



Université Paris Cité
Ecole Doctorale Physique en Ile-de-France (564)
Laboratoire Matière et Systèmes Complexes, UMR 7507

Irreversible sampling of glassy systems

Par Federico GHIMENTI

Thése de doctorat de Physique

Dirigée par Frédéric VAN WIJLAND

Soutenue publiquement le 5 Juillet 2024

Devant un jury composé de:

Frédéric VAN WIJLAND, Professeur des universités, Université Paris Cité, directeur de thèse

Liesbeth M.C. JANSSEN, Associate professor, Eindhoven University of Technology, rapporteuse

David. R. REICHMAN, Professor, Columbia University, rapporteur

Jean-Louis BARRAT, Professeur des universités, Université Grenoble Alpes, examinateur

Manon MICHEL, Chargée de recherche, Université Clermont - Auvergne, examinatrice

Ludovic BERTHIER, Directeur de recherche, Université de Montpellier, membre invité

ACKNOWLEDGEMENTS

I thank my supervisor Frédéric van Wijland for mentoring and supporting me during these years with relentless and contagious enthusiasm, and for sharing with me his vast knowledge of physics, from the *jolis petits calculs* to the longer analytical endeavours, as well as the many tricks of the trade of scientific research. Thanks for keeping the fire bright.

A large part of this thesis would not have been possible without Ludovic Berthier. His inquisitive mind and surgical precision in dealing with physical questions and with the subtle art of numerical simulations are a model and source of inspiration for me. I thank him for generously sharing with me his experience during the majority of the numerical efforts that build up this thesis. Grzegorz Szamel was another fundamental guide during these years. It was an honor for me with work with such a master of mode-coupling theory, as well as many other areas of physics, and I thank him for his help and kindness.

I wish to thank Liesbeth Janssen and David Reichman for accepting to be the referees for this thesis. Their reviews on mode-coupling theory were among the first papers I read at the beginning of my doctoral studies. It is thus a pleasure to submit to their consideration this work. Thanks to Jean-Louis Barrat and Manon Michel for dedicating a part of their precious time to be part of this jury. I am particularly grateful to Manon Michel for the many exchanges we had over the years, and for allowing me to take part in a conference on sampling problems that brought together experts from many different disciplines. I hope this thesis contains a bit of this *esprit d'ouverture*.

Giulio Biroli, Misaki Ozawa, and Gilles Tarjus supervised me during my first research internship, thus introducing me to the world of scientific research. I am grateful to them for their teachings and patience. The feedbacks from Giulio during my search for future research opportunities were precious, and I thank him for connecting me and other young enthusiastic researcher through the Beg Rohu Summer School.

A major part of this thesis builds on the work of Manon Michel and Werner Krauth. The exchanges between Werner and I date back to my time as a Master student at ENS. I thank him for the passion about physics that he conveyed me as a master student, and for the kind and insightful scientific conversations I had with him during my work as a doctoral student. I also wish to thank Jorge Kurchan, for gifting me with a beautiful intuition of his, which will lead to interesting developments.

I am grateful to Hisao Hayakawa for hosting me at the Yukawa Institute of Theoretical physics for three months. I also acknowledge Kunimasa Miyazaki, Hajime Yoshino, Harukuni and Atsushi Ikeda for showing me their lab and gifting me with the exciting experience of giving my first seminars.

Thanks also to the member of the Theory Group at MSC, Ada Altieri, Jean-Baptiste Fournier, Andrew Callan-Jones, Julien Tailleur for their kindness and the many discussions, from science to the perfect roasting of coffee grains. A warm thanks to Julien Tailleur for his support during the busy days preceding an important interview.

Thanks to Alberto, Cory, Gianmarco, Giulia, Lila, Luis, Nino and Rushi for sharing this journey together. We get by with a little help from our friends.

Last but not the least, I want to thank my family for their unconditioned love and support, and their enthusiastic celebration of any arcane draft or paper I was sending them during this years.

RÉSUMÉ COURT

ÉCHANTILLONNAGE HORS D'ÉQUILIBRE DANS LES SYSTÈMES VITREUX

L'échantillonnage d'une distribution donnée pour un système avec nombreux degrés de liberté en interaction est une tâche centrale dans plusieurs domaines scientifiques. Le temps de relaxation, c'est-a-dire l'échelle de temps typique sur laquelle la convergence est atteinte, devient extrêmement long dans de nombreux problèmes, allant du repliement des protéines à l'entraînement des réseaux neuronaux. En physique de la matière condensée, ce sont les systèmes désordonnés, des verres de spin aux liquides surrefroidis, qui constituent un défi de choix. Leur temps de relaxation augmente de plusieurs ordres de grandeur sous l'effet d'un changement modeste de température ou densité. Les stratégies suivies pour réduire le temps de relaxation reposent sur l'utilisation de dynamiques non physiques qui échantillonnent la distribution cible tout en restant réversibles. Une autre possibilité, qui trouve son origines en mathématiques appliquées, consiste à ajouter à un processus stochastique d'équilibre une force hors d'équilibre, ce qui peut donner lieu à une diminution du temps de relaxation. Cette thèse aborde quantitativement les performances des dynamiques irréversibles qui échantillonnent la distribution de Boltzmann dans les systèmes présentant un ralentissement dynamique vitreux. Dans le chapitre 1, nous décrivons plusieurs façons de s'écartez de l'équilibre tout en préservant la distribution cible, et nous identifions une implémentation minimale, obtenue en ajoutant à une dynamique de Langevin suramortie d'équilibre des forces transverses au gradient d'énergie. Dans le chapitre 2, nous étudions la dynamique avec les forces transverses pour une particule évoluant dans un potentiel extérieur. Dans le chapitre 3, nous mettons les forces transverses à l'œuvre dans un verre de spin en champ moyen, en quantifiant et comprenant l'accélération grâce à de nouvelles fonctions de corrélation croisées et un théorème de fluctuation-dissipation modifié. Dans le chapitre 3, nous explorons l'effet de forces transverses dans un liquide dense par des simulations numériques en 3d. Nous découvrons que l'accélération est une fonction non monotone de la température. Dans la région de dynamique vitreuse, l'efficacité des forces transverses diminue. Ici, à l'échelle microscopique, les trajectoires dynamiques caractéristiques des forces transverses se replient sur elles-mêmes en orbites circulaires, ce qui est quantifié en mesurant la constante de diffusion impaire, un coefficient de transport autorisé par les forces transverses. Dans les chapitres 4 et 5, nous rationalisons notre investigation numérique, en développant une théorie de champ moyen dynamique et de couplage de modes adaptées aux forces transverses. Nous abordons l'émergence des coefficients de transport (diffusivité, viscosité, mobilité), avec leur composantes impaires, et déterminons le comportement asymptotique de l'accélération lorsque l'intensité des forces transverses augmente. Dans le chapitre 7, nous évaluons les performances de l'algorithme Event Chain Monte Carlo (ECMC), une méthode d'échantillonnage hors équilibre qui réalise des translations collectives de chaînes de particules, dans un verre polydisperse de disques durs. À toutes les densités explorées, ECMC garde un avantage sur l'algorithme d'équilibre de Metropolis. Comme dans le cas de forces transverses, l'efficacité d' ECMC diminue à mesure que la densité augmente. Nous proposons ensuite un nouvel algorithme, collective Swap

(cSwap), qui réalise des échanges, collectifs et hors d'équilibre, des diamètres de particules. Il surpasse en efficacité les méthodes Monte Carlo de référence, et son efficacité augmente avec la densité, tout du moins dans notre fenêtre d'observation. En combinant cSwap et ECMC, nous obtenons une accélération de 40 par rapport aux meilleures méthodes. Le nouvel algorithme est appliqué à la production d'empilements de disque stables à des densités élevées. Nous concluons avec un résumé de nos contribution.

Mots-clés: méthodes Monte Carlo, chaines de Markov irreversibles, verres de spin, théorie de champ moyen dynamique, théorie du couplage de modes, interaction non réciproques, transition vitreuse, simulations numériques, processus stochastiques.

ABSTRACT

IRREVERSIBLE SAMPLING OF GLASSY SYSTEMS

In silico sampling of a target distribution for a system of many interacting degrees of freedom is a ubiquitous task in natural sciences. The relaxation time, the typical time scale over which convergence is achieved, becomes dauntingly large in some relevant problems, ranging from protein folding to neural networks training . The hardest instance of this problem in condensed matter is presented by disordered systems, from spin glasses to supercooled liquids, whose relaxation time grows by many orders of magnitude upon a mild change in temperature or density. The way-to-go paradigm to reduce the relaxation time relies on designing alternative, nonphysical dynamical evolution rules that sample the target distribution, which is achieved by preserving time reversibility. Another route, which has its birthplace in applied mathematics, consists in supplementing with a nonequilibrium drive an otherwise equilibrium stochastic process, which can be rewarded with a reduction of the relaxation time. This thesis addresses the quantitative performance of irreversible dynamics that sample the Boltzmann distribution in different models and system displaying glassy dynamical slowdown. In Chapter 1 we describe different ways by which the dynamics can be driven out of equilibrium while preserving the target distribution, and we identify a minimal implementation of the nonequilibrium drive, achieved by supplementing an equilibrium overdamped Langevin dynamics with forces transverse to the energy gradient. In Chapter 2 we move to the dynamics of transverse forces for a single particle evolving in an external potential. In Chapter 3, we study the dynamics of a mean field spin glass with transverse forces. We quantify and physically understand the speedup by means of novel cross correlation function and of a modified fluctuation dissipation theorem. In Chapter 4 we bring transverse forces to work in dense liquids through numerical simulations in finite dimensions. We discover that the speedup is a nonmonotonic function of the temperature and that, as we enter the region of glassy dynamics, the efficiency of transverse forces decreases. Microscopically, we find that in this region the dynamical pathways unlocked by transverse forces fold themselves in circular orbits. We characterize these trajectories by measuring the odd diffusion constant, a transport coefficient now permitted by transverse forces. In Chapter 5 and 6 we rationalize our numerical investigation, developing a dynamical mean field theory and a mode coupling theory specifically tailored for transverse forces. We address the emergence of several transport coefficients (diffusivity, viscosity, mobility), with a focus on their odd components, and determine the asymptotic behavior of the speedup as transverse forces are made increasingly strong. In Chapter 7, we probe the performance of the Event-Chain Monte Carlo algorithm, a nonequilibrium sampling method that performs driven, collective translations of chains of particles, in a polydisperse glass former of hard disks. At all densities explored, ECMC maintains an edge over the equilibrium Metropolis algorithm. Echoing what we found for transverse forces, the efficiency of ECMC decreases as the density of the system increases. We then propose a novel algorithm, collective Swap (cSwap), which performs out of equilibrium, collective swaps of particle diameters. We show that it outperforms state-of-the art Mote Carlo

algorithms, and that its efficiency increases with the density within our observation window. By combining cSwap and ECMC, we achieve a speedup of 40 over state of the art methods. As an application, we use the novel algorithm to produce stable jammed packings at remarkably high densities. In the conclusions, we summarize the contributions developed in the previous chapter, and propose future research directions.

Keywords: Monte Carlo methods, irreversible Markov chains, spin glasses, dynamical mean field theory, mode coupling theory, Non- reciprocal interactions, Glass transition, Numerical simulations, stochastic processes.

RÉSUMÉ

L'échantillonnage d'une distribution donnée pour un système avec de nombreux degrés de liberté en interaction est une tâche centrale dans plusieurs sciences naturelles et en mathématiques. Les domaines concernés incluent la biochimie, la matière condensée, les problèmes d'optimisation et d'inférence, et la physique des hautes énergies. Le paradigme pour accomplir cette tâche d'échantillonnage consiste à simuler un processus stochastique qui est réversible dans le temps. Cette propriété garantit que la distribution cible est échantillonnée une fois que la dynamique a atteint son état d'équilibre. La convergence vers l'état stationnaire est atteinte sur une échelle de temps typique connue sous le nom de temps de relaxation. Le temps de relaxation devient extrêmement long dans nombreux problèmes de physique ou autres. Quelques exemples incluent le repliement des protéines, où les structures protéïques stables et biologiquement pertinentes sont séparées par de grandes barrières énergétiques, ou dans l'apprentissage automatique, où les paramètres optimaux nécessaires pour que le réseau neuronal exécute correctement une tâche donnée doivent être identifiés dans un paysage complexe en haute dimension.

L'instance la plus difficile du problème d'échantillonnage en matière condensée est présentée par les systèmes désordonnés, des verres de spin aux liquides surfondus, qui constituent un défi de choix. Pour ces systèmes, le temps de relaxation augmente de plusieurs ordres de grandeur lors d'un léger changement de température ou de densité. L'origine de ce ralentissement brutal échappe encore à notre compréhension, ainsi que la nature du lien entre la dynamique des systèmes vitreux et leurs propriétés thermodynamiques, déterminées par la distribution de Boltzmann. Sonder la thermodynamique de ces systèmes en profondeur dans le régime vitreux est nécessaire pour étendre notre compréhension de leurs propriétés. C'est également un défi en soi, qui pourrait mener à des découvertes et des applications dans les autres domaines mentionnés où un ralentissement similaire est observé.

Pour réduire le temps de relaxation, une possibilité est de recourir à des dynamiques non physiques dotées d'une propriété de réversibilité temporelle, qui leur permet d'échantillonner la distribution de Boltzmann à l'état stationnaire. Un exemple célèbre de cette approche est un algorithme pour les verres structurels polydispersés, connu sous le nom de Swap. En permettant des échanges à l'équilibre des diamètres des particules, Swap atteint une accélération de plusieurs ordres de grandeur. D'autres exemples incluent les *cluster algorithm*, *population annealing* et *parallel tempering*.

Une autre possibilité, qui trouve sa source dans les mathématiques appliquées, consiste à ajouter à un processus stochastique d'équilibre une force hors équilibre. Un théorème stipule que recourir à une dynamique hors équilibre peut être récompensé par une réduction du temps de relaxation. De nombreuses dynamiques hors équilibre existent, et ont fait l'objet d'études approfondies en mathématiques appliquées et, plus récemment ont trouvé des applications en physique dans les systèmes ferromagnétiques et dans l'étude de la fusion en deux dimensions. Cependant, nous connaissons peu la performance de ces méthodes dans les systèmes présentant un ralentissement dynamique vitreux, notamment en ce qui concerne la dépendance de l'accélération avec la température et la densité du système et le type d'interactions entre les constituants du système. Cette thèse vise à combler cette lacune en abordant la performance quantitative des dynamiques irréversibles qui échantillonnent la distribution de Boltzmann dans

différents modèles et systèmes dont la dynamique est entravée par un ralentissement vitreux.

Dans le Chapitre 1, nous introduisons le paradigme de l'échantillonnage d'équilibre et le concept de temps de relaxation. Nous décrivons différentes manières de s'écartier de l'équilibre tout en préservant la distribution cible. Une possibilité, connue sous le nom de *lifting*, consiste à augmenter l'espace de phase du système par des variables auxiliaires, puis à exploiter la nature étendue de l'espace de phase pour injecter une impulsion hors équilibre, ajoutant une forme de persistance aux trajectoires du système. Nous présentons différents types de dynamiques augmentées, en nous inspirant des modèles de matière active. Une seconde possibilité consiste à ajouter à une dynamique de Langevin suramortie d'équilibre des forces transverses au gradient de l'énergie. Nous identifions cette dynamique avec forces transverses comme une mise en œuvre minimale des forces hors équilibre.

Dans le Chapitre 2, nous construisons une image physique de la manière dont les forces transverses opèrent en examinant différents exemples de particules dans un potentiel externe. Les forces transverses augmentent le taux d'échappement, une fréquence d'évolution microscopique typique. Ensuite, nous examinons les cas d'une particule dans un puits harmonique et du problème de franchissement de barrière, où nous quantifions l'accélération de l'échantillonnage et discutons de la manière dont les trajectoires sont modifiées en présence de forces transverses. Fait intéressant, les résultats sur l'accélération sont différents de ceux que l'on aurait pu deviner à partir de l'analyse naïve du taux d'évasion. Nous concluons en discutant de la manière dont le théorème de fluctuation-dissipation est violé par les forces transverses.

Dans le Chapitre 3, nous mettons les forces transverses à l'épreuve dans le modèle du p-spin sphérique, un verre de spin en champ moyen avec un paysage énergétique accidenté. Nous dérivons des équations dynamiques pour les fonctions de corrélation et de réponse du système, qui sont ensuite étudiées par intégration numérique directe et analytiquement, à travers une forme de relation accidentelle de fluctuation-dissipation. Nous constatons que, comme pour les dynamiques d'équilibre, il existe une température en dessous de laquelle la dynamique du système est arrêtée et l'ergodicité est brisée. Cette température n'est pas modifiée par les forces transverses : elle est la même qu'à l'équilibre. Dans la région ergodique, nous quantifions l'accélération fournie par les forces transverses et l'interprétons en termes de l'évolution de nouvelles fonctions de corrélation absentes dans le cas d'équilibre.

Dans le Chapitre 4, nous mettons les forces transverses à l'œuvre dans un modèle très utilisé des verres structurels, le mélange binaire de Kob-Andersen. Nous implementons numériquement une dynamique brownienne suramortie avec des forces transverses et mesurons l'augmentation de la constante de diffusion longitudinale produite, comme un indicateur de la réduction du temps de relaxation du système. Nous constatons que les forces transverses maintiennent un avantage sur les dynamiques d'équilibre et que, de façon surprenante, l'accélération de l'échantillonnage est une fonction non monotone de la température, diminuant à mesure que le système devient plus vitreux. Nous caractérisons les trajectoires dynamiques générées par les forces transverses en étudiant la diffusivité impaire du système, un coefficient de transport dont l'existence est rendue possible par la nature hors équilibre des forces transverses. Le comportement des constantes de diffusion longitudinale et impaire dans le régime vitreux étayez l'image des

particules étant entraînées dans un mouvement tourbillonnant à l'intérieur de la cage formée par leurs voisins locaux.

Dans les Chapitres 5 et 6, nous rationalisons nos résultats numériques, en développant une théorie dynamique de champ moyen et une théorie du couplage de modes spécifiquement adaptées aux forces transverses. Dans le Chapitre 5, nous abordons l'efficacité des forces transverses dans un liquide simple en dimension infinie, où le désordre n'est pas figé, comme pour les verres de spin, mais auto-induit par la structure amorphe du système. La limite de champ moyen est atteinte en envoyant la dimension de l'espace à l'infini, tout en redimensionnant correctement la densité. Nous développons une théorie dynamique en champ moyen pour les forces transverses. Nous quantifions l'accélération en termes du coefficient de diffusion du système, en particulier à proximité de la transition vitreuse, où la dynamique s'arrête. Nous dévoilons également la présence de coefficients de transport impairs (diffusivité impaire, viscosité impaire et mobilité impaire) et étudions leur comportement proche de l'arrêt dynamique. Notre analyse éclaire la nature des trajectoires dynamiques suivies par le liquide et comment elles évoluent à mesure que nous approchons la phase à ergodicité brisée. Dans le chapitre 6, nous nous efforçons de comprendre analytiquement comment les forces transverses opèrent en dimensions finies. Nous étendons deux schémas d'approximation, la théorie du couplage faible et la théorie du couplage de modes, à la dynamique des liquides avec des forces transverses. Le premier schéma d'approximation est valide pour le cas où les interactions sont faibles par rapport aux fluctuations thermiques et prévoit que l'efficacité des forces transverses augmente à mesure que la température diminue. Le second schéma d'approximation prévoit un arrêt dynamique en dessous d'une température de transition dynamique T_{MCT} . Comme pour le scénario de champ moyen, nous trouvons que T_{MCT} est le même que pour les dynamiques d'équilibre. Dans la phase ergodique et en approchant de la transition, nous trouvons que le gain fourni par les forces transverses est une fonction décroissante de la température. Notre analyse nous permet également de calculer de nombreux autres coefficients de transport, avec un accent particulier sur la diffusivité impaire, la mobilité impaire et la viscosité impaire. Ces résultats corroborent et rationalisent le comportement des liquides denses avec des forces transverses observés numériquement au Chapitre 4. Nous concluons en analysant la théorie du couplage de modes pour un modèle de *lifted active Brownian particles*, introduit dans le Chapitre 1. Nous trouvons des résultats similaires à ceux obtenus pour les forces transverses, suggérant que la tendance d'efficacité observée pour ce modèle minimal pourrait également tenir pour d'autres échantillonneurs irréversibles.

Dans le Chapitre 7, nous étudions le célèbre algorithme Event Chain Monte Carlo (ECMC), un schéma de Monte Carlo hors équilibre qui exploite l'idée de *lifting* pour effectuer des translations collectives entraînées de chaînes de particules, dans un modèle de disques durs polydispersés. Comme observé pour les forces transverses, l'efficacité de l'ECMC par rapport à l'algorithme standard de Metropolis diminue avec l'augmentation de la nature vitreuse du système. Cependant, les mouvements collectifs et entraînés caractéristiques de l'ECMC n'ont pas de raison de se limiter aux seules translations de particules, car en principe, d'autres degrés de liberté peuvent également ressentir une force hors équilibre. Un candidat naturel sont les diamètres mis en mouvement par l'algorithme Swap. Nous proposons un algorithme qui effectue des échanges collectifs

entraînés dans des systèmes de disques durs polydisperses continus, en exportant les idées de chaîne d'événements dans l'espace des diamètres des particules. À mesure que la nature vitreuse du système augmente, l'efficacité de notre algorithme par rapport à Swap augmente également. En combinant notre nouvel algorithme avec ECMC pour les translations de particules, nous réalisons une accélération d'environ 40 par rapport à l'état de l'art Swap. Comme application, nous montrons que notre algorithme peut être utilisé pour produire des empilements très denses de disques.

Enfin, dans les conclusions, nous résumons les contributions développées dans les chapitres précédents et proposons des directions de recherche futures.

CONTENTS

Résumé court

Échantillonnage hors d'équilibre dans les systèmes vitreux	iii
--	-----

Abstract

Irreversible sampling of glassy systems	v
---	---

Résumé

Introduction	1
--------------	---

1 Sampling Boltzmann, faster	7
-------------------------------------	---

1.1 Equilibrium sampling of the Boltzmann distribution	8
1.1.1 Equilibrium dynamics and time reversibility	9
1.2 Relaxation time	10
1.3 Nonequilibrium to the rescue	12
1.3.1 Transverse forces	13
1.3.2 Lifted Markov processes	15
1.4 Summary and outlook	17

2 Insights for transverse forces: a particle in an external potential	19
--	----

2.1 The dynamics	20
2.2 Escape rate	20
2.3 Harmonic well	21
2.3.1 Odd transport in the harmonic well	23
2.4 Barrier crossing	24
2.4.1 Heuristic argument	24
2.4.2 Instanton trajectory: no change in the exponential factor	25
2.4.3 Full expression of τ	27
2.5 Fluctuation-dissipation relations	28
2.6 Summary and Outlook	30

3 Accelerating a mean field spin glass	33
---	----

3.1 The p -spin spherical model	34
3.2 Transverse forces in the p -spin: Ichiki-Ohzeki dynamics	34
3.2.1 Numerical integration	36
3.2.2 Fluctuation-dissipation relation	38
3.2.3 Speedup and ergodicity breaking	39
3.3 Random solenoidal fields	41
3.4 Outlook	44

4 Probing transverse forces in dense liquids	47
---	----

4.1 On the choice of \mathbf{A} in three dimensions	48
4.2 Calibration	50
4.3 The behavior of the speedup with temperature	52
4.4 Odd diffusion	53
4.5 Acceleration at large γ	54

4.6	Conclusion and outlook	55
5	Transverse forces in large dimensional liquids	57
5.1	Projection operator formalism	60
5.2	Equations of motion	61
5.3	One-particle process	63
5.4	Two-particle process	66
5.4.1	General formulation	66
5.4.2	Low density expansion of the memory kernel	68
5.5	Dynamical arrest	68
5.5.1	Ergodicity breaking occurs at the same location as in equilibrium	68
5.5.2	A sanity check	70
5.6	Ergodic phase with strong nonequilibrium drive	72
5.7	Mean-squared displacement and diffusion constant	73
5.8	Emergent odd transport	76
5.8.1	Odd diffusivity	76
5.8.2	Odd mobility	77
5.8.3	Odd viscosity	78
5.9	Outlook	80
6	Mode-coupling and weak-coupling theory for transverse forces	83
6.1	Dynamics with transverse forces	86
6.2	Weak coupling approximation	87
6.2.1	Equation of motion for a tracer	87
6.2.2	Random phase approximation	87
6.2.3	Averaging over the tracer's trajectories	89
6.2.4	Weak-coupling approximation	90
6.2.5	Diffusion tensor	91
6.2.6	Mobility tensor	93
6.3	Mode-coupling theory in the presence of transverse forces	94
6.3.1	Projection operator formalism	95
6.3.2	The irreducible memory kernel	97
6.3.3	Mode-coupling expansion of the memory matrix	97
6.3.4	Schematic mode-coupling theory	101
6.3.5	New ansatz for the ergodic phase: relaxation speedup	102
6.3.6	Beyond the schematic approximation	108
6.4	Dynamics of a tracer with transverse forces in the mode-coupling approach	109
6.4.1	Equation of motion of the tracer	110
6.4.2	Mode-coupling expansion of the tracer's memory kernel	113
6.4.3	Self-intermediate scattering function	114
6.4.4	Diffusion tensor	114
6.4.5	Mobility tensor	116
6.5	Odd viscosity	118
6.5.1	Stress tensor and transverse forces	118
6.5.2	Linear response theory	119
6.5.3	The viscosity tensor	120

6.5.4	Shear viscosity	122
6.5.5	Odd viscosity	122
6.6	Lifted active Brownian particles (ABP)	123
6.6.1	Short-time dynamics	125
6.6.2	Projection operator formalism	126
6.6.3	Mode-coupling expansion	127
6.6.4	Long-time dynamics: speedup and ergodicity breaking	129
6.6.5	Diffusion constant	129
6.7	Outlook	130
7	Irreversible Monte Carlo algorithms in glass formers: Event-chain and collective Swap	133
7.1	The model	136
7.2	Monte Carlo schemes	137
7.2.1	Metropolis Monte-Carlo (MMC)	138
7.2.2	Swap Monte Carlo	138
7.2.3	Event chain Monte Carlo (ECMC)	138
7.2.4	Collective Swap (cSwap)	140
7.3	Tests of ergodicity	142
7.3.1	Numerical test	142
7.3.2	Analytical test	143
7.4	Relaxation times	145
7.4.1	Echoes from transverse forces	147
7.4.2	Faster than the fastest	147
7.5	Dense jammed packings	149
7.6	Outlook	149
Conclusions	153	
A	Facilitated dynamics	155
A1	Spatially tuned mobility	155
A2	Facilitated dynamics	156
A2.1	Pathological cases	158
A3	Facilitated dynamics in dense liquids	161
A3.1	Diffusion constant	162
A3.2	Numerical exploration	163
A4	Mode Coupling Theory	165
A4.1	Arbitrary mobility	165
A4.2	Mode coupling expansion	167
A4.3	Mode coupling theory for facilitated dynamics	168
A4.4	Ergodicity breaking within the schematic approximation	169
B	Breaking detailed balance accelerates relaxation: a proof for discrete states systems	171

C The conductance bounds the mixing time	177
C1 Definition of the mixing time	177
C2 The conductance	178
C2.1 Lifted Markov chains, and their conductance	179
C3 Proof of the lower bound for t_{mix}	180
C3.1 Preliminary lemmas	180
C3.2 Proof of Eq. (C.1)	181
D p-spin with Ichiki-Ohzeki dynamics	185
D1 Dynamical equations for the p -spin evolving under the IO dynamics . .	185
D2 Numerical Integration of the dynamical equations	192
D3 aFDT for the IO dynamics of the p -spin	193
E Chiral active baths and symmetric tracers	195
E1 Model	196
E2 Main results	196
E2.1 Swirling disk	199
E2.2 Spinning rod	199
E2.3 Steering wedge	200
E3 Effective Langevin equation for the tracer	201
E3.1 Setting up the stage	201
E3.2 Projection operator formalism	202
E3.3 Adiabatic approximation	203
E3.4 Explicit computation	204
F The irreducible memory kernel	207
G Glassy bidisperse fluids in large dimensions	209
G1 One-particle process	210
G2 Two-body process	212
G3 Long time plateau of the memory kernel	213
G4 Connection with Ikeda <i>et al.</i> [137]	214
G5 Generalization to multi-component mixtures	215
H Does swap in large dimensions work?	219
H1 Swap dynamics with continuous diameter distribution	219
H1.1 Determination of w : annealed and quenched averages	220
H1.2 Infinite-dimensional limit	221
H2 Swap rates in large dimensions	222
I Additional result for cSwap	225
I1 A model with a different polydispersity	225
I2 Changing the length of the chain in ECMC	225
I3 Efficiency of the algorithms as a function of system size	227
Bibliography	248

LIST OF FIGURES

1	Sampling a target distribution is a hard problem in some relevant fields such as (a) biochemistry, (b) optimization problems and machine learning, and (c) amorphous and disordered materials. The images are adapted respectively from [82, 7, 26].	2
2	In a liquid (a) particle diffuse rapidly, while in a glass (b), their dynamics is extremely slow. The Fourier transform of density-density correlation yields mild changes upon increasing the density (c), but on the other hand the corresponding time correlation develops a plateau that spans many orders of magnitude (d). Taken from [142]:	3
3	Examples of unphysical dynamical rules that sample the Boltzmann distribution and obey detailed balance: (a) Wolff cluster algorithm for spin systems (b) parallel tempering, (c) Dress-Krauth cluster algorithm for particle systems, (d) Swap Monte Carlo. The image is taken from [37].	4
4	Examples of out-of-equilibrium dynamics that sample the Boltzmann distribution in the steady state: (a) Dynamics where the gradient part of the energy $-\nabla V$ is supplemented by forces \mathbf{f} transverse to the energy gradient. (b) <i>Lifted</i> dynamics, where an additional set of degrees of freedom \mathbf{v} drives the dynamics out of equilibrium, (c) Event-Chain Monte Carlo, adapted from [149], is a kind of lifted dynamics where directed, collective displacement of chains of particles are performed.	4
1.1	(a) Illustration of the barrier crossing problem in one dimensions. (b) High dimensional disordered systems have a complex landscape with a large number of minima and saddle point hindering the motion.	12
2.1	(a) Zero temperature trajectories in an isotropic harmonic well with $K_{ij} = \delta_{ij}$. Without transverse forces (blue curve, $\gamma = 0$) and with transverse forces (red curve, $\gamma = 2$). (b) Plot of the relaxation time $\tau_R(\gamma)$ for an anisotropic harmonic well with $k_1 = 2$, $k_2 = 0.5$	23
2.2	(a) Gradient flow of the double well potentials for two noninteracting particles. (b) Force field for two copies of a particle in a double well potential coupled with Ichiki-Ohzeki interactions, $\gamma = 0$. (c) Instanton trajectory from Eq. (2.31) for $\gamma = 0$ and its perturbation expansion up to second order in γ for the double well potential $v(x) = \frac{1}{4}x^4 - \frac{1}{2}x^2$. The instanton starts from the minima located at $(-1, -1)$ and ends at the saddle point located at $(0, -1)$. Adapted from [112]	27
3.1	Energy per spin as a function of temperature T obtained from numerical integration (blue dots) at $\gamma = 1$ and theoretical prediction $E_\infty = -\frac{1}{2T}$ (black dashed line).	37

3.2	Correlation function of system 1, $C_{11}(t)$ for $\gamma = 2.4$ (solid lines) and $\gamma = 0$ (dashed lines) for various temperatures above and below $T_d \approx 0.6124$. The dotted curves represent the cross correlations $C_{12}(t)$ for $\gamma = 2.4$. The shift between the dashed and the solid line of a given colour, which quantifies the acceleration of the dynamics, somewhat increases as the temperature is decreased.	38
3.3	Ratio between the relaxation time of C_{11} for the IO dynamics, $\tau_\alpha(\gamma)$, and the equilibrium dynamics $\tau_\alpha(0)$ for temperatures close to T_d	39
3.4	Cross correlation C_{12} (dotted lines) and C_{21} (dashed lines) as a function of time for $T = 0.613$ at different values of γ	39
3.5	Parametric plot of the left and right hand side of the first entry of Eq. (3.11) from the integration of Eqs. (3.6, 3.7, 3.8) at $T = 0.613$ and $\gamma = 2.4$	40
4.1	(a) Structure factor for particles of type A , at two different temperatures for $\gamma = 0$ (coloured lines) and $\gamma = 8$ (dashed lines). (b) Mean squared displacement for the large particles as a function of time, for $\gamma = 0$	51
4.2	Mean-squared displacement of the A particles at $T = 0.8$ for various values of γ	51
4.3	(a) Diffusion constant $D(\gamma, T)$ normalised by its equilibrium value at $\gamma = 0$ as a function of inverse temperature. The temperature axis uses a logscale to emphasize the non-monotonic dependence. The right axis describes the odd-diffusivity as a function of T^{-1} for various values of γ . (b) Same as (a) using a linear scale to concentrate on the glassy regime below $T = 1.0$. The black dashed line corresponds to the equilibrium efficiency.	52
4.4	(a) Rendering of a short trajectory for a few particles without any transverse force at $T = 0.8$. (b) Same with transverse forces which induce circular trajectories.	53
4.5	Behavior of the ratio $D(\gamma, T)/T\gamma$ measured for $T = 100$ as a function of γ . For large values of γ , we see the scaling $D(\gamma, T) \sim \gamma$	54
5.1	(a) Ratio between the longitudinal diffusion constant $D_{ }(\beta, \gamma)$ in the presence of transverse forces and its equilibrium counterpart at $\gamma = 0$ for different values γ of the strength of the nonequilibrium drive, as a function of inverse temperature β . (b) Odd diffusivity in the presence of transverse forces. In both panels, the memory kernel used is the one obtained via a low density expansion for the case of a linear potential, as given in Eq. (5.36).	75
5.2	(a) Longitudinal mobility $\mu_{ }$ for different values of the strength γ of the non equilibrium drive, as a function of the inverse temperature $\beta \equiv T^{-1}$. (b) Odd mobility in the presence of transverse forces. In both panels, the memory kernel used is the one obtained via a low density expansion for the case of a linear potential. Its expression is given in Eq. (5.36).	78
7.1	Particle size distribution $\pi(\sigma)$ for the system investigated in this work.	136

7.2	Illustration of the Swap Monte Carlo algorithm. During a time t_{move} , a swap of the diameters of the highlighted particles is attempted. Adapted from [203].	138
7.3	Event-chain Monte Carlo algorithm: the lifted set of degrees of freedom, the active label j and the speed direction \mathbf{v} (magenta), produce a directed translational motion of a chain of three particles.	139
7.4	Collective Swap algorithm: the active particle (in magenta) inflates while other particles deflate, resulting in a directed motion in diameter space (as seen at the bottom) and a collective swap of five particles.	141
7.5	Numerical test of ergodicity for the cSwap and ECMC algorithms. (a) Equation of state $Z(\phi)$ for the polydisperse hard disks system. (b) Rescaled radial distribution function $g(r/\sigma - 1)$ as a function of the distance from its first peak $r/\sigma - 1$. (c) Probability distribution function of the packing fractions $\pi(\phi)$ explored by the system during NPT simulations at $\beta P = 16.3\overline{\sigma^2}$	142
7.6	Representation in the complex plane of the eigenvalues λ of the transition matrix P given by Eq. (7.17) for the cSwap dynamics in the case of a system of $N = 4$ particles. The dotted line is the unit circle.	146
7.7	(a) Equilibrium relaxation time of six different Monte Carlo algorithms as a function of packing fraction. MMC and the faster ECMC fall out of equilibrium much before the four swap algorithms. The large speedup offered by Swap can be further improved using irreversible MC moves, cSwapECMC providing a further speedup of about 40 near $\phi = 0.88$. (b) Equilibrium relaxation times of the six algorithms investigated in the main text, in units of CPU time. Here $t_{\text{CPU}} = 1$ second.	147
7.8	(a) The speedup offered by ECMC over MC decreases with density. (b, c) Comparison of the displacement field relative to the center of mass after a time comparable to the relaxation time starting from the same initial condition at $\phi = 0.79$ using MMC ($t = 4.6 \times 10^6 N t_{\text{move}}$) or ECMC ($t = 2.2 \times 10^5 N t_{\text{move}}$). Despite different dynamic rules, both algorithms follow similar dynamic pathways.	148
7.9	Acceleration provided by three novel algorithms (SwapECMC, cSwap, cSwapECMC) with respect to conventional swap Monte Carlo. In cSwapECMC, the combination of collective swaps and chain moves provides the fastest algorithm with a speed up increasing with ϕ and reaching 40.	148
7.10	Jamming packing fractions ϕ_J obtained after nonequilibrium compressions using different Monte Carlo algorithms, starting from fluid configurations equilibrated at ϕ_{init} . The four swap algorithms reach very large ϕ_J , nearly independently of ϕ_{init} . The light blue band covers the range of densities obtained using augmented gradient-descent techniques [44].	150

A.1	(a) Comparisons between the histogram of position sampled through numerical integration of the facilitated dynamics for $V(x)$ given by Eq (A.11) against the Boltzmann distribution at $T = 1.0$. (b) Histograms of the position sampled by the facilitated dynamics and the usual overdamped Langevin dynamics for the same potential, at a lower temperature $T = 0.1$. Both dynamics are integrated with the same time step $\Delta t = 1 \times 10^{-5}$ for 2×10^7 steps.	158
A.2	Derivative of the Mathieu function $C'(2q, q, \pm\frac{\pi}{2})$ (blue), $S'(2q, q, \pm\frac{\pi}{2})$ (orange) as a function of q . The point where the curves pass through zero determines q , and therefore λ	161
A.3	Comparison between the usual overdamped Langevin dynamics and the facilitated (here denoted 'modified') dynamics for harmonic sphere at $T = 0.1$ Left: plots of energy as a function of time. At long times, the average value of the energy and its fluctuations are the same for standard and facilitated dynamics. Center: evolution of the energy at initial times, from which we see that the facilitated dynamics has a faster convergence. Right: mean squared displacement. The mean squared displacement achieved through the facilitated dynamics is an order of magnitude higher than its standard counterpart.	164
B.1	Graphical interpretation of the proof of Ichiki and Ohzeki, taken from [136]. The plot show characteristic polynomials of W (dashed line) and S (solid line). Eq. (B.12) enforce the dashed to be above the solid line for $\text{Re } \lambda = 0^+$, while Eq. (B.13) guarantees the solid line to be above the dashed one until the horizontal axis is hit again.	174
E.1	Odd dynamics and ratchet currents of differently-shaped passive objects in a bath of cABPs. (a) A passive disc (blue) inherits chiral random motion of the opposite sign of the bath particles (yellow) through collisions. (b) This results in odd diffusion, manifesting in antisymmetric velocity correlations (solid line) which are odd under time-reversal (dashed line). (c) An immobilized rod breaks the isotropy of the bath, resulting in asymmetric accumulation of cABPs driving a net torque $\langle \Gamma \rangle_b$. (d) For a mobile rod, this torque is balanced in steady state by the angular friction, resulting in a constant angular velocity. Translational and rotational dynamics are decoupled due to central symmetry. (e) A passive wedge further breaks this central symmetry, behaving as both a rotational and translational ratchet. (f) Translation-rotation coupling and ratchet currents are visible in the time correlation of Ω and v_{\parallel} . The bottom row shows simulation results for $\ell_p = 10$ and $\ell_g = 10$. . This figure was realised by Cory Hargus.	197

G.1	Dynamical phase diagram of the bidisperse fluid for $\delta = 3.0$. $\hat{\phi}_d^{\text{mono}} \approx 4.8067$ is the critical packing fraction for the glass transition of monodisperse hard spheres. Violet points: fully ergodic phase ($\Delta_\mu = +\infty$ for $\mu = A, B$); Green points: single glass phase ($\Delta_A < +\infty$, $\Delta_B = \infty$) with particles of type A dynamical arrested; yellow points: double glass phase ($\Delta_A < +\infty$, $\Delta_B = \infty$) with both particles of type A and B dynamically frozen. This is image reproduces results reported in [137]	216
G.2	Dynamical phase diagram of a ternary mixture in infinite dimensions for $\delta_A = 6.0$, $\delta_B = 3.0$ and $\delta_C = 0$	217
I.1	Time dependence of the hexatic correlation function for a system of $N = 1024$ particles with a power law distribution of the diameters. Time is measured in units of Nt_{move} , and the efficiency of the algorithms that involve swap moves is comparable to the results shown in Fig. 2 of the main text near $\phi \approx 0.85$	226
I.2	Equilibrium correlation function for the ECMC dynamics, using different values of the chain length ℓ . Time is measured in units of (a) the number of chains displaced, and (b) Nt_{move}	226
I.3	Time dependence of the hexatic correlation function for systems of different sizes using the Swap, SwapECMC, cSwap and cSwapECMC algorithms in the NVT ensemble.	227

INTRODUCTION

The main goal of statistical mechanics is to understand the macroscopic properties of systems composed of an extremely large number of constituents, starting from their microscopic interactions. When the microscopic dynamics is reversible in time and the system exchanges heat with an external reservoir, the macroscopic properties can be obtained as averages over all the microscopic configurations of the system, weighted according to the Boltzmann distribution [59].

How can these averages be computed in practice? For the majority of strongly interacting realistic systems, the analytical evaluation of these ensemble averages is done by resorting to approximation schemes, as is the case for dense liquids [124]. The high number of degrees of freedom involved makes any exact numerical, or let alone, analytical integration unfeasible. To escape the curse of dimensionality, the way-to-go paradigm consists in simulating a stochastic dynamics for the system of interest [202, 6, 97], in the spirit of the pioneering work on the Monte Carlo algorithm by Ulam, Metropolis and Rosenbluth [189, 188, 231], or of Molecular Dynamics by Alder and Wainwright [5], or of Brownian dynamics by Turq, Lantelme and Friedman [249]. These algorithms allow the system to explore its configuration space using a stochastic process, where thermal fluctuations are combined with energy minimization flows. The dynamical evolution rules are tailored to be statistically reversible in the steady state with respect to the Boltzmann distribution. This condition ensures that, after a large enough relaxation time, the configurations explored by the simulated system are distributed according to the Boltzmann distribution.

There are however systems of physical interest characterized by an extremely rugged energy landscape, full of local minima and saddle points where the dynamics can get stuck for long times, rendering sampling a very difficult task in practice. The computational challenges of sampling the Boltzmann distribution in systems of this sort extend well beyond the realm of physics. Similar difficulties arise for instance in biochemistry, when determining the stable, functional structure of proteins [196, 58]. In this case, biologically relevant configurations are separated by high energy barriers, and using local dynamics, the transitions from one configuration to another are extremely rare. Another interesting field of application is constraint satisfaction problems [168, 95] and machine learning [8]. There, configurations are the internal weights of the neural network, and the loss function, a measure of the performance of the network in accomplishing a given feature-extraction task, plays the role of the energy of the configurations. Training a neural network involves performing a stochastic dynamics in the loss landscape [45], which is reminiscent, with some caveats [54, 195], of the dynamics discussed above for physical systems, with the common trait that the high-dimensional loss landscape is often non-convex.

In condensed matter physics, a manifestation of this hard-to-sample, rugged landscape is given by systems where some form of disorder is present. The disorder can be directly quenched in the interactions, as is the case for magnetic alloys known as spin-glasses [191], or it can be self-induced, as for structural glasses and amorphous

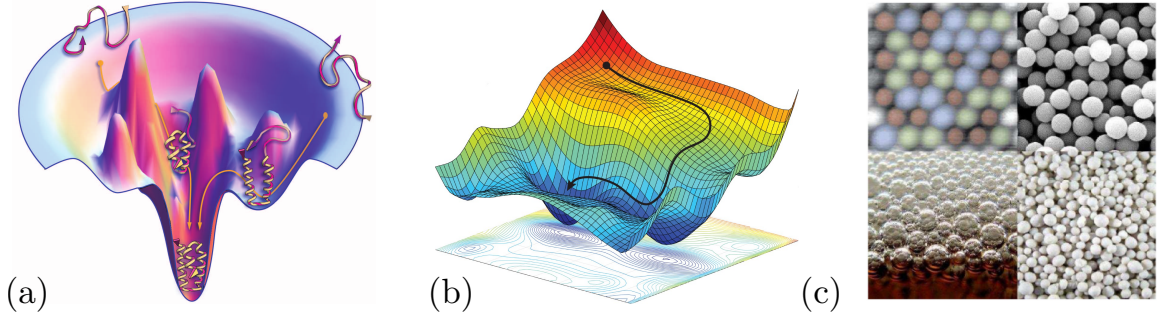


Figure 1: Sampling a target distribution is a hard problem in some relevant fields such as (a) biochemistry, (b) optimization problems and machine learning, and (c) amorphous and disordered materials. The images are adapted respectively from [82, 7, 26].

materials [26]. For these systems, as the temperature is lowered or the density increased beyond a typical threshold, the dynamics slows down by several orders of magnitude, and the particles that constitute these materials are effectively frozen, as in crystalline solids. However, on a structural level, the difference from the rapidly relaxing, liquid configurations are hard to identify. As the interplay between their structure and the slow dynamics of glasses continues to elude our understanding [10, 57, 60, 26, 28, 42], the development of algorithms capable of exploring more efficiently glassy landscapes plays a crucial role in the development and falsification of the theories of the glass transition [16, 37].

When fighting against the computationally growing timescales of glassy systems, it is a common practice to design and simulate unphysical dynamics, that reduce the time necessary to reach equilibration while preserving the target Boltzmann distribution. The latter condition can be ensured by tuning the transition rates of the dynamical process so that the stochastic dynamics is time reversible. This property, called equilibrium, or detailed balance, ensures the eventual sampling of the Boltzmann distribution. Examples of these dynamics are given by cluster algorithms for spins [242, 257] or particle systems [144, 83], where many components of the system are collectively updated, or by parallel tempering [133], where many copies of the system are simulated at different temperatures and interact with each other through configuration swaps. Recently, an efficient algorithm for polydisperse systems was developed. This so-called Swap algorithm achieves a remarkable speedup of several orders of magnitude by allowing for the exchange of radii of particles of different species [119, 203].

Another direction in the design of novel algorithms was pursued in the field of applied mathematics, and diffused gradually over the last 15 years into the field of statistical physics. The seminal idea is that imposing an equilibrium reversible dynamics is a sufficient, but not necessary, condition to grant the correct sampling of the Boltzmann distribution. One can thus design dynamics that are out-of-equilibrium, or irreversible, but that nevertheless sample the Boltzmann distribution in their steady state. A mathematical theorem [135, 134, 136] states (in spirit) that, when an equilibrium dynamics is supplemented by a nonequilibrium driving that preserves the Boltzmann distribution, the relaxation time to the steady state is shortened compared to the equilibrium

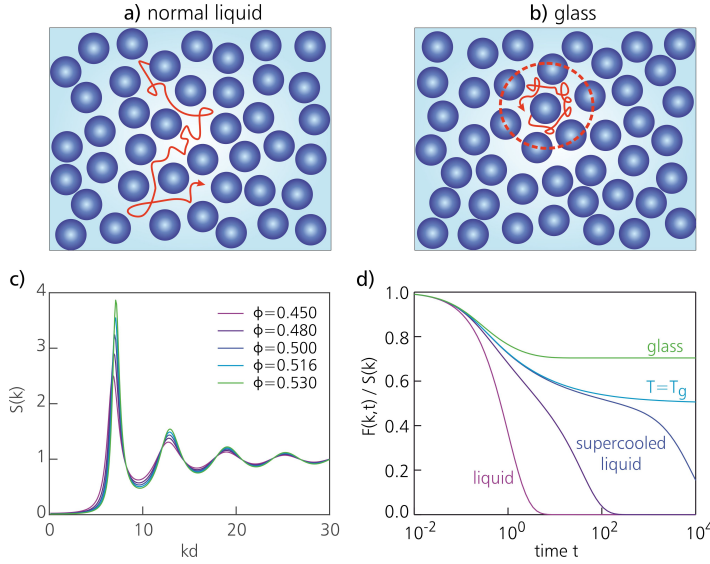


Figure 2: In a liquid (a) particle diffuse rapidly, while in a glass (b), their dynamics is extremely slow. The Fourier transform of density-density correlation yields mild changes upon increasing the density (c), but on the other hand the corresponding time correlation develops a plateau that spans many orders of magnitude (d). Taken from [142]:

case. These out of equilibrium drives can be provided by supplementing the dynamics with forces transverse to the energy gradient. Another way of implementing the nonequilibrium drive is given by the so called *lifted* dynamics [255]. In these dynamics, the original degrees of freedom of a given system are supplemented by an extra set of variables, and an out of equilibrium dynamics for the extended system is designed exploiting the extended structure of the configuration space. As shown in seminal works in the field of applied mathematics [81, 63], this procedure usually transform diffusive processes in ballistic ones, leaving room for a speedup in sampling. In the realm of physics, these ideas have been applied successfully for ferromagnetic systems close to a second-order phase transitions [248, 233, 199] and hard and soft disks [23, 22, 193] in the vicinity of the melting point, and various other directions [194, 140, 148, 182, 121]. Applications of these ideas are found also in the domain of Bayesian inference, where these dynamics go under the mathematical framework of piecewise deterministic Markov Processes [72, 198], and in machine learning [207, 106, 104]. Classical lifted dynamics have also been shown to be equivalent to class of quantum algorithms known as quantum walks [251, 11].

The physical systems where these irreversible dynamics have been applied exhibit a critical dynamical slowdown, which is by nature very different from the one observed for disordered and amorphous systems. How do these irreversible samplers of the Boltzmann distribution fare in glassy system? How big is the speedup, and how does it depends on the temperature and density of the system? Can these ideas on irreversibility be combined with state-of-the art, equilibrium algorithms, and help us advance in the "race to the bottom" [232] of the energy landscapes of disordered systems? These are the questions that this thesis addresses.

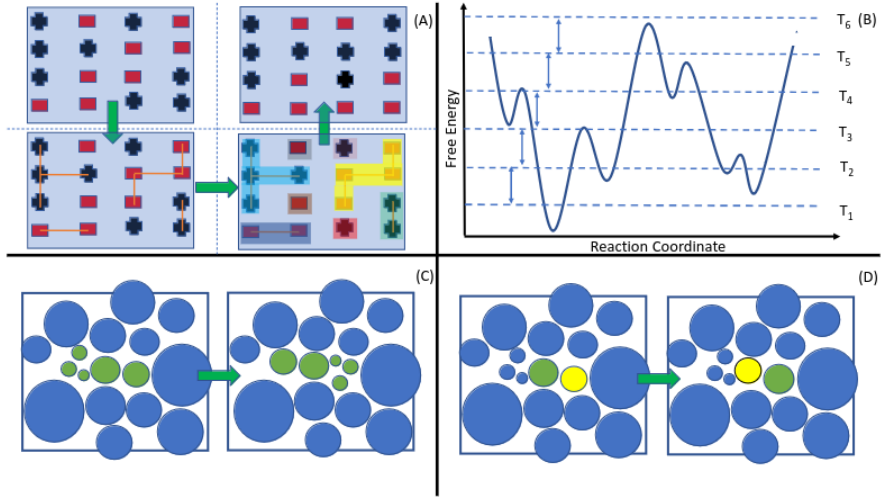


Figure 3: Examples of unphysical dynamical rules that sample the Boltzmann distribution and obey detailed balance: (a) Wolff cluster algorithm for spin systems (b) parallel tempering, (c) Dress-Krauth cluster algorithm for particle systems, (d) Swap Monte Carlo. The image is taken from [37].

Outline

This thesis is organised as follows: in Chapter 1 we describe different ways by which the dynamics can be driven out of equilibrium while preserving the target distribution, and we identify a minimal implementation of the nonequilibrium drive, achieved by supplementing an equilibrium overdamped Langevin dynamics with forces transverse to the energy gradient. In Chapter 2 we move to the dynamics of transverse forces for a single particle evolving in an external potential. In Chapter 3, which contains results from [112], we study the dynamics of a mean field spin glass with transverse forces. We quantify and physically understand the speedup by means of novel cross

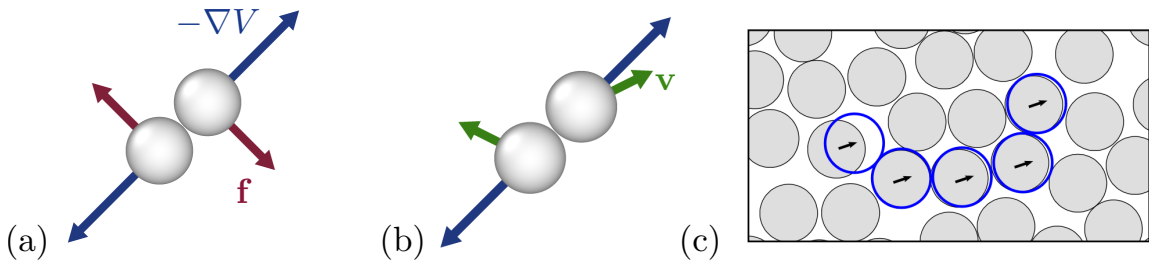


Figure 4: Examples of out-of-equilibrium dynamics that sample the Boltzmann distribution in the steady state: (a) Dynamics where the gradient part of the energy $-\nabla V$ is supplemented by forces \mathbf{f} transverse to the energy gradient. (b) *Lifted* dynamics, where an additional set of degrees of freedom \mathbf{v} drives the dynamics out of equilibrium, (c) Event-Chain Monte Carlo, adapted from [149], is a kind of lifted dynamics where directed, collective displacement of chains of particles are performed.

correlation function and of a modified fluctuation dissipation theorem. In Chapter 4, based on [108] we bring transverse forces to work in dense liquids through numerical simulations in finite dimensions. We discover that the speedup is a nonmonotonous function of the temperature and that, as we enter the region of glassy dynamics, the efficiency of transverse forces decreases. Microscopically, we find that in this region the dynamical pathways unlocked by transverse forces fold themselves in circular orbits. We characterize these trajectories by measuring the odd diffusion constant, a transport coefficient now permitted by transverse forces. In Chapter 5 and 6, based on [109, 107] we rationalize our numerical investigation, developing a dynamical mean field theory and a mode coupling theory specifically tailored for transverse forces. We address the emergence of several transport coefficients (diffusivity, viscosity, mobility), with a focus on their odd components, and determine the asymptotic behavior of the speedup as transverse forces are made increasingly strong. In Chapter 7, based on [110], we probe the performance of the Event-Chain Monte Carlo algorithm, a nonequilibrium sampling method that performs driven, collective translations of chains of particles, in a polydisperse glass former of hard disks. At all densities explored, ECMC maintains an edge over the equilibrium Metropolis algorithm. Echoing what we found for transverse forces, the efficiency of ECMC decreases as the density of the system increases. We then propose a novel algorithm, collective Swap (cSwap), which performs out of equilibrium, collective swaps of particle diameters. We show that it outperforms state-of-the art Mote Carlo algorithms, and that its efficiency increases with the density within our observation window. By combining cSwap and ECMC, we achieve a speedup of 40 over state of the art methods. As an application, we use the novel algorithm to produce stable jammed packings at remarkably high densities. In the conclusions, we summarize the contributions developed in the previous chapter, and propose future research directions.

CHAPTER 0

CHAPTER 1

SAMPLING BOLTZMANN, FASTER

In the long run we are all dead

— J. M. KEYNES, *A tract on monetary reform*

1.1	Equilibrium sampling of the Boltzmann distribution	8
1.1.1	Equilibrium dynamics and time reversibility	9
1.2	Relaxation time	10
1.3	Nonequilibrium to the rescue	12
1.3.1	Transverse forces	13
1.3.2	Lifted Markov processes	15
1.4	Summary and outlook	17

In this introductory chapter, we illustrate the paradigm of equilibrium sampling by means of an overdamped Langevin equation. We recall a widely accepted definition of time reversibility for stochastic dynamics, and we introduce a timescale that governs the convergence to the equilibrium state. We then observe that giving up time reversibility while preserving the Boltzmann distribution in the stationary state can be rewarded with a larger convergence rate, and we present several formulations of irreversible dynamics that sample the Boltzmann distribution. These examples take inspiration in their design from models of active particles, and they will be used to justify the main purpose of study for this part of the thesis: a dynamics that achieves a speedup by including forces transverse to the local energy gradient.

1.1 Equilibrium sampling of the Boltzmann distribution

We start by defining our general goal. Given a system with d real and continuous degrees of freedom encoded in a vector \mathbf{r} , and given an energy $V(\mathbf{r})$ associated to these degree of freedom, the goal is to produce independent configurations of \mathbf{r} distributed according to the Boltzmann distribution

$$\rho_B(\mathbf{r}) = \frac{1}{Z} e^{-\beta V(\mathbf{r})} \quad (1.1)$$

with $\beta^{-1} = k_B T$, with T the temperature of the system and k_B the Boltzmann constant, which we set to 1 in the rest of this thesis. The normalization factor is the partition function $Z \equiv \int d\mathbf{r} e^{-\beta V(\mathbf{r})}$. In this first part of the thesis, we address this question from a theoretical standpoint, while pinpointing elements important for practical realizations. The way-to-go paradigm to tackle this problem is to endow the system with an equilibrium, stochastic, local dynamics. To illustrate this paradigm, consider the following overdamped Langevin dynamics

$$\dot{\mathbf{r}} = -\mu_0 \nabla V(\mathbf{r}) + \sqrt{2T\mu_0} \boldsymbol{\xi}(t). \quad (1.2)$$

The mobility μ_0 sets the time-scale at which the particle is moving. The two terms on the right hand side of Eq. (1.2) play complementary roles. The first one is deterministic and drives the system toward near local minima of the energy. The second one involves a Gaussian white noise $\boldsymbol{\xi}(t)$, with correlations $\langle \boldsymbol{\xi}(t) \otimes \boldsymbol{\xi}(t') \rangle = \mathbf{1}\delta(t - t')$. It helps exploring the energy landscape by eventually kicking the particle out of saddle points and minima, where the gradient term is zero. The time derivative of the energy, upon averaging over the noise, is

$$\left\langle \frac{d}{dt} V(\mathbf{r}(t)) \right\rangle = -\mu_0 \langle [\nabla V(\mathbf{r}(t))]^2 - T \nabla^2 V(\mathbf{r}) \rangle \quad (1.3)$$

And is negative if $V(\mathbf{r})$ is convex. The stochastic dynamics given in Eq. (1.2) comes with an associated probability density distribution $\rho(\mathbf{r}, t)$, such that $\rho(\mathbf{r}, t)d\mathbf{r}$ is the probability of finding the particle in a infinitesimal phase space volume $d\mathbf{r}$ centered around \mathbf{r} at time t , and it evolves in time according to the Fokker-Planck equation

$$\partial_t \rho(\mathbf{r}, t) = \Omega_0 \rho(\mathbf{r}, t), \quad (1.4)$$

where Ω_0 is a linear operator

$$\Omega_0 = \mu_0 \nabla \cdot [(\nabla V) + T \nabla]. \quad (1.5)$$

We are adopting the convention that the gradient ∇ acts on anything to its right, unless it is enclosed by round parentheses. The Fokker-Planck operator in Eq. (1.5) is composed of a drift term and of a diffusive term, which are signatures, at the level of the dynamics of $\rho(\mathbf{r}, t)$, of gradient descent flow and of thermal fluctuations.

Due to conservation of probability $\int d\mathbf{r} \rho(\mathbf{r}, t) = 1$, the Fokker-Planck equation Eq. (1.4) can be written in the form of a continuity equation

$$\partial_t \rho(\mathbf{r}, t) = -\nabla \cdot \mathbf{j}(\mathbf{r}, t). \quad (1.6)$$

Where the probability current $\mathbf{j}(\mathbf{r}, t)$ depends on ρ and reads

$$\mathbf{j}(\mathbf{r}, t) = -\mu_0 [\nabla V + T \nabla] \rho(\mathbf{r}, t). \quad (1.7)$$

The stationary solution of Eq. (1.4) is the Boltzmann distribution defined in Eq. (1.1), since

$$\partial_t \rho_B(\mathbf{r}, t) = \Omega_0 \rho_B = 0. \quad (1.8)$$

Equivalently, we can note that $\mathbf{j}(\mathbf{r}, t)$ in the continuity equation Eq. (1.7) vanishes when evaluated for $\rho = \rho_B$. The task of sampling Boltzmann is thus accomplished once the stochastic process defined by Eq. (1.2) reaches the steady state. The question of the time taken to reach this condition is addressed in the next Section. Before turning to this issue, however, we will discuss the equilibrium nature of the overdamped Langevin process.

1.1.1 Equilibrium dynamics and time reversibility

In physics, the concept of time reversal symmetry has its origin in the deterministic Newton second law, which is invariant upon inversion of time. In statistical mechanics, where deterministic forces are combined with random fluctuations, time reversal symmetry is the hallmark of thermal equilibrium. A stochastic dynamics, such as the overdamped Langevin dynamics presented in Eq. (1.2), is an equilibrium dynamics –i.e. it is invariant under time reversal symmetry– if, in the stationary state, the probability $\mathbb{P}(\{\mathbf{r}(\tau)\}, 0 \leq \tau \leq t | \mathbf{r}(0))$ of observing a given trajectory $\{\mathbf{r}(\tau)\}$ which starts at $t = 0$ at $\mathbf{r}(0)$ and ends at $\mathbf{r}(t)$ at a final observation time t , is the same of observing its time-reversed counterpart $\{\mathbf{r}^R(\tau) \equiv \mathbf{r}(t - \tau)\}$. Taking the sampling of the steady state distribution $\rho_{ss}(\mathbf{r})$ into account for the position of the particle at the beginning of a trajectory, the equilibrium condition reads

$$\mathbb{P}(\{\mathbf{r}(\tau)\}, 0 \leq \tau \leq t | \mathbf{r}(0)) \rho_{ss}(\mathbf{r}(0)) = \mathbb{P}(\{\mathbf{r}^R(\tau), 0 \leq \tau \leq t\} | \mathbf{r}(t)) \rho_{ss}(\mathbf{r}(t)). \quad (1.9)$$

Eq. (1.9) is also known under the name of detailed balance condition. The probability of a given trajectory can be computed using a path integral approach, such as the Onsager-Machlup formalism [209, 180] for Gaussian noise. The result reads

$$\mathbb{P}(\{\mathbf{r}(\tau)\}, 0 \leq \tau \leq t | \mathbf{r}(0)) \propto e^{-S[\{\mathbf{r}(\tau)\}].} \quad (1.10)$$

Here $S[\{\mathbf{r}(t)\}]$ is the Onsager-Machlup action associated to the dynamics under consideration. For the overdamped Langevin dynamics in Eq. (1.2) in the Stratonovich discretization, it is given by

$$S(\{\mathbf{r}(\tau)\}) = \frac{1}{4T\mu_0} \int_0^t d\tau [\dot{\mathbf{r}}(t) + \mu_0 \nabla V(\mathbf{r}(t))]^2 + \frac{1}{2\mu_0} \int_0^t d\tau \nabla^2 V(\mathbf{r}(t)). \quad (1.11)$$

Using Eq. (1.11), the path probability ratio is

$$\frac{\mathbb{P}(\{\mathbf{r}(\tau)\}, 0 \leq \tau \leq t) | \mathbf{r}(0)}{\mathbb{P}(\{\mathbf{r}^R(\tau)\}, 0 \leq \tau \leq t) | \mathbf{r}(t)} = e^{-\beta[V(\mathbf{r}(t)) - V(\mathbf{r}(0))]} = \frac{\rho_B(\mathbf{r}(t))}{\rho_B(\mathbf{r}(0))}. \quad (1.12)$$

which proves the detailed balance equation Eq. (1.9) with respect to the Boltzmann distribution ρ_B , for the overdamped Langevin dynamics.

The violation of the time reversal symmetry condition given by Eq. (1.9) signals the nonequilibrium nature of the dynamics. When this occurs, it is interesting to access to the typical rate at which the irreversible nature of the process manifests itself. This inverse time scale is given by the entropy production rate σ [237, 214], defined as

$$\sigma \equiv \lim_{t \rightarrow \infty} \frac{1}{t} \int d\{\mathbf{r}(\tau)\} \rho_{ss}(\mathbf{r}(0)) e^{-S[\mathbf{r}(\tau)]} \log \frac{\rho_{ss}(\mathbf{r}(0)) \mathbb{P}(\{\mathbf{r}(\tau)\}, 0 \leq t \leq \tau | \mathbf{r}(0))}{\rho_{ss}(\mathbf{r}(t)) \mathbb{P}(\{\mathbf{r}^R(\tau)\}, 0 \leq t \leq \tau | \mathbf{r}(t))} \quad (1.13)$$

where the integral $\int d\{\mathbf{r}(\tau)\}$ signifies a sum over all the possible trajectories $\{\mathbf{r}(t)\}$. On a mathematical ground, σ is the growth rate of the Kullback-Leibler divergence between the probabilities of observing a trajectory and its time-reversed counterpart in the steady state. For systems obeying Eq. (1.9), we consistently have $\sigma = 0$. The entropy production rate can be related with the presence of a non-vanishing current in the steady state of the system, as the following equality

$$\sigma = \frac{1}{\mu_0 T} \int d\mathbf{r} \frac{\mathbf{j}_{ss}^2(\mathbf{r})}{\rho_{ss}(\mathbf{r})} \geq 0 \quad (1.14)$$

holds. A consequence of having a nonequilibrium dynamics is the presence of a nonzero, divergence-free probability current in the steady state.

After discussing the signatures of equilibrium and nonequilibrium stochastic dynamics in their steady state, let us look at the times scale necessary to enter the steady state.

1.2 Relaxation time

How much time does it take for the overdamped Langevin dynamics to reach its terminal, equilibrium state? To answer this question, we introduce a bra and ket notation from quantum mechanics. The Fokker Planck equation Eq. (1.4) can be written in the form

$$\partial_t |\rho(t)\rangle = \Omega_0 |\rho(t)\rangle \quad (1.15)$$

The distribution in real space is obtained via the projection

$$\rho(\mathbf{r}, t) = \langle \mathbf{r} | \rho(t) \rangle. \quad (1.16)$$

Since Eq. (1.15) is linear, we can write $|\rho(t)\rangle$ as a linear combination of exponentially decaying terms

$$|\rho(t)\rangle = \sum_{n=0}^{+\infty} \langle L_n | \rho(0) \rangle e^{-\lambda_n t} |R_n(t)\rangle \quad (1.17)$$

The vector $|R_n\rangle$ and $|L_n\rangle$ are the left and right eigenvectors associated to Ω_0 :

$$\begin{aligned} \Omega_0 |R_n\rangle &= \lambda_n |R_n\rangle \\ \langle L_n | \Omega_0 &= \lambda_n \langle L_n |. \end{aligned} \quad (1.18)$$

The spectrum λ_n and its properties can be determined by transforming the operator Ω_0 into a Hermitian operator W_0

$$W_0 \equiv -\rho_B(\mathbf{r})^{-\frac{1}{2}} \Omega_0 \rho_B^{\frac{1}{2}}(\mathbf{r}) = \frac{\mu_0}{T} \left[-T\boldsymbol{\nabla} + \frac{1}{2}(\boldsymbol{\nabla}V) \right] \cdot \left[T\boldsymbol{\nabla} + \frac{1}{2}(\boldsymbol{\nabla}V) \right]. \quad (1.19)$$

and rotating the vectors $|R_n\rangle$ to a new basis: $|\Psi_n\rangle = \rho_B^{-\frac{1}{2}}|R_n\rangle$. The eigenvalue problem given in Eq. (1.18) thus becomes

$$W_0 |\Psi_n\rangle = \lambda_n |\Psi_n\rangle \quad (1.20)$$

Since W_0 is Hermitian, its spectrum $\{\lambda_n\}$ is real. Moreover, one can write $W_0 = \mathbf{w} \cdot \mathbf{w}^\dagger$, with $\mathbf{w} \equiv \sqrt{\frac{\mu_0}{T}}[T\boldsymbol{\nabla} + \frac{1}{2}(\boldsymbol{\nabla}V)]$, and thus its spectrum is positive-definite, $\lambda_n \geq 0$. If the potential V is confining enough and it has no basin of attraction enclosed by infinitely high energy barriers, the stationary solution is unique, and is thus given by the Boltzmann distribution, $|R_0\rangle = |\rho_B\rangle$, with $\lambda_0 = 0$. Upon arranging the eigenvalues according to their increasing value, $0 < \lambda_1 \leq \lambda_2 \leq \lambda_3 \dots$, we can identify λ_1^{-1} as the slowest timescale over which the target Boltzmann distribution is approached. This timescale is the relaxation time τ_R

$$\tau_R \equiv \frac{1}{\lambda_1}. \quad (1.21)$$

There are situations where the relaxation time of the system can become so large that a satisfying convergence to the equilibrium distribution becomes unattainable in practice. This is the case where there are energy barriers with a height much larger than the strength of thermal fluctuations. For example, consider a one dimensional particle evolving under overdamped Langevin dynamics in the double well potential

$$V_{dw}(x) \equiv \frac{1}{4}x^4 - \frac{1}{2}x^2 \quad (1.22)$$

This potential has two symmetric minima located at $x_m^\pm = \pm x_m$ and a maximum at $x_M = 0$. The two minima are separated by an energy barrier of height $\Delta \equiv V(x_M) - V(x_m^\pm)$. If the particle is in one of the two minima, the average time required to cross the energy barrier is the Kramers' time τ_K [87, 164]

$$\tau_K = \frac{2\pi}{\mu_0 \sqrt{|V''(x_m^+)V''(x_M)|}} e^{\beta\Delta}. \quad (1.23)$$

This time contains a prefactor that depends on the stiffness of the potential at the bottom and at the top of the well, and an Arrhenius weight $e^{\beta\Delta}$ which grows exponentially in the ratio $\Delta V/T$. At low temperatures, very long times are needed to witness a barrier crossing event, which is a necessary condition to attain equilibration. For some systems with an extensive number of degrees of freedom, as amorphous materials and spin glasses, sampling the Boltzmann distribution becomes even harder, due to the presence of many minima and saddle points separated by high energy barriers.

It is thus clear that, even if in principle the equilibrium overdamped Langevin dynamics given in Eq. (1.2) is granted to converge to the Boltzmann distribution in

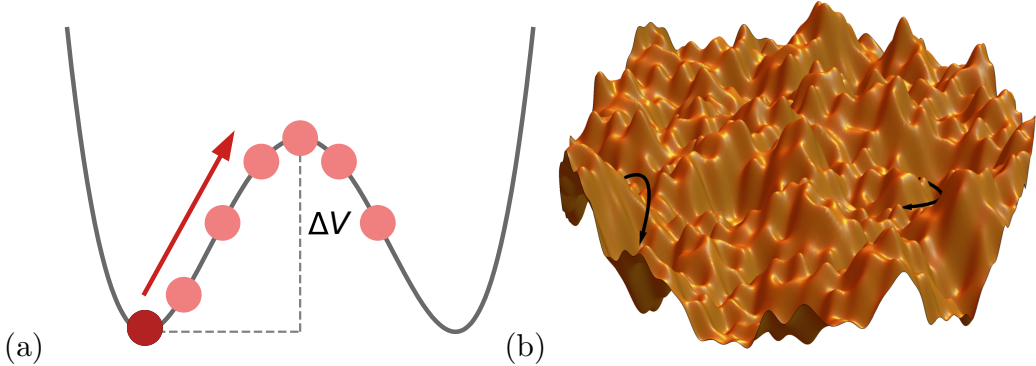


Figure 1.1: (a) Illustration of the barrier crossing problem in one dimensions. (b) High dimensional disordered systems have a complex landscape with a large number of minima and saddle point hindering the motion.

systems with a large but finite number of degrees of freedom, in practice this procedure may be numerically unfeasible, as long simulation times are needed before the quality of the sampling becomes satisfactory. This happens in regimes where interactions are much stronger than thermal fluctuations, for example at low temperature or high density, which are precisely the regimes to be probed in order to better understand the physics of disordered systems.

How to cope with the increasing sluggishness characterized above is a research field of its own. The central idea is to resort to alternative dynamical evolution rules, which might be unphysical while still granting the convergence to the target Boltzmann distribution. How to design these alternative dynamical evolution rules is a subtle art [17], which usually demands some knowledge of the system for which the dynamics is tailored. For the purposes of this thesis, we can classify these dynamics into two big families. In one family the overdamped Langevin dynamics is changed, but the detailed balance property given by Eq. (1.9) is preserved. In Appendix A, we address a dynamics belonging to this family, obtained by a spatial modulation of the mobility field. In another family, initially developed in the field of applied mathematics, the possibility that renouncing to detailed balance can be rewarded with faster relaxation is exploited. In this thesis, we will be interested in this second family of processes, which we will now look into more closely.

1.3 Nonequilibrium to the rescue

In this Section, we look at out-of-equilibrium dynamics, i.e. dynamics that violate the detailed balance equation given by Eq. (1.9), while preserving the Boltzmann distribution in the steady state.

1.3.1 Transverse forces

We start by perturbing the overdamped Langevin dynamics with a generic force field $\mathbf{f}(\mathbf{r})$, constrained to have a finite squared average over the Boltzmann distribution, $\langle |\mathbf{f}|^2 \rangle_B = 1$, with $\langle \dots \rangle_B \equiv \int d\mathbf{r} \dots \rho_B(\mathbf{r})$. Using this normalization, we can control the strength of the additional drift with a single parameter γ . The resulting overdamped Langevin equation is

$$\dot{\mathbf{r}} = -\mu_0 \nabla V + \mu_0 \gamma \mathbf{f}(\mathbf{r}) + \sqrt{2\mu_0 T} \boldsymbol{\xi}(t). \quad (1.24)$$

We now impose that the steady-state of this stochastic process to be the Boltzmann distribution ρ_B . This yields the condition

$$-\beta \mathbf{f} \cdot \nabla V + \nabla \cdot \mathbf{f} = 0, \quad (1.25)$$

which is obviously satisfied if we take \mathbf{f} to be both solenoidal and orthogonal to the gradient of the potential:

$$\begin{aligned} \nabla \cdot \mathbf{f} &= 0 \\ \mathbf{f} \cdot \nabla V &= 0 \end{aligned} \quad (1.26)$$

at every point \mathbf{r} . The resulting dynamics is now out of equilibrium, as can be seen by computing the entropy production rate

$$\sigma = \beta \langle \gamma^2 \mathbf{f}^2 \rangle_B > 0 \quad (1.27)$$

The overdamped Langevin dynamics described by Eqs. (1.24, 1.25) is an out of equilibrium process, but it admits the Boltzmann form as its nonequilibrium steady state distribution. At the level of the continuity equation for $\rho(\mathbf{r}, t)$, this means that in the steady state a nonzero, divergence-free current appears,

$$\mathbf{j}_{ss} = \gamma \mu_0 \mathbf{f} \rho_B. \quad (1.28)$$

It has been proven that the dynamics given by Eqs. (1.24, 1.25) has a relaxation time smaller or equal than the corresponding equilibrium relaxation time, obtained for $\gamma = 0$. A mathematical proof was given in [135, 134] and in [136] for the case of discrete Markov processes. The derivation of theorem in the discrete case is given in Appendix. For small γ and continuous dynamics, we propose here a simple physicist's argument [112] to account for the increase in the relaxation rate towards the steady state of the Fokker-Planck operator. We first rotate the Fokker-Planck operator associated to Eq. (1.24), as we did in Sec. 1.2, thus obtaining

$$W_\gamma \equiv -\rho_B^{-\frac{1}{2}} \Omega_\gamma \rho_B^{\frac{1}{2}} = W_0 + \gamma \delta W \quad (1.29)$$

where W_0 is the Hermitian Fokker-Planck operator in the absence of the coupling parameter γ , given by Eq. (1.19), and

$$\delta W \equiv -\mu_0 \mathbf{f} \cdot \nabla. \quad (1.30)$$

Due to the solenoidal nature of \mathbf{f} , δW is a anti-Hermitian operator, $\delta W^\dagger = \mu_0(\nabla \cdot \mathbf{f}) + \mu_0 \mathbf{f} \cdot \nabla = -\delta W$ containing the out-of-equilibrium drive. We denote by $|\Psi_n\rangle$ the eigenstates of the unperturbed Hermitian operator W_0 , and by λ_n the associated unperturbed eigenvalue. We are interested in the change $\delta\lambda$ to the spectral gap $\Delta\lambda = \lambda_1 - \lambda_0$ of the operator W between the ground state $|\Psi_0\rangle$ and the first excited state $|\Psi_1\rangle$. We first observe that the ground state and its (zero) energy are left unchanged by the perturbation. Therefore, to second order in perturbation theory, we have

$$\begin{aligned}\Delta\lambda &= -\gamma \langle \Psi_1 | \delta W | \Psi_1 \rangle \\ &\quad + \gamma^2 \sum_{n>1} \frac{|\langle \Psi_1 | \delta W | \Psi_n \rangle|^2}{\lambda_1 - \lambda_n}\end{aligned}\tag{1.31}$$

Due to the skew-Hermiticity of the perturbation the first term in Eq. (1.31) is imaginary. This is a signature of oscillations produced by the out-of-equilibrium currents, which we will show up later again in the thesis. The second term is real and positive. The eigenvalues of W are thus shifted in the opposite direction to what would occur in the case of a Hermitian perturbation. Only the real part of the spectral gap is relevant in the computation of the relaxation times, and since it is increased by the perturbation, the relaxation time toward the steady state distribution is reduced.

How can the solenoidal drift \mathbf{f} be implemented? A practical, and minimal choice for numerical implementation consists in taking $\mathbf{f} = \mathbf{A} \nabla V(\mathbf{r})$, with \mathbf{A} an antisymmetric matrix, $\mathbf{A}^T = -\mathbf{A}$. In order to have a control on the amplitude of $\langle \mathbf{A} \nabla V \rangle_B$, we impose the Frobenius norm of the matrix $\|\mathbf{A}\|_F^2 \equiv \sum_{i,j} A_{ij}^2$ to be equal to the space dimension d . The resulting dynamics with transverse forces reads

$$\dot{\mathbf{r}} = -\mu_0(\mathbf{1} + \gamma \mathbf{A}) \nabla V + \sqrt{2\mu_0 T} \boldsymbol{\xi}(t),\tag{1.32}$$

the theorem mentioned above ensures that the dynamics with transverse forces has a shorter relaxation time compared to its equilibrium counterpart given in, Eq (1.2). However, the theorem does not quantify the extent of the acceleration, nor its dependence on the relevant parameter of the problems, such as the temperature or the details of the potential landscape. Another question is whether, and for which parameters, the speedup provided by transverse forces is equivalent to a renormalization of the mobility, $\mu_0 \rightarrow \mu'_0$, a somewhat trivial way of accelerating the dynamics. For disordered and glassy systems, these question are unanswered, and will be addressed in this thesis.

Before exploring the performance of transverse forces, we illustrate an alternative way by which the dynamics can be driven out of equilibrium while preserving the Boltzmann distribution. This second method is known as *lifting*, and is presented with a style largely inspired from the physics of active particles. We also sketch a connection between a lifted dynamics and transverse forces, that gives us hope that the results obtained with transverse forces in glassy systems might be generalizable to the broader class of irreversible dynamics that sample the Boltzmann distribution.

1.3.2 Lifted Markov processes

Another way by which the dynamics of the system can be driven out of equilibrium is called *lifting*. It is a procedure that was born in the field of applied mathematics [63, 81], and it consists, broadly speaking, in supplementing the system under consideration with an additional set of degrees of freedom, called *lifted* variables—see Appendix C2.1 for a mathematical definition of lifted Markov chain—. The lifted degrees of freedom interact with the original ones, driving the system out of equilibrium. The dynamics is chosen in such a way that the steady state distribution, once marginalized over the lifted degrees of freedom, is the Boltzmann distribution for the original set of variables. Within the lifting procedure, the aim is to transform the diffusive motion typical of equilibrium process into a ballistic one. A mathematical justification for the use of lifted Markov chains is given in Appendix C, where a bound for the speed of reversible and lifted Markov chains is discussed.

In statistical mechanics, there are at least two kinds of dynamics that get very close to the idea of lifting. The first one is the underdamped Langevin dynamics, which obtained restoring the mass m and the momentum \mathbf{p} in the overdamped Langevin equation given by Eq. (1.2):

$$\begin{aligned}\dot{\mathbf{r}} &= \frac{\dot{\mathbf{p}}}{m} \\ \dot{\mathbf{p}} &= -\frac{\zeta}{m}\mathbf{p} - \nabla V + \sqrt{2T\zeta}\boldsymbol{\xi}(t).\end{aligned}\tag{1.33}$$

Here $\zeta \equiv \mu_0^{-1}$ is the friction coefficient. The overdamped Langevin result is restored by taking the limit $m \rightarrow 0$. Here, the momentum \mathbf{p} plays a role analogous to the lifting degrees of freedom. The equilibrium distribution associated to this problem is

$$\rho_B(\mathbf{r}, \mathbf{p}) = \frac{1}{Z} e^{-\beta V(\mathbf{r}) - \beta \frac{\mathbf{p}^2}{2m}}\tag{1.34}$$

and integrating out the momentum \mathbf{p} restores the Boltzmann distribution given in Eq. (1.1). In the equilibrium case, alternative dynamics can be obtained by considering stochastic process of higher order, that converge faster to the steady state, at least in convex problems [200]. Interestingly, an adaptation of this kind of dynamics to Monte Carlo schemes, the Hamiltonian Monte Carlo method [84], provided the original motivation to the introduction of lifted dynamics in the seminal work of Diaconis [81].

There is another family of dynamics of interest in statistical mechanics that present interesting resemblances with the lifted ones. It is the ensemble of active, self-propelled particles. This broad term refers to microscopic constituents that can harvest energy from some internal, and usually hidden, degree of freedom or from the environment and transform it into directed motion. A formulation for lifted dynamics in terms of active particles is the following: consider the overdamped Langevin dynamics given in Eq. (1.2), and supplement it with a lifted set of degrees of freedom \mathbf{v} . A lifted, overdamped Langevin dynamics is then

$$\dot{\mathbf{r}} = -\mu_0 \nabla V(\mathbf{r}) + \mathbf{v} + \sqrt{2\mu_0 T} \boldsymbol{\xi}(t)\tag{1.35}$$

The lifted degrees of freedom act in the form of a self propulsion. Up to now, this equation is a generic model for an active particle. The active particles studied in physics are out of equilibrium systems where the steady state distribution for the position \mathbf{r} and the self-propulsion \mathbf{v} , $\rho_{ss}(\mathbf{r}, \mathbf{v})$ that is usually not of the Boltzmann form in the steady state. However, we can try to impose on the dynamics of \mathbf{v} to be such that

$$\int d\mathbf{v} \rho_{ss}(\mathbf{r}, \mathbf{v}) = \rho_B(\mathbf{r}). \quad (1.36)$$

When this condition is realized, we have what we call a *lifted* active particle.

How should the dynamics of the self-propulsion \mathbf{v} be defined? There is no unique way by which this can be done. In the next section, we will present some examples of lifted dynamics inspired from the world of active particles. The goal is twofold: we want to give the reader a taste of the variety of choices that can be made, and provide a connection to the transverse force dynamics described earlier in this Section.

Lifted run-and-tumble

In lifted run-and-tumble particles (lRTP) the self propulsion \mathbf{v} has a constant magnitude v_0 , $\mathbf{v} = v_0 \mathbf{u}$. The direction of the self-propulsion changes from a given direction \mathbf{u} to a new one \mathbf{u}' on the unit d -dimensional sphere according to the Poisson rate

$$\Gamma(\mathbf{u} \rightarrow \mathbf{u}') = \beta v_0 \nabla V \cdot (\mathbf{u} - \mathbf{u}') \theta(\nabla V \cdot (\mathbf{u} - \mathbf{u}')) \quad (1.37)$$

with $\theta(x)$ is the Heaviside function: $\theta(x) = 0$ if $x < 0$, and 1 otherwise. If the tumbling rate was uniform, we would recover the equation of motion of a run and tumble particle in an external potential. Physically, the choice of tumbling rate given by Eq. (1.37) means that a ℓ -RTP changes its direction of self propulsion more frequently when climbing against the energy gradient, while it changes mildly when the particle is descending the potential landscape V . The steady state distribution for a ℓ -RTP is

$$\rho_{ss}(\mathbf{r}, \mathbf{u}) = \frac{1}{\Omega_d} \rho_B(\mathbf{r}). \quad (1.38)$$

with $\Omega_d = \frac{(2\pi)^{d/2}}{\Gamma(d/2)}$ the area of a unit sphere in d dimensions.

Lifted active Brownian particles

In this case, the modulus of the self propulsion is fixed, $\mathbf{v} = v_0 \mathbf{u}$, but the direction of the self propulsion velocity diffuses on the unit sphere. For a lifted active Brownian particle (ℓ ABP), the equation of motion for the self propulsion direction in d dimensions is

$$\dot{\mathbf{u}} = \frac{\beta v_0}{d-1} [(\nabla V \cdot \mathbf{u}) \mathbf{u} - \nabla V] + \sqrt{2D_r} [(\mathbf{u} \cdot \boldsymbol{\eta}(t)) \mathbf{u} - \boldsymbol{\eta}(t)] \quad (1.39)$$

with $\boldsymbol{\eta}$ a Gaussian white noise with unit correlation $\langle \boldsymbol{\eta}(t) \otimes \boldsymbol{\eta}(t') \rangle = \mathbf{1} \delta(t - t')$, and D_r is a rotational diffusivity. Without the first term in the square brackets on the right

hand side, Eq. (1.39) reduces to free Brownian motion for \mathbf{u} on the unit sphere, which is how the self propulsion speed evolves for active Brownian particles. When the term inside the square brackets is taken into account, the self propulsion tends to align to a direction opposite to the energy gradient. The steady state distribution of the ℓ ABP is

$$\rho_{ss}(\mathbf{r}, \mathbf{u}) = \frac{1}{\Omega_d} \rho_B(\mathbf{r}) \quad (1.40)$$

as for the ℓ -RTP. It is interesting to look at how Eq. (1.39) simplifies in the case $d = 2$. Here, the direction of \mathbf{u} is completely identified by the angle θ that it makes with the x axis. The dynamics for θ is

$$\dot{\theta} = \beta v_0 \mathbf{A} \mathbf{u} \cdot \nabla V + \sqrt{2D_r} \eta(t). \quad (1.41)$$

with $\mathbf{A} = \begin{bmatrix} 0 & -1 \\ 1 & 0 \end{bmatrix}$ an antisymmetric matrix, so that $\mathbf{A}\mathbf{u}$ is orthogonal to \mathbf{u} .

Lifted active Ornstein-Uhlenbeck particle

For a lifted active Ornstein-Uhlenbeck particle (ℓ AOUP), the modulus of the self propulsion fluctuates. The equations of motion read

$$\begin{aligned} \dot{\mathbf{r}} &= -\mu_0 \partial_{\mathbf{r}} V + v_0 \mathbf{u} + \sqrt{2T\mu_0} \boldsymbol{\xi}(t) \\ \dot{\mathbf{u}} &= -\mathbf{u} - \beta v_0 \partial_{\mathbf{r}} V + \sqrt{2} \boldsymbol{\chi}(t). \end{aligned} \quad (1.42)$$

Compared to an AOUP, the self-propulsion speed is driven by an the gradient of the energy V . The steady state distribution reads

$$\rho_{ss}(\mathbf{r}, \mathbf{v}) = (2\pi)^{-\frac{d}{2}} e^{-\frac{\mathbf{v}^2}{2}} \rho_B(\mathbf{r}). \quad (1.43)$$

To establish an explicit connection with transverse forces, we consider the case of a ℓ AOUP with temperature-dependent mobility, $\mu = T^{-1}$. If we introduce the extended variable $\mathbf{x} = (\mathbf{r}, \mathbf{v})^T$ and the extended potential $U(\mathbf{x}) = \beta V(\mathbf{r}) + \frac{\mathbf{v}^2}{2}$ we obtain from Eq.(1.42)

$$\dot{\mathbf{x}} = -(\mathbf{1}_{2d} + \gamma \mathbf{A}) \partial_{\mathbf{x}} U + \sqrt{2} \boldsymbol{\chi}(t) \quad (1.44)$$

with $\mathbf{A} = \begin{bmatrix} \mathbf{0}_d & -\mathbf{1}_d \\ \mathbf{1}_d & \mathbf{0}_d \end{bmatrix}$ a $2d \times 2d$ skew-symmetric matrix, $\boldsymbol{\chi}$ a Gaussian white noise with correlations $\langle \boldsymbol{\chi}(t) \otimes \boldsymbol{\chi}(t') \rangle = \delta(t - t') \mathbf{1}_{2d}$ and $\gamma \equiv v_0$. Upon considering the extended space of \mathbf{x} and rescaling the mobility of the system, we have been able to bring forth the presence of transverse forces in a lifted dynamics.

1.4 Summary and outlook

In this Chapter we saw that

- The local, equilibrium, overdamped Langevin dynamics

$$\dot{\mathbf{r}} = -\mu_0 \nabla V(\mathbf{r}) + \sqrt{2\mu_0 T} \xi(t) \quad (1.45)$$

converges to the Boltzmann distribution $\rho_B \propto e^{-\beta V(\mathbf{r})}$ over a timescale given by the relaxation time τ_R .

- τ_R can become extremely large, for instance in the presence of energy barriers separating two metastable states.
- It is possible to design alternative dynamics that are out of equilibrium, but that preserve the Boltzmann distribution in the steady state, $\rho_{ss}(\mathbf{r}) = \rho_B(\mathbf{r})$. For a class of these dynamics a theorem ensures that τ_R is reduced compared to their equilibrium counterpart.
- A minimal implementation of this out of equilibrium drive is obtained by adding forces transverse to the energy gradient:

$$\dot{\mathbf{r}} = -\mu_0(\mathbf{1} + \gamma \mathbf{A}) \nabla V(\mathbf{r}) + \sqrt{2\mu_0 T} \xi(t) \quad (1.46)$$

with $\mathbf{A}^T = -\mathbf{A}$, and γ a real number encoding the strength of the nonequilibrium drive.

There are plenty of ways by which a dynamics can be driven out of equilibrium while preserving the Boltzmann distribution. As our goal is to quantify the extent of the sampling speedup in glassy system, we need a candidate dynamics to implement and study. Transverse forces appear to be a good candidate, as they are ensured to provide a reduction of the relaxation time, and their structure represents a minimal implementation of an irreversible driving. Moreover, the link we made with a lifting model at the end of this chapter gives us hope that some properties of transverse forces might pertain to other dynamics as well, such as the ones belonging to the *lifting* family. In the next Chapter we build an intuition on how transverse forces operate using some prototypical external potentials.

CHAPTER

2

INSIGHTS FOR TRANSVERSE FORCES: A PARTICLE IN AN EXTERNAL POTENTIAL

2.1	The dynamics	20
2.2	Escape rate	20
2.3	Harmonic well	21
2.3.1	Odd transport in the harmonic well	23
2.4	Barrier crossing	24
2.4.1	Heuristic argument	24
2.4.2	Instanton trajectory: no change in the exponential factor	25
2.4.3	Full expression of τ	27
2.5	Fluctuation-dissipation relations	28
2.6	Summary and Outlook	30

In this Chapter we build an understanding of how transverse forces operate, by looking at different examples of a particle in an external potential. Transverse forces are found to increase a typical microscopic evolution frequency, the escape rate. Then we look at the cases of a particle in a harmonic well and at the barrier crossing problem, where we quantify the sampling speedup and discuss how the trajectories are modified in the presence of transverse forces. Interestingly, the result on the speedup are different from the ones that one would have guessed from the naive analysis of the escape rate. We conclude by discussing how the fluctuation-dissipation theorem is violated by transverse forces.

2.1 The dynamics

In this Section we study the overdamped Langevin equation of motion with transverse forces:

$$\dot{\mathbf{r}} = -(\mathbf{1} + \gamma \mathbf{A}) \nabla V(\mathbf{r}) + \sqrt{2T} \boldsymbol{\xi}(t) \quad (2.1)$$

with \mathbf{r} the position of the particle in d dimensions, $V(\mathbf{r})$ an external potential and T the temperature. The noise is white and Gaussian, $\langle \boldsymbol{\xi}(t) \otimes \boldsymbol{\xi}(t') \rangle = \mathbf{1}\delta(t - t')$. The matrix \mathbf{A} is antisymmetric, and creates the transverse force. In Chapter 1, we saw that this dynamics is out of equilibrium and admits the Boltzmann form $\rho_B \propto e^{-\beta V}$ as its steady state distribution.

We start our discussion by looking at a microscopic timescale characterizing the evolution of the system.

2.2 Escape rate

The escape rate [222, 103, 181] is the typical rate at which a particle moves away from a given configuration to one in its neighbourhood. To compute it, we resort to the Onsager-Machlup path integral formalism. From Eq. (2.1), the probability $P(\mathbf{r}_i + \dot{\mathbf{r}}_i dt | \mathbf{r}_i, 0)$ of observing a transition from an initial position \mathbf{r}_i to the position $\mathbf{r}_i + \dot{\mathbf{r}}_i dt$ in the infinitesimal time interval dt is

$$P(\mathbf{r}_i + \dot{\mathbf{r}}_i dt | \mathbf{r}_i, 0) \propto \exp \left\{ -dt \left[\frac{1}{4T} (\dot{\mathbf{r}} + (\mathbf{1} + \gamma \mathbf{A}) \nabla V)^2 - \frac{1}{2} \nabla^2 V \right] \right\} \quad (2.2)$$

If we set $\dot{\mathbf{r}} = 0$ in Eq. (6.48) we obtain the probability that the particle remains in its initial configuration during the infinitesimal interval dt , i.e.

$$P(\mathbf{r}_i, dt | \mathbf{r}_i, 0) \propto \exp \left\{ -dt \left[\frac{1}{4T} ((\mathbf{1} + \gamma \mathbf{A}) \nabla V)^2 - \frac{1}{2} \nabla^2 V \right] \right\}. \quad (2.3)$$

This allows us to interpret, up to an additive constant stemming from the discretization of a time interval into infinitesimal increments, the quantity $\tau_0^{-1} \equiv \frac{1}{T} \left[\frac{1}{4} ((\mathbf{1} + \gamma \mathbf{A}) \nabla V)^2 - \frac{T}{2} \nabla^2 V \right]$ as the rate at which the system escapes from its current configuration. The two terms in τ_0^{-1} have the following physical meaning: the first one expresses the fact that nonzero forces make the system move away from a given configuration. The second term tells about the influence of the concavity of the potential on the escape process.

We can average the escape rate over the steady-state Boltzmann distribution ρ_B . Using the fact that $\mathbf{A} = -\mathbf{A}^T$ and after an integration by parts we get

$$\langle \tau_0^{-1} \rangle_B = \frac{1}{4T} \left[\langle (\nabla V)^2 \rangle_B + \gamma^2 \langle (\mathbf{A} \nabla V)^2 \rangle_B \right]. \quad (2.4)$$

For $\gamma = 0$ we recover the equilibrium result $\tau_{0,\text{eq}}^{-1} = \frac{1}{4T} \langle (\nabla V)^2 \rangle_B$. If the potential is spherically symmetric, $\langle (\mathbf{A} \nabla V)^2 \rangle_B = A_{ij} A_{ik} \langle \partial_j V \partial_k V \rangle_B = \frac{1}{d} \|\mathbf{A}\|_F^2 \langle (\nabla V)^2 \rangle_B$, where $\|\mathbf{A}\|_F^2 \equiv \sum_{i,j} A_{ij}^2$ is the Frobenius norm of \mathbf{A} . We therefore conclude that

$$\tau_0^{-1} = \left(1 + \frac{1}{d} \gamma^2 \|\mathbf{A}\|_F^2 \right) \tau_{0,\text{eq}}^{-1}. \quad (2.5)$$

This result shows that transverse forces increase, through a rescaling, the escape rate of the system with respect to the equilibrium case. As a side remark, which will be useful when studying the transverse forces in infinite dimensions, for τ_0 to have a well-defined $d \gg 1$ limit we shall need to work with $\|A\|_{\text{F}}^2 \sim d$.

The analysis of the escape rate suggests that, if transverse forces act always as a rescaling of time, their speedup with respect to equilibrium dynamics should scale as γ^2 . In the next two Sections, we specialize to the case of a harmonic and of a double well potential respectively, and we compute the relaxation time. We will see that this intuition about the scaling of the sampling speedup with γ loses its validity for large γ .

2.3 Harmonic well

We now consider a two-dimensional harmonic potential $V(\mathbf{r}) = \frac{1}{2}\mathbf{r} \cdot \mathbf{K}\mathbf{r}$, with $\mathbf{K} \equiv \begin{bmatrix} k_1 & 0 \\ 0 & k_2 \end{bmatrix}$ a matrix containing the stiffness coefficients of the well. We set $k_1 \geq k_2$. Eq. (2.1) reads then

$$\dot{\mathbf{r}} = -(\mathbf{1} + \gamma \mathbf{A})\mathbf{K}\mathbf{r} + \sqrt{2T}\boldsymbol{\xi}. \quad (2.6)$$

Transverse forces are implemented via the antisymmetric matrix \mathbf{A} ,

$$\mathbf{A} \equiv \begin{bmatrix} 0 & -1 \\ 1 & 0 \end{bmatrix} \quad (2.7)$$

We first look at the relaxation time of the system, by mapping the dynamics to a quantum mechanical problem. The Fokker-Planck operator Ω_γ reads

$$\Omega_\gamma = \nabla \cdot [(\mathbf{1} + \gamma \mathbf{A})\mathbf{K}\mathbf{r} + T\nabla]. \quad (2.8)$$

It governs the evolution of the probability distribution $\rho(\mathbf{r}, t)$, $\partial_t \rho(\mathbf{r}, t) = \Omega_\gamma \rho(\mathbf{r}, t)$. The mapping to a quantum mechanical problem is performed by considering the operator

$$W_\gamma \equiv -\rho_B^{-1/2} \Omega \rho_B^{1/2} = W_0 + \gamma \mathbf{A} \mathbf{K} \mathbf{r} \cdot \nabla \quad (2.9)$$

where $W_0 = T \left(-\nabla + \frac{\beta}{2} \mathbf{K} \mathbf{r} \right) \cdot \left(\nabla + \frac{\beta}{2} \mathbf{K} \mathbf{r} \right)$ is the Hermitian operator usually found for equilibrium dynamics and the second term is a skew-Hermitian operator. Its appearance is a consequence of injecting irreversible currents into the system by means of transverse forces.

To diagonalize W_γ , we introduce a set of creation and annihilation operators

$$\begin{aligned} \mathbf{a} &\equiv \sqrt{T\mathbf{K}^{-1}} \left(\nabla + \beta \mathbf{K} \frac{\mathbf{r}}{2} \right) \\ \mathbf{a}^\dagger &\equiv \sqrt{T\mathbf{K}^{-1}} \left(-\nabla + \beta \mathbf{K} \frac{\mathbf{r}}{2} \right) \end{aligned} \quad (2.10)$$

that satisfy the commutation relations $[a_i, a_j^\dagger] = \delta_{ij}$. The operator W_γ becomes

$$W_\gamma = \mathbf{a}^\dagger \cdot \mathbf{K} \left(\mathbf{1} + \frac{\gamma}{2} \mathbf{A} \right) \cdot \mathbf{a}, \quad (2.11)$$

and it can be rewritten in a diagonal basis,

$$W_\gamma = \mathbf{b}^\dagger \begin{bmatrix} \lambda_+(\gamma) & 0 \\ 0 & \lambda_-(\gamma) \end{bmatrix} \mathbf{b}, \quad (2.12)$$

the eigenvalues $\lambda_\pm(\gamma)$ are

$$\lambda_\pm(\gamma) = \frac{1}{2} \left[k_1 + k_2 \pm \sqrt{(k_1 - k_2)^2 - \gamma^2 k_1 k_2} \right] \quad (2.13)$$

and the operators \mathbf{b} , \mathbf{b}^\dagger are rotated creation and annihilation operators

$$\begin{aligned} \mathbf{b} &= \mathbf{O}\mathbf{a} \\ \mathbf{b}^\dagger &= \mathbf{O}\mathbf{a}^\dagger, \end{aligned} \quad (2.14)$$

with $\mathbf{O} \equiv \mathbf{v}_+ \otimes \mathbf{v}_-$, \mathbf{v}_\pm being the eigenvectors associated to the matrix appearing in Eq. (2.11), with eigenvalues $\lambda_\pm(\gamma)$ respectively. As a consequence of the theory of the quantum-mechanical harmonic oscillator [256], the spectrum of W_γ is discrete and characterized by a two-dimensional vector $\mathbf{n} = (n_+, n_-)^T \in \mathbb{N}^2$:

$$\lambda_{\mathbf{n}} = n_+ \lambda_+(\gamma) + n_- \lambda_-(\gamma). \quad (2.15)$$

The ground state of W_γ , which is mapped to the Boltzmann distribution in the rotated basis, is obtained for $\mathbf{n} = \mathbf{0}$. The eigenvalue with the smallest nonzero real part is $\lambda_-(\gamma)$, and the relaxation time is given by the inverse of the real part of $\lambda_-(\gamma)$. For $\gamma = 0$, we fall back to the equilibrium case and the relaxation time is

$$\tau_R(0) = \frac{1}{k_2}. \quad (2.16)$$

If the harmonic well is isotropic $k_1 = k_2$, then $\lambda_\pm(\gamma) = k_1(1 \pm i|\gamma|)$, and the relaxation time is the same as in equilibrium, $\tau_R(\gamma) = \tau_R(0)$. We thus fall in a marginal case of the theorem stated in Sec. 1.3.1, with transverse forces that operate by generating oscillations of the particle inside the harmonic well, see Fig. 2.1(a), where a $T = 0$ trajectory at $\gamma = 0$ is compared with a $\gamma \neq 0$ one. In the latter case, the particle spirals to the bottom of the well.

In the anisotropic case, $k_1 \neq k_2$, there is room for a true reduction of the relaxation time. For $\gamma \neq 0$ and $\gamma^2 \leq \gamma_c \equiv \frac{(k_1 - k_2)^2}{k_1 k_2}$, $\lambda_\pm(\gamma)$ are real numbers and the relaxation time is

$$\tau_R(\gamma) = \frac{1}{\lambda_-(\gamma)}, \quad (2.17)$$

and $\tau_R(\gamma) < \tau_R(0)$. The relaxation time is a decreasing function of γ for $\gamma \leq \gamma_c$. For $\gamma > \gamma_c$, $\lambda_-(\gamma)$ acquires an imaginary part, and the relaxation time saturates to the value

$$\tau_R(\gamma > \gamma_c) = \frac{2}{k_1 + k_2} < \tau_R(0). \quad (2.18)$$

This is the point where oscillations start to appear, and transverse forces cease to enhance the sampling efficiency of the system. Figure 2.1(b) shows the relaxation time as a function of γ in the case of an anisotropic well.

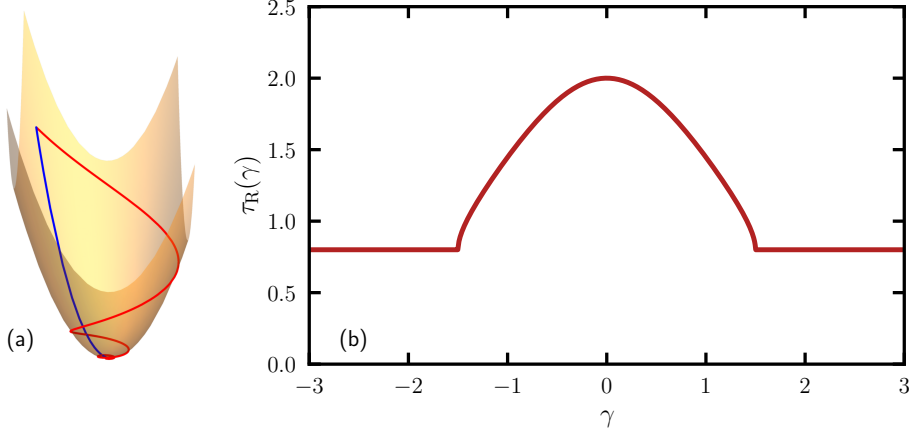


Figure 2.1: (a) Zero temperature trajectories in an isotropic harmonic well with $K_{ij} = \delta_{ij}$. Without transverse forces (blue curve, $\gamma = 0$) and with transverse forces (red curve, $\gamma = 2$). (b) Plot of the relaxation time $\tau_R(\gamma)$ for an anisotropic harmonic well with $k_1 = 2$, $k_2 = 0.5$.

2.3.1 Odd transport in the harmonic well

How do transverse forces modify the trajectories of the system? Owing to their nonequilibrium nature, transverse forces are accompanied by forms of transport that do not appear in an equilibrium situation. Here we address the relevant form of odd transport for the harmonic oscillator, odd diffusion. Other forms will be discussed when we address many body systems. Odd diffusion manifests itself in the form of a nonzero off-diagonal, anti-symmetric part of the diffusion tensor, defined as $\mathbf{D} \equiv \int_0^{+\infty} \langle \dot{\mathbf{r}}(t) \otimes \dot{\mathbf{r}}(0) \rangle$. Physically, this detects the presence of a chiral, swirling motion, and the presence of fluxes perpendicular to concentration gradients arising in the system. At the microscopic level, a Green-Kubo relation, derived in [125] identifies the odd diffusion as the time integral of the anti-symmetric part of the velocity-velocity autocorrelation tensor.

To characterize the swirling motion inside the confining harmonic well potential, we can compute the odd diffusion constant D_\perp , which is

$$D_\perp \equiv -\frac{1}{2} \int_0^{+\infty} \langle \dot{\mathbf{r}}(t) \cdot \mathbf{A} \dot{\mathbf{r}}(0) \rangle \quad (2.19)$$

where $\langle \dots \rangle$ is the average of the initial position over the Boltzmann distribution and over the realization of the noise $\xi(t)$. Note that we conventionally chose the sign of D_\perp so that $D_\perp < 0$ if the system undergoes a counterclockwise swirling motion.

We consider now the case of an isotropic harmonic well, $k_1 = k_2 = k$. Using Eq. (2.6) and the fact the realization of the noise $\xi(t)$ are independent from $\xi(0)$ and $\mathbf{r}(0)$ we get

$$D_\perp = -\frac{1}{2} \int_0^{+\infty} k^2 \langle (\mathbf{1} + \gamma \mathbf{A}) \mathbf{r}(t) \cdot \mathbf{A} (\mathbf{1} + \gamma \mathbf{A}) \mathbf{r}(0) \rangle - \sqrt{2T}k \langle (\mathbf{1} + \gamma \mathbf{A}) \mathbf{r}(t) \cdot \mathbf{A} \xi(0) \rangle. \quad (2.20)$$

Using the solution $\mathbf{r}(t)$ of Eq. (2.6):

$$\mathbf{r}(t) = \mathbf{r}(0)e^{-k(\mathbf{1}+\gamma\mathbf{A})t} + \sqrt{2T} \int_0^t d\tau e^{-k(\mathbf{1}+\gamma\mathbf{A})(t-\tau)} \boldsymbol{\xi}(\tau) \quad (2.21)$$

and the fact that $\langle \mathbf{r}(0) \otimes \mathbf{r}(0) \rangle_B = \mathbf{1} \frac{T}{k}$. Integration over time leads to

$$D_{\perp} = -\frac{T}{1+\gamma^2} \text{Tr} [(\mathbf{1}-\gamma\mathbf{A})(\mathbf{1}-\gamma\mathbf{A})\mathbf{A}(\mathbf{1}+\gamma\mathbf{A})] = -\gamma T. \quad (2.22)$$

This is the expression for the odd diffusivity of the harmonic oscillator under transverse forces. D_{\perp} does not depend on the stiffness k of the harmonic well. This is physically due to the following cancellation effect: the odd diffusivity scales as $F^2\tau_R$, where F^2 is the average squared force acting on the particle and τ_R the relaxation time of the particle. Now, $F^2 \sim k^2 \langle \mathbf{r}^2 \rangle_B \sim k$, while $\tau_k \sim k^{-1}$, see Eq. (2.16). The two factors cancel out, leaving D_{\perp} independent from the well stiffness.

In this Section, we saw how transverse forces affect the relaxation and the trajectories of a particle inside a harmonic well. We now proceed to assess the efficiency of transverse forces for a non convex problem involving the crossing of an energy barrier.

2.4 Barrier crossing

In this Section we quantify by how much transverse forces help to overcome energy barriers. For the purpose of illustration, we resort to the Ichiki-Ohzeki (IO) formulation of transverse forces [208]: two copies of a one dimensional system in an external potential interacting through antisymmetric couplings. The positions of the particles in the two copies are encoded in the vector $\mathbf{r} \equiv [r^{(1)}, r^{(2)}]^T$. The potential is $V(\mathbf{r}) = v(r^{(1)}) + v(r^{(2)})$, with $v(x)$ a non convex potential which has two minima, one of them located at x_m , separated by a energy barrier of height Δ . The energy barrier culminates at a maximum at x_M . The equation of motion in Eq. (2.1) reads

$$\begin{bmatrix} \dot{r}^{(1)} \\ \dot{r}^{(2)} \end{bmatrix} = -(\mathbf{1} + \gamma\mathbf{A}) \begin{bmatrix} v'(r^{(1)}) \\ v'(r^{(2)}) \end{bmatrix} + \sqrt{2T} \begin{bmatrix} \xi^{(1)}(t) \\ \xi^{(2)}(t) \end{bmatrix}. \quad (2.23)$$

with \mathbf{A} given by Eq. (5.10). We are interested in the situation where $T \ll \Delta$, and we will look at the rare event where particle 1 hops over the energy barrier, while particle 2 remains confined within the bottom of the well, the simultaneous crossing of both the particles happening with an exponentially smaller rate in the ratio Δ/T .

2.4.1 Heuristic argument

Before proceeding with a detailed analysis, there is a simple way to understand how a nonzero γ speeds barrier crossing up. If particle 2 is confined at the bottom of the well, its position evolves according to

$$\begin{aligned} \dot{r}^{(2)}(t) &= -v'(r^{(2)}(t)) - \gamma v'(r^{(1)}(t)) + \sqrt{2T}\xi^{(2)}(t) \\ &\simeq -k_m(r^{(2)}(t) - x_m) - \gamma V'(r^{(1)}(t)) + \sqrt{2T}\xi^{(2)}(t) \end{aligned} \quad (2.24)$$

where $k_m \equiv V''(x_m) > 0$ is the stiffness of the well. We can integrate this equation and substitute $r^{(2)}$ into the evolution equation for $r^{(1)}$:

$$\dot{r}^{(1)}(t) = - \int_0^t ds M_R(t-s) v'(r^{(1)}(s)) + \sqrt{2T} \Xi(t) \quad (2.25)$$

where $\Xi(t)$ is now a coloured Gaussian noise with correlations $\langle \Xi(t) \Xi(t') \rangle \equiv \delta(t-t') + \frac{1}{2} \gamma^2 k_m e^{-k_m|t-t'|} \equiv M_C(t-t')$. The mobility kernel $M_R(t) = \delta(t) + \gamma^2 k_m e^{-k_m t} \theta(t)$ and the correlation kernel $M_C(t) = \frac{1}{2} M_R(t) + \frac{1}{2} M_R(-t)$ are related by Kubo's fluctuation theorem for generalized Langevin equations. While the two-dimensional process $(r^{(1)}, r^{(2)})$ is a nonequilibrium one, the effective process $r^{(1)}$, forgetting the information on $r^{(2)}$, is an equilibrium process (at least when $r^{(2)}$ evolves in a quadratic well). In the large k_m limit, $M_R(t) \simeq (1+\gamma^2)\delta(t)$ and the mobility of the particle picks up a γ^2 contribution so that the barrier crossing time is reduced accordingly: $\tau \simeq e^{\beta\Delta}/(1+\gamma^2)$. This limiting case thus matches the escape rate analysis done in Sec. 2.2 within an effective equilibrium dynamics picture.

This heuristic approach suggests that the IO dynamics contributes to changes in the barrier crossing time by rescaling the prefactor of the Arrhenius formula. We now confirm this observation in the general case by looking at the most probable path taken by the system during the barrier crossing process, also known as the instanton trajectory. The process in which particle 1 overcomes the energetic barrier while particle 2 remains confined in the well corresponds, for the composite system, to a trajectory from $\mathbf{r}_m \equiv [x_m, x_m]^T$ to $\mathbf{r}_s \equiv [x_M, x_m]$ and from \mathbf{r}_s to the minimum on the other side of the saddle. We now proceed with a careful analysis of the instanton trajectory.

2.4.2 Instanton trajectory: no change in the exponential factor

The barrier crossing rate τ^{-1} can be expressed within a path-integral formulation,

$$\tau^{-1} = \int \mathcal{D}\hat{\mathbf{r}} \mathcal{D}\mathbf{r} e^{-\frac{1}{T}S[\mathbf{r}, \hat{\mathbf{r}}]} \quad (2.26)$$

where the path-integral runs over paths connecting \mathbf{r}_m to \mathbf{r}_s , and where the Janssen-De Dominicis action functional reads

$$S[\mathbf{r}, \hat{\mathbf{r}}] = \int_{-\infty}^{+\infty} dt [\dot{\mathbf{r}} \cdot \hat{\mathbf{r}} - H(\mathbf{r}, \hat{\mathbf{r}})] \quad (2.27)$$

The response field $\hat{\mathbf{r}}$ expresses the effect of the noise on the dynamics of \mathbf{r} . In the small noise $T \rightarrow 0$ limit, the path that dominates the integral minimizes S , and the resulting saddle-point trajectories follow a Hamiltonian-like dynamics (with respect to H in Eq. (2.27)) in a space of extended variables where the conjugate field $\hat{\mathbf{r}}$ stands for a momentum. The escape time τ then satisfies the logarithmic equivalence

$$\begin{cases} \tau \asymp e^{\frac{\phi}{T}} \\ \phi \equiv \min_{\mathbf{r}(t)|\mathbf{r}(-\infty)=\mathbf{r}_m, \mathbf{r}(+\infty)=\mathbf{r}_s} S[\mathbf{r}, \hat{\mathbf{r}}] \end{cases} \quad (2.28)$$

The explicit expression for $H(\mathbf{r}, \hat{\mathbf{r}})$ is

$$H(\mathbf{r}, \hat{\mathbf{r}}) \equiv \hat{\mathbf{r}}^2 - \hat{\mathbf{r}} \cdot (\mathbb{1} + \gamma \mathbf{A}) \cdot \nabla U(\mathbf{r}) \quad (2.29)$$

The minimum of S for the trajectories of interest is found by looking for the solutions of the Hamiltonian system induced by H along the $H = 0$ energy manifold, so that we have the differential equations

$$\begin{cases} \dot{\mathbf{r}} &= \frac{\partial H}{\partial \dot{\mathbf{r}}} = -(\mathbb{1} + \gamma \mathbf{A}) \cdot \nabla V(\mathbf{r}) + 2\hat{\mathbf{r}} \\ \dot{\hat{\mathbf{r}}} &= -\frac{\partial H}{\partial \mathbf{r}} = (\mathbb{1} + \gamma \mathbf{A}) \cdot \text{Hess } V(\mathbf{r}) \cdot \hat{\mathbf{r}} \end{cases} \quad (2.30)$$

together with the condition $H(\mathbf{r}, \hat{\mathbf{r}}) = 0$. Here $\text{Hess } V(\mathbf{r})_{ab} \equiv v''(r^{(a)})\delta_{ab}$ is the Hessian matrix of V . These coupled differential equations are equivalent to

$$\begin{cases} \dot{\mathbf{r}} &= (\mathbb{1} - \gamma \mathbf{A}) \cdot \nabla V(\mathbf{r}) \\ \dot{\hat{\mathbf{r}}} &= \nabla V(\mathbf{r}) \end{cases} \quad (2.31)$$

which, in principle, can be solved explicitly if a potential V is specified. We solve the instanton trajectory $\dot{\mathbf{r}}$ within perturbation theory up to second order in γ as a functional of the external potential V , assuming the $\gamma = 0$ trajectory is fully known. A linear analysis of the trajectory close to the saddle point \mathbf{r}_s shows that the perturbation expansion must have the form

$$\begin{aligned} r^{(1)} &= r_0^{(1)} + \gamma^2 r_2^{(1)} + O(\gamma^4) \\ r^{(2)} &= r_0^{(2)} + \gamma r_1^{(2)} + O(\gamma^3) \end{aligned} \quad (2.32)$$

with $\dot{r}_0^{(1)} = v'(r_0^{(1)}(t))$ and $r_0^{(2)} = 0$. By taking into account the boundary condition for the perturbation $r(+\infty)_i^{(a)} = r(-\infty)_i^{(a)} = 0$ for $a = 1, 2, i > 0$ we obtain

$$r_1^{(2)} = -e^{k_m t} \int_t^{+\infty} d\tau e^{-k_m \tau} v'(x_0^{(1)}(\tau)) \quad (2.33)$$

$$r_2^{(1)} = k_m e^{G(t)} \left[\int_t^{+\infty} d\tau e^{-G(\tau)} r_1^{(2)}(\tau) + C \right] \quad (2.34)$$

where $G(t) \equiv \int d\tau v''(r_0^{(1)}(\tau))$ and C is a constant determined by matching the asymptotic expression for $r_2^{(1)}(t)$ for $t \rightarrow +\infty$ to the linear expansion at \mathbf{r}_s . We illustrate the role played by γ in deforming the equilibrium trajectory in Fig. 2.2. As done in previous studies of the escape time out of equilibrium [50], we have chosen as an explicit potential v the well-known double well $v(x) \equiv \frac{1}{4}x^4 - \frac{1}{2}x^2$. We see that indeed system 2 finds it optimal to rise in its own energy landscape to favour the crossing of system 1 over the barrier. Interestingly, the action for the instanton trajectory is unchanged with respect to the equilibrium dynamics, namely

$$S[\mathbf{r}, \hat{\mathbf{r}}] = \int_{-\infty}^{+\infty} dt \dot{\mathbf{r}} \cdot \nabla V(\mathbf{r}) = \Delta \quad (2.35)$$

This result is identical to the one obtained with the equilibrium dynamics at $\gamma = 0$, supporting the heuristic analysis of Sec. 2.4.1. While the instanton trajectory is clearly altered, the Arrhenius factor is left unchanged by the IO dynamics. In the next section, we investigate the dependence on γ of the prefactor to the Arrhenius exponential.

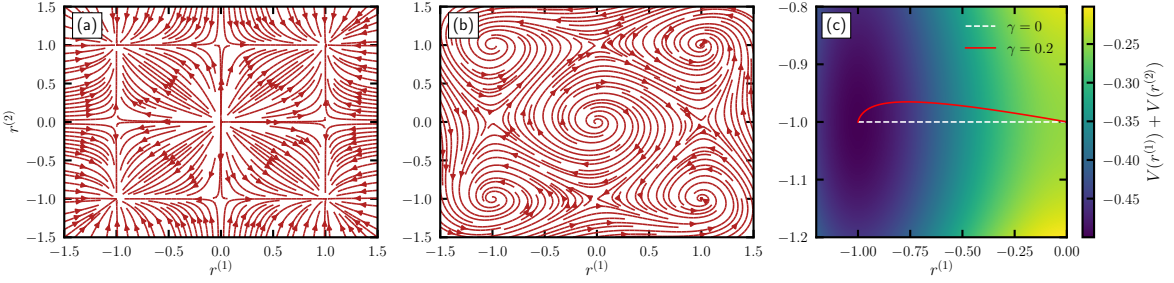


Figure 2.2: (a) Gradient flow of the double well potentials for two noninteracting particles. (b) Force field for two copies of a particle in a double well potential coupled with Ichiki-Ohzeki interactions, $\gamma = 0$. (c) Instanton trajectory from Eq. (2.31) for $\gamma = 0$ and its perturbation expansion up to second order in γ for the double well potential $v(x) = \frac{1}{4}x^4 - \frac{1}{2}x^2$. The instanton starts from the minima located at $(-1, -1)$ and ends at the saddle point located at $(0, -1)$. Adapted from [112]

2.4.3 Full expression of τ

Bouchet and Reygner [48] have derived an Eyring-Kramers formula for nonequilibrium dynamics which do not necessarily sample the Boltzmann distribution. Here we specialize their general result to the IO dynamics, which allows us to arrive at a concrete γ -dependence of the escape time. When applied to the IO dynamics the time τ reads

$$\tau = \frac{2\pi}{|\lambda_+|} \sqrt{\frac{k_M}{k_m}} e^{\frac{\Delta}{T}} \quad (2.36)$$

where $k_M \equiv -V''(x_M) > 0$, $k_m \equiv V''(x_m) > 0$, and λ_+ is the eigenvalue related to the unstable direction of the dynamics linearized around the saddle point \mathbf{r}_s :

$$|\lambda_+| = \frac{1}{2} \left[k_M - k_m + \sqrt{(k_M + k_m)^2 + 4\gamma^2 k_M k_m} \right] \quad (2.37)$$

For $\gamma = 0$ Eq. (2.36) yields the well-known Kramers' time

$$\tau = \frac{2\pi}{\sqrt{k_M k_m}} e^{\frac{\Delta}{T}} \quad (2.38)$$

while for $\gamma \neq 0$ we have $\lambda_+ > k_M$ and the time required for particle 1 to hop over the energetic barrier is reduced.

We realize *a posteriori* that the heuristic approach of Sec. 2.4.1 was physically sound. It can indeed be recovered by letting $k_m \rightarrow +\infty$ in Eq. (2.37), yielding $\lambda_+ \approx k_M(1 + \gamma^2)$. This limiting case is actually the smallest achievable value of τ at given γ , k_M and ΔV , since $\partial_{k_m} \lambda_+$ is always positive.

What happens when transverse forces are very strong? In the limit $\gamma \rightarrow \infty$, the barrier crossing time decreases as $\tau \sim \gamma^{-1}$, in contrast with the scaling suggested by the initial analysis of the escape rate done in Sec 2.2, from which a scaling $\tau \sim \gamma^{-2}$ was derived. Note that the theoretical sampling efficiency of transverse forces must

eventually saturate: this happens because the barrier crossing time can be reduced to 0, while the relaxation time inside an harmonic well saturates to a lower bound, as we saw in Sec. 2.3.

In this Section, we saw that transverse forces speedup the process of barrier crossing via a prefactor in the Kramer's time. We now want to find what happens in the case of a many-body system with several energy barrier? Before answering this question, we investigate how fluctuation dissipation relations are affected by the presence of transverse forces.

2.5 Fluctuation-dissipation relations

In this Section we look at how transverse forces affect fluctuation-dissipation relations. Our starting point is the transverse forces dynamics for a particle in d dimensions under an external potential V and an external force $\mathbf{F}^{\text{ext}}(t)$. With this modification, Eq. (2.1) reads

$$\begin{aligned}\dot{\mathbf{r}} &= -(\mathbf{1} + \gamma \mathbf{A}) \nabla V(\mathbf{r}(t)) + \mathbf{F}^{\text{ext}}(t) + \sqrt{2T} \boldsymbol{\xi}(t) \\ &\equiv \mathbf{F}^\gamma(t) + \mathbf{F}^{\text{ext}} + \sqrt{2T} \boldsymbol{\xi}(t)\end{aligned}\quad (2.39)$$

The main tool we use is a path-integral average over the dynamics. Denoting by $\mathbf{O}(t) = \mathbf{O}(\mathbf{r}(t))$ a generic vector observable that depends on the position of the particle at time t , we introduce two types of averages. The average in the presence of an external force \mathbf{F}^{ext} :

$$\langle \mathbf{O}(t_{\text{obs}}) \rangle_\gamma^{\text{ext}} \equiv \int d\mathbf{r}_0 \int \mathcal{D}\mathbf{r}(t) \mathbf{O}(t) e^{-S_\gamma^{\text{ext}}[\mathbf{r}(t)]} \rho_B(\mathbf{r}_0) \quad (2.40)$$

with S_γ^{ext} the Onsager-Machlup action associated to the transverse force dynamics, perturbed by the external force:

$$S_\gamma^{\text{ext}}[\mathbf{r}(t)] \equiv \frac{1}{4T} \int_0^{t_{\text{obs}}} dt (\dot{\mathbf{r}}(t) - \mathbf{F}^\gamma(t) - \mathbf{F}^{\text{ext}})^2, \quad (2.41)$$

and the average over the unperturbed transverse force dynamics:

$$\langle \mathbf{O}(t_{\text{obs}}) \rangle_\gamma \equiv \int d\mathbf{r}_0 \int \mathcal{D}\mathbf{r}(t) \mathbf{O}(t) e^{-S_\gamma[\mathbf{r}(t)]} \rho_B(\mathbf{r}_0) \quad (2.42)$$

with S_γ the Onsager-Machlup action associated to the transverse force dynamics when $\mathbf{F}^{\text{ext}}(t) = 0$:

$$S_\gamma[\mathbf{r}(t)] \equiv \frac{1}{4T} \int_0^{t_{\text{obs}}} dt (\dot{\mathbf{r}}(t) - \mathbf{F}^\gamma(t))^2, \quad (2.43)$$

Both averages $\langle \dots \rangle_\gamma$ and $\langle \dots \rangle_\gamma^{\text{ext}}$ involve an average over the initial condition at time $t = 0$, which follows the steady-state, Boltzmann distribution and the dynamics up to time t_{obs} , with the boundary condition $\mathbf{r}(t = 0) = \mathbf{r}_0$.

We want to establish a relation between the response function

$$R_{ab}^\gamma(t, t') \equiv \left\langle \frac{\delta O_a(t)}{\delta F_b^{\text{ext}}(t')} \right\rangle_\gamma^{\text{ext}} \Big|_{F^{\text{ext}}=0} \quad (2.44)$$

and the correlation function

$$C_{ab}^\gamma(t, t') \equiv \langle O_a(t) r_b(t') \rangle_\gamma. \quad (2.45)$$

Before doing this, however, it is useful to consider how the action behaves under time reversal. For a given path $\mathbf{r}(t)$ starting at $t = 0$ and ending at $t = t_{\text{obs}}$, define $\mathbf{r}^R(s) \equiv \mathbf{r}(t_{\text{obs}} - s)$ as its time-reversed counterpart. Then we have

$$S_\gamma[\mathbf{r}(t)] - S_{-\gamma}[\mathbf{r}^R(t)] = \frac{1}{T} [V(\mathbf{r}(t_{\text{obs}})) - V(\mathbf{r}(0))] \quad (2.46)$$

For $\gamma = 0$, we recover detailed balance. For $\gamma \neq 0$, the above equation implies that we can reverse time for the observable inside the average $\langle \dots \rangle_\gamma$, at the cost of changing the sign of γ :

$$\langle O_a(\mathbf{r}(t)) \rangle_\gamma = \langle O_a(\mathbf{r}^R(t)) \rangle_{-\gamma} \quad (2.47)$$

. Eq. (2.46) is known in the literature of lifted Markov Chains as *skew detailed balance* [255].

We can now start compute the response function. Applying the functional derivative to the Onsager-Machlup action we get

$$R_{ab}(t_{\text{obs}}, t') = \frac{1}{2T} [\langle O_a(t_{\text{obs}}) \dot{r}_b(t') \rangle_\gamma - \langle O_a(t_{\text{obs}}) F_b^\gamma(t') \rangle_\gamma] \quad (2.48)$$

On the other hand, using Eq. (2.46), and assuming that $\mathbf{O}(t)$ is even under time reversal, we have

$$R_{ab}(t', t_{\text{obs}}) = -\frac{1}{2T} [\langle O_a(t_{\text{obs}}) \dot{r}_b(t') \rangle_{-\gamma} - \langle O_a(t_{\text{obs}}) F_b^\gamma(t') \rangle_{-\gamma}] \quad (2.49)$$

If we choose $t_{\text{obs}} \geq t'$, then $R_{ab}(t', t_{\text{obs}}) = 0$ by causality, and we have

$$\begin{aligned} R_{ab}(t_{\text{obs}}, t') - R_{ab}(t', t_{\text{obs}}) &= R_{ab}(t_{\text{obs}}, t') = \frac{1}{2T} [\langle O_a(t_{\text{obs}}) \dot{r}_b(t') \rangle_\gamma + \langle O_a(t_{\text{obs}}) \dot{r}_b(t') \rangle_{-\gamma}] \\ &\quad - \frac{1}{2T} [\langle O_a(t_{\text{obs}}) F_b^\gamma(t') \rangle_\gamma - \langle O_a(t_{\text{obs}}) F_b^\gamma(t') \rangle_{-\gamma}]. \end{aligned} \quad (2.50)$$

Using time translation invariance and the matrix notation, Eq. (2.50) becomes

$$\mathbf{R}_\gamma(t) = -\frac{1}{2T} \partial_t [\mathbf{C}_\gamma(t) + \mathbf{C}_{-\gamma}(t)] - \frac{1}{2T} [\mathbf{D}_\gamma(t) - \mathbf{D}_{-\gamma}(t)] (\mathbf{1} - \gamma \mathbf{A}) \quad (2.51)$$

with $t \equiv t_{\text{obs}} - t'$, and we have introduced the matrix $\mathbf{D}_\gamma(t) \equiv \langle \mathbf{O}(t) \otimes \nabla V(\mathbf{r}(0)) \rangle_\gamma$. For $\gamma = 0$ we find the usual fluctuation dissipation relation

$$\mathbf{R}_0(t) = -\frac{1}{T} \partial_t \mathbf{C}_0(t). \quad (2.52)$$

The breaking of time reversal symmetry yields a violation of the fluctuation dissipation relation. Eq. (2.51) will be used later when studying the relation between the mobility and diffusion tensor in dense liquids.

While we expect Eq. (2.51) to hold for a generic, possibly nonconservative force applied to the system, the case where the external perturbation is obtained by shifting the energy by an amount $\delta V(\mathbf{r}) = -\mathbf{h}(t) \cdot \mathbf{w}(\mathbf{r})$, with $\mathbf{h}(t)$ a time dependent vector field and $\mathbf{w}(\mathbf{r})$ a conjugated observable, is of special interest. In this case, we can introduce a response function R' with respect to change in the field $\mathbf{h}(t)$ as

$$R'^{ab}_\gamma(t, t') = \left\langle \frac{\delta O_a(t)}{\delta h_b(t')} \right\rangle \Big|_{h=0}. \quad (2.53)$$

Since transverse forces preserve the Boltzmann distribution in the steady state, the linear response formalism can be developed as in the equilibrium case, thus obtaining [59] in the stationary regime

$$\mathbf{R}'_\gamma(t) = -\frac{1}{T} \partial_t \mathbf{C}'_\gamma(t) \quad (2.54)$$

with $\mathbf{C}'_\gamma(t - t') = \mathbf{C}'_\gamma(t, t') \equiv \langle \mathbf{O}(t) \otimes \mathbf{w}(t') \rangle_\gamma$ the correlation function between the observable \mathbf{O} and the variable $\mathbf{w}(\mathbf{r})$ conjugated to the small field $\mathbf{h}(t)$. In this case, the fluctuation dissipation theorem is restored. If we choose \mathbf{w} so that $\mathbf{w}(\mathbf{r}) = \mathbf{r}$, then $\mathbf{F}^{\text{ext}} = (\mathbf{1} + \gamma \mathbf{A}) \mathbf{h}(t)$. This means that $\mathbf{R}'(t, t') = \mathbf{R}(t, t') (\mathbf{1} + \gamma \mathbf{A})$, and $\mathbf{C}'(t, t') = \mathbf{C}(t, t')$ and therefore

$$\mathbf{R}(t)(\mathbf{1} + \gamma \mathbf{A}) = -\frac{1}{T} \partial_t \mathbf{C}(t). \quad (2.55)$$

These different formulations of the fluctuation-dissipation relation will be useful in subsequent parts of the thesis.

2.6 Summary and Outlook

In this Chapter we studied the effect of transverse forces in the motion of one particle in an external potential, and we found that

- The escape rate of the system τ_0^{-1} , i.e. the typical rate at which a particle evolves from a configuration to another, is enhanced with respect to its equilibrium $\tau_{0,\text{eq}}$ value through a rescaling:

$$\tau_0^{-1} \sim (1 + \gamma^2) \tau_{0,\text{eq}}^{-1} \quad (2.56)$$

- In an isotropic harmonic well, transverse forces do not reduce the relaxation time: $\tau_R(\gamma) = \tau_R(0)$. If the well is anisotropic, then $\tau_R(\gamma) < \tau_R(0)$, and saturation occurs at large γ .
- Even when the particle is confined in a harmonic well, a form of odd transport emerges, due to the swirling motion induced by transverse forces. This is captured by a nonzero odd diffusion constant $D_\perp = -\gamma T$.
- The time required to cross an energy barrier with transverse forces follows the Arrhenius law $\tau \sim e^{\frac{\Delta}{T}}$, but the prefactor is smaller than its equilibrium counterpart. The instanton trajectory from the bottom of the energy well to the saddle point bends when $\gamma \neq 0$. At large γ , the barrier crossing time decreases as $\tau \sim \gamma^{-1}$.

- Due to the breaking of time reversal symmetry, the fluctuation dissipation theorem is no longer valid, unless the perturbation consists in a change of the potential.

We can now move to study the performance of transverse forces in a paradigmatic model of disordered systems with a rugged energy landscape, namely the p -spin spherical model.

CHAPTER 2

CHAPTER

3

ACCELERATING A MEAN FIELD SPIN GLASS

3.1	The p -spin spherical model	34
3.2	Transverse forces in the p -spin: Ichiki-Ohzeki dynamics	34
3.2.1	Numerical integration	36
3.2.2	Fluctuation-dissipation relation	38
3.2.3	Speedup and ergodicity breaking	39
3.3	Random solenoidal fields	41
3.4	Outlook	44

In this chapter, we put transverse forces to the test in the p -spin spherical model, a mean field spin glass with a rugged energy landscape. We derive dynamical equations for the correlation and the response functions of the system. The evolution of the correlation and response functions is then studied by direct numerical integration and analytically, through a form of accidental fluctuation dissipation relation. We find that, as for equilibrium dynamics, there is a temperature below which the dynamics of the system becomes arrested and ergodicity is broken. This temperature is not modified by transverse forces: it is the same as in equilibrium. In the ergodic region, we quantify the speedup provided by transverse forces, and interpret it in terms of the evolution of novel correlation functions that are absent in the equilibrium case.

3.1 The p -spin spherical model

The spherical p -spin is a disordered, fully connected model of N interacting spins $\sigma_1, \dots, \sigma_N$ fulfilling the constraint $\sum_{i=1}^N \sigma_i^2 = N$. The energy $V[\{\sigma_i\}_{i=1,\dots,N}]$ of a configuration is

$$V[\{\sigma_i\}_{i=1,\dots,N}] = - \sum_{i_1 < \dots < i_p} J_{i_1 \dots i_p} \sigma_{i_1} \dots \sigma_{i_p} \quad (3.1)$$

where the $J_{i_1 \dots i_p}$ are independent quenched random couplings with variance $\frac{2J^2}{p!N^{p-1}}$. This model was introduced at the beginning of the 90s [66, 65] to better understand the replica symmetry breaking scenario occurring in many models of spin glasses. After its introduction, it has been instrumental in shaping up our understanding of disordered and glassy systems [67, 15, 93], including active ones [36], up to our days [91, 154, 215].

A summary of the properties relevant to the present discussion [14, 56] is that this model undergoes a transition from a paramagnetic state at high temperatures to a spin-glass phase at low temperatures $T < T_c$ [66]. From a static point of view, its peculiarity is that there exists an intermediate temperature $T_d > T_c$ such that in the temperature range $T_c < T < T_d$ an exponentially large number of metastable states appears, without however affecting the paramagnetic nature of the system. From a dynamical standpoint, while the system relaxes above T_d , it fails to explore this complex energy landscape as soon as $T < T_d$ [65], when endowed with purely relaxational equilibrium dynamics. The spin-spin correlation function

$$C(t, t') = \frac{1}{N} \sum_i \langle \sigma_i(t) \sigma_i(t') \rangle \quad (3.2)$$

In the stationary state, where $C(t, t') = C(t - t')$, the correlation function fails to relax to 0 as $t - t' \rightarrow +\infty$ for $T < T_d$, reaching instead a temperature-dependent plateau value q . For this reason, the p -spin represent an ideal test-bench to quantify the acceleration provided by new sampling protocols, such as the transverse force dynamics.

3.2 Transverse forces in the p -spin: Ichiki-Ohzeki dynamics

We implement transverse forces in the p -spin using the Ichiki-Ohzeki (IO) dynamics [208]. we consider two coupled p -spin systems (with the same realization of the disorder), with spins $\sigma_i^{(1)}$ and $\sigma_i^{(2)}$ evolving according to

$$\begin{bmatrix} \dot{\sigma}_i^{(1)} \\ \dot{\sigma}_i^{(2)} \end{bmatrix} = -(\mathbf{1}_2 + \gamma \mathbf{A}) \begin{bmatrix} \frac{\partial \mathcal{H}}{\partial \sigma_i^{(1)}} + \mu^{(1)}(t) \sigma_i^{(1)} \\ \frac{\partial \mathcal{H}}{\partial \sigma_i^{(2)}} + \mu^{(2)}(t) \sigma_i^{(2)} \end{bmatrix} + \sqrt{2T} \begin{bmatrix} \xi_i^{(1)}(t) \\ \xi_i^{(2)}(t) \end{bmatrix}. \quad (3.3)$$

The matrix $\mathbf{A} \equiv \begin{bmatrix} 0 & -1 \\ 1 & 0 \end{bmatrix}$ implements the transverse force, an antisymmetric coupling of strength γ between the two systems. The noises $\xi_i^{(a)}(t)$ are white and Gaussian, with

correlation $\langle \xi_i^{(a)}(t) \xi_j^{(b)}(t') \rangle = \delta_{ij} \delta_{ab} \delta(t - t')$. The functions $\mu^{(a)}(t)$ are adjusted so that the spherical constraint $\sum_{i=1}^N \left\langle \left(\sigma_i^{(a)}(t) \right)^2 \right\rangle = N$ is fulfilled throughout the dynamical evolution. There is a large body of literature on the effect of a nonequilibrium drive on the p -spin (or on other complex systems with a similar glassy behavior at low temperatures). In these works it has consistently been found that in the presence of a nonequilibrium drive (be it in a randomized non-relaxational dynamics [68], or in a shear [25] or with an active force [36]) a lower temperature than the equilibrium one is required in order to witness the onset of ergodicity breaking. However, in those cases the nonequilibrium stationary-state that is being sampled is not the Boltzmann distribution, and it is in general unknown. We stress that, unlike in the latter series of works, the IO dynamics does correctly sample, in its stationary state, the Boltzmann distribution $\rho_B \sim e^{-\beta \mathcal{H}}$ for $\mathcal{H} = V[\{\sigma_i^{(1)}\}] + V[\{\sigma_i^{(2)}\}]$ (with V given in Eq. (3.1)), despite being a nonequilibrium dynamics. From an analytical standpoint, a remarkable feature of the standard dynamics of the p -spin, which is preserved by Eq. (3.3) is that the mean-field nature of the problem allows us to write the stochastic evolution of a single spin in terms of unknown functions (the spin-spin correlation, the response function that enters the memory kernel, and noise correlations) that are determined self-consistently. Such a procedure can be applied to our case. Note however that in the context of the IO dynamics, the spin-spin correlation becomes a collection of four spin-spin correlations $C_{ab}(t, t') = \frac{1}{N} \langle \sum_i \sigma_i^{(a)}(t) \sigma_i^{(b)}(t') \rangle$, and the same holds for the response function

$$R_{ab}(t, t') \equiv \frac{1}{N} \sum_i \frac{\delta \langle \sigma_i^{(a)}(t) \rangle}{\delta h_i^{(b)}(t')} \quad (3.4)$$

where $h_i^a(t)$ is a time-dependent force field applied to spin i of system a . For numerical purposes, we will work with the integrated response $F_{ab}(t, t') \equiv - \int_{t'}^t d\tau R_{ab}(t, \tau)$.

Using a path integral formalism and the mean field approximation, we write an effective Langevin equation for the dynamics of a single spin $\sigma^{(1)}$ in system 1 and its counterpart $\sigma^{(2)}$ in system 2, from which self-consistent equations of motion for the correlation and the integrated response can be derived. Since our interest goes to the dynamics in the steady state we assume time translational invariance to hold, $C_{ab}(t, t') = C_{ab}(t - t')$ and $F_{ab}(t, t') = F_{ab}(t - t')$. The effective equations of motion for $\boldsymbol{\sigma}(t) \equiv [\sigma^{(1)} \ \sigma^{(2)}]^T$, for the correlation matrix \mathbf{C} and the integrated response matrix

\mathbf{F} are:

$$\begin{aligned}\partial_t \boldsymbol{\sigma}(t) = & -(\mathbf{1}_2 + \gamma \mathbf{A}) \cdot \boldsymbol{\mu}(t) \cdot \boldsymbol{\sigma}(t) + \int_0^t d\tau \mathbf{M}_{\mathbf{F}}(t-\tau) \cdot \boldsymbol{\sigma}(\tau) \\ & + \frac{1}{T} (\mathbf{1}_2 + \gamma \mathbf{A}) \cdot \mathbf{C}_0(p, t) \cdot \boldsymbol{\sigma}(0) + \boldsymbol{\Xi}(t)\end{aligned}\quad (3.5)$$

$$\partial_t \mathbf{F}(t) = -\mathbf{1}_2 - (\mathbf{1}_2 + \gamma \mathbf{A}) \cdot \boldsymbol{\mu}(t) \cdot \mathbf{F}(t) + \int_{t'}^t d\tau \mathbf{M}_{\mathbf{F}}(t-\tau) \cdot \mathbf{F}(\tau) \quad (3.6)$$

$$\partial_t \mathbf{C}(t) = -(\mathbf{1}_2 + \gamma \mathbf{A}) \cdot \boldsymbol{\mu}(t) \cdot \mathbf{C}(t) + \int_0^t d\tau \mathbf{M}_{\mathbf{F}}(t-\tau) \cdot \mathbf{C}(\tau) + \frac{1}{T} (\mathbf{1}_2 + \gamma \mathbf{A}) \cdot \mathbf{C}_0(p, t) \quad (3.7)$$

$$\begin{aligned}\boldsymbol{\mu}(t) = \text{Diag} \left[T \mathbf{1}_2 + \int_0^t d\tau \mathbf{M}(t-\tau) \cdot \mathbf{C}^T(t-\tau) + \int_0^t d\tau \mathbf{D}(t-\tau) \cdot \partial_\tau \mathbf{F}^T(t-\tau) \right. \\ \left. + \frac{1}{T} (\mathbf{1}_2 + \gamma \mathbf{A}) \cdot \mathbf{C}_0(p, t) \cdot \mathbf{C}^T(t) \right]\end{aligned}\quad (3.8)$$

where the coloured Gaussian noise has correlations $\langle \boldsymbol{\Xi}(t) \otimes \boldsymbol{\Xi}(t') \rangle = 2T \mathbf{1}_2 \delta(t-t') + \mathbf{D}(t,t')$. The three kernels $\mathbf{M}_{\mathbf{F}}$, \mathbf{C}_0 and \mathbf{D} that appear in Eqs. (3.5, 3.6, 3.7) are nonlinear functionals of the elements of \mathbf{C} and \mathbf{F} . The overall structure of these equations is similar to the equilibrium setting, and the derivation is detailed in App. D1. These equations are solved with the boundary conditions $\mathbf{C}(0) = \mathbf{1}_2$, $\mathbf{F}(0) = \mathbf{0}$, while the diagonal matrix $\boldsymbol{\mu}(t)$ enforces the spherical constraint.

In the case of standard equilibrium dynamics, the response and the correlations are related by the fluctuation-dissipation theorem (FDT), $\partial_t \mathbf{F}(t) = -\frac{1}{T} \partial_t \mathbf{C}(t)$ and it is possible to obtain a closed equation for the spin-spin correlation function of the system alone. By focusing on the long time limit of the dynamics one can then find the temperature below which the correlation function displays a nonzero plateau at infinite times when ergodicity is broken. Since the IO dynamics is a nonequilibrium one, we cannot resort to the fluctuation dissipation theorem, and analytical manipulations of Eqs. (3.5, 3.6, 3.7, 3.8) may seem, at first sight, out of reach. In the following section, however, we shall exhibit a simple argument that suggests that for the specific correlations and integrated response considered above, a relation formally similar to the FDT might still survive in the nonequilibrium steady-state.

3.2.1 Numerical integration

We integrate the dynamical equations Eqs. (3.6, 3.7, 3.8) for $p = 3$ using a finite difference method implemented in [102, 155, 27, 92] and detailed in App. D2. We check that our implementation of the IO dynamics samples the correct Boltzmann distribution by measuring the energy per spin E_∞ at long times in the ergodic phase. This is a static quantity independent of γ , for which a value of $E_\infty = -\frac{1}{2T}$ is predicted on the basis of the equilibrium statics alone [66]. In the numerical integration, we

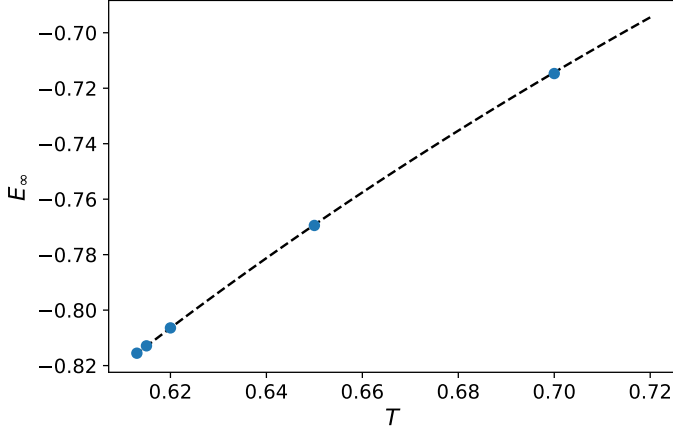


Figure 3.1: Energy per spin as a function of temperature T obtained from numerical integration (blue dots) at $\gamma = 1$ and theoretical prediction $E_\infty = -\frac{1}{2T}$ (black dashed line).

computed the energy by exploiting the relation

$$\mu(t \rightarrow +\infty) = (T - pE_\infty) \mathbf{1}_2 \quad (3.9)$$

The agreement between the measured value of E_∞ and its theoretical prediction is shown in Fig. 3.1. The errors are of order 10^{-12} and they are therefore negligible.

Having ascertained that our implementation of the IO dynamics correctly samples a static quantity, we proceed by investigating the time behavior of the correlation function of one subsystem. Our results are presented in Fig. 3.2. In the range of parameters explored, with γ up to 2.4, the IO dynamics is accelerated by a non negligible amount compared to the standard one. For $\gamma \approx 2.4$, the highest coupling achievable while preserving the convergence of the integration scheme, the convergence to 0 of the correlation function is anticipated by almost an order of magnitude. For $T < T_d$, the system freezes even at $\gamma \neq 0$, and the position of the infinite time plateau is left unchanged.

We quantify the speedup obtained by means of the IO dynamics by measuring the relaxation time $\tau_\alpha(\gamma)$, defined here as the time necessary for C_{11} to decay to the value $1/e$ in the ergodic phase. Our results are shown in Fig. 3.3. The ratio between $\tau_\alpha(\gamma)$ and the relaxation time in the standard dynamics, $\tau_\alpha(0)$ appears to scale approximately as $(1 + \gamma^2)^{-1}$. This scaling the same as the one found in Sec. 2.4.1 when heuristically discussing the Kramers' problem. We will provide the reader with further interpretation for this phenomenon in the next section.

The departure of the IO dynamics from the equilibrium dynamics is accompanied by an early growth in the cross correlations of the system. This can be seen in Fig. 3.2, where we plot C_{12} in dotted lines, and is presented in more detail in Fig. 3.4, where a close up of the cross correlations for various values of γ is shown. The dynamics of these quantities is entirely located in the region of β -relaxation of C_{11} . They exhibit a bump at short times, reaching a point of maximum modulus and then decaying to

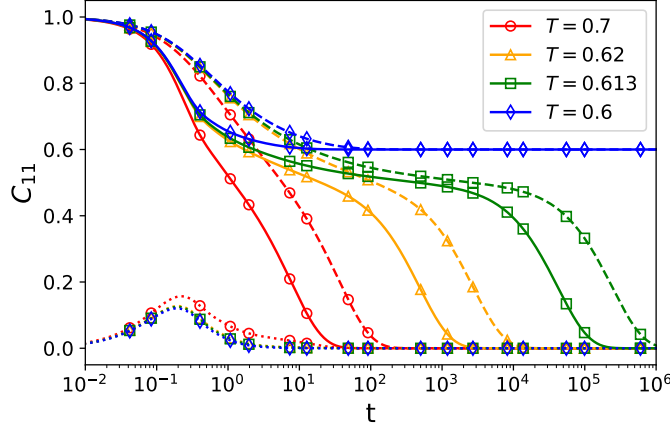


Figure 3.2: Correlation function of system 1, $C_{11}(t)$ for $\gamma = 2.4$ (solid lines) and $\gamma = 0$ (dashed lines) for various temperatures above and below $T_d \approx 0.6124$. The dotted curves represent the cross correlations $C_{12}(t)$ for $\gamma = 2.4$. The shift between the dashed and the solid line of a given colour, which quantifies the acceleration of the dynamics, somewhat increases as the temperature is decreased.

zero. This maximum grows linearly with γ for $\gamma \lesssim 1$. The location of the maximum moves left to shorter times as γ grows. This can be rationalized by observing that the entropy production rate per spin is $\frac{\sigma}{N} = 2\gamma^2\mu$, and that therefore the timescale over which non reversible effects appear decreases with γ .

3.2.2 Fluctuation-dissipation relation

In this Section, we look at how the fluctuation-dissipation relation is modified by transverse forces for the p -spin. Since in a spin system external perturbations are applied by means magnetic fields, which consist in a shift of the energy V , we expect the fluctuation dissipation theorem discussed at the end of Sec. 2.5 to hold. Since we have defined the response matrix $\mathbf{R}(t, t')$ as the response of the system with respect to an applied force, we expect that in the stationary state, a fluctuation-dissipation relation of the following form

$$\mathbf{R}(t, t')(\mathbf{1} + \gamma \mathbf{A}) = -\frac{1}{T} \partial_t \mathbf{C}(t) \quad (3.10)$$

to hold. Using the integrated response matrix \mathbf{F} , Eq. (3.10) can be rewritten as

$$\mathbf{F}(t)(\mathbf{1} + \gamma \mathbf{A}) = \frac{1}{T} [\mathbf{C}(0) - \mathbf{C}(t)] \quad (3.11)$$

A numerical test for a particular entry and particular values of T and γ of Eq. (3.11) is shown in Fig. 3.5. Similar results are obtained for other entries and other values of coupling and temperature. Eq. (3.11) can be proven analytically. We can indeed show that if Eqs. (3.7, 3.8) and the aFDT relation Eq. (3.10) are true then the remaining equation Eq. (3.6) must also hold. The details of the proof are reported in App. D3.

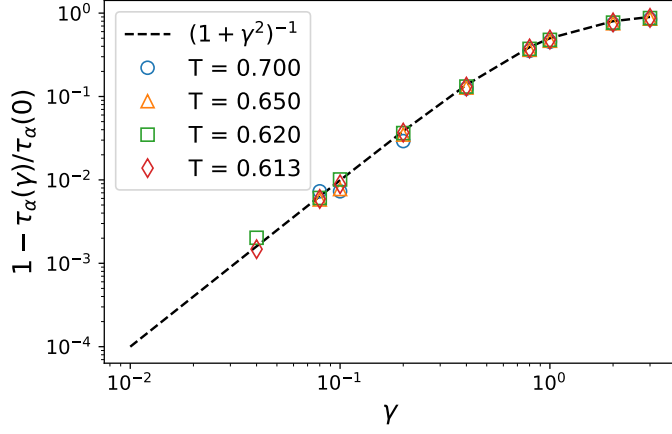


Figure 3.3: Ratio between the relaxation time of C_{11} for the IO dynamics, $\tau_\alpha(\gamma)$, and the equilibrium dynamics $\tau_\alpha(0)$ for temperatures close to T_d .

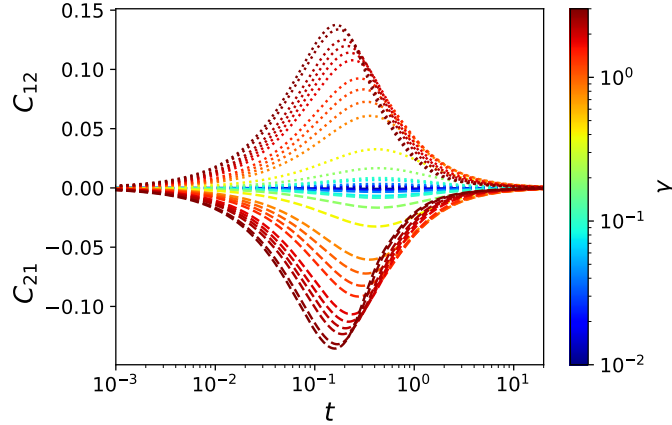


Figure 3.4: Cross correlation C_{12} (dotted lines) and C_{21} (dashed lines) as a function of time for $T = 0.613$ at different values of γ .

The numerical investigation performed in this section raises a series of questions to be answered. Can we explain the absence of a shift in the dynamical temperature T_d ? Is it possible to justify the scaling of the relaxation time of C_{11} with γ ? In the following section we shall build a theoretical understanding of our numerical findings.

3.2.3 Speedup and ergodicity breaking

By using the aFDT relation we can reduce the set of Eqs. (3.6, 3.7, 3.8) to a single equation for the correlation matrix $\mathbf{C}(t)$:

$$\begin{aligned} \partial_t \mathbf{C}(t) &= -T (\mathbf{1}_2 + \gamma \mathbf{A}) \cdot \mathbf{C}(t) \\ &\quad - \frac{1}{T} (\mathbf{1}_2 + \gamma \mathbf{A}) \int_0^t d\tau \mathbf{C}_0(p, t - \tau) \cdot \partial_\tau \mathbf{C}(\tau) \end{aligned} \tag{3.12}$$

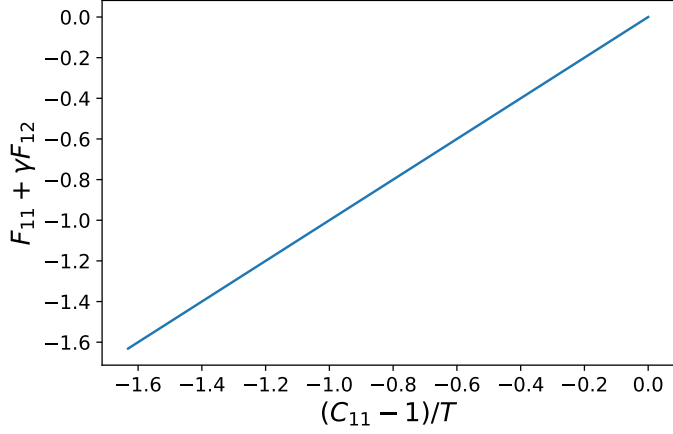


Figure 3.5: Parametric plot of the left and right hand side of the first entry of Eq. (3.11) from the integration of Eqs. (3.6, 3.7, 3.8) at $T = 0.613$ and $\gamma = 2.4$.

with $C_0(p, t)_{ij} \equiv \frac{p}{2} C_{ij}^{p-1}$. Apart from the matrix prefactor $(\mathbf{1}_2 + \gamma \mathbf{A})$ the structure of this equation is the same as the one obtained in the standard equilibrium dynamics of the p -spin [65, 14, 56]. We therefore study its long time behavior by assuming that $\lim_{t \rightarrow +\infty} \mathbf{C}(t) = \mathbf{Q}$, with \mathbf{Q} a matrix of long time plateaus generalizing the nonergodic parameter. We introduce the Laplace transform of a matrix $\mathbf{M}(t)$ as $\tilde{\mathbf{M}}(z) \equiv \int_0^{+\infty} dt \mathbf{M}(t) e^{-zt}$ and we observe that $\tilde{\mathbf{C}}(z) \approx \frac{\mathbf{Q}}{z}$ and $\tilde{\mathbf{C}}_0(p, z) \approx \frac{\mathbf{Q}_0(p)}{z}$ as $z \rightarrow 0$, with $Q_0(p)_{ij} \equiv Q_{ij}^{p-1}$. Applying the Laplace transform to both sides of Eq. (3.12) and keeping only the terms that diverge as $z \rightarrow 0$ yields

$$T\mathbf{Q} - \frac{1}{T}\mathbf{Q}_0(p) \cdot (\mathbf{1}_2 - \mathbf{Q}) = 0 \quad (3.13)$$

We now see that the dependence on Γ has simply disappeared. The form of the plateaus matrix can therefore not depend on γ . In particular, it must match the solution obtained at $\gamma = 0$. We can therefore write $\mathbf{Q} = Q\mathbf{1}_2$ and $\mathbf{Q}_0(p) = Q^{p-1}\mathbf{1}_2$. Eq. (3.13) then becomes the standard equation for the long time plateau of the p -spin equilibrium dynamics

$$\frac{2T^2}{p} = Q^{p-2}(1 - Q) \quad (3.14)$$

In analogy with the Kramers problem and the harmonic oscillator of Sec. 2.4 we see that an increased mobility $(\mathbf{1}_2 + \gamma \mathbf{A})$ arises in the IO dynamics of the p -spin. This rescaling of the mobility can always be absorbed into a rescaling of the time units. Below T_d , where the plateau extends to infinite times, the dynamical ergodicity breaking cannot be avoided while above T_d an acceleration is achieved.

We support the above picture by carrying out a perturbation expansion to second order in γ . In particular we recover the scaling of the relaxation time τ_α shown in Fig. 3.3 starting from the dynamical equation for the correlation matrix Eq. (3.12). We multiply both sides by $\mathbf{1}_2 + \gamma \mathbf{A}^T$ and we expand \mathbf{C} in powers of γ , $\mathbf{C} \approx \delta_0 \mathbf{C} +$

$\gamma\delta_1\mathbf{C} + \gamma^2\delta_2\mathbf{C}$, thereby obtaining:

$$\partial_t\mathbf{C}(t) + \gamma\mathbf{A}^T \cdot \partial_t\delta_1\mathbf{C}(t) = -(1 + \gamma^2)\left(\mathbf{C}(t) + \frac{1}{T}\int_0^t d\tau\mathbf{C}_0(p, t - \tau) \cdot \partial_\tau\mathbf{C}(\tau)\right) \quad (3.15)$$

The second term on the left hand side contains $\delta_1\mathbf{C}$, the first order perturbation of \mathbf{C} . It is a skew symmetric matrix and therefore it contributes to the expansion of the cross correlations shown in Fig. 3.4. Motivated by the numerical observation of Sec. 3.2.1 we assume that this term essentially vanishes at times larger than the time scale at which the β relaxation takes place. Moreover, because of the skew symmetry of the first order perturbation, the diagonal entries of Eq. (3.15) are not affected by the short time dynamics of $\delta_1\mathbf{C}$. We therefore obtain, to second order in γ :

$$\partial_t C_{aa}(t) = -(1 + \gamma^2)\left(T C_{aa}(t) + \frac{1}{T}\int_0^t d\tau C_{aa,0}(p, t - \tau) \partial_\tau C_{aa}(\tau)\right) \quad (3.16)$$

for $a = 1, 2$. This is the same equation as that of the equilibrium dynamics, up to a rescaling of time $t \rightarrow t/(1 + \gamma^2)$, in agreement with the findings of Fig. 3.3.

3.3 Random solenoidal fields

Let us look at the p -spin with transverse forces studied in this chapter from a more general perspective: in this chapter, we studied a mean field model whose dynamics is governed by a combination of a disordered conservative force and a solenoidal force, namely the one implemented through transverse forces. The latter is random too, since it is related with the gradient term via the antisymmetric matrix \mathbf{A} , as shown in Eq. (3.3). One could then ask what happens in a more general setting, where the random solenoidal force is not constrained to have a transverse form. This section collects some work in progress addressing this question. Consider the following overdamped Brownian Dynamics of a particle in d dimensions

$$\dot{r}_i = -\mu r_i - \frac{\partial V(\mathbf{r})}{\partial r_i} + \frac{1}{\sqrt{d}} \sum_{j=1}^d \frac{\partial A_{ij}(\mathbf{r})}{\partial r_j} + \sqrt{2T}\xi_i(t) \quad (3.17)$$

The noise is white and Gaussian, with zero mean and covariance $\langle \xi_i(t)\xi_j(t') \rangle = \delta_{ij}\delta(t - t')$. The first contribution is a restoring harmonic force with stiffness μ , that keeps the particle confined. The second and third term are respectively the gradient of a potential V and a solenoidal field, with vector potential \mathbf{A} . Both the gradient and the vector potentials are taken to be random, with correlations

$$\begin{aligned} \overline{V(\mathbf{r})V(\mathbf{r}')} &= -v^2 d\Gamma_V \left(\frac{(\mathbf{r} - \mathbf{r}')^2}{d} \right) \\ \overline{A_{ij}(\mathbf{r})A_{nm}(\mathbf{r}')} &= -a^2 d\Gamma_A \left(\frac{(\mathbf{r} - \mathbf{r}')^2}{d} \right) (\delta_{in}\delta_{jm} - \delta_{im}\delta_{jn}). \end{aligned} \quad (3.18)$$

Note the antisymmetry of the covariance for the field $A_{ij}(\mathbf{r})$. The parameters v and a encode the strength of the disorder of V and A_{ij} respectively, and the functions Γ_A, Γ_V describe the decay of the space correlations.

Eq. (3.18) represents a general Helmholtz decomposition of the forces acting on disordered systems into a conservative and a nonconservative part. For example, for $a = 0$, $v = 1$ and $\Gamma_V(x) \equiv -\frac{1}{2}(1 - \frac{x}{2})^p$, and imposing the additional spherical constraint $\langle \mathbf{r}^2(t) \rangle = d$ (which implies that the stiffness is a function of time $\mu = \mu(t)$) one falls back onto the equilibrium dynamics of the p -spin spherical model. The 0 temperature dynamics of Eq. (3.18) has been studied as a general model for the stability of ecological systems [105, 18]. In a nutshell, the nature of the fixed points of the zero temperature dynamics changes as two parameters $\tau \equiv \frac{v^2}{a^2+v^2}$, and $m \equiv \mu/\sqrt{a^2\Gamma_A''(0) + v^2\Gamma_V''(0)}$ are varied. The combination τ represents the competition between gradient and solenoidal forces, while m encodes the strength of the restoring harmonic force compared to the disordered forces. When $m > 1$, the system has only one stable fixed point. For $m_c(\tau) < m < 1$ the system has an exponentially large (in the dimension d) number of unstable fixed points, and only a sub-exponential number of minima. For $m < m_c(\tau)$, both minima and saddle points proliferate exponentially, with the number of saddle points being exponentially larger than the number of minima.

A relevant question is what happens to the dynamics of the system when $T > 0$. While the case $a = 0$ (and hence $\tau = 1$) has been extensively studied, both in its stationary and ageing regimes [157, 156, 70], where a dynamical glass transition is found for $T < T_c(\mu)$. What happens for $a \neq 0$ is an open question, that we want to address. Here we describe a first step in this direction, the derivation of the dynamical equation for the correlation and response function.

As for the study of the p -spin, we are interested in determining equations of motion for the response function $R(t, t')$ and the correlations $C(t, t')$. Since Eq. (3.18) hold also in the absence of spherical constraints, we need to study also the mean squared displacement $B(t, t')$, defined as

$$R(t, t') \equiv \frac{1}{N} \sum_{i=1}^N \langle r_i(t) \hat{r}_i(t') \rangle \quad (3.19)$$

$$C(t, t') \equiv \frac{1}{N} \sum_{i=1}^N \langle r_i(t) r_i(t') \rangle \quad (3.20)$$

$$B(t, t') \equiv \frac{1}{N} \sum_{i=1}^N \langle (r_i(t) - r_i(t'))^2 \rangle = C(t, t) + C(t', t') - 2C(t, t') \quad (3.21)$$

We resort to a path integral formalism to obtain effective equations of motion for the particle, upon averaging over the disorder. The derivation is along the lines of one for the p -spin in Appendix D1. Here we provide the relevant steps. The Janssen-De Dominicis action reads:

$$S[\mathbf{r}, \hat{\mathbf{r}}] = \sum_i \int dt i \hat{r}_i(t) \left[\dot{r}_i(t) + \mu r_i + \frac{\partial V(\mathbf{r})}{\partial r_i} - \frac{1}{\sqrt{d}} \sum_j \frac{\partial A_{ij}(\mathbf{r})}{\partial r_j} \right] + T \hat{r}_i(t)^2 \quad (3.22)$$

With $\mathbf{r}(t)$ and $\hat{\mathbf{r}}(t)$ two trajectories of the particle and the related conjugate field. The

average over the disorder for the exponential weight of a given trajectory is

$$\begin{aligned} \overline{\exp(-S[\mathbf{r}, \hat{\mathbf{r}}])} &= \exp\left(-\sum_i \int dt i\hat{r}_i(t) [\dot{r}_i(t) + \mu r_i(t)] + T\hat{r}_i(t)^2\right. \\ &\quad + \frac{1}{2} \sum_{i,j} \int dt dt' i\hat{r}_i(t) i\hat{r}_j(t') \frac{\overline{\partial V(\mathbf{r}(t))}}{\partial r_i} \frac{\overline{\partial V(\mathbf{r}(t'))}}{\partial r_j} \\ &\quad \left. + \frac{1}{2N} \sum_{i,j,k,l} \int dt dt' i\hat{r}_i(t) i\hat{r}_j(t') \frac{\overline{\partial A_{ik}(\mathbf{r}(t))}}{\partial x_k} \frac{\overline{\partial A_{jl}(\mathbf{r}(t'))}}{\partial x_l}\right) \end{aligned} \quad (3.23)$$

The force correlations for the potential and the solenoidal fields can be computed by deriving the correlators:

$$\begin{aligned} \frac{\overline{\partial V(\mathbf{r}(t))}}{\partial r_i} \frac{\overline{\partial V(\mathbf{r}(t'))}}{\partial r_j} &= 2v^2 \delta_{ij} \Gamma'_V \left(\frac{(\mathbf{r} - \mathbf{r}')^2}{d} \right) \\ &\quad - 4v^2 \frac{(r_i(t) - r_i(t'))(r_j(t) - r_j(t'))}{d} \Gamma''_V \left(\frac{(\mathbf{r} - \mathbf{r}')^2}{d} \right) \end{aligned} \quad (3.24)$$

$$\begin{aligned} \sum_{k,l} \frac{\overline{\partial A_{ik}(\mathbf{r}(t))}}{\partial x_k} \frac{\overline{\partial A_{jl}(\mathbf{r}(t'))}}{\partial x_l} &= 2a^2(d-1) \delta_{ij} \Gamma'_A \left(\frac{(\mathbf{r} - \mathbf{r}')^2}{d} \right) \\ &\quad - 4a^2 \delta_{ij} \frac{(r_i(t) - r_i(t'))^2}{d} \Gamma''_A \left(\frac{(\mathbf{r} - \mathbf{r}')^2}{d} \right) \\ &\quad + 4a^2 \frac{(r_i(t) - r_i(t'))(r_j(t) - r_j(t'))}{d} \Gamma''_A \left(\frac{(\mathbf{r} - \mathbf{r}')^2}{d} \right) \end{aligned} \quad (3.25)$$

In a saddle point approximation, one can write

$$\int dt dt' \sum_{i,j} i\hat{r}_i(t) i\hat{r}_j(t') \frac{(r_i(t) - r_i(t'))(r_j(t) - r_j(t'))}{d} = 2 \int dt dt' \sum_i i\hat{r}_i(t) R(t, t') [r_i(t) - r_i(t')] \quad (3.26)$$

and neglect contributions of order d^{-1} or higher. The effective equations for the degree of freedom $r_i(t)$ are therefore

$$\dot{r}_i(t) = -\mu r_i(t) + 4 \int_0^t ds \Gamma_D(B(t, s)) R(t, s) [r_i(t) - r_i(s)] + \xi_i(t) \quad (3.27)$$

$$\langle \xi_i(t) \xi_j(t') \rangle = \delta_{ij} [2T\delta(t-t') + 2\Gamma_F(B(t, t'))] \quad (3.28)$$

With the dissipation and fluctuation kernels Γ_D , Γ_F defined as follows:

$$\begin{aligned} \Gamma_D(B(t, t')) &\equiv v^2 \Gamma''_V(B(t, t')) \\ \Gamma_F(B(t, t')) &\equiv v^2 \Gamma'_V(B(t, t')) + a^2 \Gamma'_A(B(t, t')) \end{aligned} \quad (3.29)$$

The equations for the response, the correlation and the mean squared displacement finally read:

$$\partial_t R(t, t') = -\mu R(t, t') + 4 \int_0^t ds \Gamma_D(B(t, s)) R(t, s) [R(t, t') - R(s, t')] + \delta(t-t') \quad (3.30)$$

$$\begin{aligned}\partial_t C(t, t') = & -\mu C(t, t') + 4 \int_0^t ds \Gamma_D(B(t, s)) R(t, s) [C(t, t') - C(s, t')] \\ & + 2T R(t', t) + 2 \int_0^{t'} ds \Gamma_F(B(t, s)) R(t', s)\end{aligned}\tag{3.31}$$

$$\begin{aligned}\frac{1}{2} \frac{dC(t, t)}{dt} = & -\mu C(t, t) + T + 2 \int_0^t ds \Gamma_D(B(t, s)) R(t, s) [C(t, t) - C(s, s) + B(t, s)] \\ & + 2 \int_0^t ds \Gamma_F(B(t, s)) R(t, s)\end{aligned}\tag{3.32}$$

$$\begin{aligned}\frac{1}{2} \partial_t B(t, t') = & -\frac{\mu}{2} (C(t, t) - C(t', t') + B(t, t')) + T \\ & + 2 \int_0^t ds \Gamma_D(B(t, s)) R(t, s) [B(t, s) + B(t, t') - B(s, t)] \\ & + 2 \int_0^t ds \Gamma_F(B(t, s)) [R(t, s) - R(t', s)]\end{aligned}\tag{3.33}$$

The equilibrium case [70] is recovered for $a = 0$. The correlator of the solenoidal field enters into the expression of fluctuation kernel Γ_F , but not into the dissipation kernel Γ_D . This is a consequence of the nonequilibrium nature of Eq. (3.18).

To proceed further, these equation can be integrated numerically, as was done for the p spin with transverse transverse forces. In the presence of a solenoidal field, $\tau < 1$, it would be interesting to see how the dynamics changes in the region for $m_c(\tau) < m < 1$, where there saddles are exponentially abundant, and minima are not. We speculate that forms of chaotic behavior might arise in this situation, and that the study of the statistics of the single particle trajectories in Eq. (3.27) and the correlation function $C(t, t')$ might capture this property.

3.4 Outlook

In this chapter we provided a first test of the dynamics with transverse forces in a many body, disordered system, the spherical p -spin glass model. We interpret the fact that the temperature at which dynamical ergodicity breaking occurs is not shifted as a reflection of the fact that the transverse force dynamics accelerates the barrier crossing rate through a prefactor of the Arrhenius law, as we saw in Section 2.4. On the other hand in the ergodic phase, transverse forces maintain an edge over equilibrium dynamics. Our analysis in perturbation theory suggests that this is due to the fact that cross correlation conspire at short times to accelerate relaxation. In the spherical p -spin, the evolution of the off-diagonal elements of \mathbf{C} represent the new dynamical pathway unlocked by transverse forces. What are these new dynamical pathways in systems of interacting particles, which are free from their spherical constraint, and

what quantity can we measure associated to them? In the following chapter, we start tackling this question by looking at the mean field theory of simple liquids.

Contributions from Chapter 3

- We consider the dynamics of the mean field p -spin spherical model with transverse forces. The transverse forces are implemented by asymmetrically coupling two replicas of the same model with a coupling strength γ , following Ichiki and Ohzeki [208].
- Using a path-integral approach we derive effective dynamical equation for the response and the spin-spin correlation matrices $\mathbf{R}(t, t')$ and $\mathbf{C}(t, t')$.
- The dynamical equations are studied both numerically, through direct integration, and analytically, through an accidental fluctuation dissipation theorem.
- We find that the system has a dynamical temperature $T_d(\gamma)$, below which ergodicity is broken and dynamical arrest occurs. $T_d(\gamma)$ has the same value as in equilibrium, $T_d(\gamma) = T_d(0)$.
- In the ergodic phase, $T > T(\gamma)$, we find that transverse forces reduce the relaxation time necessary to witness the decay of $\mathbf{C}(t, t')$. Using a perturbative approach, we show that the acceleration at moderate values of γ is given by a rescaling of the relaxation time, $\tau_\alpha(\gamma) \sim \tau_\alpha(0)/(1 + \gamma^2)$.
- As a work in progress, we are considering the dynamics of a particle in high dimensions evolving under the action of a confining harmonic potential, a random Gaussian potential, and a random solenoidal force at finite temperature. Using a path integral formalism, we derive dynamical equations for the response and correlation functions and the mean squared displacement. These equation constitute the starting point for further analyzing these model and its different phases.

CHAPTER 3

CHAPTER 4

PROBING TRANSVERSE FORCES IN DENSE LIQUIDS

4.1	On the choice of \mathbf{A} in three dimensions	48
4.2	Calibration	50
4.3	The behavior of the speedup with temperature	52
4.4	Odd diffusion	53
4.5	Acceleration at large γ	54
4.6	Conclusion and outlook	55

In this Chapter we explore the sampling efficiency of transverse forces in a widely used model for structural glass formers, the binary Kob-Andersen mixture. We numerically implement an overdamped Brownian dynamics with transverse forces, and measure the increase in the longitudinal diffusion constant produced by transverse forces as a proxy of the reduction of the relaxation time of the system. We find that transverse forces maintain an edge over equilibrium dynamics and that, quite surprisingly, the sampling speedup varies non monotonically with the temperature, decreasing as the system becomes more glassy. We characterize the dynamical pathways generated by transverse forces studying the odd diffusivity of the system, a transport coefficient unlocked by the nonequilibrium nature of transverse forces. The behavior of the longitudinal and odd diffusion constants in the glassy regime supports the picture of particles being driven by transverse forces in a swirling motion inside the cage formed by their local neighbours.

We further address the question of how transverse forces perform in a finite-dimensional, structural glass model, by means of numerical simulations. We consider the Kob-Andersen model, which was originally introduced in [159, 160, 161, 162] to test the Mode Coupling theory of the glass transition, a microscopic theory for supercooled liquids, to be addressed later in the thesis. This task was also pursued in [90, 38, 39]. While the seminal papers on the Kob-Andersen mixture addressed the Hamiltonian dynamics of the model, its equilibrium Monte Carlo [35] and overdamped Langevin dynamics [90] have also been extensively studied. The Kob-Andersen model has thus been instrumental in understanding the behavior of structural glasses. A non exhaustive list of applications of this model includes aging [163], the response to an external shear [24], the study of dynamical susceptibilities [27] and novel algorithmic techniques [219, 212] for the preparation of stable glassy states. Variants of this model have also been employed in the study of active glassy systems [186, 77, 76].

The Kob-Andersen model consists of a three-dimensional mixture of two species of particles, labelled A and B respectively, with the interaction potential given by

$$V_{\alpha\beta}(r) = 4\varepsilon_{\alpha\beta} \left[\left(\frac{\sigma_{\alpha\beta}}{r} \right)^{12} - \left(\frac{\sigma_{\alpha\beta}}{r} \right)^6 \right] \theta(2.5\sigma_{\alpha\beta} - r) \quad (4.1)$$

with $\alpha, \beta \in \{A, B\}$ and $\theta(x)$ the Heaviside function. The binary nature of the system allows to explore its dynamics across a wide range of temperature, while avoiding crystallization. The number ratio of particles of type A with respect to particles of type B is 80 : 20. The quantity $\varepsilon_{AA} = 1$ sets the unit of measure of the energy, while the other energy scales are $\varepsilon_{AB} = 1.5$ and $\varepsilon_{BB} = 0.5$. Lengths are measured in units of $\sigma_{AA} = 1$. The other values of the interaction range being $\sigma_{AB} = 0.8$, $\sigma_{BB} = 0.88$.

The transverse force dynamics for this model reads

$$\begin{aligned} \dot{\mathbf{r}}_i^\alpha(t) &= \mu_0(\mathbf{1} + \gamma\mathbf{A})\mathbf{F}_i^\alpha + \sqrt{k_B T \mu_0} \boldsymbol{\xi}_i(t) \\ \mathbf{F}_i^\alpha &\equiv - \sum_{j \neq i} \sum_{\beta=A,B} \nabla_i V(|\mathbf{r}_i^\alpha - \mathbf{r}_j^\beta|) \end{aligned} \quad (4.2)$$

with $\boldsymbol{\xi}_i^\alpha(t)$ a Gaussian white noise with zero mean and correlations $\langle \boldsymbol{\xi}_i^\alpha(t) \otimes \boldsymbol{\xi}_j^\beta(t') \rangle = 1\delta(t-t')\delta_{ij}\delta_{\alpha\beta}$. Temperature is measured in units of ϵ/k_B , and the time is measured in units of $\sigma_{AA}^2/\mu_0\epsilon$.

4.1 On the choice of \mathbf{A} in three dimensions

For a concrete numerical implementation, we need to specify the values of the entries of the matrix \mathbf{A} . For concreteness, we control the strength of the nonequilibrium drive through the parameter γ while imposing the condition that the Frobenius norm of \mathbf{A} is unity, namely

$$\sqrt{\sum_{i,j} A_{ij}^2} = 1. \quad (4.3)$$

Under this condition, the matrix \mathbf{A} reads

$$\mathbf{A} = \begin{bmatrix} 0 & A_{12} & A_{13} \\ -A_{12} & 0 & A_{23} \\ -A_{13} & -A_{23} & 0 \end{bmatrix} \quad (4.4)$$

with $\sqrt{A_{12}^2 + A_{13}^2 + A_{23}^2} = 1$. We now show that upon a suitable set of rotations of coordinates the matrix \mathbf{A} can be recast in a simpler form. Indeed, if \mathbf{R} is an orthogonal matrix representing a rotation in three dimensions, i.e. $\det(\mathbf{R}) = 1$ and $\mathbf{R}^T \mathbf{R} = \mathbf{1}$, then applying \mathbf{R} to both sides of Eq. (4.2) yields (we drop here, without loss of generality, the index encoding the particle type)

$$\dot{\mathbf{r}}'_i = \mu_0 (\mathbf{1} + \gamma \mathbf{A}') \mathbf{F}'_i + \sqrt{2\mu_0 T} \boldsymbol{\xi}'_i \quad (4.5)$$

where we have defined $\mathbf{r}'_i \equiv \mathbf{R}\mathbf{r}_i$, $\mathbf{F}'_i \equiv \mathbf{R}\mathbf{F}_i$, $\boldsymbol{\xi}'_i \equiv \mathbf{R}\boldsymbol{\xi}_i$ and $\mathbf{A}' \equiv \mathbf{R}\mathbf{A}\mathbf{R}^T$. The dynamics in Eq. (4.5) is the same dynamics as Eq. (4.2), in a rotated reference frame. The force \mathbf{F}'_i is still a central force in the rotated reference frame. Using Einstein summation convention, we have

$$\begin{aligned} F'_{i,a} &= \sum_j R_{ab} \partial_{r_{i,b}} V(|\mathbf{r}_i - \mathbf{r}_j|) \\ &= \sum_j R_{ab} \frac{\partial r_{i,b}}{\partial r'_{i,c}} \partial_{r'_{i,c}} V(|\mathbf{r}_i - \mathbf{r}_j|) \\ &= \sum_j R_{ab} R_{bc}^T \partial_{r'_{i,c}} V(|\mathbf{r}'_i - \mathbf{r}'_j|) \\ &= \sum_j \partial_{r'_{i,a}} V(|\mathbf{r}'_i - \mathbf{r}'_j|), \end{aligned} \quad (4.6)$$

and the noises $\boldsymbol{\xi}'_i$ have the same statistics as the noises $\boldsymbol{\xi}_i$:

$$\begin{aligned} \langle \xi'_{i,a}(t) \xi'_{j,b}(t') \rangle &= R_{aa'} R_{bb'} \langle \xi_{i,a'}(t) \xi_{j,b'}(t') \rangle \\ &= R_{aa'} R_{bb'} \delta_{ij} \delta_{a'b'} \delta(t - t') \\ &= \delta_{ij} \delta_{ab} \delta(t - t'), \end{aligned} \quad (4.7)$$

The matrix \mathbf{A}' is still an antisymmetric matrix satisfying Eq. (4.3). Without loss of generality, we can take for \mathbf{A} the following explicit form:

$$\mathbf{A} \equiv \begin{bmatrix} 0 & -1 & 0 \\ 1 & 0 & 0 \\ 0 & 0 & 0 \end{bmatrix}. \quad (4.8)$$

which is mathematically similar to \mathbf{A} in Eq. (4.4) up to a rotation $\mathbf{R} = \mathbf{R}_x(\theta)\mathbf{R}_z(\phi)$, with $\mathbf{R}_x(\theta)$, $\mathbf{R}_z(\phi)$ rotation around the x and z axis respectively, satisfying $\tan(\phi) = -\frac{A_{23}}{A_{13}}$, $\tan(\theta) = -\frac{1}{A_{12}}\sqrt{A_{13}^2 + A_{23}^2}$. Note that for a nonzero matrix \mathbf{A} the system's dynamics is no longer isotropic. It is invariant only by rotation generated by the matrix \mathbf{A} in Eq. (6.2). We identify the plane left invariant by this rotations as the x - y plane.

4.2 Calibration

We simulate the Kob-Andersen mixture under the dynamics given by Eq. (4.2), with the matrix \mathbf{A} given by Eq. (6.2), in a cubic box of size $L = 9.4\sigma_{AA}$ with periodic boundary conditions. Eq. (4.2) is integrated numerically using the Heun [187] algorithm: the position of the particle at time $t + \Delta t$ is predicted using an intermediate step $\mathbf{r}_i^*(t)$, according to the following procedure

$$\begin{aligned}\mathbf{r}_i^*(t) &= \mathbf{r}_i(t) + \Delta t(\mathbf{1} + \gamma\mathbf{A})\mathbf{F}_i(\{\mathbf{r}_j(t)\}_{j=1\dots N}) + \sqrt{2T\Delta t}\mathbf{w}_i(t) \\ \mathbf{r}_i(t + \Delta t) &= \mathbf{r}_i(t) + \frac{\Delta t}{2} \left[\mathbf{F}_i(\{\mathbf{r}_j(t)\}_{j=1\dots N}) + \mathbf{F}_i(\{\mathbf{r}_j^*(t)\}_{j=1\dots N}) \right] + \sqrt{2T\Delta t}\mathbf{w}_i(t).\end{aligned}\quad (4.9)$$

The error introduced by this scheme is of order Δt^2 . The entries of the three-dimensional vector $\mathbf{w}_i(t)$ are independent Gaussian random numbers of mean 0 and unit variance. These numbers can be generated in a computer using random numbers uniformly distributed in the unit interval $(0, 1)$ through the Box-Muller transform [49, 6]. Note that for the algorithm to be unbiased, the random vector $\mathbf{w}_i(t)$ is used both in the intermediate and final updates.

The largest computational cost of the numerical integration comes from the evaluation of the conservative force \mathbf{F}_i . We reduce this cost by employing a Verlet neighbour list [252, 6].

We first calibrate our numerical integration scheme by looking at the structure factor for the particle of species A, $S(q)$, defined as the Fourier transform of the density-density correlation of the system [124]

$$S(q) \equiv \frac{1}{N_A} \sum_{i,j=1}^{N_A} \langle e^{i\mathbf{q} \cdot [\mathbf{r}_i^A - \mathbf{r}_j^A]} \rangle \quad (4.10)$$

where the brackets $\langle \dots \rangle$ denote an average over the Boltzmann distribution ρ_B . Fig. 4.1 compares $S(q)$ at two different temperatures, for $\gamma = 0$ and $\gamma = 8$, the largest value of γ used for long-time numerical integration. The agreement between the curves obtained with the equilibrium and the nonequilibrium dynamics is a demonstration of the fact that the steady state of Eq. (4.2) is indeed the Boltzmann distribution ρ_B . For a fixed value of γ , the agreement of the structure factor with its equilibrium counterpart is used to determine, by trial and error, the largest value of Δt that can be used before observing sensible deviations from the equilibrium case.

A direct inspection of the spectral gap of a many-body interacting system like the Kob-Andersen model is out of reach, whether numerically or analytically. To estimate the speedup of the sampling, we thus use the mean-squared displacement for particles A, $\Delta r^2(t)$,

$$\Delta r^2(t) \equiv \frac{1}{N_A} \sum_{i=1}^{N_A} \langle [\mathbf{r}_i^A(t) - \mathbf{r}_i^A(0)]^2 \rangle. \quad (4.11)$$

Its temperature evolution is shown in Fig. 4.1(b) at equilibrium. As the system is cooled down, the particles pass from a purely diffusive motion throughout the whole

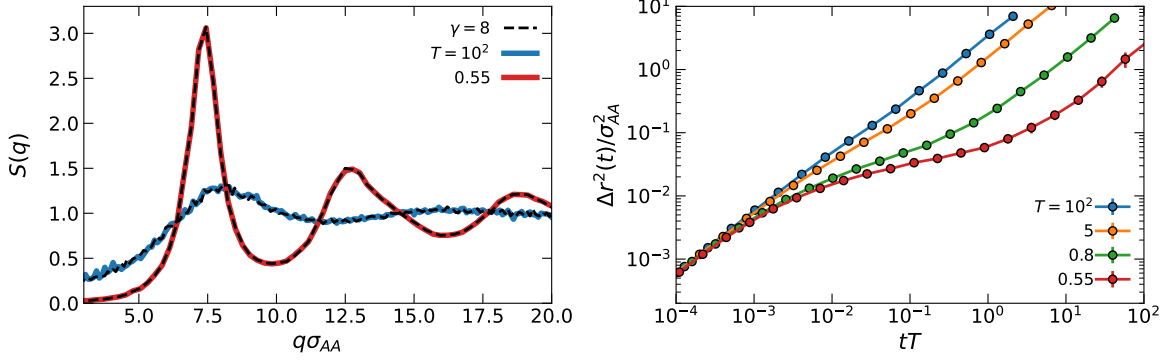


Figure 4.1: (a) Structure factor for particles of type A , at two different temperatures for $\gamma = 0$ (coloured lines) and $\gamma = 8$ (dashed lines). (b) Mean squared displacement for the large particles as a function of time, for $\gamma = 0$.

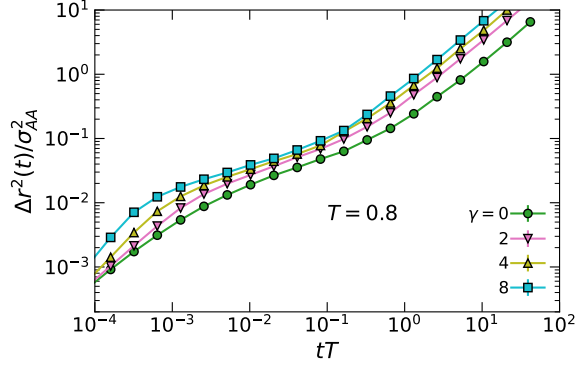


Figure 4.2: Mean-squared displacement of the A particles at $T = 0.8$ for various values of γ .

observation time to a two-step glassy dynamics below the onset temperature near $T \approx 1.0$. Here, the mean-squared displacement grows diffusively up to a plateau, which extends for several decades in time. This regime corresponds to the dynamics of particles trapped inside the cage formed by their local neighbours. At longer times, spatial rearrangement of the particles allow for the escape from the cage: the plateau is subsequently left to enter a long time diffusive regime, where

$$\lim_{t \rightarrow \infty} \Delta r^2(t) = 6D(\gamma, T)t. \quad (4.12)$$

Here $D(\gamma, T)$ is the diffusion constant of the system, which depends on the strength of the nonequilibrium drive and on the temperature.

In Fig. 4.2, we demonstrate that the introduction of transverse forces accelerates the dynamics of the system. This is done by plotting the mean squared displacement $\Delta r^2(t)$ at $T = 0.8$ for various values of γ . We clearly see that transverse forces enhance the diffusion of the particles in the system, and that increasing the strength of the driving increases the speedup.

In this calibration section, we have numerically demonstrated that transverse forces

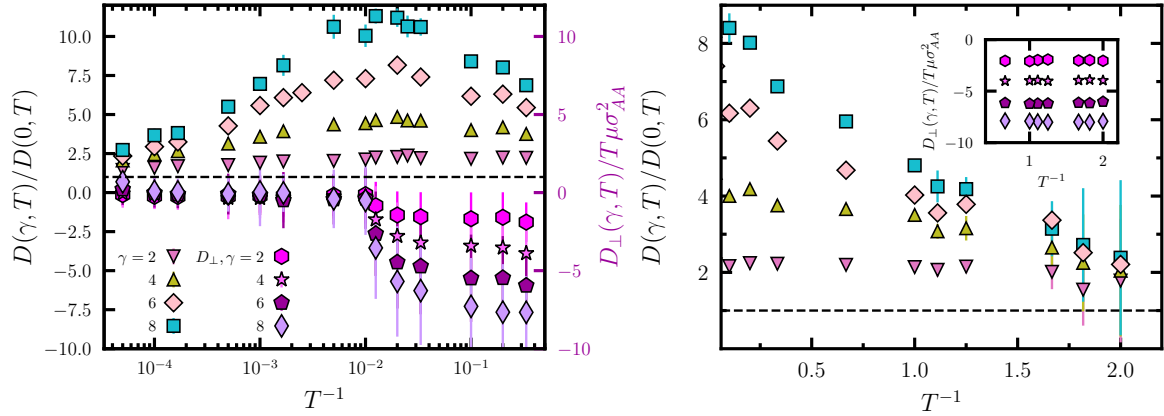


Figure 4.3: (a) Diffusion constant $D(\gamma, T)$ normalised by its equilibrium value at $\gamma = 0$ as a function of inverse temperature. The temperature axis uses a logscale to emphasize the non-monotonic dependence. The right axis describes the odd-diffusivity as a function of T^{-1} for various values of γ . (b) Same as (a) using a linear scale to concentrate on the glassy regime below $T = 1.0$. The black dashed line corresponds to the equilibrium efficiency.

preserve the Boltzmann distribution and speed the dynamics up, enhancing the diffusion of the particles. We now address how the speedup depends on temperature, and how it behaves as we enter in the glassy regime.

4.3 The behavior of the speedup with temperature

To quantify the speedup provided by transverse forces, we extract the diffusion constant, $D(\gamma, T)$, from the long-time limit of the mean-squared displacements, see Fig. 4.3(a). At fixed γ , there exists a temperature near $T^* \approx 100$ that maximizes the increase of the diffusion constant.

At high temperatures, interactions (including chiral ones) are smeared out by thermal noise which degrades the efficiency. The drop of acceleration as the temperature is lowered can be rationalized by the fact that the energy landscape remains unaffected by the transverse forces: when the supercooled regime is entered more deeply, particles spin along circular trajectories within their local cages. Short time trajectories presenting circular motion are shown in Fig. 4.4(a,b). This local motion affects only marginally the cage-breaking process. These two opposite trends account for the existence of an acceleration maximum. The enhancement of the diffusion constant in chiral systems was observed in systems with nonreciprocal interaction [20], or under the influence of an external magnetic field [145], in the dilute phase, and in [77] a non-monotonous behavior for the diffusion constant was observed in systems of dense chiral active Brownian particles. The difference of our work with respect to ones mentioned above is the fact that the Boltzmann distribution is preserved in our system and that, at the same time, we explore regimes where the dynamics is considerably slow.

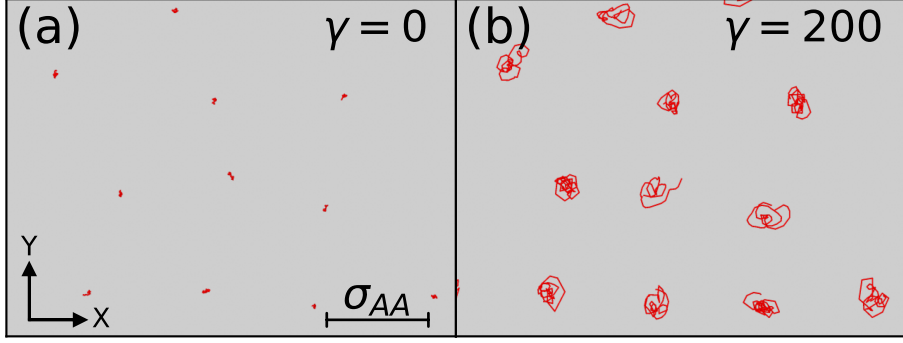


Figure 4.4: (a) Rendering of a short trajectory for a few particles without any transverse force at $T = 0.8$. (b) Same with transverse forces which induce circular trajectories.

In the next Section, we quantify the swirling motion by means of the odd diffusion constant.

4.4 Odd diffusion

To support the picture of a swirling motion inside a local cage we measure the odd diffusivity of the particles A. Odd diffusion is a form of transport which is absent in system with equilibrium dynamics due to Onsager's reciprocity relations. For system out of equilibrium, it manifests itself in the form of a nonzero off-diagonal, anti-symmetric part of the diffusion tensor. Physically, this detects the presence of chiral, swirling motion, and the presence of fluxes perpendicular to concentration gradients arising in the system. At the microscopic level, a Green-Kubo relation, derived in [125] identifies the odd diffusion as the time integral of the anti-symmetric part of the velocity-velocity autocorrelation tensor. Following this approach, we have

$$\mathbf{D}(\gamma, T) \equiv \frac{1}{N_A} \sum_{i=1}^{N_A} \int_0^{+\infty} dt \langle \dot{\mathbf{r}}_i^A(t) \otimes \dot{\mathbf{r}}_i^A(0) \rangle = \frac{D(\gamma, T)}{3} \mathbf{1} + \frac{D_{\perp}(\gamma, T)}{3} \mathbf{A}, \quad (4.13)$$

where $D(\gamma, T)$ is the longitudinal diffusion constant used to study the efficiency of the system, and $D_{\perp}(\gamma, T)$ is the odd diffusion constant. For particles of type A, it reads

$$D_{\perp} = \frac{1}{2N_A} \sum_{i=1}^{N_A} \int_0^{+\infty} dt \langle \dot{y}_i(t) \dot{x}_i(0) - \dot{x}_i(t) \dot{y}_i(0) \rangle. \quad (4.14)$$

By symmetry, D_{\perp} vanishes for an equilibrium dynamics, and its value usefully quantifies the circular motion shown in Fig. 4.4(d). For example, in the limiting case of a particle trapped in a harmonic well, we showed in Chapter 2 that $D_{\perp} = -\mu\gamma T$, with μ the mobility of the particle.

The temperature dependence of D_{\perp} for our simulated system is shown in Fig. 4.3(a) for different values of γ . Its absolute value increases with γ . At fixed γ , the odd

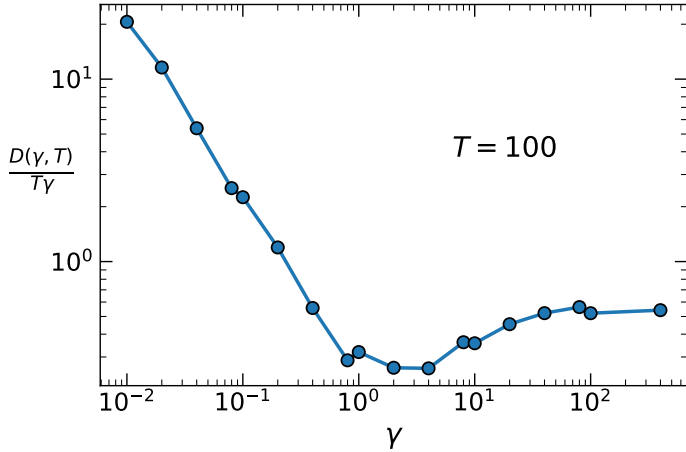


Figure 4.5: Behavior of the ratio $D(\gamma, T)/T\gamma$ measured for $T = 100$ as a function of γ . For large values of γ , we see the scaling $D(\gamma, T) \sim \gamma$.

diffusion starts from 0 at high T : as thermal fluctuations wash out interactions, they also suppress particles' chiral motion, which is induced by transverse forces. The modulus of D_{\perp} rises then steeply as a function of T^{-1} from 0 to a finite value near T^* . As the system enters its slow dynamical regime, D_{\perp} settles to a finite value as shown in the inset of Fig. 4.3(b). Interestingly, the observed behavior in the arrested glass phase, where it is presumably dominated by the in-cage circular motion created by the transverse forces, agrees with the predictions for the harmonic well. This contrasts with the translational diffusion coefficient which changes by orders of magnitude in the supercooled liquid, and vanishes in the glass.

4.5 Acceleration at large γ

How does the speedup behave asymptotically, in the limit of large γ ? Fig. 4.5 addresses this question by showing the behavior of the ratio $\frac{D(\gamma, T)}{\gamma T}$ as a function of γ , evaluated at $T = 100$. For large values of γ this quantity reaches a plateau, signaling the scaling $D(\gamma, T) \sim \gamma$, analogous to the one found for the double-well problem studied in Chapter 2, and by contrast to the naive scaling $D(\gamma, T) \sim \gamma^2$ that would have been guessed using the analysis of the escape rate in Chapter 2.

The scaling discussed here holds upon using physical units of time. In practical implementations, large values of γ produce numerical errors that impede a satisfying convergence to the Boltzmann distribution. Depending on the numerical integration scheme used, an optimal value of γ is expected to exist when the efficiency is measured in units of CPU time.

4.6 Conclusion and outlook

We found that the acceleration provided by transverse forces in a dense interacting system strongly depends on temperature, which comes as a surprise. The acceleration departs from a simple rescaling of the time, due to both interactions and emerging glassiness, which also lead to non-trivial asymptotic scaling with γ . In the glassy phase, the picture unveiled by our exploration is the one of particles swirling in the cage of their local neighbors, the driving injected by transverse forces being too much ‘uninformed’ about the structure of the system to provide a significant gain.

Can we rationalize the results obtained numerically about the efficiency and the transport properties of dense liquids with transverse forces? In the next two Chapters, we will resort to approximate theories of the glass transition to answer this question.

Contributions from Chapter 4

- We numerically integrate the overdamped Langevin dynamics of the Kob-Andersen mixture, a widely used glass-former, with transverse forces.
- We demonstrate the correct sampling of the Boltzmann distribution at finite γ , and witness the speedup provided by transverse forces, probed by looking at the diffusion of the particles in the liquid.
- We measure the diffusion constant $D(\gamma, T)$ as a function of the temperature, and we use it to study the efficiency of transverse forces, defined as $D(\gamma, T)/D(0, T)$.
- We find a surprising nonmonotonous behavior for the efficiency of transverse forces. Starting at high temperatures, the efficiency reaches a maximum in the liquid, and then decreases as the system enters the regime with glassy dynamics.
- We characterize the pathways unlocked by transverse forces by measuring the odd diffusion constant $D_{\perp}(\gamma, T)$, unveiling the swirling motion of the particles.
- We find that the $D(\gamma, T)/T$ starts from 0 at high temperatures, and then rises steeply to a constant value as the temperature is lowered. The steep rise happens around the same temperature of maximal efficiency.
- We assess the asymptotic scaling of the efficiency in the limit of large driving. When $\gamma \rightarrow +\infty$, $D(\gamma, T) \sim \gamma$. This scaling is different from the one guessed using a time rescaling argument, in the spirit of Chapter 2.1.
- Our study suggests that the dynamical pathways unlocked by transverse forces collapse onto closed orbits as the system becomes more glassy, giving rise to the picture of particles swirling inside the cages formed by their local neighbors.

CHAPTER 4

CHAPTER 5

TRANSVERSE FORCES IN LARGE DIMENSIONAL LIQUIDS

5.1	Projection operator formalism	60
5.2	Equations of motion	61
5.3	One-particle process	63
5.4	Two-particle process	66
5.4.1	General formulation	66
5.4.2	Low density expansion of the memory kernel	68
5.5	Dynamical arrest	68
5.5.1	Ergodicity breaking occurs at the same location as in equilibrium	68
5.5.2	A sanity check	70
5.6	Ergodic phase with strong nonequilibrium drive	72
5.7	Mean-squared displacement and diffusion constant	73
5.8	Emergent odd transport	76
5.8.1	Odd diffusivity	76
5.8.2	Odd mobility	77
5.8.3	Odd viscosity	78
5.9	Outlook	80

In this chapter we address the efficiency of transverse forces in a mean field simple liquid, where the disorder is not quenched, as for spin glasses, but self-induced by the amorphous structure of the system. We develop a dynamical mean field theory for simple liquids with transverse forces. The mean field limit is achieved by sending the space dimensions to infinity, while properly rescaling the number density. We quantify the acceleration in terms of the diffusion coefficient of the system, in particular in the vicinity of the glass transition, where the dynamics gets arrested. We also unravel the presence of odd transport coefficients (odd diffusivity, odd viscosity and odd mobility)

and study their behavior close to dynamical arrest. Our analysis sheds light on the nature of the dynamical pathways followed by the liquid, and how they evolve as we approach the phase with broken ergodicity.

In this chapter, we look at the efficiency of transverse forces in a mean field, dense liquid approaching the glass transition. In this system the disorder is self-induced by its own structural and dynamical properties, rather than being due to random quenched interactions as it was the case for the p -spin studied in Chapter 3.

While the physics of dense liquids approaching the glass transition remains a puzzle in finite dimensional systems [235, 47], in the mean field limit a more complete level of understanding is now available [61, 216]. For liquids, the mean field condition can be implemented [98, 169] by sending to infinity the number of spatial dimensions of the system, while properly rescaling the particle density so that the average number of neighbors per particle grows linearly with the dimension. In this limit, the dynamics of the system can be analytically studied [184, 3, 4, 177], and expressions for transport coefficients such as the diffusion constant and the viscosity can be obtained. For equilibrium dynamics, below a dynamical transition temperature, T_d , the diffusion constant vanishes, signalling a dynamical ergodicity breaking. In mean-field this dynamical transition can be inferred from a study of the thermodynamics of the system [190, 217, 216], as it corresponds to the temperature below which infinitely long-lived metastable glassy states appear [197, 94], a situation analogous to the one observed in the p -spin in Chapter 3.

The theoretical framework developed to obtain the aforementioned results makes liquids in high dimension a good candidate to obtain analytical insights on the performance of transverse forces and their transport properties. We develop here a dynamical mean field theory for liquids with transverse forces, and use the diffusion constant to probe the speedup obtained by the nonequilibrium drive. The temperature T_d at which the diffusion constant vanishes and the dynamical glass transition occurs is unaffected by the presence of transverse forces, which is in line with what was found for the p -spin, and with the idea that the infinite-dimensional transition is fully encapsulated in the equilibrium distribution preserved by the transverse forces.

On the physics side, we saw in Chapter 4 that transverse forces give rise to odd diffusivity, but our analytical effort allows to probe also other form of odd transport (mobility [224] and viscosity [13]). These coefficients usually quantify the departure from equilibrium dynamics and explain how the relaxational dynamics is driven by nonequilibrium currents, down to the dynamically arrested phase.

The spirit of the dynamical mean field theory consists in tagging a properly chosen degree of freedom of the system, while treating the other ones as a bath in which the tagged degree of freedom evolves. One thus obtains a generalized Langevin equation for the tagged degree of freedom, with memory kernels that describe the effect of the surrounding, coarse-grained bath. The infinite dimensional limit is then exploited to express these memory kernel in a self consistent manner, typical of the mean field approximation, as functional of the dynamics of the tagged degrees of freedom.

To obtain the aforementioned generalized Langevin equation, we resort to a projector operator formalism. This formalism appears, in a very similar flavour, in the next chapter, when the mode-coupling theory of liquids with transverse forces is addressed. As this formalism appears in two non-overlapping community, the one of mode-coupling

theory and the one of dynamical field theory, We sketch it here briefly, to show the spirit of the procedure.

5.1 Projection operator formalism

In this Section we review, following [227, 254] from a general standpoint the projection operator formalism introduced by Mori and Zwanzig [262]. Consider a generic observable $O(t)$ for a physical system evolving under a deterministic, or stochastic dynamics, and suppose that the evolution of $O(t)$ is governed by a linear operator \mathcal{L} ,

$$\partial_t O(t) = \mathcal{L}O(t) \quad (5.1)$$

with the initial condition $O(0) = O$. A formal solution of Eq. (5.1) is then

$$O(t) = e^{\mathcal{L}t}O \quad (5.2)$$

for stochastic dynamics, \mathcal{L} is a time dependent quantity, and Eq. (5.2) would involve a time ordered integral in the exponential. We will deal with the details of this formulation when dealing with the dynamical mean field theory. Here, for illustration purposes, we assume that \mathcal{L} is time independent.

Eq. (5.2) in the present form, is not very informative. We thus want to derive an effective equation for the observable $O(t)$. To do so, we introduce an operator \mathcal{P} :

$$\mathcal{P}\dots \equiv \langle O^* \dots \rangle \langle O^* O \rangle^{-1} O. \quad (5.3)$$

From a mathematical standpoint, the average $\langle \dots \rangle$ implements a scalar product in the Hilbert space of the observable O . From a physical standpoint, it is usually an average over the steady state distribution, or some constrained version of the latter, as is the case for the dynamical mean field theory. For example, if the steady state distribution of the system of interest has the Boltzmann form $\rho_B(\mathbf{r}^N)$, with \mathbf{r}^N the position of the N particles that constitute the system, a possible choice is $\langle \dots \rangle = \int d\mathbf{r}^N \dots \rho_B(\mathbf{r}^N)$.

From Eq. (5.3), we see that $\mathcal{P}^2 = \mathcal{P}$. \mathcal{P} is thus an operator that projects any quantity along the observable O . The projector operator \mathcal{P} is accompanied by its orthogonal counterpart, $\mathcal{Q} \equiv 1 - \mathcal{P}$.

Another useful tool is the Dyson identity

$$e^{\mathcal{L}t} = e^{\mathcal{Q}\mathcal{L}t} + \int_0^t d\tau e^{\mathcal{L}(t-\tau)} \mathcal{P} \mathcal{L} e^{\mathcal{Q}\mathcal{L}\tau} \quad (5.4)$$

which can be verified by taking a time derivative on both sides.

We can now take the time derivative of Eq. (5.2) and obtain

$$\begin{aligned} \partial_t O(t) &= e^{\mathcal{L}t} (\mathcal{P} + \mathcal{Q}) \mathcal{L} O \\ &= e^{\mathcal{L}t} \mathcal{P} \mathcal{L} O + e^{\mathcal{Q}\mathcal{L}t} \mathcal{Q} \mathcal{L} O + \int_0^t d\tau e^{\mathcal{L}(t-\tau)} \mathcal{P} \mathcal{L} e^{\mathcal{Q}\mathcal{L}\tau} \mathcal{Q} \mathcal{L} O \end{aligned} \quad (5.5)$$

Using the definition of \mathcal{P} in Eq. (5.3) and the fact that $\mathcal{Q} e^{\mathcal{L}\mathcal{Q}t} = \mathcal{Q} e^{\mathcal{Q}\mathcal{L}\mathcal{Q}t}$, we can define a frequency term ω , a memory kernel $K(t)$ and a stochastic force $f(t)$ as

$$\begin{aligned}\omega &\equiv -\langle O\mathcal{L}O \rangle \langle O^*O \rangle^{-1} \\ K(t) &\equiv \langle O\mathcal{L}\mathcal{Q} e^{\mathcal{Q}\mathcal{L}\tau} \mathcal{Q}\mathcal{L}O \rangle \langle O^*O \rangle^{-1} \\ f(t) &\equiv e^{\mathcal{Q}\mathcal{L}\mathcal{Q}t} \mathcal{Q}\mathcal{L}O,\end{aligned}\tag{5.6}$$

so that the effective dynamics for $O(t)$ reads

$$\partial_t O(t) = -\omega O(t) + \int_0^t d\tau K(\tau) O(t-\tau) + f(t).\tag{5.7}$$

The memory kernel $K(t)$ involves the time-correlation of $\mathcal{L}O$ projected in the space orthogonal to O . The dynamics governing this time correlations involves only the degrees of freedom belonging to the space orthogonal to O , due to the presence of the operator $e^{\mathcal{Q}\mathcal{L}\mathcal{Q}t}$. The random force f belongs to the space orthogonal to O , since $\mathcal{P}f(t) = 0$. Eq. (5.7) is thus an effective dynamics for O , where the effect of the degrees of freedom belonging to the space orthogonal to O have been integrated into a memory kernel and a stochastic force.

From Eq. (5.7) we can obtain an equation for the correlation function $C(t) \equiv \langle O^*(0)O(t) \rangle$. By observing that the contribution from the stochastic force is 0, since $f(t)$ belongs to the space orthogonal to O , we get

$$\partial_t C(t) = -\omega C(t) + \int_0^t d\tau K(t-\tau) C(\tau)\tag{5.8}$$

While the frequency ω can be computed exactly given the microscopic details of the dynamics, i.e. from the knowledge of \mathcal{L} , computing the memory kernel K and obtaining the full statistics of the stochastic force $f(t)$ require resorting to approximations schemes, that depend on the model under consideration. For example, in the case of a massive tracer evolving in a bath of light solvent molecules (either passive [250], or active [239]), it may happen that there exists a separation of timescales. In Appendix E, we address this kind of situation for a passive tracer in a bath of active chiral particles. In the case of the dynamical mean field theory, the infinite dimensional limit allows for substantial steps forwards, that are described in this chapter. In finite dimensions, when O encodes the density fluctuations of the system, an approximation schemes such as the mode-coupling approximation are usually employed. A mode-coupling theory for transverse forces is developed in the next chapter.

The above general discussion concludes our review of the projection operator formalism, which is now put to work in studying the dynamics of liquids in large dimensions.

5.2 Equations of motion

Our starting point is an overdamped Langevin dynamics in the presence of transverse forces for a system of interacting particles with positions \mathbf{R}_i in a space of dimension d :

$$\zeta \dot{\mathbf{R}}_i = -(\mathbb{1} + \gamma \mathbf{A}) \nabla U + \boldsymbol{\xi}(t),\tag{5.9}$$

where $U = \sum_{i < j} v(\mathbf{R}_i(t) - \mathbf{R}_j(t))$, with potential v being pairwise and spherically symmetric; ξ is a Gaussian white noise with correlations $\langle \xi(t) \otimes \xi(t') \rangle = 2\zeta T \mathbb{1} \delta(t - t')$, where ζ is the friction coefficient. As in the equilibrium case examined in [3], we will focus on the dynamics of the displacements $\mathbf{u}_i(t) \equiv \mathbf{R}_i(t) - \mathbf{R}_i(0)$ with respect to the initial positions at $t = 0$. We impose that the Frobenius norm of \mathbf{A} is $\|\mathbf{A}\|_F^2 = \sum_{i,j} A_{ij}^2 \sim d$, so that γ alone controls the intensity of the nonequilibrium drive. For convenience we assume that the spatial dimension d is even, and choose the following form of the matrix \mathbf{A} :

$$\gamma \mathbf{A} \equiv \bigoplus_{\alpha=1}^{d/2} \boldsymbol{\Gamma} \quad (5.10)$$

with $\boldsymbol{\Gamma} \equiv \gamma \begin{bmatrix} 0 & -1 \\ 1 & 0 \end{bmatrix}$ a 2×2 matrix. There is no loss of generality in choosing this form, since any antisymmetric matrix of even dimension $\gamma \mathbf{A}$, with a spectrum $\{\pm i \lambda_k\}_{k=1,\dots,d/2}$ can be rewritten via an orthogonal transformation in a block form analogous to the one of Eq. (5.10), with the γ 's replaced by $\gamma \lambda_k$ in each block. As will become clear in the course of the derivation, allowing for $\lambda_k \neq 1$ does not alter the general results discussed in the following sections (but it would require a minor alteration of some explicit formulas).

Due to the structure of \mathbf{A} it is convenient to decompose the vector $\mathbf{u}_i = \bigoplus_{\alpha=1}^{d/2} \mathbf{u}_{i,\alpha}$

$$\zeta \dot{\mathbf{u}}_{i,\alpha}(t) = (\mathbb{1} + \boldsymbol{\Gamma}) \cdot \mathbf{F}_{i,\alpha}(t) + \xi_{i,\alpha}(t), \quad (5.11)$$

where for a given d -dimensional vector \mathbf{x} we have introduced its components $\mathbf{x}_\alpha = (x_{2\alpha-1}, x_{2\alpha})^T \equiv (x_\alpha^{(1)}, x_\alpha^{(2)})^T$, a set of $d/2$ two-dimensional vectors containing the directions that affect each other non reciprocally via the transverse force. By construction it follows that $\mathbf{x} = \bigoplus_{\alpha=1}^{d/2} \mathbf{x}_\alpha$.

We first discuss the scaling of the various parameters with spatial dimension d so that the resulting $d \rightarrow \infty$ dynamics retains interesting many-body features. First, we recall the specifics of the large d limit of equilibrium dynamics. As in finite dimensional models, each particle interacts with typically d neighbors. The notion of neighbor makes sense when the range ℓ of the pair interaction potential is finite, as assumed here. Then the typical number of neighbors per particle is $\rho V_d(\ell)$ where $V_d(\ell) = \frac{\pi^{d/2}}{\Gamma(d/2+1)} \ell^d$ is the volume of the interaction sphere. As $d \rightarrow \infty$ we want to maintain $\rho V_d(\ell)$ of order d^1 . Then, to ensure that the energy is extensive in the number dN of degrees of freedom, the pair potential $v(r)$ needs to admit the following scaling behavior,

$$v(r) \equiv \bar{v}(h), \quad h = d \left(\frac{r}{\ell} - 1 \right), \quad (5.12)$$

where $\bar{v}(h)$ remains finite as $d \rightarrow \infty$. This implies that the forces scale as $v'(r) \sim d \bar{v}'(h) \sim d$. On the other hand, the displacement $\Delta r \equiv |\mathbf{r}_0^{(a)} + \mathbf{u}^{(a)}| - r_0$ of a given particle is of order d^{-1} , as h needs to be of order unity. It follows then from the expansion $\Delta r \approx \hat{\mathbf{r}} \cdot \mathbf{u} + \frac{\mathbf{u}^2}{2r_0}$ that $u_\mu^{(a)} \sim d^{-1}$. To keep all the terms of Eq. (5.11) of the same order in d , we need to scale the friction as $\zeta = \hat{\zeta} d^2$. Finally, we need to discuss the main new element in Eq. (5.11), *i.e.* the transverse forces. With our choice (5.10) of matrix \mathbf{A} , in order for these forces to act in a nontrivial yet non singular way, we need to keep γ fixed as $d \rightarrow +\infty$.

5.3 One-particle process

We consider $N + 1$ particles labeled by $i = 0, \dots, N$ and we now proceed to derive in the infinite dimensional limit an exact equation for a tagged, appropriate degree of freedom pertaining to particle 0. In an equilibrium setting, the authors of [177] understood that the proper cavity variable could not be a full d -dimensional position vector (because the number of degrees of freedom of the cavity cannot be extensive in d). In our situation, however, we identify the proper degree of freedom to be the vectors $\mathbf{u}_{0,\alpha} = (u_{0,2\alpha-1}, u_{0,2\alpha})^T$, with α fixing the pair of space directions.

With this identification, we start by writing a Liouville operator $L(t)$ governing the dynamics of the $N + 1$ particles:

$$L(t) \equiv \sum_{i=0}^N \sum_{\mu=1}^{d/2} \frac{1}{\zeta} \left[-(\mathbf{1}_2 + \boldsymbol{\Gamma}) \cdot \nabla_{i,\mu} U(t) + \boldsymbol{\xi}_{i,\alpha}(t) + T \nabla_{i,\mu} \right]^T \cdot \nabla_{i,\mu} \quad (5.13)$$

for a given realization of the stochastic forces. Then one can write for a generic vector $\mathbf{x}_{i,\mu}(t) = \mathcal{U}[L](t, 0) \cdot \mathbf{x}_{i,\mu}$, where $\mathbf{x}_{i,\mu} \equiv \mathbf{x}_{i,\mu}(0)$ and

$$\mathcal{U}[L](t, 0) \equiv \exp \left(\mathcal{T} \int_0^t d\tau L(\tau) \right). \quad (5.14)$$

The operator \mathcal{T} is the time ordering operator from left to right, so that $\partial_t \mathcal{U}(t, 0) = \mathcal{U}(t, 0) L(t)$ [141].

We associate to the Liouvillian operator an irreducible version L^{irr} :

$$\begin{aligned} L^{\text{irr}}(t) &\equiv L(t) - \delta L(t), \\ \delta L(t) &\equiv \frac{1}{\zeta} \left[-(\mathbf{1}_2 + \boldsymbol{\Gamma}) \cdot \nabla_{0,\alpha} U(t) + \boldsymbol{\xi}_{0,\alpha}(t) + T \nabla_{0,\alpha} \right]^T \cdot \mathcal{P} \cdot \nabla_{0,\alpha} \end{aligned} \quad (5.15)$$

where the projection operator \mathcal{P} is defined by

$$\begin{aligned} \mathcal{P}\mathbf{x}(t) &\equiv \left\langle \frac{\int d\mathbf{r}_0^\perp \prod_{i>0,\mu} d\mathbf{r}_{i,\mu} e^{-\beta U} \mathbf{x}(t)}{\int d\mathbf{r}_0^\perp \prod_{i>0,\mu} d\mathbf{r}_{i,\mu} e^{-\beta U}} \right\rangle_{\boldsymbol{\xi}_0, \dots, \boldsymbol{\xi}_N} \\ &\equiv \langle \mathbf{x}(t) \rangle_0, \end{aligned} \quad (5.16)$$

where $d\mathbf{r}_0^\perp \equiv \prod_{\mu \neq \alpha} d\mathbf{r}_{0,\mu}$ indicates integration over all the component of particle 0 with the exclusion of the pair of tagged directions α . The average $\langle \dots \rangle_{\boldsymbol{\xi}_0, \dots, \boldsymbol{\xi}_N} \equiv \langle \dots \rangle_0$ is an average over realizations of the noise of all the particle and coordinates, including the tagged one. In short, \mathcal{P} averages over all the degrees of freedom except for the tagged ones.

We now express the force $\nabla_{0,\alpha} U(t)$ using the irreducible Liouvillian. To do this, we exploit the identity

$$\mathcal{U}([L](t; 0)) = \mathcal{U}([L^{\text{irr}}](t; 0)) + \int_0^t d\tau \mathcal{U}([L](\tau; 0)) \delta L(\tau) \mathcal{U}([L^{\text{irr}}](t; \tau)), \quad (5.17)$$

which is a generalization of the Dyson identity written in Eq. (5.4), to write

$$-(\mathbf{1}_2 + \boldsymbol{\Gamma}) \cdot \nabla_{0,\alpha} U(t) = -(\mathbf{1}_2 + \boldsymbol{\Gamma}) \cdot \nabla_{0,\alpha} U^\dagger(t) - \int_0^t d\tau \mathcal{U}[L](\tau, 0) \delta L(\tau) \mathcal{U}[L^{\text{irr}}](t, \tau) (\mathbf{1}_2 + \boldsymbol{\Gamma}) \cdot \nabla_{0,\alpha} U, \quad (5.18)$$

where we defined $\nabla_{0,\alpha} U^\dagger(t) \equiv \mathcal{U}[L^{\text{irr}}](t, 0) \cdot \nabla_{0,\alpha} U$. We show in what follows that the first and second terms on the right hand side of Eq. (5.18) are respectively a fluctuating force and an effective friction. In order to make this identification explicit, we simplify the term under the integral of Eq. (5.18) into

$$\begin{aligned} & \left\{ \mathcal{U}[L](\tau, 0) \delta L(\tau) \mathcal{U}[L^{\text{irr}}](t, \tau) (\mathbf{1}_2 + \boldsymbol{\Gamma}) \cdot \nabla_{0,\alpha} U \right\}^{(a)} = \beta \\ & \times \left\{ (\mathbf{1}_2 + \boldsymbol{\Gamma}) \cdot \left\langle \nabla_{0,\alpha} U^\dagger(t - \tau) \otimes \nabla_{0,\alpha} U^\dagger \right\rangle_0 \cdot \dot{\mathbf{u}}_{0,\alpha}(\tau) \right\}^{(a)}, \end{aligned} \quad (5.19)$$

where we recall that $u_\alpha^{(a)}$ is the a -th component of the two dimensional vector \mathbf{u}_α . Eq. (5.11) for the coordinate α of particle 0 reads

$$\begin{aligned} \zeta \dot{\mathbf{u}}_{0,\alpha}(t) &= -(\mathbf{1}_2 + \boldsymbol{\Gamma}) \cdot \nabla_{0,\alpha} U^\dagger(t) \\ &- \beta \int_0^t d\tau (\mathbf{1}_2 + \boldsymbol{\Gamma}) \cdot \left\langle \nabla_{0,\alpha} U^\dagger(t - \tau) \otimes \nabla_{0,\alpha} U^\dagger \right\rangle_0 \cdot \dot{\mathbf{u}}_{0,\alpha}(\tau) \\ &+ \boldsymbol{\xi}_{0,\alpha}(t). \end{aligned} \quad (5.20)$$

It is important to realize that so far Eq. (5.20) is exact. This equation expresses the decomposition of a force into the sum of an effective noise and of a friction term, as customarily obtained through the projection operator formalism [261]. However, we shall establish that in the infinite dimensional limit the memory kernel is further simplified by substituting $\nabla_{0,\alpha} U^\dagger(t)$ with $\nabla_{0,\alpha} \tilde{U}(t)$, the force exerted by the fluid where the coordinates α of particle 0 have been fixed. To do so we first fully write the expression of L^{irr} , with $\mathcal{Q} \equiv 1 - \mathcal{P}$:

$$\begin{aligned} L^{\text{irr}}(t) &= \frac{1}{\zeta} [-(\mathbf{1}_2 + \boldsymbol{\Gamma}) \cdot \nabla_{0,\alpha} U + \boldsymbol{\xi}_{0,\alpha}(t) + T \nabla_{0,\alpha}]^T \cdot \mathcal{Q} \nabla_{0,\alpha} \\ &+ \sum_{\mu \neq \alpha}^{d/2} \frac{1}{\zeta} [-(\mathbf{1}_2 + \boldsymbol{\Gamma}) \cdot \nabla_{0,\mu} U + \boldsymbol{\xi}_{0,\mu}(t) + T \nabla_{0,\mu}]^T \cdot \nabla_{0,\mu} \\ &+ \sum_{i>0}^N \sum_{\mu=1}^{d/2} \frac{1}{\zeta} [-(\mathbf{1}_2 + \boldsymbol{\Gamma}) \cdot \nabla_{i,\mu} U + \boldsymbol{\xi}_{i,\mu}(t) + T \nabla_{i,\mu}]^T \cdot \nabla_{i,\mu} \\ &\equiv \frac{1}{\zeta} [-(\mathbf{1}_2 + \boldsymbol{\Gamma}) \cdot \nabla_{0,\alpha} U + \boldsymbol{\xi}_{0,\alpha}(t) + T \nabla_{0,\alpha}]^T \cdot \mathcal{Q} \nabla_{0,\alpha} \\ &+ L^0(t), \end{aligned} \quad (5.21)$$

from which we see that $\nabla_{0,\alpha} \tilde{U}(t) = \mathcal{U}[L^0](t, 0) \nabla_{0,\alpha} U$. By using the last line of Eqs. (5.17, 5.21) we can express the force $\nabla_{0,\alpha} U^\dagger(t)$ in terms of a Dyson series

$$\begin{aligned} \nabla_{0,\alpha} U^\dagger(t) &= \nabla_{0,\alpha} \tilde{U}(t) \\ &+ \int_0^t d\tau \mathcal{U}[L^0](t, \tau) \frac{1}{\zeta} \left[(\mathbf{1}_2 + \boldsymbol{\Gamma}) \cdot \nabla_{0,\alpha} U + \boldsymbol{\xi}_{0,\alpha}(\tau) + T \nabla_{0,\alpha} \right]^T \cdot \mathcal{Q} \nabla_{0,\alpha} \mathcal{U}[L^0](\tau, 0) \nabla_{0,\alpha} U \\ &+ \dots \end{aligned} \quad (5.22)$$

We now argue that all the terms of this series excluding the first are sub-leading in the infinite dimensional limit, provided that this limit is taken for a finite time t . For example, the second term of the series can be rewritten as

$$\int_0^t d\tau \mathcal{U}[L^0](t, \tau) \frac{1}{\zeta} \left[(\mathbf{1}_2 + \boldsymbol{\Gamma}) \cdot \nabla_{0,\alpha} U + \boldsymbol{\xi}_{0,\alpha}(\tau) + T \nabla_{0,\alpha} \right]^T \cdot \left[[\tilde{\mathbf{k}}_\alpha(\tau) - \langle \tilde{\mathbf{k}}_\alpha(\tau) \rangle_0] \right], \quad (5.23)$$

where $\tilde{k}_\alpha^{(ab)}(0) \equiv \sum_{j>0} \nabla_\alpha^{(a)} \nabla_\alpha^{(b)} v(r_{0j}^{(ab)}) \delta_{ab}$. The fluctuations of this term are of order $d^{3/2}$. Therefore for finite times the integral scales as $\frac{1}{d} d^{3/2} \sim d^{1/2}$, and is sub-leading compared to the first term of the series which is of order d . Terms of the series of order n all contain additional powers of the friction coefficient ζ , leading to the scaling $d^{3/2-n}$. In conclusion, we can rewrite Eq. (5.20) as

$$\begin{aligned} \zeta \dot{\mathbf{u}}_{0,\alpha}(t) &= -(\mathbf{1}_2 + \boldsymbol{\Gamma}) \cdot \nabla_{0,\alpha} \tilde{U}(t) \\ &\quad - \beta \int_0^t d\tau (\mathbf{1}_2 + \boldsymbol{\Gamma}) \cdot \langle \nabla_{0,\alpha} \tilde{U}(t-\tau) \otimes \nabla_{0,\alpha} \tilde{U} \rangle_0 \cdot \dot{\mathbf{u}}_{0,\alpha}(\tau) \\ &\quad + \boldsymbol{\xi}_{0,\alpha}(t). \end{aligned} \quad (5.24)$$

We have thus obtained an effective equation for the degree of freedom $\mathbf{u}_{0,\alpha}(t)$, the coordinates α of the position for particle 0. The force-force correlation can be rewritten as

$$\begin{aligned} \langle \nabla_{0,\alpha}^{(a)} \tilde{U}(t) \nabla_{0,\alpha}^{(b)} \tilde{U} \rangle_0 &= \left\langle \sum_{i,j \neq 0} \nabla_{0,\alpha}^{(a)} v(\tilde{r}_{0i}(t)) \nabla_{0,\alpha}^{(b)} v(\tilde{r}_{0j}) \right\rangle_0 \\ &= \left\langle \sum_{i \neq 0} \nabla_{0,\alpha}^{(a)} v(\tilde{r}_{0i}(t)) \nabla_{0,\alpha}^{(b)} v(\tilde{r}_{0i}) \right\rangle_0 \\ &= \frac{2}{d} \left\langle \sum_{\mu=1}^{d/2} \sum_{i \neq 0} \nabla_{0,\mu}^{(a)} v(\tilde{r}_{0i}(t)) \nabla_{0,\mu}^{(b)} v(\tilde{r}_{0i}) \right\rangle_0 \\ &= \frac{2}{dN} \left\langle \sum_{\mu=1}^{d/2} \sum_{i \neq 0} \nabla_{0,\mu}^{(a)} v(r_{0i})(t) \nabla_{0,\mu}^{(b)} v(r_{0i}) \right\rangle \\ &\equiv M^{(ab)}(t), \end{aligned} \quad (5.25)$$

where we have used, in order:

- the fact that force between particle 0 and particle i and the force between particle 0 and particle j are uncorrelated, for $i \neq j$, in the large dimensional limit;
- the equivalent roles played by the $d/2$ blocks;
- the fact that in the large dimensional limit the average $\langle \dots \rangle_{0,\alpha}$ over the dynamics with the frozen direction α of particle 0 can be replaced by an average over the dynamics of the full, unfrozen system, and that such an average can be carried out for all the N particles of the system.

Moreover, we observe that in the high dimensional limit the force $\nabla_{0,\alpha} \tilde{U}(t)$ has a zero average, and its statistics are entirely determined by its second moment. The

dynamical equation obtained for particle 0 can be generalized to any particle in the liquid, since they are all identical. The resulting equation reads

$$\begin{aligned} \zeta \dot{\mathbf{u}}_{i,\alpha} &= -\beta \int_0^t d\tau (\mathbf{1} + \boldsymbol{\Gamma}) \cdot \mathbf{M}(t - \tau) \dot{\mathbf{u}}_{i,\alpha}(\tau) + \boldsymbol{\Xi}_{i,\alpha}(t) \\ \langle \boldsymbol{\Xi}_{i,\alpha}(t) \rangle &= 0 \\ \langle \boldsymbol{\Xi}_{i,\alpha}(t) \otimes \boldsymbol{\Xi}_{j,\beta}(t') \rangle &= \delta_{ij} \delta_{\alpha\beta} \left[2T\zeta \mathbf{1}_d \delta(t - t') + (\mathbf{1}_2 + \boldsymbol{\Gamma}) \cdot \mathbf{M}(t - t') \cdot (\mathbf{1}_2 + \boldsymbol{\Gamma}^T) \right]. \end{aligned} \quad (5.26)$$

The memory kernel $\mathbf{M}(t)$ encoding pairwise force-force correlations is self-consistently determined by the dynamics of two interacting particles. The latter can be obtained from the microscopic dynamics in the same way as in Eq. (5.26). However, we first observe that the memory kernel at the initial time is completely determined by the equilibrium properties of the system. Therefore, it has the same expression as its equilibrium counterpart, and in particular it is diagonal:

$$\mathbf{M}(0) = \mathbf{1}_2 \frac{\rho}{d} \int d\mathbf{r}_0 g(\mathbf{r}_0) |v'(r_0)|^2, \quad (5.27)$$

with $g(\mathbf{r}) = e^{-\beta v(r)}$ the radial distribution function in the infinite-dimensional limit. The physical simplifying idea that we use to proceed is that a diagonal kernel at initial times implies, in the large dimensional limit, a diagonal kernel at successive times. In the following Section, we will derive the equations of motion for the two particle process under the self consistent assumption of a diagonal kernel $\mathbf{M} = \mathbf{1}M(t)$. In this case the dynamics for the full displacement of particle i in d dimensions reads

$$\begin{aligned} \zeta \mathbf{u}_i(t) &= -\beta \int_0^t d\tau M(t - \tau) (\mathbf{1}_d + \gamma \mathbf{A}) \cdot \dot{\mathbf{u}}_i(\tau) + \boldsymbol{\Xi}(t) \\ \langle \boldsymbol{\Xi}_i(t) \otimes \boldsymbol{\Xi}_j(t) \rangle &= \mathbf{1}_d \delta_{ij} \left[2T\zeta \delta(t - t') + (1 + \gamma^2) M(t - t') \right] \\ M(t) &= \frac{\rho}{d} \int d\mathbf{r}_0 g(\mathbf{r}_0) \langle \hat{\mathbf{r}}(t) v'(r(t)) \rangle_{\mathbf{r}_0} \cdot \hat{\mathbf{r}}_0 v'(r_0), \end{aligned} \quad (5.28)$$

where the definition of the kernel $M(t)$ comes from an extension by continuity of Eq. (5.27).

5.4 Two-particle process

5.4.1 General formulation

We consider two particles, which we label 0 and 1, and we focus on the dynamics of their separation $\mathbf{r}(t) \equiv \mathbf{R}_0(t) - \mathbf{R}_1(t)$. A derivation analogous to the one performed for the one-particle process, along the lines of [177], gives:

$$\begin{aligned} \frac{\zeta}{2} \dot{\mathbf{r}} &= -(\mathbf{1}_d + \gamma \mathbf{A}) \hat{\mathbf{r}} v'(r(t)) - \frac{\beta}{2} \int_0^t d\tau M(t - \tau) (\mathbf{1}_d + \gamma \mathbf{A}) \dot{\mathbf{r}}(\tau) + \sqrt{2} \boldsymbol{\Xi}(t) \\ \langle \boldsymbol{\Xi}(t) \otimes \boldsymbol{\Xi}(t') \rangle &= \mathbf{1}_d \left[2T\zeta \delta(t - t') + (1 + \gamma^2) M(t - t') \right]. \end{aligned} \quad (5.29)$$

Equation (5.29) can intuitively be derived from the one-particle process of Eq. (5.28), singling the force between particles 0 and 1 out of the expression of M . This is a legitimate operation which yields a negligible correction in the large dimensional limit.

From Eq. (5.29) using Itō calculus one can obtain equations of motion for the dynamics of the distance $r = \|\mathbf{r}\|$ and the unit vector $\hat{\mathbf{r}}$ along \mathbf{r} :

$$\begin{aligned} \frac{\zeta}{2} \dot{r}(t) &= \frac{T(d-1)}{r(t)} - \frac{\beta}{2} \int_0^t d\tau M(t-\tau) \hat{\mathbf{r}}(\tau) \cdot (\mathbf{1}_d + \gamma \mathbf{A}) \dot{\mathbf{r}}(\tau) + \sqrt{2} \hat{\mathbf{r}}(t) \cdot \boldsymbol{\Xi}(t) \\ \frac{\zeta}{2} \dot{\hat{\mathbf{r}}}(t) &= -\frac{T(d-1)}{r(t)^2} \hat{\mathbf{r}}(t) - \gamma \mathbf{A} \hat{\mathbf{r}}(t) v'(r(t)) \\ &\quad - \frac{\beta}{2r(t)} \int_0^t d\tau M(t-\tau) \cdot \mathbf{\Pi}_{\perp}(t) (\mathbf{1}_d + \gamma \mathbf{A}) \dot{\mathbf{r}}(\tau) \\ &\quad + \sqrt{2} \mathbf{\Pi}_{\perp}(t) \cdot \boldsymbol{\Xi}(t), \end{aligned} \quad (5.30)$$

with $\mathbf{\Pi}_{\perp}(t) \equiv \mathbf{1}_d - \hat{\mathbf{r}}(t) \otimes \hat{\mathbf{r}}(t)$ the operator projecting along a direction orthogonal to $\hat{\mathbf{r}}(t)$. At $t = 0$ the dynamics of $\hat{\mathbf{r}}$ reads

$$\frac{\zeta}{2} \dot{\hat{\mathbf{r}}}(0) = -\frac{T(d-1)}{r(0)^2} \hat{\mathbf{r}}(0) - \gamma \mathbf{A} \hat{\mathbf{r}}(0) v'(r(0)) + \sqrt{2} \mathbf{\Pi}_{\perp}(t) \cdot \boldsymbol{\Xi}(0). \quad (5.31)$$

The left hand side of this equation scales as $d^{3/2}$, while the right hand side contains terms of order at most d . We therefore conclude that the orientation of the vector \mathbf{r} does not change to leading order in d with respect to its initial orientation. We can thus assume that $\hat{\mathbf{r}}(t) = \hat{\mathbf{r}}(0)$ at all times. Then the evolution of $\hat{\mathbf{r}}(t)$ in Eq. (5.30) becomes

$$\begin{aligned} \frac{\zeta}{2} \dot{\hat{\mathbf{r}}}(t) &= -\frac{T(d-1)}{r(t)^2} \hat{\mathbf{r}}(0) - \gamma \mathbf{A} \hat{\mathbf{r}}(0) v'(r(t)) - \frac{\gamma \beta}{2r(t)} \int_0^t d\tau M(t-\tau) \mathbf{A} \dot{\mathbf{r}}(\tau) \\ &\quad + \sqrt{2} \mathbf{\Pi}_{\perp}(t) \cdot \boldsymbol{\Xi}(t). \end{aligned} \quad (5.32)$$

The scaling for the different terms reads as above, and the new term introduced, which is of order $d^2 \times d^{-1} = d$, remains subleading. This proves self-consistently that, as was the case in equilibrium, the orientation of the inter particle separation is constant throughout the dynamics, which was not an *a priori* expected property due to the presence of transverse forces. The equation for the interparticle distance reads:

$$\begin{aligned} \frac{\zeta}{2} \dot{r}(t) &= -v'(r(t)) - \frac{T(d-1)}{r(t)} - \frac{\beta}{2} \int_0^t d\tau M(t-\tau) r(\tau) + \sqrt{2} \Xi(t) \\ \langle \Xi(t) \Xi(t') \rangle &= 2T\zeta \delta(t-t') + (1+\gamma^2) M(t-t') \\ M(t) &= \frac{\rho \Omega_d}{d} \int dr_0 g(r_0) \langle v'(r(t)) \rangle_{r_0} v'(r_0). \end{aligned} \quad (5.33)$$

Note that the two-particle process is still an out of equilibrium one, since the noise and the friction terms do not respect the fluctuation-dissipation theorem. One expects therefore a different value of the memory kernel $M(t)$ compared to the $\gamma = 0$ case. The analytical determination of $M(t)$ at all times is an open question, even in the equilibrium case, where progress has been made either by numerical integration or by a low density expansion [185]. We turn to the latter approach, in order to produce an expression of $M(t)$ which will be useful in the following sections, where we discuss the efficiency of the transverse forces.

5.4.2 Low density expansion of the memory kernel

The main idea is to expand the memory kernel in the form of a perturbative series

$$M(t) = \sum_{n=1}^{\infty} M^{(n)}(t), \quad (5.34)$$

where $M^{(n)} \sim O(\rho^n)$ can be self-consistently determined from the two particle process given by Eq. (5.33), evaluated up to order $O(\rho^{n-1})$. Therefore, the lowest order $M^{(1)}$ is determined by the process

$$\begin{aligned} \frac{\zeta}{2} \dot{r}^{(0)}(t) &= \frac{T(d-1)}{r^{(0)}(t)} - v'(r^{(0)}(t)) + \sqrt{2}\Xi^{(0)}(t) \\ \langle \Xi^{(0)}(t)\Xi^{(0)}(t') \rangle &= 2T\zeta\delta(t-t'), \end{aligned} \quad (5.35)$$

which is the same as the one obtained at equilibrium [185]. Low densities suppress the action of transverse forces at the level of the two-body process. In particular, one can consider the case of a linear potential $v(r) = \epsilon(\frac{r}{\ell} - 1)$, for which $M^{(1)}(t)$ was determined in Ref. [185]. We give here the expression of its time integral $\widehat{M^{(1)}} \equiv \int_0^{+\infty} dt M^{(1)}(t)$, which will be useful later. It reads

$$\beta \widehat{M^{(1)}} = \frac{\widehat{\phi}}{2} \frac{\beta^2(2+\beta)}{(1+\beta)^3}, \quad (5.36)$$

with $\widehat{\phi} \equiv \rho V_d \frac{\ell^d}{d}$ the rescaled packing fraction, and with V_d the volume of a sphere of unit radius in d dimensions. Below, we will address the issues of the long time limit of M and of its asymptotic behavior as γ goes to infinity.

5.5 Dynamical arrest

5.5.1 Ergodicity breaking occurs at the same location as in equilibrium

The mean field glass transition in fluids can be found by looking at the long time behavior of $M(t)$. Following the existing literature [115, 216] we split the kernel M into a decaying part and an asymptotic plateau value at t becomes large: $M(t) = M_f(t) + M_p$, with $M_f(t \rightarrow \infty) = 0$ and $M_p \geq 0$ a constant. A glass transition occurs when the density or the temperature of the system are such that $M_p > 0$. In this Section we will show that this happens at the same parameters as for equilibrium dynamics.

The plateau value M_p is given by:

$$M_p = \lim_{t \rightarrow \infty} M(t) = \frac{\rho}{d} \int d\mathbf{r}_0 \langle v'(r) \rangle_{ss} v'(r_0), \quad (5.37)$$

where $\langle \dots \rangle_{\text{ss}}$ is an average over the steady state value of the dynamics for the distance between two particles, given by Eq. (5.29). Such a steady state distribution depends on the value of M_p , thus yielding a self-consistent relation that can be exploited to determine the plateau value.

Using the aforementioned decomposition for $M(t)$ the equation of motion for \mathbf{r} can be rewritten as a nonequilibrium dynamics for a particle in d dimensions inside an effective potential $w(\mathbf{r})$, under the action of a constant Gaussian drift Ξ_p (induced by the long time dynamics of $M(t)$) and fluctuating Gaussian noises Ξ_f, ξ with eventually decaying correlations:

$$\frac{\zeta}{2}\dot{\mathbf{r}} = (\mathbf{1}_d + \gamma\mathbf{A}) \cdot \left[-\nabla w(\mathbf{r}) - \frac{\beta}{2} \int_0^t d\tau M_f(t-\tau) \dot{\mathbf{r}}(\tau) + \Xi_f(t) \right] + \sqrt{T}\xi(t), \quad (5.38)$$

with

$$w(\mathbf{r}) = v(|\mathbf{r}|) + \frac{\beta}{4}M_p[\mathbf{r} - \mathbf{r}_0]^2 + \Xi_p \cdot \mathbf{r}, \quad (5.39)$$

the correlations of the constant random drive Ξ_p and the time dependent noises $\Xi_f(t)$, $\xi(t)$ being respectively $\langle \xi(t) \otimes \xi(t') \rangle = \mathbf{1}_d T \zeta \delta(t-t')$, $\langle \Xi_f(t) \otimes \Xi_f(t') \rangle = \mathbf{1}_d \frac{1}{2} M_f(t-t')$, $\langle \Xi_p \otimes \Xi_p \rangle = \mathbf{1}_d \frac{1}{2} M_p$.

We briefly review the equilibrium case ($\gamma = 0$) for which we have

$$\frac{\zeta}{2}\dot{\mathbf{r}} = -\nabla w(\mathbf{r}) - \frac{\beta}{2} \int_0^t d\tau M_f(t-\tau) \dot{\mathbf{r}}(\tau) + \Xi_f(t) + \sqrt{T}\xi(t). \quad (5.40)$$

This is an equilibrium dynamics with memory under an external potential $w(\mathbf{r})$. The equilibrium distribution is the Boltzmann one:

$$p_B(\mathbf{r}|M_p, \Xi_p, \mathbf{r}_0) \equiv \frac{e^{-\beta w(\mathbf{r})}}{\int d\mathbf{r} e^{-\beta w(\mathbf{r})}}. \quad (5.41)$$

We note that the steady state distribution depends on the plateau value of the memory kernel, and it is conditioned on the realizations of the field Ξ_f and on the initial condition \mathbf{r}_0 . The steady state value of the force appearing in the self-consistent equation Eq. (5.37) is

$$\langle v'(r) \rangle_{\text{eq}, \mathbf{r}_0} = \frac{1}{(\pi M_p)^{d/2}} \int d\Xi_p e^{-\frac{\Xi_p^2}{M_p}} \int d\mathbf{r} p_B(\mathbf{r}, |M_p, \Xi_p, \mathbf{r}_0) v'(|\mathbf{r}|). \quad (5.42)$$

Substitution in Eq. (5.37) yields the desired self-consistent relation. We refer the reader to Refs. [184, 216] for a detailed discussion of its solution. Here it is sufficient to use the fact that Eq. (5.37) admits a nonzero value for M_p below a critical temperature (or above a critical density ρ_d) T_d , meaning that the system is no longer ergodic below T_d (above ρ_d).

After having reviewed the equilibrium limit, we now return to the $\gamma \neq 0$ case of interest. The steady state distribution of the process given by Eq. (5.38) is the same as the equilibrium one. This means that the self-consistent relation given by Eq. (5.37) yields a nonzero value of M_p for the same critical parameter as in the equilibrium dynamics, thus proving the statement that opened this Section. This reflects the fact that

the transverse force dynamics is constructed to preserve the Boltzmann distribution in the steady state. Any ergodicity breaking that takes its root in the thermodynamics, as the one observed in mean field fluids, will be observed also in the presence of transverse forces at the same point as in equilibrium. However, even if the location of glass transition point is unchanged, it is interesting to observe how the dynamics conspires to produce this result, and how it differs from its equilibrium counterpart.

5.5.2 A sanity check

The spirit of the dynamical mean-field theory is to integrate out in an exact fashion an extensive number of degrees of freedom. This integration step transforms the Markovian dynamics into one with memory. From an analysis of the dynamics, it is thus not easy to see that the steady-state distribution for the non-Markovian process is the Boltzmann one. We know however that this must be the case, because the integration can be done at the static level using replicas [216], and we know that in equilibrium, the analysis of the dynamics [184] confirms the results of the statics. This subsection may thus seem a somewhat superfluous sanity check, but it is in principle needed. We want to prove directly the invariance of the steady state distribution of Eq. (5.38). We express the memory kernel $M_f(t)$ as a sum of exponentials:

$$\frac{1}{2}M_f(t) = \sum_k c_k e^{-t/\tau_k}, \quad (5.43)$$

where the c_k 's and the τ_k 's are appropriately distributed [225]. Using this decomposition, we can rewrite the non-Markovian equation of motion for \mathbf{r} as a Markovian one, at the cost of introducing an extra set of degrees of freedom, \mathbf{y}_k , coupled to \mathbf{r} :

$$\begin{aligned} \frac{\zeta}{2}\dot{\mathbf{r}}(t) &= -(\mathbf{1}_d + \gamma\mathbf{A}) \cdot \nabla w(\mathbf{r}) + \sum_k \sqrt{c_k\beta}(\mathbf{1}_d + \gamma\mathbf{A}) \cdot \left[\mathbf{y}_k(t) - \sqrt{c_k\beta}[\mathbf{r}(t) - \mathbf{r}_0] \right] \\ &\quad + \sqrt{T}\boldsymbol{\xi}, \\ \dot{\mathbf{y}}_k &= -\frac{1}{\tau_k} \left[\mathbf{y}_k - \sqrt{c_k\beta}[\mathbf{r}(t) - \mathbf{r}_0] \right] + \sqrt{\frac{2T}{\tau_k}}\boldsymbol{\eta}_k \\ \langle \boldsymbol{\eta}_i(t) \otimes \boldsymbol{\eta}_j(t') \rangle &= \mathbf{1}_d \delta_{ij} \delta(t - t') \\ \langle \boldsymbol{\xi}_i(t) \otimes \boldsymbol{\xi}_j(t') \rangle &= \mathbf{1}_d \delta(t - t'). \end{aligned} \quad (5.44)$$

We choose $\mathbf{y}_k(0)$ to be independent random variables drawn from a Gaussian distribution of variance T for all k . Upon averaging over the Markovian evolution and the initial condition of the \mathbf{y}_k variables, Eq. (5.44) is then identical to Eq. (5.38). The dynamics of \mathbf{y}_k reads:

$$\mathbf{y}_k(t) = \mathbf{y}_k(0)e^{-t/\tau_k} + \int_0^t d\tau e^{-\frac{t-\tau}{\tau_k}} \left[\frac{\sqrt{c_k\beta}}{\tau_k} [\mathbf{r}(\tau) - \mathbf{r}_0] + \sqrt{\frac{2T}{\tau_k}}\boldsymbol{\eta}_k(\tau) \right], \quad (5.45)$$

which, after an integration by parts, becomes

$$\begin{aligned}\mathbf{y}_k(t) &= \mathbf{y}_k(0)e^{-t/\tau_k} + \sqrt{c_k\beta}[\mathbf{r}(t) - \mathbf{r}_0] \\ &\quad - \sqrt{c_k\beta} \int_0^t d\tau e^{-\frac{t-\tau}{\tau_k}} \dot{\mathbf{r}}(\tau) + \sqrt{\frac{2T}{\tau_k}} \int_0^t d\tau e^{-\frac{t-\tau}{\tau_k}} \boldsymbol{\eta}_k(\tau).\end{aligned}\tag{5.46}$$

Substitution into the equation for \mathbf{r} yields

$$\begin{aligned}\frac{\zeta}{2} \dot{\mathbf{r}}(t) &= -(\mathbf{1}_d + \gamma\mathbf{A}) \nabla w(\mathbf{r}) - \beta \int_0^t d\tau \sum_k c_k e^{-\frac{t-\tau}{\tau_k}} (\mathbf{1}_d + \gamma\mathbf{A}) \cdot \dot{\mathbf{r}}(\tau) \\ &\quad + (\mathbf{1}_d + \gamma\mathbf{A}) \cdot \boldsymbol{\nu}(t) + \sqrt{T} \boldsymbol{\xi}(t) \\ \boldsymbol{\nu}(t) &\equiv \sum_k \sqrt{c_k\beta} \mathbf{y}_k(0) e^{-t/\tau_k} + \sqrt{\frac{2c_k}{\tau_k}} \int_0^t d\tau e^{-\frac{t-\tau}{\tau_k}} \boldsymbol{\eta}_k(\tau).\end{aligned}\tag{5.47}$$

The second term on the right hand side is $\frac{\beta}{2} \int_0^t d\tau M_f(t-\tau)(\mathbf{1}_d + \gamma\mathbf{A}) \cdot \dot{\mathbf{r}}(\tau)$. The contribution $\boldsymbol{\nu}(t)$ is a Gaussian noise whose correlations are given by

$$\langle \boldsymbol{\nu}(t) \otimes \boldsymbol{\nu}(t') \rangle = \mathbf{1}_d \sum_k c_k e^{\frac{|t-t'|}{\tau_k}} = \frac{1}{2} \mathbf{1}_d M_f(|t-t'|),\tag{5.48}$$

and therefore $\boldsymbol{\nu}(t) = \boldsymbol{\Xi}_f(t)$. This concludes the proof of equivalence between Eq. (5.38) and Eq. (5.44).

To obtain the steady state distribution of the joint process for \mathbf{r} and \mathbf{y} , we first rewrite the equation in the following form:

$$\begin{aligned}\frac{\zeta}{2} \dot{\mathbf{r}}(t) &= -(\mathbf{1}_d + \gamma\mathbf{A}) [\nabla w(\mathbf{r}) + \nabla \tilde{w}(\mathbf{r}, \{\mathbf{y}_k\})] + \sqrt{T} \boldsymbol{\xi}(t) \\ \mathbf{y}_k(t) &= -\frac{1}{\tau_k} \boldsymbol{\partial}_k \tilde{w}(\mathbf{r}, \{\mathbf{y}_k\}) + \sqrt{\frac{2T}{\tau_k}} \boldsymbol{\eta}(t),\end{aligned}\tag{5.49}$$

where $\tilde{w}(\mathbf{r}, \{\mathbf{y}_k\}) = \sum_k \frac{1}{2} (\mathbf{y}_k - \sqrt{c_k\beta}\mathbf{r})^2$ and $\boldsymbol{\partial}_k \equiv \frac{\partial}{\partial \mathbf{y}_k}$. This is an overdamped Langevin dynamics under the action of an external potential $w + \tilde{w}$ and transverse forces acting on the \mathbf{r} variables. Therefore, it admits the steady state distribution

$$p_{ss}(\mathbf{r}, \{\mathbf{y}_k\} | M_p, \boldsymbol{\Xi}_p, \mathbf{r}_0) \propto e^{-\beta(w + \tilde{w}(\mathbf{r}, \{\mathbf{y}_k\}))}.\tag{5.50}$$

Upon integrating out the auxiliary variables \mathbf{y}_k , we obtain

$$p_{ss}(\mathbf{r} | M_p, \boldsymbol{\Xi}_p, \mathbf{r}_0) = \frac{e^{-\beta w(\mathbf{r})}}{\int d\mathbf{r} e^{-\beta w(\mathbf{r})}} = p_B(\mathbf{r} | M_p, \boldsymbol{\Xi}_p, \mathbf{r}_0).\tag{5.51}$$

This result implies a self-consistent equation for M_p identical to the one holding in equilibrium, and therefore an identical glass transition temperature. This maybe does not come as a surprise given that, at least in infinite dimensions, the glass transition point can also be found by resorting to equilibrium statistical mechanics methods [216], and the transverse forces are designed to preserve the equilibrium statistics and thermodynamics.

5.6 Ergodic phase with strong nonequilibrium drive

The calculation of the previous Section has demonstrated that the behavior of the plateau value of the force-force correlation for transverse forces is identical to the one for equilibrium dynamics. However, in the presence of transverse forces the two-particle process at any finite time is different from its equilibrium counterpart, and we therefore expect $M(t)$ to be affected by the nonequilibrium forces in the ergodic region. The explicit determination of the memory kernel for arbitrary temperature and density is out of reach, and already in equilibrium the numerical integration of the equation of motion and the self-consistent relation is a formidable task [185]. Here, we address the scaling of the memory kernel $M(t)$ in the limit $\gamma \rightarrow \infty$.

The starting point is the dynamics of the interparticle distance:

$$\begin{aligned} \frac{\zeta}{2} \dot{r}(t) &= \frac{T(d-1)}{r(t)} - v'(r(t)) \\ &\quad - \frac{\beta}{2} \int_0^t d\tau M(t-\tau) \dot{r}(\tau) + \Xi(t) \\ \langle \Xi(t) \Xi(t') \rangle &= T\zeta \delta(t-t') + \frac{1}{2}(1+\gamma^2)M(t-t'). \end{aligned} \tag{5.52}$$

We recall that the memory kernel $M(t)$ is determined from the two-body dynamics itself, see Eq. (5.33).

We now rescale time, $\bar{t} \equiv \gamma t$, and we define the new functions $\bar{f}(\bar{t}) \equiv f\left(\frac{\bar{t}}{\gamma}\right)$, obtaining

$$\begin{aligned} \gamma \frac{\zeta}{2} \dot{\bar{r}}(\bar{t}) &= \frac{T(d-1)}{\bar{r}(\bar{t})} - v'(\bar{r}(\bar{t})) \\ &\quad - \frac{\beta}{2} \int_0^{\frac{\bar{t}}{\gamma}} d\tau \bar{M}(\bar{t}-\tau) \dot{\bar{r}}(\tau) + \bar{\Xi}(\bar{t}) \\ \langle \bar{\Xi}(\bar{t}) \bar{\Xi}(\bar{t}') \rangle &= \gamma T\zeta \delta(\bar{t}-\bar{t}') + \frac{1}{2}(1+\gamma^2)\bar{M}(\bar{t}-\bar{t}'), \end{aligned} \tag{5.53}$$

with $\bar{M}(\bar{t}) = \frac{\rho}{d} \int d\mathbf{r}_0 g(\mathbf{r}_0) \langle v'(\bar{r}(\bar{t})) \rangle_{\mathbf{r}_0} v'(r_0)$. If we now send $\gamma \rightarrow \infty$ and keep only the leading terms, we obtain

$$\begin{aligned} \frac{\zeta}{2} \dot{\bar{r}}(\bar{t}) &= \bar{\Xi}(\bar{t}) \\ \langle \bar{\Xi}(\bar{t}) \bar{\Xi}(\bar{t}') \rangle &= \frac{1}{2} \bar{M}(\bar{t}-\bar{t}'). \end{aligned} \tag{5.54}$$

Note that in the rescaled units this equation is no longer dependent on γ , and as a consequence $\bar{M}(\bar{t})$ cannot depend on γ . Using this result, we can determine the scaling

of the zero frequency mode of the memory kernel, $\widehat{M}(0)$:

$$\begin{aligned}\widehat{M}(0) &= \int_0^{+\infty} M(t) dt \\ &= \frac{1}{\gamma} \int_0^{+\infty} M\left(\frac{\bar{t}}{\gamma}\right) d\bar{t} \\ &= \frac{1}{\gamma} \int_0^{+\infty} \overline{M}(\bar{t}) d\bar{t} \sim \frac{1}{\gamma}.\end{aligned}\tag{5.55}$$

We have thus found the large γ behavior of the zero-frequency mode of the memory kernel. Interestingly, this is the same scaling found for the barrier crossing time in Chapter 2, and it differs from the γ^2 scaling that would have been naively guessed when looking at the escape rate of the particles, as was done in Chapter 2.1.

5.7 Mean-squared displacement and diffusion constant

In this Section, we explore how the transverse forces dynamics influences the diffusivity of the particles. We are interested in the mean-squared displacement

$$\Delta(t) \equiv \frac{1}{N} \sum_i \langle [\mathbf{R}_i(t) - \mathbf{R}_i(0)]^2 \rangle = \langle \mathbf{u}_0(t)^2 \rangle.\tag{5.56}$$

In the long time limit we expect diffusive behavior

$$\lim_{t \rightarrow \infty} \Delta(t) = 2dD_{\parallel}(T, \gamma)t.\tag{5.57}$$

Our aim is to obtain an expression for $D_{\parallel}(T, \gamma)$. The starting point of our calculation is the one-particle dynamics (we omit the particle index since they are all equivalent)

$$\zeta \dot{\mathbf{u}}(t) = - \int_0^t d\tau M(t - \tau) (\mathbf{1}_d + \gamma \mathbf{A}) \dot{\mathbf{u}}(\tau) + \boldsymbol{\Xi}(t),\tag{5.58}$$

with the noise correlations $\langle \boldsymbol{\Xi}(t) \otimes \boldsymbol{\Xi}(t') \rangle = \mathbf{1}_d [2T\zeta\delta(t - t') + (1 + \gamma^2)M(t - t')]$. Introducing the Laplace transform $\hat{f}(s) \equiv \int_0^{+\infty} dt e^{-st} f(t)$, we can write the mean-squared displacement using the Bromwich inversion integral [43]

$$\Delta(t) = - \frac{1}{4\pi^2} \int_{z-i\infty}^{z+i\infty} \int_{z-i\infty}^{z+i\infty} ds ds' e^{st+s't} \langle \hat{\mathbf{u}}(s) \cdot \hat{\mathbf{u}}(s') \rangle,\tag{5.59}$$

with z greater than the real part of all the singularities of the integrand. Applying the Laplace transform to both sides of Eq. (5.58) and noting that $\mathbf{A}\mathbf{A}^T = \mathbf{1}_d$ we get

$$\begin{aligned}\mathbf{u}(s) &= \frac{(\zeta + \beta \widehat{M}(s)) \mathbf{1}_d - \gamma \beta \widehat{M}(s) \mathbf{A}}{(\zeta + \beta \widehat{M}(s))^2 + (\gamma \beta \widehat{M}(s))^2} \cdot \frac{\widehat{\boldsymbol{\Xi}}(s)}{s} \\ &\equiv \widehat{\mathbf{K}}(s) \cdot \frac{\widehat{\boldsymbol{\Xi}}(s)}{s}.\end{aligned}\tag{5.60}$$

We also need to know the noise correlations in Laplace space, which read

$$\begin{aligned}\langle \widehat{\Xi}(s) \otimes \widehat{\Xi}^T(s') \rangle &= \mathbf{1}_d \frac{2T\zeta + (1 + \gamma^2) (\widehat{M}(s) + \widehat{M}(s'))}{s + s'} \\ &\equiv \mathbf{1}_d \frac{C(s, s')}{s + s'}.\end{aligned}\quad (5.61)$$

Equation (5.59) now reads

$$\Delta(t) = -\frac{1}{4\pi^2} \int_{z-i\infty}^{z+i\infty} \int_{z-i\infty}^{z+i\infty} ds ds' \frac{e^{st+s't}}{ss'(s+s')} C(s, s') \text{Tr}[\widehat{\mathbf{K}}(s) \cdot \widehat{\mathbf{K}}^T(s')]. \quad (5.62)$$

Since we are interested in the large time limit, we make the change of variables $w \equiv st$, $w' \equiv s't$:

$$\Delta(t) = -\frac{t}{4\pi^2} \int_{zt-i\infty}^{zt+i\infty} \int_{zt-i\infty}^{zt+i\infty} dw dw' \frac{e^{w+w'}}{ww'(w+w')} C\left(\frac{w}{t}, \frac{w'}{t}\right) \text{Tr}\left[\widehat{\mathbf{K}}\left(\frac{w}{t}\right) \cdot \widehat{\mathbf{K}}^T\left(\frac{w'}{t}\right)\right]. \quad (5.63)$$

The diffusion constant is obtained sending $t \rightarrow +\infty$:

$$D_{\parallel}(\gamma, T) = \frac{\text{Tr}[\widehat{\mathbf{K}}(0) \cdot \widehat{\mathbf{K}}^T(0)] C(0, 0)}{2d} \lim_{t \rightarrow +\infty} \left(\frac{1}{4\pi^2}\right) \int_{zt-i\infty}^{zt+i\infty} \int_{zt-i\infty}^{zt+i\infty} dw dw' \frac{e^{w+w'}}{ww'(w+w')} \quad (5.64)$$

Carrying out the computation explicitly yields

$$D_{\parallel}(\gamma, T) = T \frac{\zeta + (1 + \gamma^2)\beta\widehat{M}(0)}{\left(\zeta + \beta\widehat{M}(0)\right)^2 + \left(\gamma\beta\widehat{M}(0)\right)^2}. \quad (5.65)$$

This is the central result of this Section. For $\gamma = 0$ we obtain the known equilibrium expression of the diffusion constant:

$$D_{\parallel}(0, T) = \frac{T}{\zeta + \beta\widehat{M}(0)}. \quad (5.66)$$

The nonequilibrium diffusion constant is always larger than the equilibrium one, $D_{\parallel}(\gamma, T) \geq D_{\parallel}(0, T)$, as long as $\widehat{M}(0)$ is equal to or smaller than its equilibrium counterpart. For large nonequilibrium drives, the zero-frequency mode of the memory kernel scales as γ^{-1} (see Sec. 5.6 above), and the diffusion constant grows linearly with γ :

$$D_{\parallel}(T, \gamma \rightarrow \infty) \sim c(T)\gamma, \quad (5.67)$$

with $c(T)$ a temperature-dependent coefficient.

Concerning the temperature behavior of D_{\parallel} , two limits are of interest. The first one is the infinite temperature limit. In this case $\widehat{M}(0) = 0$ and one obtains

$$D_{\parallel}(T \rightarrow \infty, \gamma) = \frac{T}{\zeta} = D_{\parallel}(T \rightarrow \infty, 0). \quad (5.68)$$

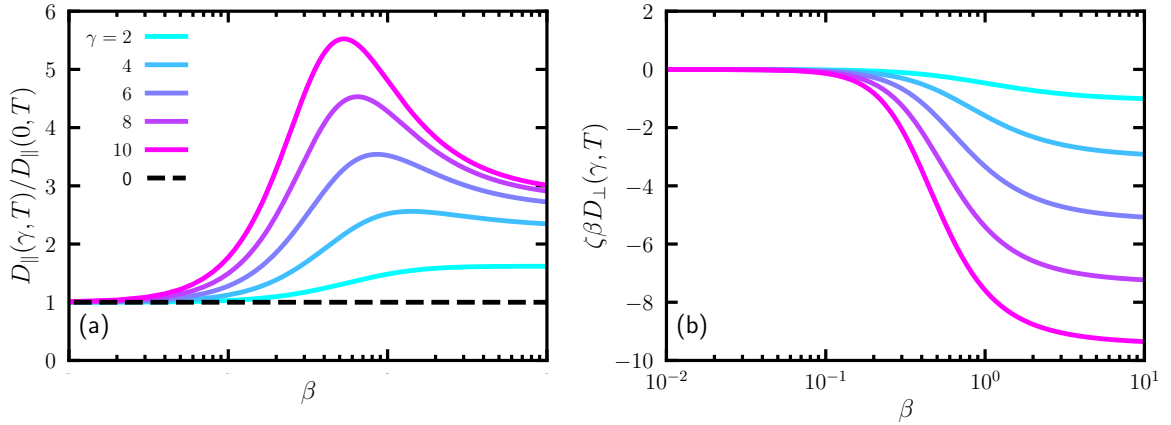


Figure 5.1: (a) Ratio between the longitudinal diffusion constant $D_{\parallel}(\beta, \gamma)$ in the presence of transverse forces and its equilibrium counterpart at $\gamma = 0$ for different values γ of the strength of the nonequilibrium drive, as a function of inverse temperature β . (b) Odd diffusivity in the presence of transverse forces. In both panels, the memory kernel used is the one obtained via a low density expansion for the case of a linear potential, as given in Eq. (5.36).

Since thermal fluctuations dominate over the interactions when $T \rightarrow \infty$, the transverse forces fail to accelerate the dynamics, and the nonequilibrium nature of the process is washed out by the thermal noise. The second limit of interest is for $T \rightarrow T_d$, the glass transition temperature. Here $\widehat{M}(0)$ diverges and the diffusion constant goes to 0, signaling dynamical arrest.

To conclude this Section, we explicitly compare $D_{\parallel}(\gamma, T)$ and its equilibrium counterpart in the low density regime for a linear potential, where $\widehat{M}(0)$ takes the form given in Eq. (5.36). The results are shown in Fig. 5.1(a). The efficiency of transverse forces, defined as the ratio $\frac{D_{\parallel}(\gamma, T)}{D_{\parallel}(\gamma, 0)}$ changes non monotonically with the temperature for the highest values of γ .

Our investigation of the diffusion constant suggests the following picture: upon reducing the temperature from the $T \rightarrow \infty$ regime dominated by thermal noise, transverse forces emerge from thermal fluctuations and accelerate the dynamics. However, as memory effects become stronger and the glass transition is approached, the enhancement of the diffusion is reduced. We are thus led to the question of what is the effect of transverse forces in the low temperature regime. In the next Section we show that they mostly give rise to odd transport coefficients rather than providing a stronger dynamical speedup.

5.8 Emergent odd transport

5.8.1 Odd diffusivity

In this subsection we prove, and quantify, the presence of odd diffusion in the infinite dimensional fluid driven by transverse forces. Odd diffusion manifests itself in the form of a nonzero off-diagonal, anti-symmetric part of the diffusion tensor. Physically, this detects the presence of chiral, swirling motion, and the presence of fluxes perpendicular to concentration gradients arising in the system. At the microscopic level, a Green-Kubo relation, derived in [125] identifies the odd diffusion as the time integral of the anti-symmetric part of the velocity-velocity autocorrelation tensor. Following this approach, we have

$$\mathbf{D}(\gamma, T) \equiv \frac{1}{N} \sum_{i=1}^N \int_0^{+\infty} dt \langle \dot{\mathbf{u}}_i(t) \otimes \dot{\mathbf{u}}_i(0) \rangle = \frac{D_{\parallel}(\gamma, T)}{d} \mathbf{1} + \frac{D_{\perp}(\gamma, T)}{d} \mathbf{A}. \quad (5.69)$$

The conventional longitudinal diffusion constant $D_{\parallel}(\gamma, T)$ given by Eq. (5.65) appears in the diagonal entries of the diffusion tensor. The anti-symmetric contribution is proportional to the odd diffusion constant $D_{\perp}(T, \gamma)$. It is defined as:

$$\begin{aligned} D_{\perp} &\equiv \frac{1}{dN} \sum_{i=1}^N \int_0^{\infty} \langle \dot{\mathbf{u}}_i(t) \cdot \mathbf{A} \dot{\mathbf{u}}_i(0) \rangle \\ &= \frac{1}{\zeta N d} \sum_{i=1}^N \lim_{z \rightarrow 0} \langle s \hat{\mathbf{u}}_i(s) \cdot \mathbf{A} \Xi_i(0) \rangle \\ &= \frac{1}{\zeta d} \lim_{s \rightarrow 0} \langle s \hat{\mathbf{u}}(s) \cdot \mathbf{A} \Xi(0) \rangle. \end{aligned} \quad (5.70)$$

In the second equality we have used a representation in terms of the Laplace transform of the displacement $\mathbf{u}_{i,\alpha}$, and in the third equality the fact that all particles are equivalent. Using Eq. (5.60) and the fact that:

$$\langle \hat{\Xi}(s) \otimes \Xi(0) \rangle = \mathbf{1}_d T \left[\zeta + (1 + \gamma^2) \beta \widehat{M}(s) \right] \quad (5.71)$$

we obtain

$$D_{\perp} = -\frac{T}{\zeta d} \text{Tr}[\widehat{\mathbf{K}}(0) \mathbf{A}] \left[\zeta + (1 + \gamma^2) \beta \widehat{M}(0) \right], \quad (5.72)$$

with $\widehat{\mathbf{K}}(0)$ defined in Eq. (5.60). An explicit computation of the trace yields

$$D_{\perp} = -\frac{T\gamma}{\zeta} \frac{\beta \widehat{M}(0) + (1 + \gamma^2) (\beta \widehat{M}(0))^2}{\left(\zeta + \beta \widehat{M}(0) \right)^2 + \left(\gamma \beta \widehat{M}(0) \right)^2}, \quad (5.73)$$

thus proving the presence of a finite odd diffusivity in the system whenever $\gamma \neq 0$. Upon approaching the glass transition, the odd diffusivity converges to the nonzero value $\gamma \frac{T}{\zeta}$: even when ergodicity is broken and the system is confined in a long-lived metastable state, a form of odd transport persists, analogous to the swirling motion of a particle trapped in an harmonic well in the presence of transverse forces [108].

As we shall see now, odd diffusion is not the only emergent odd transport coefficient.

5.8.2 Odd mobility

Odd mobility [224] is a transport coefficient closely related to the odd diffusivity. In this subsection we show that its behavior upon approaching the glass transition is distinctly different from the odd diffusivity as we find that odd mobility vanishes in the nonergodic phase.

Odd mobility describes the transverse motion of a tracer upon applying a constant force. Specifically, we consider the case where a constant force \mathbf{F}^{ext} is applied at $t = 0$ on particle 0, which thus assumes the role of a tracer. The system thus evolves under the action of the operator $L^{\text{ext}}(t)$, defined as

$$L^{\text{ext}}(t) = L(t) + \frac{1}{\zeta} \sum_{\beta=1}^{d/2} \mathbf{F}_{\beta}^{\text{ext}} \cdot \nabla_{0,\beta}, \quad (5.74)$$

with $L(t)$ the evolution operator of the unperturbed system, displayed in Eq. (5.13). Following a linear response formalism, we have, to first order in \mathbf{F}^{ext} ,

$$\mathcal{U}[L^{\text{ext}}](t, 0) \approx \mathcal{U}[L](t, 0) + \frac{1}{\zeta} \sum_{\beta=1}^{d/2} \int_0^t d\tau \mathcal{U}[L](t, \tau) \mathbf{F}_{\beta}^{\text{ext}} \cdot \nabla_{0,\beta} \mathcal{U}[L](0, \tau). \quad (5.75)$$

To obtain the equation of motion of the perturbed tracer in the linear response, we have to compute $\mathcal{U}[L^{\text{ext}}](t, 0) \mathbf{F}_{0,\alpha}$. However, we observe that $\mathcal{U}[L](t, 0) \mathbf{F}_{0,\alpha}$ is translationally invariant. This implies that only the first term on the right hand side of Eq. (5.75) contributes to the evolution of $\mathbf{F}_{0,\alpha}$, and therefore

$$\mathcal{U}[L^{\text{ext}}](t, 0) \mathbf{F}_{0,\alpha}(t) = \mathcal{U}[L](t, 0) \mathbf{F}_{0,\alpha} + O((\mathbf{F}^{\text{ext}})^2). \quad (5.76)$$

The equation of motion of the perturbed tracer in the infinite dimensional limit thus becomes

$$\zeta \dot{\mathbf{u}}_i(t) = \mathbf{F}^{\text{ext}} - \int_0^t d\tau M(t - \tau) (\mathbf{1}_d + \gamma \mathbf{A}) \cdot \dot{\mathbf{u}}_i(\tau) + \boldsymbol{\Xi}(t), \quad (5.77)$$

with the noise $\boldsymbol{\Xi}(t)$ and the memory kernel $M(t)$ corresponding to the one of the unperturbed dynamics in Eq. (5.28). The mobility of the tracer is defined via the relation

$$\lim_{t \rightarrow +\infty} \langle \dot{\mathbf{u}}_0(t) \rangle = \boldsymbol{\mu} \mathbf{F}^{\text{ext}}. \quad (5.78)$$

Applying a Laplace transform to Eq. (5.77), taking the 0-frequency limit and keeping the leading diverging terms we obtain the following expression for $\boldsymbol{\mu}$:

$$\boldsymbol{\mu} = \frac{[\zeta + \beta \widehat{M}(0)] \mathbf{1} - \gamma \beta \widehat{M}(0) \mathbf{A}}{[\zeta + \beta \widehat{M}(0)]^2 + (\gamma \beta \widehat{M}(0))^2} \equiv \mu_{\parallel} \mathbf{1} + \mu_{\perp} \mathbf{A}. \quad (5.79)$$

For $\gamma = 0$ we fall back to the equilibrium case, $\boldsymbol{\mu} = \frac{1}{\zeta + \beta \widehat{M}(0)} \mathbf{1}$ and the Einstein relation is satisfied, $T \boldsymbol{\mu} = \mathbf{D}$. When $\gamma \neq 0$, the Einstein relation breaks down. Note in passing that this violation takes a compact form for the longitudinal component of

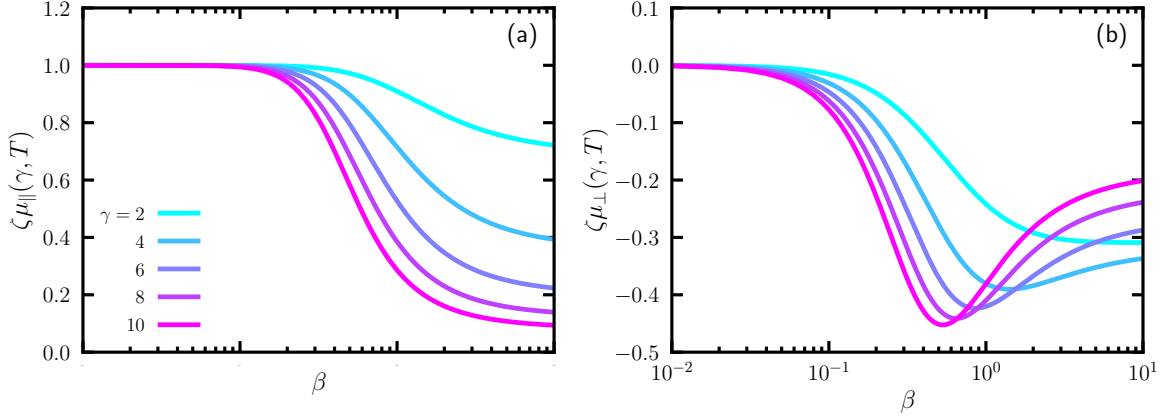


Figure 5.2: (a) Longitudinal mobility μ_{\parallel} for different values of the strength γ of the non equilibrium drive, as a function of the inverse temperature $\beta \equiv T^{-1}$. (b) Odd mobility in the presence of transverse forces. In both panels, the memory kernel used is the one obtained via a low density expansion for the case of a linear potential. Its expression is given in Eq. (5.36).

the diffusivity tensor, namely $\mathbf{D}_{\parallel} = [(\mathbf{1} + \gamma \mathbf{A})\boldsymbol{\mu}]_{\parallel}$. The mobility is composed of a longitudinal term, μ_{\parallel} , and of an odd component, μ_{\perp} . The ratio $\frac{D_{\parallel}}{T\mu_{\parallel}} = 1 + \gamma^2 \frac{\beta \widehat{M}(0)}{1 + \beta \widehat{M}(0)}$ is greater than one, which hints at a more efficient exploration of configurations than in equilibrium, but this effective temperature [69] is not the one that drives dynamical arrest.

A plot of longitudinal and transverse mobilities as a function of the inverse temperature is shown in Fig. 5.2, where the low density approximation of the memory kernel $\widehat{M}(0) \approx \widehat{M}^{(1)}$ [see Eq. (5.36)] was used. The longitudinal mobility decreases with temperature from its free particle high- T value, while the modulus of the odd mobility has a non-monotonic behavior, with a maximum located in the same region where the odd diffusion steeply rises, and where the efficiency of transverse forces starts decreasing, which was depicted in Fig. 5.1. This simultaneous occurrence of a similar behavior in all these quantities supports the physical picture of transverse forces operating at their best in the mildly interacting regime.

We also see from Eq. (5.79) that both the longitudinal and transverse mobilities vanish at the glass transition T_d . Physically, the above result implies the absence of a long-time systematic displacement in the non-ergodic phase both along the direction of the external force and in the direction transverse to it.

5.8.3 Odd viscosity

This subsection is devoted to the computation of the odd viscosity. Odd viscosity appears as an anti-symmetric component of the viscous tensor. Upon application of an external shear stress, a system with odd viscosity develops a flow in the plane orthogonal to the one along which the shear stress is applied. A Green-Kubo approach,

developed in Ref. [85], relates the odd viscosity of a nonequilibrium system to the time integral of stress-stress correlation functions. Within this framework, using linear response theory, the viscous tensor in the hydrodynamic limit reads

$$\eta_{abcd} = \frac{\beta}{V} \int_0^{+\infty} dt \left\langle \sigma_{ab}(t) \sigma_{cd}^{\text{IK}}(0) \right\rangle. \quad (5.80)$$

The average of the integrand is meant both with respect to the initial condition and with respect to the realizations of the noise. The notation σ_{ab}^{IK} refers to the Irving-Kirkwood stress tensor for overdamped dynamics:

$$\sigma_{ab}^{\text{IK}} = -\frac{1}{2} \sum_{i \neq j} \frac{r_{ij,a}(t) r_{ij,b}(t)}{r_{ij}(t)} v'(r_{ij}(t)), \quad (5.81)$$

and σ_{ab} is the stress tensor in the presence of transverse forces

$$\sigma_{ab} = (\mathbf{1}_d + \gamma \mathbf{A})_{bc} \sigma_{ac}^{\text{IK}}. \quad (5.82)$$

The odd viscosity is finally defined as

$$\eta_{\perp} \equiv \frac{1}{2} (\eta_{xyxx} - \eta_{xxxxy}), \quad (5.83)$$

where $x = 2a - 1$ and $y = 2a$ with $a = 1, \dots, d/2$. To be explicit, we focus on the $x = 0, y = 1$ case. The odd viscosity then becomes

$$\eta_{\perp} = \frac{\beta}{2V} \int_0^{+\infty} dt \left\langle \sigma_{xy}^{\text{IK}}(t) \sigma_{xx}^{\text{IK}}(0) \right\rangle - \left\langle \sigma_{xx}^{\text{IK}}(t) \sigma_{xy}^{\text{IK}}(0) \right\rangle + \gamma \left\langle \sigma_{xx}^{\text{IK}}(t) \sigma_{xx}^{\text{IK}}(0) \right\rangle + \gamma \left\langle \sigma_{xy}^{\text{IK}}(t) \sigma_{xy}^{\text{IK}}(0) \right\rangle. \quad (5.84)$$

The first two terms inside the integrand vanish because they are odd upon rotation in the xy plane. The latter terms are

$$\begin{aligned} & \left\langle \sigma_{xx}^{\text{IK}}(t) \sigma_{xx}^{\text{IK}}(0) \right\rangle + \left\langle \sigma_{xy}^{\text{IK}}(t) \sigma_{xy}^{\text{IK}}(0) \right\rangle \\ &= \frac{1}{4} \left\langle \sum_{i \neq j, k \neq l} \frac{r_{ij,x}(t) r_{ij,x}(t) r_{kl,x}(0) r_{kl,x}(0) + r_{ij,x}(t) r_{ij,y}(t) r_{kl,x}(0) r_{kl,y}(0)}{r_{ij,x}(t) r_{kl,x}(0)} v'(r_{ij}(t)) v'(r_{kl}(0)) \right\rangle \\ &= \frac{1}{4} \left\langle \sum_{i \neq j} \frac{r_{ij,x}(t) r_{ij,x}(t) r_{ij,x}(0) r_{ij,x}(0) + r_{ij,x}(t) r_{ij,y}(t) r_{ij,x}(0) r_{ij,y}(0)}{r_{ij,x}(t) r_{ij,x}(0)} v'(r_{ij}(t)) v'(r_{ij}(0)) \right\rangle \\ &\sim \frac{1}{2d^2} \left\langle \sum_{i \neq j} \frac{|\mathbf{r}_{ij} \cdot \mathbf{r}_0|^2}{r_{ij}(t) r_{ij}(0)} v'(r(t)) v'(r_{ij}(0)) \right\rangle \\ &= \frac{\rho^2 V}{2d^2} \int d\mathbf{r}_0 g(\mathbf{r}_0) \left\langle \frac{|\mathbf{r}(t) \cdot \mathbf{r}_0|^2}{r_{ij}(t) r_{ij}(0)} v'(r(t)) v'(r_{ij}(0)) \right\rangle_{\text{dyn}} \\ &= \frac{\rho V l^2}{2d} M(t), \end{aligned} \quad (5.85)$$

where $\langle \dots \rangle_{\text{dyn}}$ is an average over the realization of the noise in the two-body dynamics. In the last passage we have used the fact that the direction of the interparticle

separation is constant throughout the dynamics and that to leading order in d we have $r(t) \sim \ell$, with ℓ the characteristic interaction length of the potential. The odd viscosity is therefore

$$\eta_{\perp} = \frac{\gamma\beta\rho_0\ell^2}{4d}\widehat{M}(0). \quad (5.86)$$

As the glass transition is approached, the odd viscosity diverges. The physical interpretation of this phenomenon is that infinitely long-lived memory develops also at the level of stress fluctuations with respect to transverse perturbations, a consequence of the chiral interaction produced by the nonequilibrium drive. Below T_d , small external shear stresses applied to the system generate neither longitudinal nor transverse flows, consistently with the picture of a dynamically arrested glass, and both viscosities are formally infinite.

5.9 Outlook

In this chapter, we have studied how transverse forces speedup the dynamics in a mean field liquid. Consistently with what we found for the p -spin, the dynamical ergodicity breaking temperature is not changed by transverse forces. As the transition is approached, the efficiency of transverse forces decreases while, quite surprisingly, at higher temperatures the behavior of the speedup is nonmonotonous. Close to the glass transition, the study of odd transport coefficients corroborates the picture, which was already emerging from the numerical analysis of Chapter 4, of an arrested liquid where the particles swirl within the cages induced by the interaction with their neighbors. Can we provide an analogous analytical characterization in finite dimensional settings? We address this question in the next chapter, where two finite dimensional theories for liquid with transverse forces are developed, the weak-coupling and the mode-coupling theory.

Contributions from Chapter 4

- We adapt the dynamical mean field theory to dense liquids with transverse forces in the large dimensional limit.
- Our approach allows to obtain equation of motion for a tagged particle in the fluid, and for the collision process between two particles. Both the dynamical process involve the force-force autocorrelation function between a pair of interacting particles. This autocorrelation function is self-consistently, implicitly determined through the two-body process.
- The central result of our approach is an expression for the longitudinal diffusion constant $D_{\parallel}(\gamma, T)$ of the system, as a function of the zero-frequency mode of the force-force autocorrelation function.
- We find that there exists a dynamical temperature $T_d(\gamma)$, such that $D(\gamma, T < T_d(\gamma)) = 0$. In this region, ergodicity is broken. The dynamical temperature is independent from the strength of transverse forces, and it is the same as in equilibrium, $T_d(\gamma) = T_d(0)$.
- The efficiency of transverse forces is given by the ratio $D_{\parallel}(\gamma, T)/D_{\parallel}(0, T)$. We study its behavior as a function of the temperature. For $T \rightarrow \infty$, this ratio tends to 1. For $T \rightarrow T_d$, the ratio tends to a constant that depends on γ .
- Through a low density treatment of the memory kernel for a linear potential we discover that the has a nonmonotonous behavior as a function of the temperature, reaching a maximum before going to regions of higher densities.
- We find that in the asymptotic limit of large transverse forces, $\gamma \rightarrow \infty$ at fixed T , the efficiency grows linearly in γ .
- We determine, in the ergodic region and close to dynamical arrest, odd transport coefficient unlocked by transverse forces: the odd diffusivity D_{\perp} , the odd mobility μ_{\perp} , and the odd viscosity η_{\perp}
- We characterize the behavior of the odd transport coefficient as the glass transition is approached. As $T \rightarrow T_d$, $D_{\perp} \rightarrow -\gamma T_d$, $\mu_{\perp} \rightarrow 0$, $\eta_{\perp} \rightarrow +\infty$.
- Our study of the transport coefficients suggest that, as the glass transition is approached, particles in the fluid get progressively slowed down by the cage formed by their neighbors. At the glass transition, an arrested liquid is formed, with particles swirling inside local cages.

CHAPTER 5

CHAPTER

6

MODE-COUPLING AND WEAK-COUPLING THEORY FOR TRANSVERSE FORCES

6.1	Dynamics with transverse forces	86
6.2	Weak coupling approximation	87
6.2.1	Equation of motion for a tracer	87
6.2.2	Random phase approximation	87
6.2.3	Averaging over the tracer's trajectories	89
6.2.4	Weak-coupling approximation	90
6.2.5	Diffusion tensor	91
6.2.6	Mobility tensor	93
6.3	Mode-coupling theory in the presence of transverse forces	94
6.3.1	Projection operator formalism	95
6.3.2	The irreducible memory kernel	97
6.3.3	Mode-coupling expansion of the memory matrix	97
6.3.4	Schematic mode-coupling theory	101
6.3.5	New ansatz for the ergodic phase: relaxation speedup .	102
6.3.6	Beyond the schematic approximation	108
6.4	Dynamics of a tracer with transverse forces in the mode-coupling approach	109
6.4.1	Equation of motion of the tracer	110
6.4.2	Mode-coupling expansion of the tracer's memory kernel	113
6.4.3	Self-intermediate scattering function	114
6.4.4	Diffusion tensor	114
6.4.5	Mobility tensor	116
6.5	Odd viscosity	118
6.5.1	Stress tensor and transverse forces	118
6.5.2	Linear response theory	119
6.5.3	The viscosity tensor	120
6.5.4	Shear viscosity	122
6.5.5	Odd viscosity	122
6.6	Lifted active Brownian particles (ABP)	123
6.6.1	Short-time dynamics	125
6.6.2	Projection operator formalism	126
6.6.3	Mode-coupling expansion	127
6.6.4	Long-time dynamics: speedup and ergodicity breaking	129
6.6.5	Diffusion constant	129
6.7	Outlook	130

In this Chapter we bring the endeavour of understanding analytically how transverse forces operate to the finite dimensional realm. We extend two approximations schemes, the weak-coupling theory and the mode-coupling theory, to the dynamics of liquids with transverse forces. The former approximation scheme is valid for case where the interactions are weak compared to thermal fluctuations, and predicts that the efficiency of transverse forces increases as the the temperature decreases. The sec-

ond approximation schemes predicts a dynamical arrest below a dynamical transition temperature T_{MCT} . As for the mean field scenario, we find that T_{MCT} is the same as for equilibrium dynamics. In the ergodic phase, and approaching the transition, we find that the gain provided by transverse forces is a monotonously decreasing function of the temperature. Our analysis allows us also to compute many other transport coefficients, with a particular emphasis on odd diffusivity, odd mobility and odd viscosity. These findings corroborate and rationalize the behavior of dense liquids with transverse forces observed numerically in Chapter 4. We conclude by analyzing the mode-coupling theory for a model of lifted active Brownian particles, introduced in Chapter 1. We find results similar to the ones obtained for transverse forces, suggesting that the trend of the efficiency witnessed for this minimal model might hold also for other irreversible samplers.

When interested in the dynamics of dense liquids [26], the mode-coupling approximation [116, 115] is a method of choice. It is a versatile tool designed to analyze the dynamics of simple liquids and of other soft-matter systems in realistic space dimensions ($d = 2$ or 3). It has famously been applied to critical dynamics [153], to glass-formers [115], to polymers [236] and colloidal assemblies [158, 220] up to hard-condensed matter systems [238]. These systems share the common trait that they are in thermal equilibrium. In recent years, the mode-coupling approximation has been extended to some nonequilibrium settings, such as sheared liquids [100], granular fluids [128, 165], or, even more recently, to systems of self-propelled particles [244, 176, 243, 76]. Here, our goal is to use these works as an inspiration to develop a mode-coupling approximation for transverse forces.

Before dwelling into mode-coupling theory, however, we first explore the dynamics of a tracer in a weak fluctuation regime. This approximation scheme, known as the weak-coupling approximation [79, 78], is a way to implement dynamically the random-phase approximation [124], used to describe correlation functions in dense liquids. It has been applied to the diffusion of tracer particle in the passive, active [79] and driven [78] case, and also in the presence of non-reciprocal interactions [20]. Here, it is instrumental in providing a first, insightful picture of how transverse forces influence the dynamics in the high temperature regime.

6.1 Dynamics with transverse forces

Our starting point is the following dynamics for a fluid of interacting particles with positions \mathbf{r}_i in three dimensions

$$\dot{\mathbf{r}}_i = \mu_0 (\mathbf{1} + \gamma \mathbf{A}) \mathbf{F}_i + \sqrt{2\mu_0 T} \boldsymbol{\xi}_i, \quad (6.1)$$

with $\mathbf{F}_i \equiv -\sum_j \nabla_i V(|\mathbf{r}_i - \mathbf{r}_j|)$ a conservative force arising from a pairwise, isotropic interaction potential, and the $\boldsymbol{\xi}_i$'s are independent Gaussian white noises with independent components. The bare mobility μ_0 and the temperature T are related to the diffusion constant of a free particle D_0 through Einstein's relation $D_0 = \mu_0 T$, setting the Boltzmann constant to unity. This dynamics differs from its overdamped equilibrium counterpart due to the presence of an antisymmetric matrix $\mathbf{A} = -\mathbf{A}^T$. The resulting additional transverse force $\mathbf{AF}_i = A_{\alpha\beta} F_{i,\beta}$ injects into the system a nonequilibrium current that nevertheless preserves the Boltzmann distribution in the nonequilibrium steady-state. Following the discussion of Sec. 4.1, we choose for \mathbf{A} the form

$$\mathbf{A} \equiv \begin{bmatrix} 0 & -1 & 0 \\ 1 & 0 & 0 \\ 0 & 0 & 0 \end{bmatrix}. \quad (6.2)$$

We proceed by studying Eq. (6.1) using the weak-coupling approximation.

6.2 Weak coupling approximation

We consider the problem of a tracer diffusing in a system interacting with transverse forces in the special case in which fluctuations in the surrounding fluid can be considered as weak. Following [78], we assume that the tracer produces a small perturbation in the density field of its environment, a procedure known as the random phase approximation, and derive an expression for the transport coefficients of the tracer, namely the longitudinal and the odd diffusion constants. This gives a first grasp on the speedup generated by transverse forces. In spite of throwing an interesting physical light, this approach does not easily extend to low temperatures where the weak coupling hypothesis is not fulfilled.

6.2.1 Equation of motion for a tracer

We consider a tagged particle with position \mathbf{r}_0 diffusing in a fluid under the action of transverse forces. We include the possibility for the tagged particle to be subjected to a constant external force \mathbf{F}^{ext} , which will be used to probe the mobility of the tagged particle. The equation of motion for the tracer is

$$\dot{\mathbf{r}}_0 = \mu_0 \mathbf{F}^{\text{ext}} - \mu_0 (\mathbf{1} + \gamma \mathbf{A}) \sum_{i>0} \nabla_0 V(\mathbf{r}_0(t) - \mathbf{r}_i(t)) + \sqrt{2\mu_0 T} \boldsymbol{\xi}_0. \quad (6.3)$$

This is Eq. (6.1), with the role of particle 0 being singled out. All other particles in the fluid also interact according to Eq. (6.1). We introduce the density field of the fluid without the tracer, $n(\mathbf{r}, t) \equiv \sum_{i>0} \delta(\mathbf{r} - \mathbf{r}_i(t))$ and we can then rewrite Eq. (6.3) as

$$\dot{\mathbf{r}}_0 = \mu_0 \mathbf{F}^{\text{ext}} - (\mathbf{1} + \gamma \mathbf{A})(\nabla V * n)(\mathbf{r}_0(t), t) + \sqrt{2\mu_0 T} \boldsymbol{\xi}_0(t). \quad (6.4)$$

with the convolution between two functions denoted by $*$: $(f * g)(\mathbf{r}) \equiv \int d\mathbf{r}' f(\mathbf{r} - \mathbf{r}') g(\mathbf{r}')$. Equation (6.4) needs to be complemented with the Dean-Kawasaki [74] equation for $n(\mathbf{r}, t)$:

$$\begin{aligned} \partial_t n(\mathbf{r}, t) &= \mu_0 T \nabla^2 n(\mathbf{r}, t) + \mu_0 \nabla \cdot [(\mathbf{1} + \gamma \mathbf{A}) n(\mathbf{r}, t) (\nabla V * n)(\mathbf{r}, t)] \\ &\quad + \mu_0 \nabla \cdot [(\mathbf{1} + \gamma \mathbf{A}) \cdot n(\mathbf{r}, t) \nabla V(\mathbf{r} - \mathbf{r}_0(t))] + \nabla \cdot \sqrt{2T\mu_0 n(\mathbf{r}, t)} \boldsymbol{\chi}(\mathbf{r}, t), \end{aligned} \quad (6.5)$$

where the Gaussian noise $\boldsymbol{\chi}(\mathbf{r}, t)$ has correlations $\langle \boldsymbol{\chi}(\mathbf{r}, t) \otimes \boldsymbol{\chi}(\mathbf{r}', t') \rangle = \mathbf{1} \delta(\mathbf{r} - \mathbf{r}') \delta(t - t')$. In order to solve Eqs. (6.4, 6.5) we resort to the random phase approximation.

6.2.2 Random phase approximation

In the language of the collective coordinate n , the random phase approximation is a simple linearization of the Dean-Kawasaki equation (6.5) for the local and fluctuating density field $n(\mathbf{r}, t) = \sum_i \delta(\mathbf{r} - \mathbf{r}_i(t))$ [78, 79, 143, 20]. Assuming that the homogeneous

density of the system $\rho_0 \equiv \frac{N}{V}$ is large enough so that density fluctuations remain small, we split $n(\mathbf{r}, t)$ into

$$n(\mathbf{r}, t) = \rho_0 \left(1 + \frac{1}{\sqrt{\rho_0}} \phi(\mathbf{r}, t) \right) \quad (6.6)$$

with $\phi(\mathbf{r}, t)$ a fluctuating field. To linear order in $\phi/\sqrt{\rho_0}$, which we assume to be small, Eq. (6.5) becomes

$$\partial_t \phi = \mu_0 T \nabla^2 \phi + \mu_0 \nabla \cdot (\nabla \rho_0 V * \phi)(\mathbf{r}, t) + \mu_0 \nabla^2 \sqrt{\rho_0} V(\mathbf{r} - \mathbf{r}_0(t)) + \nabla \cdot \sqrt{2T\mu_0} \boldsymbol{\chi}(\mathbf{r}, t). \quad (6.7)$$

In deriving Eq. (6.7) from Eq. (6.5) we used the fact that, to linear order in $\phi/\sqrt{\rho_0}$, $\nabla \cdot \gamma \mathbf{A} n(\mathbf{r}, t) (\nabla V * n)(\mathbf{r}, t) = 0$ because \mathbf{A} is anti-symmetric, while the nonzero contribution from $\nabla \cdot \gamma \mathbf{A} \cdot n(\mathbf{r}, t) \nabla V(\mathbf{r} - \mathbf{r}_0(t))$ is of order ρ_0^{-1} . The linearized equation for the density field is therefore not directly influenced by the presence of the transverse forces. Instead the latter manifestly appear in the equation of motion of the tracer. To proceed toward the weak coupling approximation, we consider the case where the interaction potential between the particle is soft, with $V(r)$ finite as $r \rightarrow 0$. Upon introducing the Fourier transform of a function f by the convention $f(\mathbf{k}) \equiv \int d\mathbf{r} e^{-i\mathbf{k}\cdot\mathbf{r}} f(\mathbf{r})$, we obtain from Eq. (6.4):

$$\dot{\mathbf{r}}_0(t) = \mu_0 \mathbf{F}^{\text{ext}} - i\mu_0 (\mathbf{1} + \gamma \mathbf{A}) \int \frac{d\mathbf{k}}{(2\pi)^d} e^{i\mathbf{k}\cdot\mathbf{r}_0(t)} \mathbf{k} \sqrt{\rho_0} V(\mathbf{k}) \phi(\mathbf{k}, t) + \sqrt{2T\mu_0} \boldsymbol{\xi}_0(t), \quad (6.8)$$

where γ appears explicitly in the right-hand side. It is formally possible to express $\phi(\mathbf{k}, t)$ as a functional of the tracer position \mathbf{r}_0 upon integrating Eq. (6.7), and then Eq. (6.8) becomes a self-contained equation for \mathbf{r}_0 . We assume that the bath and the tracer have evolved for very long times before we start observing them so that the initial condition for the density fluctuation $\phi(\mathbf{k}, t)$ can be overlooked, namely

$$\phi(\mathbf{k}, t) = \int_{-\infty}^t ds \left[-\mu_0 k^2 \sqrt{\rho_0} V(\mathbf{k}) e^{-i\mathbf{k}\cdot\mathbf{r}_0(s)} + i\sqrt{2\mu_0 T} \mathbf{k} \cdot \boldsymbol{\chi}(\mathbf{k}, s) \right] e^{-\mu_0 T k^2 [1 + \beta \rho_0 V(\mathbf{k})](t-s)}, \quad (6.9)$$

the correlations of the noise in Fourier space being $\langle \boldsymbol{\chi}(\mathbf{k}, t) \otimes \boldsymbol{\chi}(\mathbf{k}', t') \rangle = \mathbf{1}(2\pi)^d \delta(t - t') \delta(\mathbf{k} + \mathbf{k}')$. Substitution of Eq. (6.9) into Eq. (6.8) leads to

$$\dot{\mathbf{r}}_0(t) = \mu_0 \mathbf{F}^{\text{ext}} + \mu_0 \int_{-\infty}^t ds \mathbf{F}(\mathbf{r}_0(t) - \mathbf{r}_0(s), t - s) + \boldsymbol{\Xi}(\mathbf{r}(t), t) + \sqrt{2\mu_0 T} \boldsymbol{\xi}_0(t). \quad (6.10)$$

The interaction between the tracer and the bath splits into a deterministic force

$$\mathbf{F}(\mathbf{r}_0(t), t) \equiv i\mu_0 \int \frac{d\mathbf{k}}{(2\pi)^3} (\mathbf{1} + \gamma \mathbf{A}) \cdot \mathbf{k} k^2 \rho_0 V^2(\mathbf{k}) e^{i\mathbf{k}\cdot\mathbf{r}_0(t) - \mu_0 T k^2 [1 + \beta \rho_0 V(\mathbf{k})] t}, \quad (6.11)$$

and a Gaussian colored noise $\boldsymbol{\Xi}$, independent of $\boldsymbol{\xi}_0$. The memory kernel $\langle \boldsymbol{\Xi}(\mathbf{r}(t), t) \otimes \boldsymbol{\Xi}(\mathbf{r}_0(t'), t') \rangle = \mathbf{G}(\mathbf{r}_0(t) - \mathbf{r}_0(t'), t - t')$ has the following expression:

$$\mathbf{G}(\mathbf{r}_0(t), t) \equiv \frac{(T\mu_0)^2}{\rho_0} \int_{\mathbf{k}} (\mathbf{1} + \gamma \mathbf{A}) \hat{\mathbf{k}} \otimes \hat{\mathbf{k}} (\mathbf{1} - \gamma \mathbf{A}) \frac{[\beta \rho_0 V(\mathbf{k})]^2}{1 + \beta \rho_0 V(\mathbf{k})} e^{i\mathbf{k}\cdot\mathbf{r}_0(t) - \mu_0 T k^2 [1 + \beta \rho_0 V(\mathbf{k})] t}. \quad (6.12)$$

We are now in a position to define, and then to determine, the various transport coefficients quantifying the dynamics of the tracer. Our computation rests on a path-integral formalism, which we briefly outline in the next subsection.

6.2.3 Averaging over the tracer's trajectories

We are interested in the computation of the diffusivity tensor, obtained from the velocity-velocity autocorrelation function [125]

$$\mathbf{D} \equiv \int_0^{+\infty} dt \langle \dot{\mathbf{r}}_0(t) \otimes \dot{\mathbf{r}}_0(0) \rangle = \lim_{t_f \rightarrow \infty} \langle [\mathbf{r}_0(t_f) - \mathbf{r}_0(0)] \otimes \dot{\mathbf{r}}_0(0) \rangle, \quad (6.13)$$

with $\mathbf{F}^{\text{ext}} = \mathbf{0}$, along with that of the mobility tensor $\boldsymbol{\mu}$, defined by the response to an external force as

$$\langle \mathbf{r}_0(t_f) - \mathbf{r}_0(0) \rangle \equiv \boldsymbol{\mu} \mathbf{F}^{\text{ext}} t_f \quad (6.14)$$

as $t_f \rightarrow \infty$ and $\mathbf{F}^{\text{ext}} \rightarrow 0$. The angular brackets denote averages over the realization of the noise. Using a path-integral formalism, these averages over the noise realization can be rewritten as weighted averages over the tracer's trajectories. If $f(\mathbf{r}_0(t_f))$ is a generic function of the tracer position at the final time t_f then within the path-integral formalism we have

$$\langle f(\mathbf{r}_0(t_f)) \rangle = \int \mathcal{D}\mathbf{p}_0(t) \mathcal{D}\mathbf{r}_0(t) f(\mathbf{r}_0(t_f)) e^{-S[\mathbf{r}_0(t), \mathbf{p}_0(t)]}, \quad (6.15)$$

where the Janssen-De Dominicis functional integral $\int \mathcal{D}\mathbf{p}_0(t) \mathcal{D}\mathbf{r}_0(t)$ is over all the trajectories $\mathbf{r}_0(t), \mathbf{p}_0(t)$. The response field $\mathbf{p}_0(t)$ is an auxiliary field encoding stochastic fluctuations. The trajectories are weighted by a trajectory-dependent exponential factor $e^{-S[\mathbf{r}_0(t), \mathbf{p}_0(t)]}$. The corresponding action features two contributions, expressing respectively the motion of a free tracer and its interactions with the bath:

$$S[\mathbf{r}_0(t), \mathbf{p}_0(t)] = S_{\text{free}}[\mathbf{r}_0(t), \mathbf{p}_0(t)] + S_{\text{int}}[\mathbf{r}_0(t), \mathbf{p}_0(t)], \quad (6.16)$$

with

$$S_{\text{free}}[\mathbf{r}_0(t), \mathbf{p}_0(t)] \equiv -i \int dt \mathbf{p}_0(t) \cdot [\dot{\mathbf{r}}_0(t) - \mu_0 \mathbf{F}^{\text{ext}}] + \mu_0 T \int dt \mathbf{p}_0(t)^2, \quad (6.17)$$

and

$$\begin{aligned} S_{\text{int}}[\mathbf{r}_0(t), \mathbf{p}_0(t)] &\equiv i \int dt \int_{-\infty}^t ds \mathbf{p}_0(t) \cdot \mathbf{F}(\mathbf{r}_0(t) - \mathbf{r}_0(s), t-s) \\ &+ \int dt \int_{-\infty}^t ds \mathbf{p}_0(t) \cdot \mathbf{G}(\mathbf{r}_0(t) - \mathbf{r}_0(s), t-s) \cdot \mathbf{p}_0(s). \end{aligned} \quad (6.18)$$

To evaluate the dynamical averages in Eqs. (6.13, 6.14), we resort to a small coupling approximation between the bath and the tracer and expand in powers of the small coupling parameter. This is carried out explicitly in the next subsection.

6.2.4 Weak-coupling approximation

We now assume that the coupling between the bath and the tracer is weak with respect to the thermal forces. This is expressed by requiring that

$$h \equiv \frac{\sqrt{\rho_0}V}{T} \ll 1. \quad (6.19)$$

From Eqs. (6.11, 6.12) we see that both \mathbf{F} and \mathbf{G} are of order h^2 . From Eq. (6.18), this implies that S_{int} is of order h^2 as well. To second-order in h , dynamical averages can thus be computed by expanding the exponential e^{-S} :

$$\langle f(\mathbf{r}_0(t_f)) \rangle = \frac{\langle f(\mathbf{r}_0(t_f)) \rangle_{\text{free}} - \langle f(\mathbf{r}_0(t_f)) S_{\text{int}} \rangle_{\text{free}}}{1 - \langle S_{\text{int}} \rangle_{\text{free}}} + O(h^4), \quad (6.20)$$

where $\langle \dots \rangle_{\text{free}} \equiv \int \mathcal{D}\mathbf{r}_0(t) \mathcal{D}\mathbf{p}_0(t) \dots e^{-S_{\text{free}}}$ refers to an average over the dynamics of a free tracer. The action S_{free} is quadratic, which ensures that linear and quadratic functionals of the trajectories $\mathbf{r}_0(t)$, $\mathbf{p}_0(t)$ can be computed exactly. Since we are interested in the tracer's displacement, we define the one-point quantity $\Delta\mathbf{r}_0(t, s) \equiv \mathbf{r}_0(t) - \mathbf{r}_0(s)$ with $t \geq s$. We then have

$$\begin{aligned} \langle \Delta\mathbf{r}_0(t, s) \rangle_{\text{free}} &= \mu_0 \mathbf{F}^{\text{ext}}(t-s), \\ \langle \mathbf{p}_0(t) \rangle_{\text{free}} &= 0, \end{aligned} \quad (6.21)$$

from which we recover the result that the mobility tensor for the free tracer is $\boldsymbol{\mu}_{\text{free}} = \mu_0 \mathbf{1}$. The two-point averages read

$$\begin{aligned} \langle \mathbf{p}_0(t) \otimes \mathbf{p}_0(s) \rangle_{\text{free}} &= \mathbf{0} \\ \langle \Delta\mathbf{r}_0(t, s) \otimes \mathbf{p}_0(s') \rangle_{\text{free}} &= -i \mathbf{1} \chi_{[s,t)}(s') \\ \langle [\Delta\mathbf{r}_0(t, 0) - \mu_0 \mathbf{F}^{\text{ext}} t] \otimes [\Delta\mathbf{r}_0(t', s') - \mu_0 \mathbf{F}^{\text{ext}}(t'-s')] \rangle_{\text{free}} &= 2 \mathbf{1} \mu_0 T L([s, t] \cap [s', t']), \end{aligned} \quad (6.22)$$

where $\chi_{[s,t)}(s')$ is the characteristic function of the interval $[s, t)$ (it is 1 if $s' \in [s, t)$ and 0 otherwise). The quantity $L[a, b]$ returns the length of the interval $[a, b]$. Note that for $\mathbf{F}^{\text{ext}} = 0$ the last equality in Eq. (6.22) yields the mean-squared displacement of a free particle, $\langle \Delta\mathbf{r}_0(t_f, 0)^2 \rangle_{\text{free}} = 2d\mu_0 T t_f$.

We now evaluate $\langle S_{\text{int}} \rangle_{\text{free}}$. This average requires the evaluation over the dynamical action for a free particle of two contributions. The first one is

$$\langle \mathbf{p}_0(t) e^{i\mathbf{k} \cdot \Delta\mathbf{r}_0(t,s)} \rangle_{\text{free}} = i e^{-\mu_0 T k^2(t-s) + i\mathbf{k} \cdot \mathbf{F}^{\text{ext}}(t-s)} \langle \mathbf{p}_0(t) \Delta\mathbf{r}_0(t, s) \rangle_{\text{free}} \cdot \mathbf{k} = \mathbf{0}, \quad (6.23)$$

where we made use of Wick's theorem and of the second equality of Eq. (6.22). Similarly one can show that the other term vanishes, namely $\langle \mathbf{p}_0(t) \otimes \mathbf{p}_0(s) e^{i\mathbf{k} \cdot \Delta\mathbf{r}_0(t,s)} \rangle = \mathbf{0}$. We thus conclude that

$$\langle S_{\text{int}} \rangle_{\text{free}} = 0. \quad (6.24)$$

In the next two subsections we will compute the diffusion and the mobility tensors to leading order in h .

6.2.5 Diffusion tensor

We specialize the calculation to the case where no external force is applied to the tracer particle, $\mathbf{F}^{\text{ext}} = 0$. The calculation of the diffusion tensor to second order in the weak coupling h requires computing two free-particle dynamical averages, stemming respectively from the drift term \mathbf{F} of Eq. (6.11) and from the memory term \mathbf{G} of Eq. (6.12). They are given by (with $s \leq t$):

$$\begin{aligned} \langle \Delta r_{0,a}(t_f, 0) \dot{r}_{0,b}(0) p_{0,c}(t) e^{i\mathbf{k} \cdot \Delta \mathbf{r}(t, s)} \rangle_{\text{free}} &= -2i\delta_{ac}\mu_0 T e^{-\mu_0 T k^2 [1 + \beta\rho_0 V(\mathbf{k})](t-s)} \\ &\quad \times k_b \chi_{[s, t]}(0) \chi_{[0, t_f]}(t) \\ \langle \Delta r_{0,a}(t_f, 0) \dot{r}_{0,b}(0) p_{0,c}(t) p_{0,d}(s) e^{i\mathbf{k} \cdot \Delta \mathbf{r}_0(t, s)} \rangle_{\text{free}} &= [\delta_{bd}\delta_{ac}\delta(s-0) - 2\mu_0 T \delta_{ac} k_d k_b \chi_{[s, t]}(0)] \\ &\quad \times \chi_{[0, t_f]}(t) e^{-\mu_0 T k^2 (t-s)}. \end{aligned} \quad (6.25)$$

Using these results, one can directly compute the diffusivity matrix

$$\begin{aligned} \mathbf{D}(\gamma, T) &\approx \mu_0 T \mathbf{1} - \lim_{t_f \rightarrow \infty} \langle \Delta \mathbf{r}_0(t_f, 0) \otimes \mathbf{r}_0(0) S_{\text{int}} \rangle_{\text{free}} \\ &= \mu_0 T \mathbf{1} - \lim_{t_f \rightarrow +\infty} i \int dt \int_{-\infty}^t ds \langle \Delta \mathbf{r}_0(t_f, 0) \otimes \mathbf{r}_0(0) [\mathbf{p}_0(t) \cdot \mathbf{F}(\Delta \mathbf{r}_0(t, s), t-s)] \rangle_{\text{free}} \\ &\quad - \lim_{t_f \rightarrow +\infty} \int dt \int_{-\infty}^t ds \langle \Delta \mathbf{r}_0(t_f, 0) \otimes \mathbf{r}_0(0) [\mathbf{p}_0(t) \cdot \mathbf{G}(\Delta \mathbf{r}_0(t, s), t-s) \cdot \mathbf{p}_0(s)] \rangle_{\text{free}} \\ &= \mu_0 T \left[\mathbf{1} - \frac{1}{2\rho_0} \int_{\mathbf{k}} (\mathbf{1} + \gamma \mathbf{A}) \hat{\mathbf{k}} \otimes \hat{\mathbf{k}} \frac{[\beta\rho_0 V(\mathbf{k})]^2}{\left[1 + \frac{1}{2}\beta\rho_0 V(\mathbf{k})\right]^2} \right. \\ &\quad \left. + \frac{1}{4\rho_0} \int_{\mathbf{k}} (\mathbf{1} + \gamma \mathbf{A}) \hat{\mathbf{k}} \otimes \hat{\mathbf{k}}^T (\mathbf{1} - \gamma \mathbf{A}) \frac{[\beta\rho_0 V(\mathbf{k})]^3}{\left[1 + \frac{1}{2}\beta\rho_0 V(\mathbf{k})\right]^2 [1 + \beta\rho_0 V(\mathbf{k})]} \right]. \end{aligned} \quad (6.26)$$

For $\gamma = 0$, we obtain

$$\begin{aligned} \mathbf{D}(0, T) &= \mu_0 T \left[\mathbf{1} - \frac{1}{2\rho_0} \int_{\mathbf{k}} \hat{\mathbf{k}} \otimes \hat{\mathbf{k}} \frac{[\beta\rho_0 V(\mathbf{k})]^2}{\left[1 + \frac{1}{2}\beta\rho_0 V(\mathbf{k})\right] [1 + \beta\rho_0 V(\mathbf{k})]} \right] \\ &= \mu_0 T \mathbf{1} \left[1 - \frac{1}{2d\rho_0} \int_{\mathbf{k}} \frac{[\beta\rho_0 V(\mathbf{k})]^2}{\left[1 + \frac{1}{2}\beta\rho_0 V(\mathbf{k})\right] [1 + \beta\rho_0 V(\mathbf{k})]} \right], \end{aligned} \quad (6.27)$$

where we used, in the second line, the fact that upon integration over all the wavevectors $\hat{\mathbf{k}} \otimes \hat{\mathbf{k}}$ can be replaced, using the isotropy of the integrand in Eq. (6.27), by $d^{-1} \mathbf{1}$. We thus recover the equilibrium result for the longitudinal diffusion constant obtained in [79, 78]. The equilibrium diffusion tensor of Eq. (6.27) is diagonal, and the interaction of the tracer with the bath reduces its ability to diffuse. When $\gamma \neq 0$, the diffusion tensor acquires an antisymmetric contribution proportional to γ , and the diagonal part picks up a contribution proportional to γ^2 . These additional terms lead respectively to odd diffusivity and enhanced diffusion. To see this explicitly, we can write the tensor products of Eq. (6.26) in the (xyz) basis. In this basis, the matrix \mathbf{A} displayed

in Eq. (6.2) reads $\mathbf{A} = \mathbf{e}_y \otimes \mathbf{e}_x - \mathbf{e}_x \otimes \mathbf{e}_y$. The second tensor product inside the brackets of Eq. (6.26) is, neglecting the term that vanishes upon integration over all the wavevectors,

$$(\mathbf{1} + \gamma \mathbf{A})\hat{\mathbf{k}} \otimes \hat{\mathbf{k}} = \sum_{i=x,y,z} \hat{k}_i^2 \mathbf{e}_i \otimes \mathbf{e}_i + \gamma [\mathbf{e}_y \otimes \mathbf{e}_x \hat{k}_x^2 - \mathbf{e}_x \otimes \mathbf{e}_y \hat{k}_y^2]. \quad (6.28)$$

The term proportional to γ is antisymmetric upon integration over the wavevector \mathbf{k} , and it contributes to the odd diffusivity.

The third tensor in Eq. (6.26) is

$$\begin{aligned} (\mathbf{1} + \gamma \mathbf{A})\hat{\mathbf{k}} \otimes \hat{\mathbf{k}} (\mathbf{1} - \gamma \mathbf{A}) &= \sum_{i=x,y,z} \hat{k}_i^2 \mathbf{e}_i \otimes \mathbf{e}_i + \gamma [\mathbf{e}_x \otimes \mathbf{e}_y \hat{k}_x^2 - \mathbf{e}_y \otimes \mathbf{e}_x \hat{k}_y^2] \\ &\quad + \gamma [\mathbf{e}_y \otimes \mathbf{e}_x \hat{k}_x^2 - \mathbf{e}_x \otimes \mathbf{e}_y \hat{k}_y^2] + \gamma^2 [\mathbf{e}_x \otimes \mathbf{e}_x \hat{k}_x^2 + \mathbf{e}_y \otimes \mathbf{e}_y \hat{k}_y^2]. \end{aligned} \quad (6.29)$$

Upon integration over \mathbf{k} the terms proportional to γ cancel out, leaving only a contribution proportional to γ^2 to the longitudinal diffusion.

The diffusion tensor in the (xyz) basis is therefore given by

$$\mathbf{D} = D_{xx}(\gamma) [\mathbf{e}_x \otimes \mathbf{e}_x + \mathbf{e}_y \otimes \mathbf{e}_y] + D_{zz} \mathbf{e}_z \otimes \mathbf{e}_z + D_{\perp} (\mathbf{e}_y \otimes \mathbf{e}_x - \mathbf{e}_x \otimes \mathbf{e}_y), \quad (6.30)$$

with $D_{\parallel}(\gamma)$ given by

$$\begin{aligned} D_{\parallel}(\gamma) &= \mu_0 T \left(1 - \frac{1}{2d\rho_0} \int_{\mathbf{k}} \frac{[\beta\rho_0 V(\mathbf{k})]^2}{[1 + \beta\rho_0 V(\mathbf{k})] [1 + \frac{1}{2}\beta\rho_0 V(\mathbf{k})]} \right. \\ &\quad \left. + \frac{\gamma^2}{4d\rho_0} \int_{\mathbf{k}} \frac{[\beta\rho_0 V(\mathbf{k})]^3}{[1 + \beta\rho_0 V(\mathbf{k})] [1 + \frac{1}{2}\beta\rho_0 V(\mathbf{k})]^2} \right). \end{aligned} \quad (6.31)$$

The odd diffusion constant reads

$$D_{\perp}(\gamma) = -\gamma \frac{\mu_0 T}{2d\rho_0} \int_{\mathbf{k}} \frac{[\beta\rho_0 V(\mathbf{k})]^2}{[1 + \beta\rho_0 V(\mathbf{k})] [1 + \frac{1}{2}\beta\rho_0 V(\mathbf{k})]}. \quad (6.32)$$

For systems with equilibrium dynamics (that is, when $\gamma = 0$), Onsager reciprocity relations impose this quantity to vanish. However, when departing from equilibrium, as is the case in the presence of transverse forces, odd transport coefficients need not vanish as they are *a priori* not prohibited by time-reversal invariance. In our case, a nonzero odd diffusivity reveals the presence of a directed swirling motion for the tagged particle. Of course, for $\gamma = 0$, the odd diffusivity vanishes, as expected in equilibrium.

We see from Eq. (6.31) that the diffusivity of the tracer is enhanced by transverse forces, as the contribution proportional to γ^2 is positive. It is remarkable that this diffusion enhancement is captured even for a system where the linearized bath relaxation is not affected by the transverse forces. An enhancement of diffusion in odd system was also found in the case where the oddity is induced by external magnetic fields [145, 146], and is not, as in our case, a consequence of the nonequilibrium dynamics of the system.

We now take advantage of these explicit expressions to discuss the temperature dependence of the speedup. First, we observe that both terms in the integrals of Eq. (6.31) are decreasing functions of the temperature. This implies that the quantity $D_{\parallel}(0)/\mu_0 T$ is an increasing function of the temperature. Thus the efficiency of the transverse forces, defined as the ratio of the diffusion coefficient with and without transverse forces, is

$$\frac{D_{\parallel}(\gamma)}{D_{\parallel}(0)} = 1 + \gamma^2 \frac{I}{D_{\parallel}(0)/\mu_0 T}, \quad (6.33)$$

with $I \equiv \frac{1}{2d\rho_0} \int_{\mathbf{k}} \frac{[\beta\rho_0 V(\mathbf{k})]^3}{[1+\beta\rho_0 V(\mathbf{k})][1+\frac{1}{2}\beta\rho_0 V(\mathbf{k})]^2}$. We conclude that the efficiency of transverse forces increases upon cooling down the system. This is consistent with the increase of the odd diffusivity of the tracer. An analogous trend was recently found for binary mixture with nonreciprocal interactions between particles of different species [20].

It would be remarkable that the monotonous trend of the efficiency extends to low temperatures or high densities. In the following sections, using the mode coupling theory, we will show that this trend does not hold for very cool or very dense systems, where the small coupling approximation in Eq. (6.19) breaks down. Before moving to the mode-coupling formalism, we briefly examine the mobility of the tracer which contains additional information, since the Einstein relation between the diffusivity and mobility tensors does not necessarily hold.

6.2.6 Mobility tensor

The mobility tensor of the tracer can be obtained from the weak coupling expansion of Eq. (6.14):

$$\langle \Delta \mathbf{r}_0(t_f, 0) \rangle = \mu_0 T \mathbf{F}^{\text{ext}} t_f - \langle \Delta \mathbf{r}_0(t_f, 0) S_{\text{int}} \rangle_{\text{free}} + o(t_f). \quad (6.34)$$

The second term involves the following averages, which can be obtained using Wick's theorem and the dynamical averages of a free tracer displayed in Eq. (6.22):

$$\begin{aligned} \langle \Delta r_{0,a}(t_f, 0) \mathbf{p}_{0,b}(t) e^{i\mathbf{k} \cdot \Delta \mathbf{r}_0(t, s)} \rangle_{\text{free}} &= i\delta_{ab} \chi_{[0, t_f]} e^{-\mu_0 T k^2(t-s) + i\mu_0 \mathbf{k} \cdot \mathbf{F}^{\text{ext}}} \\ \langle \Delta r_{0,a}(t_f, 0) p_{0,b}(t) p_{0,c}(s) e^{i\mathbf{k} \cdot \Delta \mathbf{r}_0(t, s)} \rangle_{\text{free}} &= -i\delta_{ab} k_c \chi_{[0, t_f]} e^{-\mu_0 T k^2(t-s) + i\mu_0 \mathbf{k} \cdot \mathbf{F}^{\text{ext}}}. \end{aligned} \quad (6.35)$$

Plugging these results into Eq. (6.34) we obtain

$$\begin{aligned} \langle \Delta \mathbf{r}(t_f, 0) \rangle &\approx \mu_0 \mathbf{F}^{\text{ext}} t_f - (\mathbf{1} + \gamma \mathbf{A}) \mathbf{F}^{\text{ext}} \frac{\mu_0}{2d\rho_0} \int_{\mathbf{k}} \frac{[\rho_0 \beta V(\mathbf{k})]^2}{[1 + \beta \rho_0 V(\mathbf{k})][1 + \frac{1}{2} \beta \rho_0 V(\mathbf{k})]} t_f \\ &\equiv (\mathbf{1} \mu_{\parallel} + \mathbf{A} \mu_{\perp}) \mathbf{F}^{\text{ext}} t_f. \end{aligned} \quad (6.36)$$

When $\gamma = 0$, the Einstein relation $D_{\parallel}(0, T) = T \mu_{\parallel}(0, T)$ is recovered. When $\gamma \neq 0$, the presence of a transverse component to the force on the tracer does not affect the longitudinal mobility of the tracer, and its expression is the same as in equilibrium [78]. However, an odd mobility coefficient [224] proportional to γ appears. If the tracer is pulled by a force \mathbf{F}^{ext} along a given direction in the (xy) plane, it will also move along

the transverse direction parallel to \mathbf{AF}^{ext} : this is the physical meaning of the emergent odd mobility. As the temperature is lowered, the longitudinal mobility decreases while the odd mobility increases.

The main take-home message of this section is the increase of the sampling efficiency upon decreasing the temperature. In what follows we analyse what happens when the small coupling approximation breaks down. When the strength of transverse forces increases, we ask about the asymptotic behavior of the efficiency.

6.3 Mode-coupling theory in the presence of transverse forces

The dynamical evolution of the system of N particles with positions \mathbf{r}_i is governed by the operator Ω_γ

$$\Omega_\gamma \equiv D_0 \sum_i \nabla_i \cdot [\nabla_i - (\mathbf{1} + \gamma \mathbf{A}) \beta \mathbf{F}_i]. \quad (6.37)$$

When $\gamma = 0$, Ω_γ is the usual Smoluchowski evolution operator of the equilibrium dynamics. The evolution of the probability distribution $\rho(\mathbf{r}^N, t)$ of the system reads

$$\partial_t \rho(\mathbf{r}^N, t) = \Omega_\gamma \rho(\mathbf{r}^N, t). \quad (6.38)$$

We can thus write the formal expression for $\rho(\mathbf{r}^N, t)$ given its initial condition $\rho(\mathbf{r}^N)$:

$$\rho(\mathbf{r}^N, t) = e^{\Omega_\gamma t} \rho(\mathbf{r}^N, 0). \quad (6.39)$$

We denote the average value of any function $f(\mathbf{r}^N, t)$ by $\langle f(\mathbf{r}^N, t) \rangle$, and it is fully determined by the knowledge of $\rho(\mathbf{r}^N, t)$:

$$\begin{aligned} \langle f(\mathbf{r}^N, t) \rangle &\equiv \int d\mathbf{r}^N f(\mathbf{r}^N) e^{\Omega_\gamma t} \rho(\mathbf{r}^N) = \int d\mathbf{r}^N \left[e^{\Omega_\gamma^\dagger t} f(\mathbf{r}^N) \right] \rho(\mathbf{r}^N) \\ &= \int d\mathbf{r}^N e^{\Omega_{-\gamma} t} f(\mathbf{r}^N) \rho(\mathbf{r}^N) = \langle e^{\Omega_{-\gamma} t} f(\mathbf{r}^N) \rangle, \end{aligned} \quad (6.40)$$

where we have used the adjoint operator Ω_γ^\dagger , defined as

$$\Omega_\gamma^\dagger \equiv D_0 \sum_i [\nabla_i + (\mathbf{1} + \gamma \mathbf{A}) \beta \mathbf{F}_i] \cdot \nabla_i, \quad (6.41)$$

and the following identity, which is a consequence of the breaking of detailed balance:

$$\dots \Omega_\gamma f(\mathbf{r}^N) \Big\rangle = \dots \left(\Omega_{-\gamma}^\dagger f(\mathbf{r}^N) \right) \Big\rangle. \quad (6.42)$$

The steady state solution of Eq. (6.39) is the Boltzmann distribution $\rho_B(\mathbf{r}^N) = \frac{e^{-\beta \mathcal{H}(\mathbf{r}^N)}}{\int d\mathbf{r}^N e^{-\beta \mathcal{H}(\mathbf{r}^N)}}$ with $\mathcal{H}(\mathbf{r}^N) \equiv \frac{1}{2} \sum_{i \neq j} V(|\mathbf{r}_i - \mathbf{r}_j|)$. Since we are interested in the steady state dynamics of the system, we assume that the initial condition is also sampled from the Boltzmann distribution, i.e. $\rho(\mathbf{r}^N) = \rho_B(\mathbf{r}^N)$.

We are interested in the fluctuating density mode $n(\mathbf{q}, t)$, defined as the Fourier transform of the fluctuating density field $n(\mathbf{r}, t) = \sum_i \delta(\mathbf{r} - \mathbf{r}_i(t)) - \rho_0$:

$$n(\mathbf{q}, t) \equiv \sum_i e^{-i\mathbf{q}\cdot\mathbf{r}_i(t)}, \quad (6.43)$$

evaluated at the wavevector \mathbf{q} , and the dynamical structure factor $S(\mathbf{q}, t)$:

$$S(\mathbf{q}, t) \equiv \frac{1}{N} \left\langle n^*(\mathbf{q}) \left(e^{\Omega_\gamma^\dagger t} n(\mathbf{q}) \right) \right\rangle = \frac{1}{N} \left\langle n^*(\mathbf{q}) e^{\Omega_{-\gamma} t} n(\mathbf{q}) \right\rangle. \quad (6.44)$$

The initial condition $S(\mathbf{q})$ is the equilibrium structure factor of the system. Another quantity of interest is the self-part of the intermediate scattering function, $F_s(q, t)$:

$$F_s(\mathbf{q}, t) \equiv \frac{1}{N} \sum_i \left\langle n_i^*(\mathbf{q}) e^{\Omega_{-\gamma} t} n_i(\mathbf{q}) \right\rangle, \quad (6.45)$$

with $n_i(\mathbf{q}) \equiv e^{-i\mathbf{q}\cdot\mathbf{r}_i}$.

In the next section, we implement the Mori-Zwanzig projection operator formalism, described in its generalities in Section 5.1 to obtain an equation of motion for the dynamical density correlations.

6.3.1 Projection operator formalism

We start our calculation by introducing the Laplace transform

$$S(\mathbf{q}, z) \equiv \int_0^{+\infty} S(\mathbf{q}, t) e^{-zt}, \quad (6.46)$$

which, once applied to the time derivative of Eq. (6.44) yields

$$zS(\mathbf{q}, z) - S(\mathbf{q}) = \frac{1}{N} \left\langle n^*(\mathbf{q}) \Omega_{-\gamma} \frac{1}{z - \Omega_{-\gamma}} n(\mathbf{q}) \right\rangle. \quad (6.47)$$

We introduce an operator that projects along the density mode $n(\mathbf{q})$:

$$\mathcal{P} \equiv \frac{1}{NS(\mathbf{q})} n(\mathbf{q}) \left\langle n^*(\mathbf{q}), \right\rangle \quad (6.48)$$

and its orthogonal counterpart $\mathcal{Q} \equiv \mathcal{I} - \mathcal{P}$. Using the resolvent identity [115]

$$\mathcal{Q} \frac{1}{z - \Omega_{-\gamma}} = \mathcal{Q} \frac{1}{z - \Omega_{-\gamma} \mathcal{Q}} + \mathcal{Q} \frac{1}{z - \Omega_{-\gamma} \mathcal{Q}} \mathcal{Q} \Omega_{-\gamma} \mathcal{P} \frac{1}{z - \Omega_{-\gamma}}, \quad (6.49)$$

we obtain

$$\begin{aligned} zS(\mathbf{q}, z) - S(\mathbf{q}) &= \frac{1}{N} \left\langle n^*(\mathbf{q}) \Omega_{-\gamma} \frac{1}{z - \Omega_{-\gamma}} (\mathcal{P} + \mathcal{Q}) n(\mathbf{q}) \right\rangle \\ &= \left[\frac{1}{NS(q)} \left\langle n^*(\mathbf{q}) \Omega_{-\gamma} n(\mathbf{q}) \right\rangle \right. \\ &\quad \left. + \frac{1}{NS(q)} \left\langle n^*(\mathbf{q}) \Omega_{-\gamma} \mathcal{Q} \frac{1}{z - \mathcal{Q} \Omega_{-\gamma} \mathcal{Q}} \mathcal{Q} \Omega_{-\gamma} n(\mathbf{q}) \right\rangle \right] S(\mathbf{q}, z). \end{aligned} \quad (6.50)$$

Using the projection operators, we have separated the contributions to the evolution of the structure factor into an exponentially decaying part with frequency $-N^{-1} \langle n^*(\mathbf{q}) \Omega_{-\gamma} n(\mathbf{q}) \rangle$ and a memory kernel. The frequency term reads

$$-\frac{1}{N} \langle n(\mathbf{q})^* \Omega_{-\gamma} n(\mathbf{q}) \rangle = i \frac{D_0}{N} \mathbf{q} \cdot \sum_i \langle e^{i\mathbf{q} \cdot \mathbf{r}_i} \cdot [(\nabla_i - \gamma \mathbf{A} \beta \mathbf{F}_i) n(\mathbf{q})] \rangle = -D_0 q^2. \quad (6.51)$$

This term, which encodes the diffusive decay of the structure factor in the absence of interactions, is left unaffected by the transverse forces.

Using an integration by parts, together with the fact that the Boltzmann distribution describes the steady state of the system, the memory kernel $\widetilde{\mathbf{M}}$ can be written as

$$\begin{aligned} \mathbf{q} \cdot \frac{(D_0 \beta)^2}{V \rho_0} & \left\langle \sum_i e^{i\mathbf{q} \cdot \mathbf{r}_i} ((\mathbf{1} - \gamma \mathbf{A}) \mathbf{F}_i + iT \mathbf{q}) \mathcal{Q} \frac{1}{z - \mathcal{Q} \Omega_{-\gamma} \mathcal{Q}} \right. \\ & \times \left. \mathcal{Q} \sum_j e^{i\mathbf{q} \cdot \mathbf{r}_j} (\mathbf{F}_i (\mathbf{1} - \gamma \mathbf{A}) - iT \mathbf{q}) \right\rangle \cdot \mathbf{q} \equiv D_0 \mathbf{q} \cdot \widetilde{\mathbf{M}}(\mathbf{q}, z) \cdot \mathbf{q}. \end{aligned} \quad (6.52)$$

Due to the presence of projection operators \mathcal{Q} , the formula for $\widetilde{\mathbf{M}}$ can be simplified,

$$\begin{aligned} \widetilde{\mathbf{M}}(\mathbf{q}, z) &= \frac{(D_0 \beta)^2}{V \rho_0} \left\langle \sum_i e^{i\mathbf{q} \cdot \mathbf{r}_i} ((\mathbf{1} - \gamma \mathbf{A}) \mathbf{F}_i + iT \mathbf{q}) \mathcal{Q} \frac{1}{z - \mathcal{Q} \Omega_{-\gamma} \mathcal{Q}} \mathcal{Q} \sum_j e^{i\mathbf{q} \cdot \mathbf{r}_j} (\mathbf{F}_i (\mathbf{1} - \gamma \mathbf{A}) - iT \mathbf{q}) \right\rangle \\ &= \frac{(D_0 \beta)^2}{V \rho_0} \left\langle \sum_i e^{i\mathbf{q} \cdot \mathbf{r}_i} ((\mathbf{1} - \gamma \mathbf{A}) \mathbf{F}_i) \mathcal{Q} \frac{1}{z - \mathcal{Q} \Omega_{-\gamma} \mathcal{Q}} \mathcal{Q} \sum_j e^{i\mathbf{q} \cdot \mathbf{r}_j} \mathbf{F}_i (\mathbf{1} - \gamma \mathbf{A}) \right\rangle. \end{aligned} \quad (6.53)$$

The memory kernel can be expressed in terms of the correlations between projected force density Fourier modes,

$$\mathcal{Q} \mathbf{j}(\mathbf{q}) \equiv \mathcal{Q} \sum_i \mathbf{F}_i e^{-i\mathbf{q} \cdot \mathbf{r}_i}. \quad (6.54)$$

Note that due to the projection operator we have $\dots \mathcal{Q} \sum_i \mathbf{F}_i e^{-i\mathbf{q} \cdot \mathbf{r}_i} \rangle = \dots \mathcal{Q} T \sum_i \nabla_i e^{-i\mathbf{q} \cdot \mathbf{r}_i}$ and it is the latter form that is used in the derivation of the mode-coupling approximation, Eq. (6.65). The memory kernel $\widetilde{\mathbf{M}}$ thus reads

$$\widetilde{\mathbf{M}}(\mathbf{q}, z) = (1 - \gamma \mathbf{A}) \widetilde{\mathbf{K}}(\mathbf{q}, z) (1 - \gamma \mathbf{A}), \quad (6.55)$$

with

$$\widetilde{\mathbf{K}}(\mathbf{q}, z) \equiv \frac{D_0 \beta^2}{V \rho_0} \left\langle \mathbf{j}(\mathbf{q})^* \mathcal{Q} \frac{1}{z - \mathcal{Q} \Omega_{-\gamma} \mathcal{Q}} \mathcal{Q} \mathbf{j}(\mathbf{q}) \right\rangle. \quad (6.56)$$

Equation (6.50) becomes

$$z S(\mathbf{q}, z) - S(q) = \frac{D_0}{S(q)} \mathbf{q} \cdot [-\mathbf{1} + \widetilde{\mathbf{M}}(\mathbf{q}, z)] \cdot \mathbf{q} S(\mathbf{q}, z). \quad (6.57)$$

When $\gamma = 0$, the memory kernel $\widetilde{\mathbf{M}}$ is diagonal, and only the correlations among longitudinal particle currents contribute. We thus fall back onto the equilibrium case.

In the presence of transverse forces, correlations arising from transverse currents contribute to the dynamics of the structure factor. Cross-correlations among longitudinal and transverse currents might as well influence the dynamics. This is the new feature entering the design of our mode-coupling approximation. In the next section, we expand on the irreducible representation of the memory kernel.

6.3.2 The irreducible memory kernel

We now introduce the irreducible memory kernel. Following Kawasaki [152] and Vogel and Fuchs [253] we define an irreducible operator

$$\Omega_{-\gamma}^{\text{irr}} \equiv D_0 \mathcal{Q} \sum_j \nabla_j \mathcal{Q}_j \cdot (\mathbf{1} - \gamma \mathbf{A}) [-\beta \mathbf{F}_j + \nabla_j] \mathcal{Q}, \quad (6.58)$$

with $\mathcal{Q}_j \equiv 1 - \mathcal{P}_j$ and $\mathcal{P}_j \equiv e^{-i\mathbf{q}\cdot\mathbf{r}_j} \langle e^{i\mathbf{q}\cdot\mathbf{r}_j} \rangle$ a single-particle projection operator. The definition of the irreducible operator comes from a formal extension of the equilibrium case. Using the fact that particles are statistically equivalent we obtain $\mathcal{Q}\Omega_{-\gamma}\mathcal{Q} = \Omega_{-\gamma}^{\text{irr}} - \delta\Omega_{-\gamma}$, with

$$\delta\Omega_{-\gamma} = \frac{D_0\beta^2}{N} \mathcal{Q} \mathbf{j}(\mathbf{q}) \cdot (\mathbf{1} - \gamma \mathbf{A}) \langle \mathbf{j}(\mathbf{q})^* \mathcal{Q} \rangle. \quad (6.59)$$

Using Eq. (6.59) and the resolvent identity

$$\frac{1}{z - \mathcal{Q}\Omega_{-\gamma}\mathcal{Q}} = \frac{1}{z - \Omega_{-\gamma}^{\text{irr}}} + \frac{1}{z - \Omega_{-\gamma}^{\text{irr}}} \delta\Omega_{-\gamma} \frac{1}{z - \mathcal{Q}\Omega_{-\gamma}\mathcal{Q}}, \quad (6.60)$$

we can express the reducible memory kernel $\widetilde{\mathbf{K}}$ in Eq. (6.56) as a function of an irreducible memory kernel $\mathbf{K}(\mathbf{q}, z)$, where the evolution of the system is governed by $\Omega_{-\gamma}^{\text{irr}}$:

$$\mathbf{K}(\mathbf{q}, z) \equiv \frac{D_0\beta^2}{\rho_0 V} \left\langle \mathbf{j}(\mathbf{q})^* \mathcal{Q} \frac{1}{z - \Omega_{-\gamma}^{\text{irr}}} \mathcal{Q} \mathbf{j}(\mathbf{q}) \right\rangle. \quad (6.61)$$

The relationship between the reducible and the irreducible memory kernels is

$$\widetilde{\mathbf{K}}(\mathbf{q}, z) = [\mathbf{1} + \mathbf{K}(\mathbf{q}, z)(\mathbf{1} - \gamma \mathbf{A})]^{-1} \mathbf{K}(\mathbf{q}, z). \quad (6.62)$$

The introduction of the irreducible memory kernel is a necessary step in order to avoid an unphysical negative viscosity in the system, which may appear within an approximate evaluation of the reducible kernel [64].

Approximations are now needed to compute $\mathbf{K}(\mathbf{q}, z)$. In the next section we apply the mode-coupling approximation to the memory kernel.

6.3.3 Mode-coupling expansion of the memory matrix

To perform the mode-coupling expansion, we follow Szamel and Löwen [247]. The basic idea behind the mode-coupling approximation is to decompose the current field into a

sum of products of density modes:

$$\mathcal{Q}\mathbf{j}(\mathbf{q}) \approx \frac{1}{2} \sum_{\mathbf{k}} \frac{n(\mathbf{k})n(\mathbf{q}-\mathbf{k})}{N^2 S(\mathbf{k})S(\mathbf{q}-\mathbf{k})} \langle n^*(\mathbf{k})n^*(\mathbf{q}-\mathbf{k})\mathcal{Q}\mathbf{j}(\mathbf{q}) \rangle, \quad (6.63)$$

where the factor $\frac{1}{2}$ comes from a Gaussian factorization of a static multi-point density correlator. The central mode-coupling approximation is the factorization of the time-dependent multi-point density correlator, combined to the approximation $\Omega_{-\gamma}^{\text{irr}} \approx \Omega_{-\gamma}$:

$$\begin{aligned} \langle n(\mathbf{k}')^*n(\mathbf{q}-\mathbf{k}')^* e^{\Omega_{-\gamma}^{\text{irr}} t} n(\mathbf{k})n(\mathbf{q}-\mathbf{k}) \rangle &\approx \langle n^*(\mathbf{k}')e^{\Omega_{-\gamma} t} n(\mathbf{k}) \rangle \langle n^*(\mathbf{q}-\mathbf{k}') e^{\Omega_{-\gamma} t} n(\mathbf{q}-\mathbf{k}) \rangle \\ &\quad + \langle n^*(\mathbf{k}') e^{\Omega_{-\gamma} t} n(\mathbf{q}-\mathbf{k}) \rangle \langle n^*(\mathbf{q}-\mathbf{k}') e^{\Omega_{-\gamma} t} n(\mathbf{k}) \rangle \\ &= N^2 S(\mathbf{k}, t) S(\mathbf{q}-\mathbf{k}, t) [\delta_{\mathbf{k},\mathbf{k}'} + \delta_{\mathbf{k}'\mathbf{q}-\mathbf{k}}]. \end{aligned} \quad (6.64)$$

We now compute the expectation value in Eq. (6.63) with the aid of a convolution approximation

$$\begin{aligned} \langle n(\mathbf{k})^*n(\mathbf{q}-\mathbf{k})^*\mathcal{Q}\mathbf{j}(\mathbf{q}) \rangle &= \langle n(\mathbf{k})^*n(\mathbf{q}-\mathbf{k})^*\mathbf{j}(\mathbf{q}) \rangle - \frac{1}{NS(\mathbf{q})} \langle n(\mathbf{k})^*n(\mathbf{q}-\mathbf{k})^*n(\mathbf{q}) \rangle \langle n(\mathbf{q})\mathbf{j}(\mathbf{q}) \rangle \\ &\approx T \left\langle n(\mathbf{k})^*n(\mathbf{q}-\mathbf{k}) \sum_i \nabla_i e^{-i\mathbf{q}\cdot\mathbf{r}_i} \right\rangle \\ &\quad - \frac{T}{NS(\mathbf{q})} NS(\mathbf{k})S(\mathbf{q}-\mathbf{k})S(\mathbf{q}) \left\langle n(\mathbf{q})^* \sum_i \nabla_i e^{-i\mathbf{q}\cdot\mathbf{r}_i} \right\rangle \\ &= -T \left\langle \sum_i \nabla_i [n(\mathbf{k})^*n(\mathbf{q}-\mathbf{k})^*] e^{-i\mathbf{q}\cdot\mathbf{r}_i} \right\rangle \\ &\quad + \frac{T}{NS(\mathbf{q})} NS(\mathbf{k})S(\mathbf{q}-\mathbf{k})S(\mathbf{q}) \left\langle \sum_i \nabla_i [n(\mathbf{q})^*] e^{-i\mathbf{q}\cdot\mathbf{r}_i} \right\rangle \\ &= -iNT [\mathbf{k}S(\mathbf{q}-\mathbf{k}) + (\mathbf{q}-\mathbf{k})S(\mathbf{k}) - \mathbf{q}S(\mathbf{k})S(\mathbf{q}-\mathbf{k})] \\ &= iNT\rho_0 S(\mathbf{k})S(\mathbf{q}-\mathbf{k}) [\mathbf{k}c(\mathbf{k}) + (\mathbf{q}-\mathbf{k})c(\mathbf{q}-\mathbf{k})], \end{aligned} \quad (6.65)$$

where in the last step we have introduced the direct correlation function $c(\mathbf{k})$, related to $S(\mathbf{k})$ via the Ornstein-Zernike relation $\rho_0 c(\mathbf{k}) = 1 - \frac{1}{S(\mathbf{k})}$. We can now inject the expansion (6.63) into the memory kernel \mathbf{K} of Eq. (6.61). We then use Eq. (6.64) and Eq. (6.65). After replacing the sum over the wavevectors with an integral, $\sum_{\mathbf{k}} \rightarrow V \int_{\mathbf{k}}$, we obtain

$$\mathbf{K}(\mathbf{q}, t) \approx \frac{D_0\rho_0}{2} \int_{\mathbf{k}} \mathbf{V}_{\mathbf{k},\mathbf{q}} \otimes \mathbf{V}_{\mathbf{k},\mathbf{q}} S(\mathbf{k}, t) S(\mathbf{q}-\mathbf{k}, t), \quad (6.66)$$

where the vertex

$$\mathbf{V}_{\mathbf{k},\mathbf{q}} \equiv \mathbf{k}c(k) + (\mathbf{q}-\mathbf{k})c(|\mathbf{q}-\mathbf{k}|) \quad (6.67)$$

is the mode-coupling vertex of the equilibrium dynamics.

To proceed further, we decompose the kernel \mathbf{K} over an orthonormal basis that depends on the wavevector \mathbf{q} and on the matrix \mathbf{A} . The axes of this basis are defined

by

$$\begin{aligned}\mathbf{e}_1 &\equiv \mathbf{e}_{\mathbf{q}1} \equiv \frac{\mathbf{A}^T \mathbf{A} \mathbf{q}}{|\mathbf{A} \mathbf{q}|} \\ \mathbf{e}_2 &\equiv \mathbf{e}_{\mathbf{q}2} \equiv \frac{\mathbf{A} \mathbf{q}}{|\mathbf{A} \mathbf{q}|} \\ \mathbf{e}_3 &\equiv \mathbf{e}_{\mathbf{q}3} \equiv \frac{(\mathbf{1} - \mathbf{A}^T \mathbf{A}) \mathbf{q}}{|(\mathbf{1} - \mathbf{A}^T \mathbf{A}) \mathbf{q}|}.\end{aligned}\quad (6.68)$$

Looking at the expression for \mathbf{A} in Eq. (6.2), we see that \mathbf{e}_1 is the normalized projection of \mathbf{q} on the (xy) plane, \mathbf{e}_2 is the normalized vector orthogonal to \mathbf{e}_1 in the (xy) plane, as selected by the matrix \mathbf{A} , and \mathbf{e}_3 is the normalized projection of \mathbf{q} along the z -direction. We refer to this basis as the $\mathbf{A} - \mathbf{q}$ basis. The matrix $\mathbf{K}(\mathbf{q}, t)$ is diagonal in the basis defined in Eq. (6.68), within the mode-coupling approximation. To prove this, we consider the decomposition of $\mathbf{K}(\mathbf{q}, t)$ in the $\mathbf{A} - \mathbf{q}$ basis, namely

$$\mathbf{K}(\mathbf{q}, t) = \sum_{i,j=1}^3 K_{ij}(\mathbf{q}, t) \mathbf{e}_i \otimes \mathbf{e}_j. \quad (6.69)$$

The matrix element K_{ij} reads

$$\begin{aligned}K_{ij}(\mathbf{q}, t) &= \frac{D_0 \rho_0}{2} \int_{\mathbf{k}} [k_i c(k) + (q_i - k_i) c(|\mathbf{q} - \mathbf{k}|)] \\ &\quad [k_j c(k) + (q_j - k_j) c(|\mathbf{q} - \mathbf{k}|)] S(\mathbf{k}, t) S(\mathbf{q} - \mathbf{k}, t).\end{aligned}\quad (6.70)$$

We now consider the symmetries of the dynamics with transverse forces. The first symmetry transformation we exploit is a reflection of direction 3 (the axis z). This symmetry imposes

$$\mathbf{K}(\mathcal{R}_3 \mathbf{q}, t) = \mathbf{K}(\mathbf{q}, t), \quad (6.71)$$

with $\mathcal{R}_3 \mathbf{q} \equiv \mathbf{q} - 2\mathbf{e}_3(\mathbf{q} \cdot \mathbf{e}_3)$ the operator that reflects a vector with respect to direction 3. By construction, we have $\mathbf{e}_{\mathbf{q}i} = \mathbf{e}_{\mathcal{R}_3 \mathbf{q}i}$ for $i = 1, 2$, and $\mathbf{e}_{\mathbf{q}3} = -\mathbf{e}_{\mathcal{R}_3 \mathbf{q}3}$. This implies that $K_{3i}(\mathbf{q}, t) = K_{3i}(\mathcal{R}_3 \mathbf{q}, t)$ for $i = 1, 2$. On the other hand, a change of variable $k_3 \rightarrow -k_3$ in the momentum integration of $K_{3i}(\mathcal{R}_3 \mathbf{q}, t)$ shows that

$$K_{3i}(\mathcal{R}_3 \mathbf{q}, t) = -K_{3i}(\mathbf{q}, t), \quad (6.72)$$

where we used the fact that $S(\mathcal{R}_3 \mathbf{k}, t) = S(\mathbf{k}, t)$ due to the symmetries of the dynamics with transverse forces. Combining Eqs. (6.71, 6.72) we see that $K_{3i}(\mathbf{q}, t) = -K_{3i}(\mathbf{q}, t)$ for $i = 1, 2$, thus implying that $K_{3i}(\mathbf{q}, t) = 0$ for $i = 1, 2$.

The second symmetry we exploit is obtained by considering a rotation within the (xy) plane by an angle $\pi/2$. The resulting invariance imposes

$$\mathbf{K}(\mathcal{R}_{\frac{\pi}{2}} \mathbf{q}, t) = \mathbf{K}(\mathbf{q}, t), \quad (6.73)$$

with $\mathcal{R}_{\frac{\pi}{2}} \mathbf{q} \equiv \mathbf{A} \mathbf{q} + \mathbf{e}_3 q_3$ the operator that rotates a vector by an angle $\pi/2$ in the (xy) plane. By construction, $\mathbf{e}_{\mathbf{q}3} = \mathbf{e}_{\mathcal{R}_{\frac{\pi}{2}} \mathbf{q}3}$, $\mathbf{e}_{\mathbf{q}1} = -\mathbf{e}_{\mathcal{R}_{\frac{\pi}{2}} \mathbf{q}2}$ and $\mathbf{e}_{\mathbf{q}2} = \mathbf{e}_{\mathcal{R}_{\frac{\pi}{2}} \mathbf{q}1}$. This implies

$K_{12}(\mathbf{q}, t) = -K_{21}(\mathcal{R}_{\frac{\pi}{2}}\mathbf{q}, t)$. On the other hand, a change of variable $\mathbf{k} \rightarrow \mathcal{R}_{\frac{\pi}{2}}\mathbf{k}$ in the momentum integral of $K_{21}(\mathcal{R}_{\frac{\pi}{2}}\mathbf{q}, t)$ shows that

$$K_{21}(\mathcal{R}_{\frac{\pi}{2}}\mathbf{q}, t) = -K_{12}(\mathbf{q}, t), \quad (6.74)$$

where we used the fact that $S(\mathcal{R}_{\frac{\pi}{2}}\mathbf{k}, t) = S(\mathbf{k}, t)$ due to the symmetries of the dynamics with transverse forces. Combining Eqs. (6.73, 6.74) we see that $K_{12}(\mathbf{q}, t) = -K_{12}(\mathbf{q}, t)$ for $i = 1, 2$, thus implying that $K_{12}(\mathbf{q}, t) = K_{21}(\mathbf{q}, t) = 0$. This concludes our proof that the kernel $\mathbf{K}(\mathbf{q}, t)$ is diagonal in the $\mathbf{A} - \mathbf{q}$ basis, i.e.

$$\mathbf{K}(\mathbf{q}, t) = \sum_{i=1}^3 K_{ii}(\mathbf{q}, t) \mathbf{e}_i \otimes \mathbf{e}_i. \quad (6.75)$$

Using this diagonal approximation, we can give an expression of $\widetilde{\mathbf{K}}(\mathbf{q}, z)$. Noting that the matrix \mathbf{A} reads, in the $\mathbf{A} - \mathbf{q}$ basis,

$$\mathbf{A} = \mathbf{e}_2 \otimes \mathbf{e}_1 - \mathbf{e}_1 \otimes \mathbf{e}_2, \quad (6.76)$$

we can invert the matrix in Eq. (6.62), substitute the result in Eq. (6.55) and Eq. (6.57) to finally obtain

$$\begin{aligned} zS(\mathbf{q}, z) - S(\mathbf{q}) &= -D_0 \mathbf{q} \cdot \left[\frac{1 + (1 + \gamma^2)K_{22}}{(1 + K_{11})(1 + K_{22}) + \gamma^2 K_{11} K_{22}} \mathbf{e}_1 \otimes \mathbf{e}_1 + \frac{1}{1 + K_{33}} \mathbf{e}_3 \otimes \mathbf{e}_3 \right. \\ &\quad + \gamma \frac{K_{11} + K_{22} + (1 + \gamma^2)K_{11}K_{22}}{(1 + K_{11})(1 + K_{22}) + \gamma^2 K_{11} K_{22}} [\mathbf{e}_1 \otimes \mathbf{e}_2 - \mathbf{e}_2 \otimes \mathbf{e}_1] \\ &\quad \left. + \frac{(1 + K_{11})K_{22} + K_{11}(K_{22} - 1)\gamma^2}{(1 + K_{11})(1 + K_{22}) + \gamma^2 K_{11} K_{22}} \mathbf{e}_2 \otimes \mathbf{e}_2 \right] \cdot \mathbf{q} S(\mathbf{q}, z), \end{aligned} \quad (6.77)$$

where we have omitted the dependence on (\mathbf{q}, z) of the memory kernel K_{ii} , for simplicity. Note that only the first line of the term in the square bracket contributes to the decay of $S(\mathbf{q}, z)$, due to the projection along the mode \mathbf{q} . The off-diagonal, anti-symmetric term on the second line hints at the odd transport properties of the dynamics, which will be investigated below.

Before turning to the discussion of longitudinal and odd transport, we study the decay of the dynamical structure factor to a (possibly nonzero) plateau. To do so, we introduce the normalized dynamical density correlations $\phi(\mathbf{q}, t) \equiv \frac{S(\mathbf{q}, t)}{S(\mathbf{q})}$. Its dynamics is readily obtained from Eq. (6.77):

$$z\phi(\mathbf{q}, z) - 1 = -\frac{D_0}{S(q)} \mathbf{q} \cdot \left[\frac{1 + (1 + \gamma^2)K_{22}}{(1 + K_{11})(1 + K_{22}) + \gamma^2 K_{11} K_{22}} \mathbf{e}_1 \otimes \mathbf{e}_1 + \frac{1}{1 + K_{33}} \mathbf{e}_3 \otimes \mathbf{e}_3 \right] \cdot \mathbf{q} \phi(\mathbf{q}, z). \quad (6.78)$$

For $\gamma = 0$, we are back to the known equilibrium situation. The isotropy of the dynamics is restored, $K_{11} = K_{33}$ and we consistently find:

$$z\phi(\mathbf{q}, z) - 1 = -\frac{D_0}{S(q)} q^2 \frac{\phi(\mathbf{q}, z)}{1 + K_{\parallel}(\mathbf{q}, z)} \quad (6.79)$$

where K_{\parallel} is the longitudinal mode-coupling kernel

$$K_{\parallel}(\mathbf{q}, t) = \frac{D_0 \rho_0}{2q^2} \int_{\mathbf{k}} [\mathbf{q} \cdot \mathbf{k} c(k) + \mathbf{q} \cdot (\mathbf{q} - \mathbf{k}) c(|\mathbf{q} - \mathbf{k}|)]^2 S(\mathbf{k}, t) S(\mathbf{q} - \mathbf{k}, t). \quad (6.80)$$

For the general situation with $\gamma \neq 0$, it is instructive to consider the case where $q_3 = 0$ and rewrite Eq. (6.78) in the time domain:

$$\begin{aligned} & \partial_t \phi(\mathbf{q}, t) + D_0 q^2 \phi(\mathbf{q}, t) \\ & + D_0 q^2 (1 + \gamma^2) K_{22} * \phi(\mathbf{q}, t) = - \left[(K_{11} + K_{22}) + (1 + \gamma^2) K_{11} * K_{22} \right] * \partial_t \phi(\mathbf{q}, t), \end{aligned} \quad (6.81)$$

where $*$ denotes a convolution in time, $f * g(t) = \int_0^t dt f(t - \tau) g(\tau)$. With this expression, it is clear that when $\gamma \neq 0$ the transverse currents affect both the relaxation rate and the friction kernel of the system.

In order to extract a physical picture from these equations, we inject an approximate form for the static structure factor in which the structure is sharply localized at a given wavevector. As a result, the next subsection explores the resulting so-called schematic approximation.

6.3.4 Schematic mode-coupling theory

The first schematic approximation we consider follows the historical one [19] where the structure factor is strongly peaked for a wavevector of modulus q_0 , $S(\mathbf{q}) \approx 1 + S_0 \delta(|\mathbf{q}| - q_0)$, which implies in turn that $\rho_0 c(\mathbf{q}) = 1$ if $|\mathbf{q}| = q_0$ and 0 otherwise. Within this approximation, $K_{22} = 0$. In this case, Eq. (6.78) has the following property: if $\phi(\mathbf{k}, t)$ is rotationally invariant at $t = 0$, then $\phi(\mathbf{k}, t)$ remains rotationally invariant at all subsequent times t . The memory kernel thus reads

$$\begin{aligned} K_{11}(q_0, t) &= K_{33}(q_0, t) \\ &= \frac{D_0 S_0^2}{2\rho_0} \int_{|\mathbf{k}|=|\mathbf{q}-\mathbf{k}|=q_0} \frac{d\mathbf{k}}{(2\pi)^3} \phi(\mathbf{k}, t) \phi(\mathbf{q} - \mathbf{k}, t) \\ &= \lambda_{\text{eq}} \phi^2(q_0, t). \end{aligned} \quad (6.82)$$

where $\lambda_{\text{eq}} \equiv \frac{\sqrt{3}}{16\pi^2} \frac{D_0 S_0^2 q_0^3}{\rho_0} \phi^2(q_0, t)$. Upon substitution into Eq. (6.78) we obtain, denoting by $\phi_2(q_0, z)$ the Laplace transform of $\phi^2(q_0, t)$,

$$z\phi(q_0, z) - 1 = -D_0 q_0^2 \frac{1}{1 + \lambda_{\text{eq}} \phi_2(q_0, z)} \phi(q_0, z). \quad (6.83)$$

This equation is identical to the one obtained in the equilibrium case for $\gamma = 0$.

We briefly review here how an ergodicity breaking scenario is predicted from this equation [172]. If we denote by f_0 the nonergodicity parameter $f_0 \equiv \lim_{t \rightarrow +\infty} \phi(q_0, t)$,

we have

$$\begin{aligned}\lim_{z \rightarrow 0} \phi(q_0, z) &= \frac{f_0}{z}, \\ \lim_{z \rightarrow 0} \phi_2(q_0, z) &= \frac{f_0^2}{z}.\end{aligned}\tag{6.84}$$

Taking the limit $z \rightarrow 0$ on both sides of Eq. (6.83) and keeping only the diverging part yields

$$\frac{f_0}{1 - f_0} = \frac{\lambda_{\text{eq}}}{D_0 q_0^2} f_0^2.\tag{6.85}$$

Equation (6.85) admits a nonzero solution if and only if $\frac{\lambda_{\text{eq}}}{D_0 q_0^2} \geq 4$. This is the ergodicity breaking predicted by the mode-coupling theory of the colloidal glass transition in equilibrium [247].

We now give an expression for the high-temperature relaxation time in the equilibrium case. Let us assume that the system is ergodic, $\lambda_{\text{eq}} < 4D_0 q^2$, and that $\phi(q_0, t) = e^{-\frac{t}{\tau_0}}$, from which it follows that $\phi(q_0, z = 0) = \tau_0$ and $\phi_2(q_0, z = 0) = \frac{\tau_0}{2}$. Equation (6.83) evaluated at $z = 0$ gives an expression for the relaxation time τ_0

$$\tau_0 = \frac{1}{q_0^2 D_0 - \frac{\lambda_{\text{eq}}}{2}}.\tag{6.86}$$

This result is physical only for $\lambda_{\text{eq}} < 2q_0^2 D_0$, which corresponds to the ergodic phase. At higher values of λ_{eq} another functional form for the decay of ϕ must be assumed [19, 172].

Implementing the conventional schematic approximation does not allow us to capture any qualitative change in the evolution equation of the dynamical structure factor. However, the fact that dynamics is accelerated is a mathematical statement, and so we should blame the nature of the schematic approximation. There is also the possibility that the mode-coupling approximation itself does not capture the acceleration provided by transverse forces, but our analysis, developed in the remainder of the paper, shows that this is not the case.

The historical schematic approximation spuriously transforms a set of anisotropic equations for time-correlations into an isotropic one. We thus need to take a step back and consider an alternative schematic approximation that does not overlook the anisotropy, which we believe is an essential ingredient. This is what we implement in the next subsection.

6.3.5 New ansatz for the ergodic phase: relaxation speedup

We now resort to an approximate form of the static structure factor that preserves the chiral character of the dynamics, and which, as will appear, implies a faster relaxation in the ergodic phase.

We keep the main ingredient of the schematic approximation, namely the idea that the structure factor is sharply localized for wavevectors around a given modulus

q_0 . Nevertheless, we replace the sharp delta-function with a rounded peak of nonzero width ϵ , which is assumed to be small with respect to q_0 , but nonzero. This will be enough to produce an interesting interplay of modes in various directions. In practice, we resort to the following approximate forms for $S(k)$ and for the product $S(\mathbf{k})S(\mathbf{q} - \mathbf{k})$:

$$\begin{aligned} S(k) &\approx 1 + S_0 \frac{1}{\epsilon^d} \eta \left(\frac{k - q_0}{\epsilon} \right) \\ S(|\mathbf{k}|)S(\mathbf{q} - \mathbf{k}) &\approx \frac{S_0^2}{\epsilon^d} \eta \left(\frac{k - q_0}{\epsilon} \right) \eta \left(\frac{|\mathbf{q} - \mathbf{k}| - q_0}{\epsilon} \right) \end{aligned} \quad (6.87)$$

with $\epsilon^{-1}\eta(k)$ a function normalized to unity with an absolute maximum at $k = 0$. An example of such $\eta(k)$ could be a Gaussian function

$$\epsilon^{-d}\eta(k) \equiv \frac{1}{\sqrt{2\pi\epsilon^{2d}}} e^{-\frac{k^2}{2\epsilon^2}}, \quad (6.88)$$

but the specific shape of η is not relevant. Such a function will serve as an approximation of the Dirac distribution. Using the Ornstein-Zernike relation, the direct correlation function is given by

$$\rho_0 c(k) \approx \frac{\frac{S_0}{\epsilon^d} \eta \left(\frac{k - q_0}{\epsilon} \right)}{1 + \frac{S_0}{\epsilon^d} \eta \left(\frac{k - q_0}{\epsilon} \right)}. \quad (6.89)$$

When computing $K_{22}(\mathbf{q}, t)$, we focus on a wavevector \mathbf{q} such that $|\mathbf{q}| = q_0$ and expand around wavevectors \mathbf{k}_0 such that $k_0 = q_0$ and $|\mathbf{q} - \mathbf{k}_0| = q_0$. We then rewrite \mathbf{k} as

$$\mathbf{k} = \mathbf{k}_0 + \epsilon \mathbf{p} \quad (6.90)$$

in the integrals of Eq. (6.70). Note that ϵ has the dimension of a wavevector, and hence \mathbf{p} is dimensionless. The approximate values of k and $|\mathbf{q} - \mathbf{k}|$ up to order ϵ^2 are then

$$\begin{aligned} k &= |\mathbf{k}_0 + \epsilon \mathbf{p}| = q_0 + \epsilon \frac{\mathbf{p} \cdot \mathbf{k}_0}{q_0} + \frac{\epsilon^2}{2q_0} \left[p^2 - \frac{(\mathbf{p} \cdot \mathbf{k}_0)^2}{q_0^2} \right] \\ |\mathbf{q} - \mathbf{k}| &\approx q_0 + \epsilon \frac{\mathbf{p} \cdot (\mathbf{q} - \mathbf{k}_0)}{q_0} + \frac{\epsilon^2}{2q_0} \left[p^2 - \frac{(\mathbf{p} \cdot (\mathbf{q} - \mathbf{k}_0))^2}{q_0^2} \right]. \end{aligned} \quad (6.91)$$

We now expand the direct correlation function in powers of ϵ . We assume the function η to be even, so that $\rho_0 c'(q_0) = 0$. We thus obtain

$$\begin{aligned} \rho_0 c(k) &\approx \rho_0 c(q_0) + \epsilon^2 \frac{(\mathbf{p} \cdot \mathbf{k}_0)^2}{2q_0^2} \rho_0 c''(q_0) \\ &= 1 + \epsilon^2 \frac{(\mathbf{p} \cdot \mathbf{k}_0)^2}{2S_0 q_0^2} \frac{\eta_0''}{\eta_0^2}, \end{aligned} \quad (6.92)$$

where we used the notation $\eta_0 \equiv \eta(0)$, $\eta_0'' \equiv \eta''(0)$. Substituting Eq. (6.92) into the expression for the memory kernel $K_{22}(\mathbf{q}, t)$, given in Eq. (6.70), we find to lowest order

in ϵ ,

$$\begin{aligned} K_{22}(\mathbf{q}, t) &= \frac{D_0 \rho_0}{2} \int_{\mathbf{k}} \left(\frac{\mathbf{Aq} \cdot \mathbf{k}}{|\mathbf{Aq}|} \right)^2 [c(k) - c(|\mathbf{q} - \mathbf{k}|)]^2 S(k) S(|\mathbf{q} - \mathbf{k}|) \phi(\mathbf{k}, t) \phi(\mathbf{q} - \mathbf{k}, t) \\ &\approx \epsilon^4 \frac{D_0 (\eta''_0)^2}{8 \rho_0 q_0^4 \eta_0^4} \int_{\mathbf{p}} \left(\frac{\mathbf{Aq} \cdot \mathbf{k}_0}{|\mathbf{Aq}|} \right)^2 (\mathbf{p} \cdot \mathbf{q})^2 [2\mathbf{p} \cdot \mathbf{k}_0 - \mathbf{p} \cdot \mathbf{q}]^2 \eta \left(\frac{\mathbf{p} \cdot \mathbf{k}_0}{q_0} \right) \eta \left(\frac{\mathbf{p} \cdot (\mathbf{q} - \mathbf{k}_0)}{q_0} \right) \\ &\quad \times \phi(\mathbf{k}_0, t) \phi(\mathbf{q} - \mathbf{k}_0, t). \end{aligned} \tag{6.93}$$

The integrand is nonzero as long as $\mathbf{Aq} \neq 0$. Allowing for a small momentum shell of thickness ϵ was enough for anisotropy to play a role, in contrast to the standard schematic approximation.

The previous result justifies the following approximation for the memory kernel $\mathbf{K}(\mathbf{q}, z)$, when $|\mathbf{q}| = q_0$ and $\mathbf{Aq} \neq 0$:

$$\mathbf{K}(\mathbf{q}, z) = \lambda \phi_2(q_0, z) (\mathbf{e}_1 \otimes \mathbf{e}_1 + \mathbf{e}_3 \otimes \mathbf{e}_3) + \nu \phi_2(q_0, z) \mathbf{e}_2 \otimes \mathbf{e}_2, \tag{6.94}$$

with λ and ν two parameters that depend continuously on density and temperature. Moreover, as a further simplification, we assume that all the modes relax as the ones in the (xy) plane. We speculate that the anisotropy of the system would simply lead to a renormalization of γ for our theory, thus weakly affecting the results discussed in the following.

Within the above approximation, Eq. (6.78) reads

$$z\phi - 1 = -q_0^2 D_0 \phi \frac{1 + \nu \phi_2(1 + \gamma^2)}{1 + \phi_2(\lambda + \nu) + \phi_2^2 \lambda \nu (1 + \gamma^2)}. \tag{6.95}$$

For $\gamma = 0$, this expression must match its equilibrium counterpart. Therefore we must have $\lambda = \lambda_{\text{eq}}$. In the next paragraph we investigate the glass transition and the dynamic acceleration in the ergodic phase.

Ergodicity Breaking

We substitute Eq. (6.84) into Eq. (6.95) and keep only the leading diverging terms of order $1/z^2$:

$$\lambda_{\text{eq}} \nu (1 + \gamma^2) (1 - f_0) f_0 = q_0^2 D_0 \nu (1 + \gamma^2). \tag{6.96}$$

This expression simplifies into Eq. (6.85), namely $\frac{1}{1-f_0} = \frac{\lambda_{\text{eq}}}{q_0^2 D_0} f_0$, which establishes that dynamic ergodicity breaking occurs at exactly the same location as in equilibrium.

Speedup of the relaxation time

Using $\phi(q_0, z = 0) = \tau_0$, $\phi_2(q_0, 0) = \frac{\tau_0}{2}$ and substituting into Eq. (6.95) with $z = 0$ we obtain an equation for τ_0 :

$$\tau_0^2 \left[(1 + \gamma^2) \left(\frac{\lambda}{4} - q_0^2 D_0 \right) \nu \right] + \tau_0 \left[\frac{1}{2} (\lambda + \nu) - q_0^2 D_0 \right] + 1 = 0. \tag{6.97}$$

The positive solution for any value of γ is

$$\tau_0^{-1}(\gamma) = \frac{4}{-\lambda - \nu + 2q_0^2 D_0 + \sqrt{\lambda^2 + \nu^2 + 4\nu q_0^2 D_0(1 + 2\gamma^2) + 4q_0^2 D_0^2 - 2\lambda(\nu + 2\gamma^2\nu + 2q_0^2 D_0)}}. \quad (6.98)$$

This describes the relaxation time for exponential relaxation in the ergodic phase. The relaxation is exponential as long as $\lambda_{\text{eq}} < 2q_0^2 D_0$, as in equilibrium. As a consistency check, $\tau_0(0)$ matches the equilibrium solution, while $\tau_0(\gamma) < \tau_0(0)$ for all values of γ . This proves that transverse forces accelerate the relaxation of the system.

In the limit $\gamma \rightarrow \infty$, the relaxation time reads:

$$\tau_0(\gamma) = \frac{1}{\gamma\nu} \sqrt{\frac{2}{\left(q_0^2 D_0 - \frac{\lambda}{2}\right)}}. \quad (6.99)$$

In this limit, the relaxation time goes to 0 linearly in $1/\gamma$. If correct, this implies a relaxation time that goes to zero for a large amplitude of the transverse forces. However, in numerical applications this method would be hindered by errors in the discretized equation of motion as increasing γ would in practice demand smaller and smaller timesteps. Note also that the γ^1 -dependence of the acceleration at large γ differs from the naive γ^2 acceleration one might anticipate based on a simpler dimensional analysis as argued in [108]. This modified scaling results from a many-body correlation effect.

We now move to lower temperatures close to the dynamical glass transition, where the exponential form for the relaxation is no longer valid.

Early and late β -relaxations close to the transition

We now study the time-dependence of ϕ near its intermediate-time plateau within the ergodic phase, but very close to the mode-coupling critical temperature. We study whether the known power-law regimes in this region, as found in [19], are affected by the transverse forces. Our starting point is Eq. (6.95), which we recall here:

$$\frac{q_0^2 D_0 \phi(z)}{1 - z\phi(z)} = \frac{1 + (\lambda + \nu) \phi_2(z) + (1 + \gamma^2) \lambda \nu \phi_2(z)^2}{1 + (1 + \gamma^2) \nu \phi_2(z)}. \quad (6.100)$$

The system loses ergodicity for $\lambda \geq 4q_0^2 D_0$. In the glass state close to the ergodicity breaking we set $\lambda = 4q_0^2 D_0(1 + \varepsilon)$ with $\varepsilon \ll 1$, and we obtain

$$\lim_{t \rightarrow +\infty} \phi(t) = \frac{1}{2} \left(1 + \varepsilon^{1/2}\right). \quad (6.101)$$

If instead we set

$$\lambda = 4q_0^2 D_0 (1 - \varepsilon) \quad (6.102)$$

we are in the ergodic phase close to the glass transition. To describe the approach of ϕ to the plateau we assume, in the limit $\varepsilon \rightarrow 0$ the following scaling form, taken from Eq. (6.101):

$$\phi(t) = \frac{1}{2} + \varepsilon^{1/2} g(\tau), \quad (6.103)$$

with $\tau \equiv \varepsilon^\alpha t$ a rescaled time. We begin by assuming that $\alpha > 1$ and we shall later check that this is self-consistently correct. When considering the Laplace transform, we use a rescaled variable $z \equiv \varepsilon^\alpha \zeta$. The Laplace transforms of $\phi(t)$ and $\phi^2(t)$ are therefore

$$\begin{aligned}\phi(\zeta) &= \varepsilon^{-\alpha} \left[\frac{1}{2\zeta} + \varepsilon^{1/2} g(\zeta) \right], \\ \phi_2(\zeta) &= \varepsilon^{-\alpha} \left[\frac{1}{4\zeta} + \varepsilon^{1/2} g(\zeta) + \varepsilon g_2(\zeta) \right].\end{aligned}\tag{6.104}$$

We thus substitute Eq. (6.104) into Eq. (6.100) and search for the leading order in ε . To do so, we assume that we are in a regime where $|\varepsilon^{1/2} g(\tau)| \ll 1$. The orders ε^0 and $\varepsilon^{1/2}$ are self-consistently satisfied, while at order ε we obtain

$$8\zeta g^2(\zeta) - 4g_2(\zeta) = -\frac{1}{\zeta}.\tag{6.105}$$

This is the same equation as that obtained in equilibrium [19]. The exponents controlling the approach to and the departure from the plateau are left unchanged by the transverse dynamics.

For completeness, we also recall how to compute these exponents below. For the early β -relaxation we take

$$g(\tau) \equiv a_0 \tau^{-a}\tag{6.106}$$

for $\tau \ll 1$, which implies that

$$\begin{aligned}g(\zeta) &= a_0 \zeta^{a-1} \Gamma(1-a), \\ g_2(\zeta) &= a_0^2 \zeta^{2a-1} \Gamma(1-2a),\end{aligned}\tag{6.107}$$

for $\zeta \gg 1$, with $\Gamma(x) \equiv \int_0^{+\infty} t^{x-1} e^{-t} dt$ the gamma function. Substitution into Eq. (6.105) yields to leading order in ζ

$$4a_0^2 \zeta^{2a-1} \left[2\Gamma(1-a)^2 - \Gamma(1-2a) \right] = 0.\tag{6.108}$$

This equation has two solutions $a = -1$ and $a = 0.395$. Among these, we retain only the physical one with $a = 0.395$. This solution is consistent with the earlier assumption that $\alpha > 1$. In fact, if we want

$$\phi(t) = \frac{1}{2} + a_0 t^{-a}\tag{6.109}$$

to hold, then we must have $\alpha = 1/2a > 1$. We also assess in which range of times this solution is valid. Since we want $|\varepsilon^{1/2} g(\tau)| \ll 1$ and $\tau \ll 1$ we must have

$$\varepsilon^{\frac{1}{2a}} a_0^{1/a} \ll \tau \ll 1,\tag{6.110}$$

which implies

$$a_0^{1/a} \ll t \ll \varepsilon^{-1/2a}.\tag{6.111}$$

For the late β -relaxation we assume

$$g(\tau) \equiv -b_0 \tau^b\tag{6.112}$$

for $\tau \gg 1$, which implies that

$$\begin{aligned} g(\zeta) &= -b_0 \zeta^{-b-1} \Gamma(1+b), \\ g_2(\zeta) &= b_0^2 \zeta^{-2b-1} \Gamma(1+2b), \end{aligned} \quad (6.113)$$

for $\zeta \ll 1$. Substitution in Eq. (6.105) yields to leading order in ζ

$$4a_0^2 \zeta^{-2b-1} [2\Gamma(1+b)^2 - \Gamma(1+2b)] = 0. \quad (6.114)$$

This equation has the solution $b = 1$. We also assess in which range of times this solution is valid. Since we want $|\varepsilon^{1/2}g(\tau)| \ll 1$ and $\tau \gg 1$ we must have

$$1 \ll \tau \ll \varepsilon^{\frac{1}{2b}} b_0^{-1/b}, \quad (6.115)$$

which implies

$$\varepsilon^{-1/2a} \ll t \ll \varepsilon^{-\frac{1}{2a}-\frac{1}{2b}} b_0^{-1/b}. \quad (6.116)$$

This approach does not allow us to compute the values of the two constants a_0 and b_0 . These will however exhibit a dependence on γ , which, we expect, should result in a marginal shortening of the time required to approach and leave the plateau in the temperature regime close to the ergodicity breaking transition.

Divergence of the relaxation time

In this subsection we show that the exponent characterizing the divergence of the relaxation time close to criticality is also unchanged by the transverse forces.

We start by assuming the following form for $\phi(t)$ for $t \gg a_0^{1/\alpha}$:

$$\phi(t) \equiv \frac{1}{2} e^{2\varepsilon^{1/2}g(\varepsilon^\alpha t)}. \quad (6.117)$$

This expression naturally gives Eq. (6.103) whenever $|\varepsilon^{1/2}g(\varepsilon^\alpha t)| \ll 1$, which corresponds to the plateau regime investigated earlier. When $t \gg \varepsilon^{-\frac{1}{2a}-\frac{1}{2b}} b_0^{-1/b}$ we have

$$\phi(t) = \frac{1}{2} e^{-2b_0\varepsilon^{\alpha+1/2}t}. \quad (6.118)$$

The Laplace transforms read

$$\begin{aligned} \phi(z) &= \frac{1}{2(z + 2b_0\varepsilon^{\alpha+1/2})}, \\ \phi_2(z) &= \frac{1}{4(z + 4b_0\varepsilon^{\alpha+1/2})}. \end{aligned} \quad (6.119)$$

Using the scaling $z = \varepsilon^{\alpha+1/2}\zeta$ we see that, to leading order in ε , Eq. (6.119) satisfies Eq. (6.100), which confirms that the ansatz of Eq. (6.118) is correct. Our schematic mode-coupling theory therefore predicts that, close to the critical temperature T_{MCT} , the relaxation time τ_α diverges as a power law,

$$\tau_\alpha \sim (T - T_{\text{MCT}})^{-1/2a+1/2b}, \quad (6.120)$$

with $\frac{1}{2a} + \frac{1}{2b} \approx 1.7658$, which is again the same exponent as in equilibrium [19].

6.3.6 Beyond the schematic approximation

Using insights gained from the schematic approximation, we now prove some general properties of the dynamics with transverse forces, as derived in Eq. (6.78), in particular regarding the location of the glass transition and the acceleration of the dynamics.

Location of the glass transition

To locate the glass transition, we assume that when ergodicity breaking occurs, the plateau is the same for all wavevectors with the same modulus:

$$\begin{aligned}\phi(\mathbf{q}, z \rightarrow 0) &\approx \frac{\phi_\infty(\mathbf{q})}{z}, \\ K_{11}(\mathbf{q}, z \rightarrow 0) &\approx K_{33}(\mathbf{q}, z \rightarrow 0) \approx \frac{K_{\parallel,\infty}(\mathbf{q})}{z}, \\ K_{22}(\mathbf{q}, z \rightarrow 0) &\approx \frac{K_{\perp,\infty}(\mathbf{q}, z \rightarrow 0)}{z}.\end{aligned}\tag{6.121}$$

Taking the limit $z \rightarrow 0$ in Eq. (6.78), and using Eq. (6.121), the contribution from transverse forces cancels, leading to

$$q^2 D_0 \frac{\phi_\infty(\mathbf{q})}{1 - \phi_\infty(\mathbf{q})} = K_{\parallel,\infty}(\mathbf{q}).\tag{6.122}$$

This equation is the same as the one governing the equilibrium case. This establishes that the glass transition takes place for the same value of the parameters (density, temperature) as in equilibrium when $\gamma = 0$.

Acceleration in the ergodic phase

In the ergodic phase, however, some acceleration can be achieved even if the location of the glass transition is the same. To support this assertion, we begin by self-consistently assuming that transverse forces accelerate the decay of the dynamical structure factor. In practice, we start from the postulate that

$$\phi_f(\mathbf{q}) \leq \phi_{eq,f}(\mathbf{q}),\tag{6.123}$$

where $\phi_f \equiv \phi(\mathbf{q}, z = 0) \equiv \int_0^{+\infty} d\tau \phi(\mathbf{q}, \tau)$ is the time-integrated normalized dynamical structure factor, and $\phi_{eq,f}$ is the same quantity for equilibrium dynamics, obtained from Eq. (6.78) when $\gamma = 0$. Due to the mode-coupling expression of the memory kernel, Eq. (6.70), it follows that $K_{ij,f}(\mathbf{q}) \equiv K_{ij}(\mathbf{q}, z = 0) \leq K_{ij,eq,f}(\mathbf{q}) \equiv K_{ij,eq}(\mathbf{q}, z = 0)$. This means that

$$\frac{1 + (1 + \gamma^2)K_{22,f}}{(1 + K_{11,f})(1 + K_{22,f}) + \gamma^2 K_{11,f} K_{22,f}} \geq \frac{1}{1 + K_{11,eq,f}},\tag{6.124}$$

where we omitted the dependence on the \mathbf{q} argument for clarity. This inequality self-consistently proves that the transverse force dynamics accelerates the decay rate of ϕ in the ergodic phase.

Limits behavior for large γ

We explore the asymptotic behavior of the relaxation in the ergodic in the presence of very strong transverse forces. In the ergodic phase, the $z \rightarrow 0$ limit of Eq. (6.78) reads

$$1 = -D_0 \mathbf{q} \cdot \left[\frac{1 + (1 + \gamma^2)K_{22,f}}{(1 + K_{11,f})(1 + K_{22,f}) + \gamma^2 K_{11,f} K_{22,f}} \mathbf{e}_1 \otimes \mathbf{e}_1 + \frac{1}{1 + K_{33,f}} \mathbf{e}_3 \otimes \mathbf{e}_3 \right] \cdot \mathbf{q} \phi_f. \quad (6.125)$$

The analysis of the exponential relaxation in the schematic approximation suggests that, in the limit $\gamma \rightarrow \infty$, one should expect

$$\lim_{\gamma \rightarrow \infty} \phi_f = \frac{\bar{\phi}_f}{\gamma}, \quad (6.126)$$

where $\bar{\phi}_f$ is a constant that does not depend on γ . Our starting point is the assumption that a similar scaling holds for the memory kernels, namely

$$\lim_{\gamma \rightarrow \infty} K_{ii,f} = \frac{\bar{K}_{ii,f}}{\gamma}, \quad (6.127)$$

with $\bar{K}_{ii,f}$ a quantity independent from γ . This scaling can be explicitly checked in the case of exponential relaxation. If we substitute the asymptotic behaviors of Eqs. (6.126, 6.127) into Eq. (6.125), the dependence on γ disappears. This result consistently demonstrates that the relaxation time decreases linearly in γ^{-1} in the limit of strong transverse forces. Note that, by contrast to the discussion in Sec. 6.3.5 which was limited to exponential decays, this result is valid over the whole ergodic phase.

In this section, we have investigated the relaxation properties of the collective density modes in the presence of transverse forces, demonstrating the existence of a speedup, and establishing its asymptotic behavior for strong drift. We have also realized that transverse forces do not affect the location of the transition to the nonergodic regime. This, in turn, triggers a number of questions related to the microscopic mechanisms and dynamical pathways opened by transverse forces that support these observed collective behaviors. To answer this question, we turn to the analysis of the motion of an individual particle. The transport coefficients of this tracer, along with the diffusivity and mobility tensors, will help us shape a qualitative picture.

6.4 Dynamics of a tracer with transverse forces in the mode-coupling approach

We now analyze the motion of a tracer within the mode-coupling framework. We first introduce the general setting and the relevant dynamical quantities.

Following Ernst and Dorfman [86], we consider the motion of a tagged tracer particle with label 0 in a liquid of N particles with transverse forces. The tracer initial position

at time $t = 0$, \mathbf{r}_0 , is fixed at the origin, and it influences the distribution of the surrounding bath. The initial condition for the probability distribution of the total system thus reads

$$P_{N+1}(\mathbf{r}^{N+1}, t = 0) = V\delta(\mathbf{r}_0)\rho_B(\mathbf{r}^{N+1}). \quad (6.128)$$

Averages over the initial distribution $P_{N+1}(\mathbf{r}^{N+1}, 0)$ will be denoted by $\langle \dots \rangle_0$. Averages over the Boltzmann distribution are denoted by $\langle \dots \rangle$, as usual. Starting from $t = 0$, a constant external force \mathbf{F}_{ext} is applied on the tracer. The evolution operator becomes $\Omega_\gamma^{\text{ext}}$, defined as

$$\begin{aligned} \Omega_{\gamma,\text{ext}} &= \Omega_\gamma + \delta\Omega^{\text{ext}} \\ &= D_0 \sum_i \nabla_i \cdot [\nabla_i - (\mathbf{1} + \gamma \mathbf{A}) \beta \mathbf{F}_i] - D_0 \nabla_0 \cdot \beta \mathbf{F}_{\text{ext}}. \end{aligned} \quad (6.129)$$

We denote the Fourier transform of the tracer density as

$$n_0(\mathbf{q}) \equiv e^{-i\mathbf{q}\cdot\mathbf{r}_0}. \quad (6.130)$$

The large-time, long-wavelength limit of this Fourier transform can be used to obtain relevant transport coefficients. A small \mathbf{q} expansion of the time derivative of Eq. (6.130) yields constitutive equations of motion for the tracer

$$\begin{aligned} \langle \partial_t n_0(\mathbf{q}, t) \rangle_0 &= -i\mathbf{q} \cdot \langle \dot{\mathbf{r}}_0(t) \rangle_0 - \mathbf{q} \cdot \int_0^t d\tau \langle \dot{\mathbf{r}}_0(\tau) \otimes \dot{\mathbf{r}}_0(0) \rangle_0 \cdot \mathbf{q} \\ &\quad - \mathbf{q} \cdot \langle \dot{\mathbf{r}}_0(t) \otimes \mathbf{r}_0 \rangle_0 \cdot \mathbf{q} + O(q^3) \\ &\approx -i\mathbf{q} \cdot \boldsymbol{\mu} \cdot \mathbf{F}^{\text{ext}} - \mathbf{q} \cdot \mathbf{D} \cdot \mathbf{q}. \end{aligned} \quad (6.131)$$

In the second line, we have taken a large time limit, $t \rightarrow \infty$, and used the definition of the diffusivity tensor \mathbf{D} , given by Eq. (6.13), and the mobility tensor $\boldsymbol{\mu}$, given by Eq. (6.14). Note that the mobility and the diffusivity are computed within a linear response formalism, where the intensity of the external force is small, $|\mathbf{F}^{\text{ext}}| \rightarrow 0$. Moreover, as for the weak coupling analysis of the tracer, we are interested in the expression of the diffusivity tensor obtained for $\mathbf{F}^{\text{ext}} = 0$, and neglect the dressing of the diffusivity that comes from the presence of the dragging external force.

6.4.1 Equation of motion of the tracer

We introduce a projection operator tailored to the space of the tracer density fluctuations

$$\mathcal{P}_0 \equiv \sum_{\mathbf{q}} \dots n_0^*(\mathbf{q}) \langle n_0(\mathbf{q}) \dots \rangle \quad (6.132)$$

and the associated orthogonal projector $\mathcal{Q}_0 \equiv \mathcal{I} - \mathcal{P}_0$. Note that, in contrast with the other projection operators used in this work, \mathcal{P}_0 contains a summation over all wavevectors, since these are all included inside the δ -function of the initial condition

in Eq. (6.128). With this definition, we have

$$\begin{aligned}
 \mathcal{P}_0 P_{N+1}(\mathbf{r}^{N+1}; t = 0) &= \frac{1}{V} \sum_{\mathbf{q}} n_0(\mathbf{q}) \langle n_0^*(\mathbf{q}) V \delta(\mathbf{r}_0) \rangle \\
 &= \sum_{\mathbf{q}} n_0(\mathbf{q}) \rangle \\
 &= V \delta(\mathbf{r}_0) \rho_B(\mathbf{r}^{N+1}) \\
 &= P_{N+1}(\mathbf{r}^N; t = 0),
 \end{aligned} \tag{6.133}$$

and thus

$$\mathcal{Q}_0 P_{N+1}(\mathbf{r}^N, t = 0) = 0. \tag{6.134}$$

Our goal is to derive an equation of motion for the evolution of the average tracer density, $\langle n_0(\mathbf{q}) e^{\Omega_{\gamma,\text{ext}} t} \rangle_0$. In this notation, the probability distribution $P_{N+1}(\mathbf{r}^{N+1}, 0)$ stands to the right of the evolution operator $e^{\Omega_{\gamma,\text{ext}} t}$, which acts on the said distribution. The time derivative of this quantity reads, after a Fourier transformation

$$\begin{aligned}
 \left\langle n_0(\mathbf{q}) \Omega_{\gamma,\text{ext}} \frac{1}{z - \Omega_{\gamma,\text{ext}}} \right\rangle_0 &= \left\langle n_0(\mathbf{q}) \Omega_{\gamma,\text{ext}} \mathcal{P}_0 \frac{1}{z - \Omega_{\gamma,\text{ext}}} \right\rangle_0 + \left\langle n_0(\mathbf{q}) \Omega_{\gamma,\text{ext}} \mathcal{Q}_0 \frac{1}{z - \Omega_{\gamma,\text{ext}}} \right\rangle_0 \\
 &= \left[\langle n_0(\mathbf{q}) \Omega_{\gamma,\text{ext}} n_0^*(\mathbf{q}) \rangle \right. \\
 &\quad \left. + \left\langle n_0(\mathbf{q}) \Omega_{\gamma,\text{ext}} \mathcal{Q}_0 \frac{1}{z - \Omega_{\gamma,\text{ext}} \mathcal{Q}_0} \mathcal{Q}_0 \Omega_{\gamma,\text{ext}} n_0^*(\mathbf{q}) \right\rangle \right] n_0(\mathbf{q}, z),
 \end{aligned} \tag{6.135}$$

with $n_0(\mathbf{q}, z) = \left\langle n_0(\mathbf{q}) \frac{1}{z - \Omega_{\gamma,\text{ext}}} \right\rangle_0$. We used the same resolvent identity as in Eq. (6.60) (with \mathcal{P}_0 and \mathcal{Q}_0 instead of \mathcal{P} and \mathcal{Q}), namely

$$\frac{1}{z - \Omega_{\gamma,\text{ext}}} = \frac{1}{z - \Omega_{\gamma,\text{ext}} \mathcal{Q}_0} + \frac{1}{z - \Omega_{\gamma,\text{ext}} \mathcal{Q}_0} \mathcal{Q}_0 \Omega_{\gamma,\text{ext}} \mathcal{P}_0 \frac{1}{z - \Omega_{\gamma,\text{ext}}}, \tag{6.136}$$

together with the fact that $\left\langle \dots \mathcal{Q}_0 \frac{1}{z - \Omega_{\gamma,\text{ext}} \mathcal{Q}_0} \right\rangle_0 = 0$. The frequency matrix reads

$$\langle n_0(\mathbf{q}) \Omega_{\gamma,\text{ext}} n_0^*(\mathbf{q}) \rangle = -D_0 q^2 - i D_0 \beta \mathbf{q} \cdot \mathbf{F}^{\text{ext}}, \tag{6.137}$$

and it contains the mobility of a free tracer, $D_0 \beta$.

The memory kernel reads instead

$$\begin{aligned}
 \left\langle n_0(\mathbf{q}) \Omega_{\gamma,\text{ext}} \mathcal{Q}_0 \frac{1}{z - \mathcal{Q}_0 \Omega_{\gamma,\text{ext}} \mathcal{Q}_0} \mathcal{Q}_0 \Omega_{\gamma,\text{ext}} n_0^*(\mathbf{q}) \right\rangle &= \left\langle n_0^*(\mathbf{q}) \Omega_{-\gamma,\text{ext}} \mathcal{Q}_0 \frac{1}{z - \mathcal{Q}_0 \Omega_{-\gamma,\text{ext}} \mathcal{Q}_0} \mathcal{Q}_0 \Omega_{-\gamma,\text{ext}} n_0(\mathbf{q}) \right\rangle \\
 &= -i \mathbf{q} \cdot D_0^2 \left\langle e^{i \mathbf{q} \cdot \mathbf{r}_0} [(\mathbf{1} - \gamma \mathbf{A}) \cdot \beta \mathbf{F}_0 - i \mathbf{q} + \beta \mathbf{F}^{\text{ext}}] \mathcal{Q}_0 \frac{1}{z - \mathcal{Q}_0 \Omega_{-\gamma,\text{ext}} \mathcal{Q}_0} \right. \\
 &\quad \left. \times \mathcal{Q}_0 \nabla_0 e^{-i \mathbf{q} \cdot \mathbf{r}_0} \right\rangle \cdot [(1 - \gamma \mathbf{A}) \cdot i \mathbf{q} - \beta \mathbf{F}^{\text{ext}}].
 \end{aligned} \tag{6.138}$$

The first term \mathbf{F}^{ext} on the right hand side does not contribute, since it belongs to the space of the tracer's density modes. It thus vanishes when the projector \mathcal{Q}_0 acts on its right. To extract the mobility of the tracer, we are interested in terms linear in \mathbf{F}^{ext} . One of these terms comes from the last \mathbf{F}^{ext} appearing on the right-hand side of Eq. (6.138). Another term comes in principle from the expansion of the operator $\Omega_{\gamma,\text{ext}}$. However, the physical meaning of this term is a dressing of the diffusion matrix by means of the external force, as it yields a contribution proportional to q^2 . The tracer's equation of motion can thus be cast in the form

$$z\langle n_0(q, z) \rangle_0 - 1 = [-i\mathbf{q} \cdot \boldsymbol{\mu}(\mathbf{q}, z) \cdot \mathbf{F}^{\text{ext}} - \mathbf{q} \cdot [\mathbf{D}(\mathbf{q}, z) + |\mathbf{F}^{\text{ext}}| \delta \mathbf{D}(\mathbf{q}, z)] \cdot \mathbf{q}] \mathbf{n}(\mathbf{q}, z), \quad (6.139)$$

where $\delta \mathbf{D}(\mathbf{q}, z)$ is the correction to the diffusivity tensor due to the applied external force. We are not interested in this term, and we focus on the mobility and diffusivity tensors, that read respectively

$$\boldsymbol{\mu}(\mathbf{q}, z) = D_0 \beta [\mathbf{1} - (\mathbf{1} - \gamma \mathbf{A}) \widetilde{\mathbf{K}}_0(\mathbf{q}, z)], \quad (6.140)$$

and

$$\mathbf{D}(\mathbf{q}, z) = D_0 [\mathbf{1} - (\mathbf{1} - \gamma \mathbf{A}) \widetilde{\mathbf{K}}_0(\mathbf{q}, z) (\mathbf{1} - \gamma \mathbf{A})]. \quad (6.141)$$

The tracer-memory kernel can be expressed in terms of the projected longitudinal tracer force density Fourier modes

$$\widetilde{\mathbf{K}}_0(\mathbf{q}, z) \equiv D_0 \beta^2 \left\langle \mathbf{j}_0^*(\mathbf{q}) \mathcal{Q}_0 \frac{1}{z - \mathcal{Q}_0 \Omega_{-\gamma} \mathcal{Q}_0} \mathcal{Q}_0 \mathbf{j}_0(\mathbf{q}) \right\rangle, \quad (6.142)$$

with $\mathcal{Q}_0 \mathbf{j}_0(\mathbf{q}) \equiv \mathcal{Q}_0 \mathbf{F}_0 e^{-i\mathbf{q} \cdot \mathbf{r}_0}$. Note that due to the projection operator we have $\dots \mathcal{Q}_0 \mathbf{F}_0 e^{-i\mathbf{q} \cdot \mathbf{r}_0} \rangle = \dots \mathcal{Q}_0 T \nabla_0 e^{-i\mathbf{q} \cdot \mathbf{r}_0} \rangle$ and it is the latter form that is used in the definition of the irreducible evolution operator, Eq. (6.146) and the derivation of the mode-coupling vertex, Eq. (6.149).

Equations (6.140, 6.141) express the transport coefficients of the tracer as a function of the current-current, memory tensor $\widetilde{\mathbf{K}}_0$. As usual in a mode-coupling approach, we first give an irreducible representation of this memory kernel and then expand it within the mode-coupling approximation.

The reduction of $\widetilde{\mathbf{K}}$ is achieved by introducing an irreducible evolution operator

$$\Omega_{-\gamma}^{\text{irrs}} = \Omega_{-\gamma} + D_0 \beta^2 \sum_{\mathbf{k}} \mathcal{Q}_0 \mathbf{j}_0(\mathbf{k}) \cdot (\mathbf{1} - \gamma \mathbf{A}) \cdot \langle \mathbf{j}_0^*(\mathbf{k}) \mathcal{Q}_0 \rangle \quad (6.143)$$

and exploiting the identity

$$\frac{1}{z - \mathcal{Q}_0 \Omega_{-\gamma} \mathcal{Q}_0} = \frac{1}{z - \Omega_{-\gamma}^{\text{irrs}}} \left[1 - \frac{D_0 \beta^2}{V} \sum_{\mathbf{k}} \mathcal{Q}_0 \mathbf{j}_0(\mathbf{k}) \right] \cdot (\mathbf{1} - \gamma \mathbf{A}) \cdot \left\langle \mathbf{j}_0^*(\mathbf{k}) \mathcal{Q}_0 \frac{1}{z - \mathcal{Q}_0 \Omega_{-\gamma} \mathcal{Q}_0} \right\rangle. \quad (6.144)$$

We obtain from Eq. (6.142)

$$\widetilde{\mathbf{K}}_0(\mathbf{q}, z) = [\mathbf{1} + \mathbf{K}_0(\mathbf{q}, z) (\mathbf{1} - \gamma \mathbf{A})]^{-1} \cdot \mathbf{K}_0(\mathbf{q}, z), \quad (6.145)$$

where we have introduced the irreducible memory kernel for the tracer

$$\mathbf{K}_0(\mathbf{q}, z) \equiv \beta^2 D_0 \left\langle \mathbf{j}_0^*(\mathbf{q}) \mathcal{Q}_0 \frac{1}{z - \Omega_{-\gamma}^{\text{irrs}}} \mathcal{Q}_0 \mathbf{j}_0(\mathbf{q}) \right\rangle. \quad (6.146)$$

As a consequence of the linear response treatment in the definition of the $\mathbf{K}_0(\mathbf{q}, z)$ the evolution operator involves the dynamics with transverse forces in the absence of the external perturbation. This allows us to simplify the tracer's memory kernel, as was done previously for the memory kernel related to the dynamics structure factor, $\mathbf{K}(\mathbf{q}, z)$. Before discussing further this point, we apply the mode-coupling approximation scheme to \mathbf{K}_0 .

6.4.2 Mode-coupling expansion of the tracer's memory kernel

The mode-coupling expansion can be carried out in an analogous way to what was done in Sec. 6.3.3. The tracer's current is expanded along the following density product:

$$\mathcal{Q}_0 \mathbf{j}_0(\mathbf{q}) \approx \sum_{\mathbf{k}} \frac{n(\mathbf{k}) n_0(\mathbf{q} - \mathbf{k})}{NS(\mathbf{k})} \langle n^*(\mathbf{k}) n_0^*(\mathbf{q} - \mathbf{k}) \mathcal{Q}_0 \mathbf{j}_0(\mathbf{q}) \rangle. \quad (6.147)$$

The Gaussian approximation now becomes

$$\begin{aligned} \langle n^*(\mathbf{k}') n_0^*(\mathbf{q} - \mathbf{k}') e^{\Omega_{-\gamma}^{\text{irrs}} t} n(\mathbf{k}) n_0(\mathbf{q} - \mathbf{k}) \rangle &\approx \langle n^*(\mathbf{k}') e^{\Omega_{-\gamma} t} n(\mathbf{k}) \rangle \langle n_0^*(\mathbf{q} - \mathbf{k}') e^{\Omega_{-\gamma} t} n_0(\mathbf{q} - \mathbf{k}) \rangle \\ &\quad + \langle n^*(\mathbf{k}') e^{\Omega_{-\gamma} t} n_0(\mathbf{q} - \mathbf{k}) \rangle \langle n_0^*(\mathbf{q} - \mathbf{k}') e^{\Omega_{-\gamma} t} n(\mathbf{k}) \rangle \\ &= NS(\mathbf{k}, t) F_s(\mathbf{q} - \mathbf{k}, t) \delta_{\mathbf{k}, \mathbf{k}'} + S(\mathbf{k}, t) S(\mathbf{q} - \mathbf{k}, t) \delta_{\mathbf{k}', \mathbf{q} - \mathbf{k}} \\ &\approx NS(\mathbf{k}, t) F_s(\mathbf{q} - \mathbf{k}, t) \delta_{\mathbf{k}, \mathbf{k}'}. \end{aligned} \quad (6.148)$$

In the last passage we have neglected the term of order 1 compared to the term of order N^2 . In addition, we noted that since the tracer is equivalent to any other particle, we have $\langle n_0^*(\mathbf{q} - \mathbf{k}') e^{\Omega_{-\gamma} t} n_0(\mathbf{q} - \mathbf{k}) \rangle = F_s(\mathbf{q} - \mathbf{k})$, with the self-intermediate correlation function F_s defined in Eq. (6.45).

We now compute the average in Eq. (6.147) with the help of a convolution approximation

$$\begin{aligned} \langle n(\mathbf{k})^* n_0^*(\mathbf{q} - \mathbf{k}) \mathcal{Q}_0 \mathbf{j}_0(\mathbf{q}) \rangle &= \langle n(\mathbf{k})^* n_0^*(\mathbf{q} - \mathbf{k}) \mathbf{j}_0(\mathbf{q}) \rangle - \langle n(\mathbf{k})^* n_0^*(\mathbf{q} - \mathbf{k}) n_0(\mathbf{q}) \rangle \langle n_0^*(\mathbf{q}) \mathbf{j}_0(\mathbf{q}) \rangle \\ &= T \left\langle n(\mathbf{k})^* n_0^*(\mathbf{q} - \mathbf{k}) \nabla_0 e^{-i\mathbf{q}\cdot\mathbf{r}_0} \right\rangle \\ &\quad - TS(k) \left\langle n_0^*(\mathbf{q}) \nabla_0 e^{-i\mathbf{q}\cdot\mathbf{r}_0} \right\rangle \\ &= -T \left\langle \nabla_0 [n(\mathbf{k})^* n_0^*(\mathbf{q} - \mathbf{k})] e^{-i\mathbf{q}\cdot\mathbf{r}_0} \right\rangle \\ &\quad + TS(k) \left\langle \nabla_0 [n_0^*(\mathbf{q})] e^{-i\mathbf{q}\cdot\mathbf{r}_0} \right\rangle \\ &= -iT [\mathbf{k} + (\mathbf{q} - \mathbf{k}) S(k) - \mathbf{q} S(k)] \\ &= -iT \rho_0 S(k) c(k) \mathbf{k}, \end{aligned} \quad (6.149)$$

with $\rho_0 c(k) = 1 - \frac{1}{S(k)}$ the direct correlation function. With these results, substitution of Eq. (6.147) in the irreducible memory kernel of Eq. (6.146) yields

$$\mathbf{K}_0(\mathbf{q}, t) \approx D_0 \rho_0 \int_{\mathbf{k}} \mathbf{k} \otimes \mathbf{k} c(k)^2 F_s(\mathbf{q} - \mathbf{k}, t) S(\mathbf{k}, t). \quad (6.150)$$

This is the mode-coupling expression of the tracer's memory kernel. Using the symmetries of the dynamics, as done in Sec. 6.3.3, one can show that \mathbf{K}_0 is diagonal in the $\mathbf{A} - \mathbf{q}$ basis given by Eq. (6.68):

$$\mathbf{K}_0(\mathbf{q}, t) = \sum_i K_{0,ii}(\mathbf{q}, t) \mathbf{e}_i \otimes \mathbf{e}_i. \quad (6.151)$$

Now that we have a diagonal decomposition of the tracer's memory kernel, we can focus on physical quantities of interest for the tracer dynamics.

6.4.3 Self-intermediate scattering function

The dynamics of the self-intermediate scattering function F_s can be read from the tracer's dynamics. It is given by

$$zF_s(\mathbf{q}) - 1 = -D_0 \mathbf{q} \cdot \left[\frac{1 + (1 + \gamma^2)K_{0,22}}{(1 + K_{0,11})(1 + K_{0,22}) + \gamma^2 K_{0,11} K_{0,22}} \mathbf{e}_1 \otimes \mathbf{e}_1 + \frac{1}{1 + K_{0,33}} \mathbf{e}_3 \otimes \mathbf{e}_3 \right] \cdot \mathbf{q} F_s(\mathbf{q}, z). \quad (6.152)$$

This equation of motion is formally similar to Eq. (6.78), with the collective memory kernel being replaced by the tracer's memory kernel. For a wavevector \mathbf{q} lying in the (xy) plane, we get, using an inverse Laplace transform

$$\partial_t F_s + D_0 q^2 F_s + D_0 q^2 (1 + \gamma^2) K_{0,22} * F_s = - \left[(K_{0,11} + K_{0,22}) + (1 + \gamma^2) K_{0,11} * K_{0,22} \right] * \partial_t F_s, \quad (6.153)$$

where the dependence on (\mathbf{q}, t) has been omitted for clarity. This equation was announced in a recent work (Eq. (11) in [108]). The properties of this dynamics can be analyzed in the same way illustrated for the dynamical structure factor in Sec. 6.3.5.

6.4.4 Diffusion tensor

The diffusion tensor at any finite wavevector and frequency is obtained by substituting the mode-coupling expression for \mathbf{K}_0 , given in Eq. (6.151), into Eq. (6.141). The result

reads, in the $\mathbf{A} - \mathbf{q}$ basis introduced in Eq. (6.68)

$$\begin{aligned} \mathbf{D}(\mathbf{q}, z) = D_0 & \left[\frac{1 + (1 + \gamma^2)K_{0,22}}{(1 + K_{0,11})(1 + K_{0,22}) + \gamma^2 K_{0,11} K_{0,22}} \mathbf{e}_1 \otimes \mathbf{e}_1 + \frac{1}{1 + K_{0,33}} \mathbf{e}_3 \otimes \mathbf{e}_3 \right. \\ & + \gamma \frac{K_{0,11} + K_{0,22} + (1 + \gamma^2)K_{0,11}K_{0,22}}{(1 + K_{0,11})(1 + K_{0,22}) + \gamma^2 K_{0,11} K_{0,22}} [\mathbf{e}_1 \otimes \mathbf{e}_2 - \mathbf{e}_2 \otimes \mathbf{e}_1] \\ & \left. + \frac{(1 + K_{0,11})K_{0,22} + K_{0,11}(K_{0,22} - 1)\gamma^2}{(1 + K_{0,11})(1 + K_{0,22}) + \gamma^2 K_{0,11} K_{0,22}} \mathbf{e}_2 \otimes \mathbf{e}_2 \right]. \end{aligned} \quad (6.154)$$

The expression of the diffusion tensor is one of the main results of this work. From the large wavelength, small frequency limit of Eq. (6.154) we obtain the diffusion matrix \mathbf{D} . In Cartesian coordinates, it reads

$$\mathbf{D} = D_{\parallel,x} [\mathbf{e}_x \otimes \mathbf{e}_x + \mathbf{e}_y \otimes \mathbf{e}_y] + D_{\parallel,z} \mathbf{e}_z \otimes \mathbf{e}_z + D_{\perp} [\mathbf{e}_y \otimes \mathbf{e}_x - \mathbf{e}_z \otimes \mathbf{e}_y]. \quad (6.155)$$

We now discuss the expression and the behavior of the different diffusion constants that appear in the diffusion tensor \mathbf{D} .

Longitudinal diffusion

The dynamics with transverse forces is anisotropic. As a consequence, there are two types of longitudinal diffusion constants, one related to the diffusion in the (xy) plane (within which rotational invariance is preserved), $D_{\parallel,x}$ and one related to the diffusion along the z direction, $D_{\parallel,z}$. Their expressions are

$$\begin{aligned} D_{\parallel,x}(\gamma) &= D_0 \frac{1 + (1 + \gamma^2)K_{0,11}^\infty}{(1 + K_{0,11}^\infty)(1 + K_{0,22}^\infty) + \gamma^2 K_{0,11}^\infty K_{0,22}^\infty} \\ D_{\parallel,z}(\gamma) &= D_0 \frac{1}{1 + K_{0,33}^\infty}, \end{aligned} \quad (6.156)$$

where we introduced the notation $K_{0,ii}^\infty \equiv K_{0,ii}(\mathbf{q} \rightarrow 0, z \rightarrow 0)$ to denote the long wavelength, zero frequency of the tracer's memory kernel. This coefficient reads explicitly

$$K_{0,ii}^\infty = \frac{D_0}{\rho_0} \int_0^{+\infty} dt \int_{\mathbf{k}} [k_i \rho_0 c(k)]^2 F_s(-\mathbf{k}, t) S(\mathbf{k}, t). \quad (6.157)$$

For $\gamma = 0$, the equilibrium result is duly recovered:

$$D_{aa,\text{eq}} = D_0 \frac{1}{1 + K_{0,\parallel,\text{eq}}^\infty}, \quad (6.158)$$

for $a = x, y, z$. When $\gamma \neq 0$ the anisotropy of the dynamics is revealed through the different expressions of the diffusion constants.

The dynamics is indeed accelerated. If we assume that in the ergodic phase $K_{0,ii}^\infty \leq K_{0,ii,\text{eq}}^\infty$, we self-consistently obtain $D_{aa}(\gamma) \geq D_{aa}(0)$.

In the ergodic phase in the limit of strong drive, the memory kernel scales as γ^{-1} . This implies that the efficiency of transverse forces with respect to the equilibrium dynamics, computed as the ratio $D(\gamma) \equiv \sum_{a=x,y,z} D_{aa}(\gamma)$ over $D(0)$, grows as

$$\frac{D(\gamma)}{D(0)} \sim \gamma. \quad (6.159)$$

We now investigate two limiting cases: in the high temperature regime, the memory kernels vanish because the fluid enters an effectively noninteracting limit and therefore $D(\gamma) = D_0$, while at $T = T_{\text{MCT}}$ the memory kernels diverge as predicted by the schematic approach of Sec. 6.3.4, implying that $D(\gamma) = 0$ and dynamical arrest occurs. We have therefore

$$\begin{aligned} \lim_{T \rightarrow \infty} \frac{D(\gamma)}{D(0)} &= c(\gamma), \\ \lim_{T \rightarrow T_{\text{MCT}}} \frac{D(\gamma)}{D(0)} &= 1, \end{aligned} \quad (6.160)$$

With $c(\gamma) > 1$ a constant that depends on the intensity of the driving force. These conditions, together with the acceleration in the ergodic phase, demonstrate that the ratio of the diffusion constants $\frac{D(\gamma)}{D_0}$ exhibits a maximum as a function of the temperature in the ergodic phase. This maximum is observed in numerical simulations [108].

Odd diffusivity

The odd diffusion constant is encoded in the antisymmetric part of the diffusivity tensor:

$$D_{\perp}(T, \gamma) = -D_0 \gamma \frac{K_{0,11}^{\infty} + K_{0,22}^{\infty} + (1 + \gamma^2) K_{0,11}^{\infty} K_{0,22}^{\infty}}{(1 + K_{0,11}^{\infty})(1 + K_{0,22}^{\infty}) + \gamma^2 K_{0,11}^{\infty} K_{0,22}^{\infty}}. \quad (6.161)$$

For an asymptotically large driving, $\gamma \rightarrow \infty$, the odd diffusion constant grows linearly in γ , $D_{\perp}(\gamma, T) \sim \gamma$. This suggests that strong transverse forces manifest themselves with an increasingly swirling motion.

Close to ergodicity breaking where the memory kernel diverges, we obtain

$$\lim_{T \rightarrow T_{\text{MCT}}} D_{\perp} = -\gamma D_0. \quad (6.162)$$

Therefore, even if the longitudinal diffusion constant associated to particle transport goes to 0 at the critical temperature, the odd diffusion constant remains nonzero. Together with the vanishing of the diffusion constant, this suggests a physical picture where particles perform a swirling motion inside the permanent local cage made by their neighbors. An analogous situation can be shown to arise in the much simpler model of a particle in an harmonic well under the action of transverse forces [108].

6.4.5 Mobility tensor

The mobility tensor is an alternative quantity characterizing the nature of the dynamics with a physical content distinct from that of the diffusivity tensor due to the breaking

of the Einstein relation. The mobility tensor is obtained from Eq. (6.140), using the mode-coupling expansion of the tracer's memory kernel given in Eq. (6.151). The result reads

$$\boldsymbol{\mu}(\mathbf{q}, z) = D_0\beta \left[\frac{1 + K_{22}}{(1 + K_{11})(1 + K_{22}) + \gamma^2 K_{11}K_{22}} \mathbf{e}_1 \otimes \mathbf{e}_1 + \frac{1}{1 + K_{33}} \mathbf{e}_3 \otimes \mathbf{e}_3 \right. \\ \left. + \frac{\gamma(K_{0,11}\mathbf{e}_2 \otimes \mathbf{e}_1 - K_{0,22}\mathbf{e}_1 \otimes \mathbf{e}_2)}{(1 + K_{11})(1 + K_{22}) + \gamma^2 K_{11}K_{22}} + \frac{1 + K_{11}}{(1 + K_{11})(1 + K_{22}) + \gamma^2 K_{11}K_{22}} \mathbf{e}_2 \otimes \mathbf{e}_2 \right]. \quad (6.163)$$

In the small frequency and large wavelength limit of these expression, we obtain the mobility of the tracer,

$$\boldsymbol{\mu} = \mu_{\parallel,x} [\mathbf{e}_x \otimes \mathbf{e}_x + \mathbf{e}_y \otimes \mathbf{e}_y] + \mu_{\parallel,z} \mathbf{e}_z \otimes \mathbf{e}_z \\ + \mu_{\perp} [\mathbf{e}_x \otimes \mathbf{e}_y - \mathbf{e}_y \otimes \mathbf{e}_x], \quad (6.164)$$

with the longitudinal mobilities $\mu_{\parallel,x}, \mu_{\parallel,z}$, and odd mobility μ_{\perp} given by

$$\mu_{\parallel,x} = D_0\beta \frac{1 + K_{0,11}^{\infty}}{(1 + K_{0,11}^{\infty})^2 + \gamma^2 K_{0,11}^{\infty}}, \\ \mu_{\parallel,z} = D_0\beta \frac{1}{1 + K_{0,33}^{\infty}}, \\ \mu_{\perp} = -\gamma D_0\beta \frac{K_{0,11}^{\infty}}{(1 + K_{0,11}^{\infty})^2 + \gamma^2 K_{0,11}^{\infty}}. \quad (6.165)$$

The anisotropic character of transverse forces in three dimensions manifests itself through the fact that $\mu_{\parallel,z} \neq \mu_{\parallel,x}$. In the large γ -limit, all nonzero entries of the mobility tensor converge (in modulus) to the mobility of a free tracer, $D_0\beta$. This is in contrast with the behavior of the diffusivity tensor, whose nonzero entries grow linearly in γ . This is a consequence of the breakdown of the fluctuation-dissipation theorem, arising from the nonequilibrium nature of the dynamics. A variant of the fluctuation-dissipation theorem survives for the longitudinal components of the diffusion and mobility tensor, as $[\mu(\mathbf{1} + \gamma\mathbf{A})]_{aa} = \beta[\mathbf{D}]_{aa}$ with $a = x, y, z$. This variant of the fluctuation-dissipation theorem was also derived in the dynamical mean-field treatment of transverse forces [109].

As the glass transition is approached, all components of the mobility tensor vanish. Physically, this means that in the dynamically arrested glass, a weak external force cannot set the particles in motion, neither in the longitudinal nor in the transverse direction with respect to the external force.

The vanishing of longitudinal and odd mobilities is one of the facets of the glass transition in the mode-coupling theory of transverse forces. Another facet is the divergence of the viscosity tensor, which will be explored in the next section.

6.5 Odd viscosity

This section is devoted to the study of the emerging odd viscosity [12, 13, 85, 127, 99]. Following [253, 85], we compute the viscosity tensor in the long wavelength and long times limits by looking at the response of the stress to an external perturbation. To do so, we define a microscopic stress tensor in the presence of transverse forces and develop its linear response theory, leading to the definition of the viscosity tensor, and in particular to the identification of its odd component.

6.5.1 Stress tensor and transverse forces

Following [253], we start by defining the microscopic stress tensor in the presence of transverse forces from the equation

$$\partial_t n(\mathbf{q}) = \Omega_\gamma^\dagger n(\mathbf{q}) \equiv -D_0 \beta q_a q_b \sigma_{ab}(\mathbf{q}). \quad (6.166)$$

This identity, which only holds when inserted into the average $\langle \dots \rangle$, yields

$$\sigma_{ab}(\mathbf{q}) \equiv \sum_i \left[i(\delta_{bc} + \gamma A_{bc}) \frac{q_a F_{i,c}}{q^2} + T \delta_{ab} \right] e^{-i\mathbf{q}\cdot\mathbf{r}_i}. \quad (6.167)$$

For $\gamma = 0$, we recover the expression of the microscopic equilibrium stress tensor, $\sigma^{eq}(\mathbf{q})$, given by

$$\sigma_{ab}^{eq}(\mathbf{q}) \equiv \sum_i \left[i \frac{q_a F_{i,b}}{q^2} + T \delta_{ab} \right] e^{-i\mathbf{q}\cdot\mathbf{r}_i}. \quad (6.168)$$

For equilibrium dynamics, the viscosity is defined as the response function of $\mathcal{Q}\sigma^{eq}$ to particle current fluctuations, as discussed in [130] for underdamped Langevin dynamics and extended in [253] for the overdamped case. In the presence of transverse forces one must substitute σ^{eq} with σ given by Eq. (6.167). This gives rise to coupling between parallel and longitudinal components of the stress tensor, which eventually results in odd viscosity.

Note that the projection of the stress tensor in the space orthogonal to the density fluctuations, $\mathcal{Q}\sigma_{ab}(\mathbf{q})$, is related with its equilibrium counterpart by the following relation

$$\mathcal{Q}\sigma_{ab}(\mathbf{q}) = \mathcal{Q}\sigma_{ac}^{eq}(\delta_{cb} - \gamma A_{cb}), \quad (6.169)$$

where the Einstein summation convention is being used. We also have

$$\mathcal{Q}j_a(\mathbf{q}) = -iq_b \mathcal{Q}\sigma_{ba}^{eq}(\mathbf{q}), \quad (6.170)$$

with $\mathcal{Q}j_a(\mathbf{q})$ the projected force density Fourier modes defined in Eq. (6.54).

In the next section, we pursue our program by developing a linear response theory of the microscopic stress.

6.5.2 Linear response theory

We consider the perturbation produced by a weak external velocity field made by a single Fourier mode $\mathbf{v}(\mathbf{r}, t) \equiv \mathbf{v}(t) e^{i\mathbf{q}\cdot\mathbf{r}}$. The evolution operator associated to the system is now $\Omega_\gamma + \delta\Omega$, with

$$\delta\Omega \equiv - \sum_i \nabla_i \cdot \mathbf{v}(t) e^{i\mathbf{q}\cdot\mathbf{r}_i}. \quad (6.171)$$

As a consequence of the perturbation, the probability distribution associated to the system becomes $\rho_B(\mathbf{r}^N) + \delta\rho(\mathbf{r}^N, t)$. The equation of motion for the perturbation $\delta\rho(\mathbf{r}^N, t)$ reads, to linear order,

$$\partial_t \delta\rho(\mathbf{r}^N, t) = \Omega_\gamma \delta\rho(\mathbf{r}^N, t) + \delta\Omega(t) \rho_B(\mathbf{r}^N). \quad (6.172)$$

The solution to this equation is given by

$$\begin{aligned} \delta\rho(\mathbf{r}^N, t) &= \int_{-\infty}^t d\tau e^{\Omega_\gamma(t-\tau)} \delta\Omega(\tau) \rho_B(\mathbf{r}^N) \\ &= -\frac{\beta}{V} \int_{-\infty}^t d\tau e^{\Omega_\gamma(t-\tau)} v_b(\tau) i q_a \sigma_{ab}^{\text{eq}*}(\mathbf{q}) \rho_B(\mathbf{r}^N). \end{aligned} \quad (6.173)$$

The average of the stress tensor in linear response reads

$$\begin{aligned} \langle \mathcal{Q}\sigma_{ab}(\mathbf{q}, t) \rangle^{\text{lr}} &= -\frac{\beta}{V} \int_{-\infty}^t d\tau i q_c v_d(\tau) \left\langle \sigma_{cd}^{\text{eq}*}(\mathbf{q}) e^{\Omega_{-\gamma}(t-\tau)} \mathcal{Q}\sigma_{ab}(\mathbf{q}) \right\rangle \\ &= -\frac{\beta}{V} \int_{-\infty}^t d\tau i q_c v_d(\tau) \left\langle \sigma_{cd}^{\text{eq}*}(\mathbf{q}) e^{\Omega_{-\gamma}(t-\tau)} \mathcal{Q}\sigma_{ab}(\mathbf{q}) \right\rangle \theta(t-\tau). \end{aligned} \quad (6.174)$$

The average $\langle \dots \rangle^{\text{lr}}$ is an average over the dynamics described by the operator $\Omega_\gamma + \delta\Omega$, neglecting terms of order higher than linear in $\mathbf{v}(t)$. We are interested in computing the variation of the stress with respect to the small perturbation. To do this, it is more suitable to work in Fourier space, by denoting the Fourier transform of a function $f(t)$ as $f(\omega) \equiv \int_{-\infty}^{+\infty} f(t) e^{-i\omega t}$. Within the linear response framework, we can take the perturbation \mathbf{v} to be a monochromatic plane wave, i.e. $\mathbf{v}(t) = \mathbf{v}(\omega) e^{-i\omega t + 0_+}$. The symbol 0_+ has to be understood as a small positive infinitesimal quantity used to ensure that the perturbation goes to 0 at $t = -\infty$. Substitution into Eq. (6.174) yields

$$\frac{\partial \langle \mathcal{Q}\sigma_{ab}(\mathbf{q}, \omega) \rangle^{\text{lr}}}{\partial i q_c v_d} = \frac{\beta}{V} \left\langle \sigma_{cd}^{\text{eq}*}(\mathbf{q}) \frac{1}{-i\omega - \Omega_{-\gamma}} \mathcal{Q}\sigma_{ab}(\mathbf{q}) \right\rangle. \quad (6.175)$$

This is the response of $\mathcal{Q}\sigma_{ab}(\mathbf{q})$ to an external velocity gradient. To obtain the viscosity, we need to work out the response of $\mathcal{Q}\sigma_{ab}(\mathbf{q})$ to a change in the gradients of the particle current. However, within linear response, we can work out a relation between the particle currents and the applied velocity field, thus making the calculation of the viscosity tensor possible. This is done next.

6.5.3 The viscosity tensor

Following [130, 64, 253], we introduce the average particle current $\mathbf{J}(\mathbf{q}, t)$, governing the evolution of the density mode $n(\mathbf{q})$

$$\langle \partial_t n(\mathbf{q}, t) \rangle^{\text{lr}} \equiv i\rho_0 \mathbf{q} \cdot \mathbf{J}(\mathbf{q}, t). \quad (6.176)$$

The left hand side of Eq. (6.176) splits into

$$\langle \partial_t n(\mathbf{q}, t) \rangle^{\text{lr}} = \langle n(\mathbf{q}, t) \delta\Omega(t) \rangle + \langle n(\mathbf{q}, t) \Omega_\gamma \rangle^{\text{lr}}, \quad (6.177)$$

which implies

$$J_a(\mathbf{q}, t) = v_a(\mathbf{q}, t) - \frac{D_0\beta}{\rho_0} q_b \langle \sigma_{ab}(\mathbf{q}, t) \rangle^{\text{lr}}. \quad (6.178)$$

Thus, the particle current corresponds to sum of the imposed solvent velocity \mathbf{v} and of a term that originates from the change in the stress tensor.

The viscosity tensor is defined as the response function describing the change of the projected stress tensor due to the gradient of the average particle current [130]:

$$\eta_{abcd}(\mathbf{q}, \omega) \equiv \frac{\partial \langle \mathcal{Q}\sigma_{ab}(\mathbf{q}, \omega) \rangle^{\text{lr}}}{\partial i q_c J_d(\mathbf{q}, \omega)}. \quad (6.179)$$

Our aim is now to show that the viscosity tensor is related to the following correlation function,

$$C_{abcd}^{\text{irr}}(\mathbf{q}, \omega) \equiv \frac{\beta}{V} \left\langle \sigma_{ab}^{\text{eq}*}(\mathbf{q}) \mathcal{Q} \frac{1}{-i\omega - \Omega_{-\gamma}^{\text{irr}}} \mathcal{Q} \sigma_{cd}(\mathbf{q}) \right\rangle, \quad (6.180)$$

which encodes the correlation between the equilibrium stress tensor and the stress tensor in presence of transverse forces, evolving with the irreducible operator $\Omega_{-\gamma}^{\text{irr}}$ defined in Eq. (6.58).

We first introduce an auxiliary correlation function $C_{abcd}^{\mathcal{Q}}$,

$$C_{abcd}^{\mathcal{Q}} \equiv \frac{\beta}{V} \left\langle \sigma_{ab}^{\text{eq}*}(\mathbf{q}) \mathcal{Q} \frac{1}{-i\omega - \mathcal{Q}\Omega_{-\gamma}\mathcal{Q}} \mathcal{Q} \sigma_{cd}(\mathbf{q}) \right\rangle, \quad (6.181)$$

which is the analogue of C_{abcd}^{irr} but evolves with the projected evolution operator $\mathcal{Q}\Omega_{-\gamma}\mathcal{Q}$. Using the operator identity

$$\frac{1}{-i\omega - \mathcal{Q}\Omega_{-\gamma}} = \frac{1}{-i\omega - \Omega_{-\gamma}} + \frac{1}{-i\omega - \Omega_{-\gamma}} \mathcal{P}\Omega_{-\gamma} \frac{1}{-i\omega - \mathcal{Q}\Omega_{-\gamma}}, \quad (6.182)$$

we obtain

$$\frac{\partial \langle \mathcal{Q}\sigma_{ab}(\mathbf{q}) \rangle^{\text{lr}}}{\partial i q_c v_d} = \left[\delta_{ce} \delta_{dg} - \frac{D_0\beta}{S(q)} q_f \frac{\partial \langle n(\mathbf{q}, t) \rangle^{\text{lr}}}{\partial i q_c v_d} (\delta_{fg} + \gamma A_{fg}) q_e \right] C_{egab}^{\mathcal{Q}}. \quad (6.183)$$

On the other hand, the correlators C_{abcd}^Q and C_{abcd}^{irr} are related to each other. We can exploit the resolvent identity given by Eq. (6.60) and the fact that the operator $\delta\Omega_{-\gamma}$ defined in Eq. (6.59) can be expressed in terms of the stress tensor through Eq. (6.170),

$$\delta\Omega_{-\gamma} = \frac{D_0\beta^2}{N} q_a q_d Q \sigma_{ab}^{\text{eq}}(\mathbf{q}) \langle \delta_{bc} - \gamma A_{bc} \rangle \langle \sigma_{dc}^{\text{eq}} Q \rangle. \quad (6.184)$$

This yields

$$\begin{aligned} C_{abcd}^{\text{irr}} &= C_{abcd}^Q - \frac{D_0\beta^2}{\rho_0 V} q_e q_f \langle \sigma_{ab}^{\text{eq}*}(\mathbf{q}) \frac{1}{-i\omega - Q\Omega_{-\gamma} Q} Q \sigma_{ef}^{\text{eq}}(\mathbf{q}) \rangle (\delta_{fg} - \gamma A_{fg}) C_{fgcd}^{\text{irr}} \\ &= C_{abcd}^Q - \frac{D_0\beta}{\rho_0} q_e q_f C_{abeg}^Q C_{fgcd}^{\text{irr}}. \end{aligned} \quad (6.185)$$

This equation is analogous to the relation between the memory kernels \mathbf{K} and $\widetilde{\mathbf{K}}$ given by Eq. (6.62). Contracting both sides of Eq. (6.185) with the quantity inside the brackets in Eq. (6.183) and rearranging the terms gives

$$\frac{\partial \langle Q\sigma_{ab}(\mathbf{q}) \rangle^{\text{lr}}}{\partial i q_c v_d} = \left[\delta_{ce} \delta_{df} + \frac{D_0\beta}{\rho_0} q_e q_g \frac{\partial \langle Q\sigma_{gf}(\mathbf{q}) \rangle^{\text{lr}}}{\partial i q_c v_d} - q_e q_g \frac{D_0}{\rho_0 S(q)} \frac{\partial \langle n(\mathbf{q}) \rangle^{\text{lr}}}{\partial i q_c v_d} (\delta_{gf} + \gamma A_{gf}) \right] C_{efab}^{\text{irr}}. \quad (6.186)$$

On the other hand, from Eq. (6.178) we have

$$\begin{aligned} \frac{\partial i q_e J_f}{\partial i q_c v_d} &= \delta_{ce} \delta_{df} + \frac{D_0\beta}{\rho_0} q_e q_g \frac{\partial \langle Q\sigma_{hf}(\mathbf{q}) \rangle^{\text{lr}}}{\partial i q_c v_d} \\ &\quad - q_e q_g \frac{D_0}{\rho_0 S(q)} \frac{\partial \langle n(\mathbf{q}) \rangle^{\text{lr}}}{\partial i q_c v_d} \delta_{gf}. \end{aligned} \quad (6.187)$$

Combining Eqs. (6.186, 6.187), using the chain rule and the definition of the viscosity tensor given by Eq. (6.179) we obtain

$$\frac{\partial i q_e J_f}{\partial i q_c v_d} \eta_{abef}(\mathbf{q}, \omega) = \left[\frac{\partial i q_e J_f}{\partial i q_c v_d} - \gamma q_e q_g \frac{D_0}{\rho_0 S(q)} \frac{\partial \langle n(\mathbf{q}) \rangle^{\text{lr}}}{\partial i q_c v_d} A_{gf} \right] C_{efab}^{\text{irr}}(\mathbf{q}, \omega). \quad (6.188)$$

This equation relates the irreducible stress-stress correlator with the viscosity. For $\gamma = 0$, we recover the relation derived in [253],

$$\eta_{abcd}(\mathbf{q}, \omega) = \frac{\beta}{V} \langle \sigma_{cd}^{\text{eq}*}(\mathbf{q}) \frac{1}{-i\omega - \Omega_0^{\text{irr}}} Q \sigma_{ab}^{\text{eq}}(\mathbf{q}) \rangle. \quad (6.189)$$

When $\gamma \neq 0$, and additional term stemming from the influence of the transverse forces and proportional to the response of the density field to external currents appears. Moreover, the stress-stress correlator C^{irr} depends on γ both through the definition of the stress σ_{ab} and the dynamical evolution operator $\Omega_{-\gamma}^{\text{irr}}$.

In the hydrodynamic limit, when $q \rightarrow 0$ and $\omega \rightarrow 0$, the second term on the right hand side of Eq. (6.188) is subleading compared to the first one, leading to

$$\eta_{abcd}(\mathbf{q} \rightarrow 0, \omega \rightarrow 0) = C_{cdab}^{\text{irr}}(\mathbf{q} \rightarrow 0, \omega \rightarrow 0). \quad (6.190)$$

This equation relates the hydrodynamic viscosity with the stress-stress irreducible correlator. In the next two sections, we use this formula to compute, within the mode-coupling approximation, the shear and odd viscosities.

6.5.4 Shear viscosity

We start with the shear viscosity η_{xyxy} . Due to the rotational invariance of the dynamics in the (xy) plane, we evaluate the $\mathbf{q} \rightarrow 0$ limit with $\mathbf{q} = q\mathbf{e}_x$. From Eq. (6.190) we obtain

$$\begin{aligned}\eta_{xyxy} &= \lim_{q \rightarrow 0} \lim_{\omega \rightarrow 0} \frac{\beta}{V} \left\langle \sigma_{xy}^{\text{eq}*}(\mathbf{q}) \mathcal{Q} \frac{1}{-i\omega - \Omega_{-\gamma}^{\text{irr}}} \mathcal{Q} \sigma_{xy}^{\text{eq}}(\mathbf{q}) \right\rangle \\ &\quad - \gamma \frac{\beta}{V} \left\langle \sigma_{xy}^{\text{eq}*}(\mathbf{q}) \mathcal{Q} \frac{1}{-i\omega - \Omega_{-\gamma}^{\text{irr}}} \mathcal{Q} \sigma_{xx}^{\text{eq}}(\mathbf{q}) \right\rangle.\end{aligned}\quad (6.191)$$

We now replace $\mathcal{Q}\sigma_{ab}^{\text{eq}}(\mathbf{q})$ with $i\mathcal{Q}_{q^2}^{q_2} j_b(\mathbf{q})$. In this way, the stress-stress correlations is expressed in terms of the projected force-force correlations, encoded by the memory kernel \mathbf{K} given by Eq. (6.61). We therefore get, using the $\mathbf{A} - \mathbf{q}$ basis,

$$\eta_{xyxy} = \lim_{q \rightarrow 0} \lim_{\omega \rightarrow 0} \frac{\rho_0}{D_0 \beta} [K_{22}(q\mathbf{e}_x, -i\omega) - \gamma K_{21}(q\mathbf{e}_x, -i\omega)]. \quad (6.192)$$

Using the expression of \mathbf{K} given by the mode-coupling approximation, Eq.(6.70), and the fact that within this approximation the off-diagonal terms in \mathbf{K} are 0 in the $\mathbf{A} - \mathbf{q}$ basis, we have

$$\begin{aligned}\eta_{xyxy} &= \lim_{q \rightarrow 0} \lim_{\omega \rightarrow 0} \frac{\rho_0}{q^2 D_0 \beta} K_{22}(q\mathbf{e}_x, -i\omega) \\ &= \lim_{q \rightarrow 0} \frac{\rho_0^2}{2q^2 \beta} \int_0^{+\infty} dt \int_{\mathbf{k}} [k_y(c(k) - c(|q\mathbf{e}_x - \mathbf{k}|))]^2 S(\mathbf{k}, t) S(q\mathbf{e}_x - \mathbf{k}, t). \\ &= \frac{1}{2\beta} \int_0^{+\infty} dt \int_{\mathbf{k}} [\hat{k}_x k_y \rho_0 c'(k)]^2 |S(\mathbf{k}, t)|^2\end{aligned}\quad (6.193)$$

In this expression, the dependence on γ enters through the dynamical evolution of $S(\mathbf{k}, t)$. For $\gamma = 0$, rotational symmetry is restored, and we recover the equilibrium, mode-coupling result [201]:

$$\eta_{xyxy}^{\text{eq}} = \frac{1}{60\pi^2 \beta} \int_0^{+\infty} dk k^4 \left[\frac{1}{S(k)} S'(k) \right]^2 \phi(k, t)^2. \quad (6.194)$$

Since the relaxation of $S(\mathbf{k}, t)$ is faster in the presence of transverse forces we have $\eta_{xyxy}(\gamma) \leq \eta_{xyxy}^{\text{eq}}$. Also, the shear viscosity diverges at the glass transition.

6.5.5 Odd viscosity

We now address the odd viscosity. We identify the following contribution as the odd viscosity:

$$\eta_{\text{odd}} \equiv \frac{1}{2} (\eta_{xyxx} - \eta_{xxxy}). \quad (6.195)$$

Physically, a nonzero η_{odd} means that attempts at compressing the system along the x -direction generate shear flows in the (xy) plane. In a nonreciprocal fashion, shear

stresses applied on the (xy) plane will generate an expansion of the liquid along the x -direction. In equilibrium dynamics we have $\eta_{abcd} = \eta_{cdba}$ and therefore $\eta_{\text{odd}} = 0$. We address now how this situation changes when transverse forces are present.

Performing a computation similar to the one done in Eq. (6.192) gives

$$\begin{aligned}\eta_{\text{odd}} &= \frac{1}{2} \lim_{q \rightarrow 0} \lim_{\omega \rightarrow 0} \frac{\rho_0}{q^2 D_0 \beta} [(K_{21}(q\mathbf{e}_x, -i\omega) + K_{12}(q\mathbf{e}_x, -i\omega)) \\ &\quad - \gamma(K_{11}(q\mathbf{e}_x, -i\omega) + K_{22}(q\mathbf{e}_x, -i\omega))].\end{aligned}\quad (6.196)$$

Within the mode-coupling approximation, the first two terms on the right hand side of Eq. (6.196) are 0. Taking the hydrodynamic limit of the mode-coupling expression of K_{ii} given by Eq. (6.70), we obtain

$$\begin{aligned}\eta_{\text{odd}} &= -\frac{\gamma}{2} \lim_{q \rightarrow 0} \lim_{\omega \rightarrow 0} \frac{\rho_0}{q^2 D_0 \beta} [K_{11}(q\mathbf{e}_x, -i\omega) + K_{22}(q\mathbf{e}_x, -i\omega)] \\ &= -\frac{\gamma}{4\beta} \int_0^{+\infty} dt \int_{\mathbf{k}} [[\rho_0 c(k) + k_x \hat{k}_x \rho_0 c'(k)]^2 + [\hat{k}_x k_y \rho_0 c'(k)]^2] S(\mathbf{k}, t)^2.\end{aligned}\quad (6.197)$$

As the glass transition is approached the odd viscosity diverges. Physically, this means that in the glassy state no form of transport is possible, and the transverse, as well as the longitudinal, dynamical pathways through which the liquid relaxes, are blocked. This directly impacts all viscosity coefficients.

The above discussion on the viscosity tensor concludes our mode-coupling treatment of the dynamics of dense liquids with transverse forces. In the following Section, we address the mode-coupling theory for a model of lifted active particles, with the goal of providing some insights on the generalities of the results obtained for transverse forces.

6.6 Lifted active Brownian particles (ABP)

In this Section, we develop a mode-coupling theory for a model of lifted-active Brownian particles, constructed following the examples provided in Section 1.3.2. The lifted-ABP dynamics of N particles in two dimensions is given by

$$\begin{cases} \dot{\mathbf{r}}_i &= v_0 \hat{\mathbf{u}}_i \\ \dot{\theta}_i &= v_0 \beta \mathbf{F}_i \cdot \mathbf{A} \hat{\mathbf{u}}_i + \sqrt{2D_r} \chi_i, \end{cases} \quad (6.198)$$

where $\hat{\mathbf{u}}_i = (\cos \theta_i, \sin \theta_i)$ is a unit vector denoting the direction of the self-propulsion speed of particle i . The vector $\hat{\mathbf{u}}_i$ forms an angle θ_i with respect to the x -axis. χ_i is a Gaussian white noise, $\langle \chi_i(t) \chi_j(t') \rangle = \delta_{ij} \delta(t-t')$. The self-propulsion orientation is subjected to diffusion with a diffusion constant D_r as for standard ABPs, but is in addition subjected to a drift that depends on the interaction force $\mathbf{F}_i = -\sum_j \nabla_{j \neq i} V(\mathbf{r}_i - \mathbf{r}_j)$ between the particles in position space. The latter enforces the stationarity of the Boltzmann distribution in the steady state because the matrix $\mathbf{A} \equiv \begin{bmatrix} 0 & -1 \\ 1 & 0 \end{bmatrix}$ ensures that the drift is always perpendicular to $\hat{\mathbf{u}}_i$. The drift term makes the ABP equations of motion non-conventional, hence the ‘lifted-ABP’ name for Eq. (6.198).

In the absence of interactions when $\mathbf{F}_i = 0$, Eq. (6.198) describes freely diffusing ABPs, with diffusion constant $\frac{v_0^2}{2D_r}$. When interactions are added, lifted-ABPs sample the equilibrium Boltzmann distribution of the interacting system at fixed temperature T , and this can be done at various values of $\frac{v_0^2}{2D_r}$. This is to be compared with the equilibrium dynamics where temperature simultaneously fixes the Boltzmann distribution and the free diffusion constant $D_0 = \mu_0 T$.

The evolution of the probability distribution $\rho(\mathbf{r}^N, \theta^N, t)$ of lifted-ABPs is governed by the operator Ω_{v_0} :

$$\Omega_{v_0} \equiv - \sum_i \nabla_i \cdot v_0 \hat{\mathbf{u}}_i + \sum_i \partial_{\theta_i} [-v_0 \beta \mathbf{F}_i \cdot \mathbf{A} \hat{\mathbf{u}}_i + D_r \partial_{\theta_i}], \quad (6.199)$$

so that

$$\partial_t \rho(\mathbf{r}^N, \theta^N, t) = \Omega_{v_0} \rho(\mathbf{r}^N, \theta^N, t). \quad (6.200)$$

The steady state solution of Eq. (6.200) is a product of independent distributions in the respective subspaces spanned by \mathbf{r}^N and by \mathbf{u}^N :

$$\rho_{ss} = \frac{1}{(2\pi)^N} \rho_B(\mathbf{r}^N) = \frac{1}{Z} e^{-\beta \sum_{i < j} V(\mathbf{r}_i - \mathbf{r}_j)}. \quad (6.201)$$

with $Z \equiv (2\pi)^N \int d\mathbf{r}^N e^{-\beta \sum_{i < j} V(\mathbf{r}_i - \mathbf{r}_j)}$.

The operator Ω_{v_0} has the following property, which is a reflection of the breaking of detailed balance reminiscent of Eq. (6.42) for transverse forces:

$$\Omega_{v_0} f(\mathbf{r}^N, \hat{\mathbf{u}}^N) \Big\rangle = \left(\Omega_{-v_0}^\dagger f(\mathbf{r}^N, \hat{\mathbf{u}}^N) \right) \Big\rangle. \quad (6.202)$$

We are interested in the evolution of the density mode $n(\mathbf{q})$:

$$n(\mathbf{q}, t) \equiv \sum_i e^{-i\mathbf{q} \cdot \mathbf{r}_i(t)} \quad (6.203)$$

and of its correlation function, the dynamical structure factor $S(\mathbf{q}, t)$:

$$S(\mathbf{q}, t) \equiv \frac{1}{N} \langle n^*(\mathbf{q}) n(\mathbf{q}, t) \rangle. \quad (6.204)$$

The following identity holds when inserted into an average:

$$\partial_t n(\mathbf{q}, t) = \Omega_{v_0}^\dagger n(\mathbf{q}, t), \quad (6.205)$$

so that $n(\mathbf{q}, t) = e^{\Omega_{v_0}^\dagger t} n(\mathbf{q}, 0)$. This, together with Eq. (6.202) allows us to write

$$S(\mathbf{q}, t) = \frac{1}{N} \langle n^*(\mathbf{q}) e^{\Omega_{-v_0} t} n(\mathbf{q}, 0) \rangle. \quad (6.206)$$

Another important quantity is the time derivative of the density mode at $t = 0$:

$$\partial_t n(\mathbf{q}) = -i v_0 q \hat{u}_{||}(\mathbf{q}), \quad (6.207)$$

which is the projection of the velocity $\hat{\mathbf{u}}_i$ along the wavevector \mathbf{q} :

$$\hat{u}_{\parallel}(\mathbf{q}) \equiv \sum_i (\hat{\mathbf{q}} \cdot \hat{\mathbf{u}}_i) e^{-i\mathbf{q} \cdot \mathbf{r}_i}. \quad (6.208)$$

We are also interested in the self-intermediate scattering function $F_s(\mathbf{q}, t)$. Here we re-write the definition (6.45) by putting the time dependence entirely into $n_i(\mathbf{q}, t)$,

$$F_s(\mathbf{q}, t) \equiv \frac{1}{N} \sum_{i=1}^N \langle n_i^*(\mathbf{q}) n_i(\mathbf{q}, t) \rangle. \quad (6.209)$$

We have $\partial_t n_i(\mathbf{q}) = -iv_0 q u_{\parallel,i}(\mathbf{q})$, with

$$\hat{u}_{\parallel,i}(\mathbf{q}) \equiv \hat{\mathbf{q}} \cdot \hat{\mathbf{u}}_i e^{-i\mathbf{q} \cdot \mathbf{r}_i} \quad (6.210)$$

encoding the Fourier transform of the longitudinal self-propulsion velocity with respect to the wavevector \mathbf{q} . The small- q expansion of the self-intermediate scattering function yields the mean-squared displacement

$$\Delta(t) \equiv \sum_{i=1}^N \langle [\mathbf{r}_i(t) - \mathbf{r}_i(0)]^2 \rangle. \quad (6.211)$$

Using the isotropy of the dynamics given by Eq. (6.198) we can also connect F and Δ :

$$F_s(\mathbf{q}, t) = 1 - \frac{q^2}{4} \Delta(t) + O(q^3). \quad (6.212)$$

An equation for Δ is obtained at the end of the section.

6.6.1 Short-time dynamics

To gain insights on the dynamics we consider a short-time expansion of $S(\mathbf{q}, t)$:

$$\begin{aligned} S(\mathbf{q}, t) &\approx S(q) + \frac{t}{N} \langle n^*(\mathbf{q}) \Omega_{-v_0} n(\mathbf{q}) \rangle + \frac{t^2}{2N} \langle n^*(\mathbf{q}) \Omega_{-v_0} \Omega_{-v_0} n(\mathbf{q}) \rangle \\ &= S(q) - iv_0 q \langle n^*(\mathbf{q}) \hat{u}_{\parallel}(\mathbf{q}) \rangle - \frac{t^2}{2} v_0^2 q^2 \langle \hat{u}_{\parallel}^*(\mathbf{q}) \hat{u}_{\parallel}(\mathbf{q}) \rangle. \end{aligned} \quad (6.213)$$

The second term on the right hand side of Eq. (6.213) vanishes due to rotational invariance. For the third term we have, using Einstein notation for the components of the vectors $\hat{\mathbf{q}}$ and $\hat{\mathbf{u}}_i$,

$$\begin{aligned} \langle \hat{u}_{\parallel}^*(\mathbf{q}) \hat{u}_{\parallel}(\mathbf{q}) \rangle &= \left\langle \sum_{i,j} \hat{u}_{i,\alpha} \hat{u}_{j,\beta} \hat{q}_{\alpha} \hat{q}_{\beta} e^{-i\mathbf{q} \cdot (\mathbf{r}_i - \mathbf{r}_j)} \right\rangle \\ &= \sum_{i,j} \langle \hat{u}_{\alpha,i} \hat{u}_{\beta,j} \rangle \langle \delta_{i,j} \delta_{\alpha\beta} \hat{q}_{\alpha} \hat{q}_{\beta} e^{-i\mathbf{q} \cdot (\mathbf{r}_i - \mathbf{r}_j)} \rangle \\ &= \frac{N}{2}, \end{aligned} \quad (6.214)$$

and therefore we obtain

$$S(\mathbf{q}, t) = S(q) - \frac{v_0^2 q^2}{4} t^2 + O(t^3). \quad (6.215)$$

This yields two results. First, we see that increasing v_0 produces a faster decay of the dynamic structure factor at short times. Moreover, in contrast with equilibrium overdamped Brownian dynamics, the decrease is quadratic in time (in line with the ballistic nature of the dynamics at short times), instead of being linear. This suggests that we should study the dynamics of $S(\mathbf{q}, t)$ to second order in time, as done in the next section.

6.6.2 Projection operator formalism

We want to find an evolution equation for $S(\mathbf{q}, t)$. The starting point is to write its second time derivative:

$$\begin{aligned} \partial_t^2 S(\mathbf{q}, t) &= \frac{1}{N} \left\langle n^*(\mathbf{q}) \Omega_{-v_0} e^{\Omega_{-v_0} t} \Omega_{-v_0} n(\mathbf{q}) \right\rangle \\ &= -\frac{i v_0 q}{N} \left\langle \hat{u}_\parallel^*(\mathbf{q}) \Omega_{-v_0} e^{\Omega_{-v_0} t} n(\mathbf{q}) \right\rangle. \end{aligned} \quad (6.216)$$

By taking the Laplace Transform on both sides of Eq. (6.216) we get

$$z^2 S(\mathbf{q}, z) - z = -\frac{i v_0 q}{N} \left\langle \hat{u}_\parallel^*(\mathbf{q}) \Omega_{-v_0} \frac{1}{z - \Omega_{-v_0}} n(\mathbf{q}) \right\rangle. \quad (6.217)$$

We now have to choose a projection operator \mathcal{P} tailored to the relevant degrees of freedom. We assume these relevant modes to be the density field and its time derivative, which leads to the following expression for \mathcal{P} :

$$\mathcal{P} \equiv \frac{1}{N S(q)} n(\mathbf{q}) \langle n^*(\mathbf{q}) \rangle + \frac{2}{N} \hat{u}_\parallel(\mathbf{q}) \langle \hat{u}_\parallel^*(\mathbf{q}) \rangle. \quad (6.218)$$

With this choice and a resolvent identity akin to Eq. (6.49) previously used for transverse forces

$$\begin{aligned} \frac{1}{z - \Omega_{-v_0}} &= \frac{1}{1 - \mathcal{Q} \Omega_{-v_0} \mathcal{Q}} \\ &+ \left(1 + \frac{1}{z - \mathcal{Q} \Omega_{-v_0} \mathcal{Q}} \Omega_{-v_0} \right) \mathcal{P} \frac{1}{z - \Omega_{-v_0}} \mathcal{P} \left(1 + \Omega_{-v_0} \frac{1}{z - \mathcal{Q} \Omega_{-v_0} \mathcal{Q}} \right), \end{aligned} \quad (6.219)$$

Eq. (6.217) becomes

$$\begin{aligned} z^2 S(\mathbf{q}, z) - z S(q) &= -\frac{i v_0 q}{N} \left[\left\langle \hat{u}_\parallel^*(\mathbf{q}) \Omega_{-v_0} n(\mathbf{q}) \right\rangle \frac{1}{N S(q)} \langle n^*(\mathbf{q}) R(z) n(\mathbf{q}) \rangle \right. \\ &+ \left\langle \hat{u}_\parallel^*(\mathbf{q}) \Omega_{-v_0} \hat{u}_\parallel(\mathbf{q}) \right\rangle \frac{2}{N} \left\langle \hat{u}_\parallel^*(\mathbf{q}) R(z) n(\mathbf{q}) \right\rangle \\ &\left. + \left\langle \hat{u}_\parallel^*(\mathbf{q}) \Omega_{-v_0} \mathcal{Q} R_\mathcal{Q}(z) \mathcal{Q} \Omega_{-v_0} \hat{u}_\parallel(\mathbf{q}) \right\rangle \frac{2}{N} \left\langle \hat{u}_\parallel^*(\mathbf{q}) R(z) n(\mathbf{q}) \right\rangle \right]. \end{aligned} \quad (6.220)$$

An explicit computation gives:

$$\begin{aligned} \langle \hat{u}_\parallel^*(\mathbf{q}) \Omega_{-v_0} n(\mathbf{q}) \rangle &= -i \frac{v_0 q N}{2}, \\ \langle \hat{u}_\parallel^*(\mathbf{q}) \Omega_{-v_0} \hat{u}_\parallel(\mathbf{q}) \rangle &= -\frac{N}{2} D_r, \\ -\frac{iv_0 q}{N} \left\langle \hat{u}_\parallel^*(\mathbf{q}) \frac{1}{z - \Omega_{-v_0}} n(\mathbf{q}) \right\rangle &= z S(\mathbf{q}, z) - S(q). \end{aligned} \quad (6.221)$$

Putting everything together and taking an inverse Laplace transform yields

$$\begin{aligned} \partial_t^2 S(\mathbf{q}, t) &= -\frac{v_0^2 q^2}{2S(q)} S(\mathbf{q}, t) - D_r \partial_t S(\mathbf{q}, t) \\ &\quad - \int_0^t d\tau M(\mathbf{q}, t - \tau) \partial_\tau S(\mathbf{q}, \tau). \end{aligned} \quad (6.222)$$

This is an evolution equation for the dynamical structure factor for the lifted-ABP dynamics. It allows for underdamped oscillations in the presence of a memory kernel given by

$$M(\mathbf{q}, t) \equiv -\frac{2}{N} \left\langle \hat{u}_\parallel^*(\mathbf{q}) \Omega_{-v_0} \mathcal{Q} e^{\mathcal{Q}\Omega_{-v_0} \mathcal{Q}t} \mathcal{Q} \Omega_{-v_0} \hat{u}_\parallel(\mathbf{q}) \right\rangle. \quad (6.223)$$

With a similar approach, one can derive an equation for $F_s(\mathbf{q}, t)$. In practice the step above must be repeated using the single particle projection operator

$$\mathcal{P}_i \equiv n_i(\mathbf{q}) \langle n_i^*(\mathbf{q}) + 2u_{\parallel,i}(\mathbf{q}) \rangle \langle \hat{u}_{\parallel,i}^*(\mathbf{q}), \quad (6.224)$$

instead of \mathcal{P} and employ particle equivalence. The result is

$$\partial_t^2 F_s(\mathbf{q}, t) = -\frac{v_0^2 q^2}{2} F_s(\mathbf{q}, t) - D_r \partial_t F_s(\mathbf{q}, t) - \int_0^t d\tau M_s(\mathbf{q}, t - \tau) \partial_\tau F_s(\mathbf{q}, \tau), \quad (6.225)$$

with the self-memory kernel defined as

$$M_s(\mathbf{q}, t) \equiv -\frac{2}{N} \sum_{i=1}^N \left\langle \hat{u}_{\parallel,i}^*(\mathbf{q}) \Omega_{-v_0} \mathcal{Q} e^{\mathcal{Q}\Omega_{-v_0} \mathcal{Q}t} \mathcal{Q} \Omega_{-v_0} \hat{u}_{\parallel,i}(\mathbf{q}) \right\rangle. \quad (6.226)$$

All the steps performed so far are exact. To proceed, approximations are needed to compute M and M_s . In the next section, we approximate the memory kernels using the mode-coupling scheme.

6.6.3 Mode-coupling expansion

We expand the memory kernel as a product of density mode correlations. The physical justification for this choice is that the non-trivial part in the time evolution of $\hat{u}_\parallel(\mathbf{q})$ comes from the coupling with the fluid, which involves pairwise forces between particles. We therefore write

$$\mathcal{Q} \Omega_{-v_0} \hat{u}_\parallel(\mathbf{q}) \rangle = \frac{1}{2} \sum_{\mathbf{k}} \left\langle \frac{\langle n^*(\mathbf{k}) n^*(\mathbf{q} - \mathbf{k}) \mathcal{Q} \Omega_{-v_0} \hat{u}_\parallel(\mathbf{q}) \rangle}{N^2 S(k) S(|\mathbf{q} - \mathbf{k}|)} n(\mathbf{k}) n(\mathbf{q} - \mathbf{k}) \right\rangle, \quad (6.227)$$

with the factor $\frac{1}{2}$ inserted to avoid double counting of the density modes products. We now calculate the expectation value on the right hand side of Eq. (6.227) thanks to the convolution approximation $\langle n^*(\mathbf{k})n^*(\mathbf{q} - \mathbf{k})n(\mathbf{q}) \rangle \approx NS(q)S(k)S(|\mathbf{q} - \mathbf{k}|)$:

$$\begin{aligned}
 \langle n^*(\mathbf{k})n^*(\mathbf{q} - \mathbf{k})\mathcal{Q}\Omega_{-v_0}\hat{u}_{\parallel}(\mathbf{q}) \rangle &= \langle n^*(\mathbf{k})n^*(\mathbf{q} - \mathbf{k})\Omega_{-v_0}\hat{u}_{\parallel}(\mathbf{q}) \rangle - \langle n^*(\mathbf{k})n^*(\mathbf{q} - \mathbf{k})\mathcal{P}\Omega_{-v_0}\hat{u}_{\parallel}(\mathbf{q}) \rangle \\
 &= \left\langle \left[\Omega_{-v_0}^\dagger(n^*(\mathbf{k})n^*(\mathbf{q} - \mathbf{k})) \right] \hat{u}_{\parallel}(\mathbf{q}) \right\rangle \\
 &\quad - \langle n^*(\mathbf{k})n^*(\mathbf{q} - \mathbf{k})n(\mathbf{q}) \rangle \frac{1}{NS(q)} \langle n^*(\mathbf{q})\Omega_{-v_0}\hat{u}_{\parallel}(\mathbf{q}) \rangle \\
 &= -iv_0 \left\langle \sum_{i,j,k} (\hat{u}_{i,\alpha}\hat{q}_\alpha) [\hat{u}_{j,\beta}k_\beta + \hat{u}_{k,\beta}(q_\beta - k_\beta)] e^{i\mathbf{k}\cdot\mathbf{r}_j} e^{i(\mathbf{q}-\mathbf{k})\cdot\mathbf{r}_k} e^{-i\mathbf{q}\cdot\mathbf{r}_i} \right\rangle \\
 &\quad + i\frac{Nv_0q}{2} S(k)S(|\mathbf{q} - \mathbf{k}|) \\
 &= i\frac{Nv_0}{2} \left[qS(k)S(|\mathbf{q} - \mathbf{k}|) - (\hat{\mathbf{q}} \cdot \mathbf{k})S(|\mathbf{q} - \mathbf{k}|) - \hat{\mathbf{q}} \cdot (\mathbf{q} - \mathbf{k})S(k) \right] \\
 &= i\frac{Nv_0\rho_0}{2} [(\hat{\mathbf{q}} \cdot \mathbf{k})c(k) + \hat{\mathbf{q}} \cdot (\mathbf{q} - \mathbf{k})c(|\mathbf{q} - \mathbf{k}|)],
 \end{aligned} \tag{6.228}$$

where the direct correlation function $\rho_0 c(q)$ and the particle density of the system ρ_0 were defined below Eq. (6.149) and above Eq. (6.7), respectively.

We can now give the expression for the mode-coupling memory kernel. To this end, we resort to the approximation

$$e^{\mathcal{Q}\Omega_{-v_0}\mathcal{Q}t} \approx e^{\Omega_{-v_0}t}, \tag{6.229}$$

and use a Gaussian factorization for computing the two-body density correlation. Moreover, due to the irreversibility of the dynamics, we have

$$\langle n^*(\mathbf{k})n^*(\mathbf{q} - \mathbf{k})\mathcal{Q}\Omega_{-v_0}\hat{u}_{\parallel}(\mathbf{q}) \rangle = \langle \hat{u}_{\parallel}(\mathbf{q})\Omega_{-v_0}\mathcal{Q}n(\mathbf{k})n(\mathbf{q} - \mathbf{k}) \rangle. \tag{6.230}$$

The memory kernel reads, in the mode-coupling approximation

$$M(\mathbf{q}, t) \approx \frac{v_0^2\rho_0}{4} \int \frac{d\mathbf{k}}{(2\pi)^2} [(\hat{\mathbf{q}} \cdot \mathbf{k})c(k) + \hat{\mathbf{q}} \cdot (\mathbf{q} - \mathbf{k})c(|\mathbf{q} - \mathbf{k}|)]^2 S(\mathbf{k}, t)S(\mathbf{q} - \mathbf{k}, t). \tag{6.231}$$

A similar expression can be obtained for M_s , using as a starting point the expansion

$$\mathcal{Q}\Omega_{-v_0}\hat{u}_{\parallel,i}(\mathbf{q}) = \sum_{\mathbf{k}} \frac{\langle n^*(\mathbf{k})n_i^*(\mathbf{q} - \mathbf{k})\mathcal{Q}\Omega_{-v_0}\hat{u}_{\parallel,i}(\mathbf{q}) \rangle}{NS(k)} n(\mathbf{k})n_i(\mathbf{q} - \mathbf{k}). \tag{6.232}$$

The final result reads

$$M_s(\mathbf{q}, t) \approx \frac{v_0^2\rho_0}{2} \int \frac{d\mathbf{k}}{(2\pi)^2} [\hat{\mathbf{q}} \cdot \mathbf{k}c(k)]^2 F(|\mathbf{q} - \mathbf{k}|, t)S(\mathbf{k}, t). \tag{6.233}$$

Note that the structure of the memory kernels M and M_s is the same as the one obtained for equilibrium dynamics, their magnitude being now determined by the magnitude of the self-propulsion speed v_0 .

In the next sections we study the ergodicity breaking transition and the behavior of the diffusion constant stemming from these approximate expressions for the memory kernels.

6.6.4 Long-time dynamics: speedup and ergodicity breaking

To study the long-time dynamics we introduce the normalized dynamical structure function $\phi(\mathbf{q}, t) \equiv \frac{S(\mathbf{q}, t)}{S(q)}$. Its equation of motion reads

$$\partial_t^2 \phi(\mathbf{q}, t) = -\frac{v_0^2 q^2}{2S(q)} \phi(\mathbf{q}, t) - D_r \partial_t \phi(\mathbf{q}, t) - \int_0^t d\tau M(\mathbf{q}, t - \tau) \partial_\tau \phi(\mathbf{q}, \tau). \quad (6.234)$$

We first study the ergodicity breaking transition. We define the long-time limits of the normalized structure factor and the memory kernel

$$\begin{aligned} \lim_{t \rightarrow +\infty} \phi(\mathbf{q}, t) &= \phi_\infty(\mathbf{q}), \\ \lim_{t \rightarrow +\infty} M(\mathbf{q}, t) &= M_\infty(\mathbf{q}). \end{aligned} \quad (6.235)$$

In the long-time limit, Eq. (6.234) becomes a self-consistent equation for the plateau value of the correlation function:

$$\frac{\phi_\infty(\mathbf{q})}{1 - \phi_\infty(\mathbf{q})} = \frac{2S(q)\rho_0}{q^2} \int \frac{d\mathbf{k}}{(2\pi)^2} [(\hat{\mathbf{q}} \cdot \mathbf{k})c(k) + \hat{\mathbf{q}} \cdot (\mathbf{q} - \mathbf{k})c(|\mathbf{q} - \mathbf{k}|)]^2 \phi_\infty(\mathbf{k})\phi_\infty(\mathbf{q} - \mathbf{k}). \quad (6.236)$$

This equation is the same as the one obtained for overdamped equilibrium dynamics [247]. It follows that ergodicity breaking is expected to occur at the same critical density as in equilibrium.

To study the relaxation of the system in the ergodic regime, we introduce a relaxation time

$$\tau \equiv \int_0^{+\infty} dt \phi(\mathbf{q}, t). \quad (6.237)$$

Integration of Eq. (6.234) in t from 0 to $+\infty$ gives

$$\begin{aligned} \tau &= \frac{2S(q)D_r}{v_0^2 q^2} \\ &+ \frac{2S(q)\rho_0}{q^2} \int_0^{+\infty} dt \int \frac{d\mathbf{k}}{(2\pi)^2} [(\hat{\mathbf{q}} \cdot \mathbf{k})c(k) + \hat{\mathbf{q}} \cdot (\mathbf{q} - \mathbf{k})c(|\mathbf{q} - \mathbf{k}|)]^2 \phi(\mathbf{k}, t)\phi(\mathbf{q} - \mathbf{k}, t). \end{aligned} \quad (6.238)$$

This expression for τ is formally identical to the equilibrium case with the bare diffusion coefficient D_0 now being replaced with $\frac{v_0^2}{2D_r} = D_0$. While D_0 is slaved to the temperature in equilibrium, $\frac{v_0^2}{2D_r}$ can be independently varied in the lifted-ABP model, potentially leading to an accelerated dynamics.

6.6.5 Diffusion constant

We obtain an equation of motion for the mean-squared displacement $\Delta(t)$ by substituting Eq. (6.212) in Eq. (6.225) and retaining only the leading term in the limit $q \rightarrow 0$:

$$\partial_t^2 \Delta(t) = 2v_0^2 - D_r \partial_t \Delta(t) - \int_0^t d\tau M_s(\mathbf{q} \rightarrow 0, t - \tau) \partial_\tau \Delta(\tau). \quad (6.239)$$

We now assume a diffusive behavior at large times: $\Delta(t) \sim 4Dt$. Substituting into Eq. (6.239) we obtain an expression for the diffusion constant D :

$$D = \frac{v_0^2}{2D_r} \frac{1}{1 + \frac{v_0^2}{2D_r} m_s^\infty}, \quad (6.240)$$

where the memory kernel is given by

$$m_s^\infty = \rho_0 \int_0^{+\infty} dt \int \frac{d\mathbf{k}}{(2\pi)^2} [\hat{\mathbf{q}} \cdot \mathbf{k} c(k)]^2 F_s(k, t) S(k, t). \quad (6.241)$$

The formal expression of m_s^∞ is the same as in equilibrium, while the one for D is also formally similar, with the replacement D_0 by $\frac{v_0^2}{2D_r}$. In the ergodic phase when m_s^∞ is finite, the diffusion constant D can be enhanced with respect to equilibrium by increasing $\frac{v_0^2}{2D_r} > D_0$, which plays the role of the driving force. Differently from the transverse force case, the acceleration survives the high-temperature limit, since $D = \frac{2v_0^2}{D_r}$ in this limit. In the opposite limit of temperature approaching the dynamic transition, $m_{s,\infty}$ diverges and thus D exactly recovers its equilibrium expression and the lifted-ABP dynamics is no longer felt. This suggests that lifted dynamics acceleration plummets as the kinetic glass transition is approached.

6.7 Outlook

This Chapter concludes our investigations on transverse forces. Using analytical approximations schemes for the microscopic dynamics of finite dimensional liquids, we rationalized the picture brought forth by the numerical analysis of Chapter 4. Our approach goes of course much beyond this task, as allowed us to study several individual and collective transport coefficient, from the diffusivity and mobility tensors to the viscosity. This Chapter opens at least two immediate research directions. The first one has to do with the collective behavior of dense assemblies of chiral active particles [175, 77], for which a mode-coupling analysis will surely closely follow the footsteps developed in our work. The second one is more subtle: it is concerned with the numerical integration of the derived mode-coupling equations. This will surely be a highly non-trivial task due to the loss of isotropy and the appearance of multiple time integrals in the equation of motion. However, we hope to proceed further in this direction, taking also advantage from recently developed numerical software that handle the integration of general mode-coupling equations [221].

The mode-coupling theory developed for lifted-ABPs in Section 6.6 suggests that also lifting schemes might share a fate similar to the one of transverse forces in the glassy phase of dense liquids, at least when the driving is supplemented at the level of the translational degrees of freedom. Our investigation for transverse forces leaves us thus with two questions: does the fate of more sophisticated lifting schemes echo the one of transverse forces? And, if this is true for translational degrees of freedom, are there other degrees of freedom in glassy system that can be targeted by nonequilibrium currents, and thus speedup the dynamics in a more effective way? The next Chapter aims at addressing these questions.

Contributions from Chapter 6

- We build a specific weak-coupling approximation for the dynamics of a tracer with transverse forces.
- In the weak coupling approximation, we witness the emergence of odd mobility and diffusivity, and an enhancement of longitudinal diffusivity. Both the odd transport properties and the longitudinal diffusion grow as the temperature is reduced.
- We construct a mode-coupling theory tailored for transverse forces.
- We find that a dynamical ergodicity breaking transition happens, in the presence of transverse forces, at the same values of temperature T_{MCT} (or density) for equilibrium dynamics.
- In the ergodic phase, we witness a speedup of transverse forces on equilibrium dynamics, both in the form of a reduced relaxation time for the decay of density-density correlations and an enhancement of longitudinal diffusion.
- From the dynamics of collective and individual density-density autocorrelators, we obtain expressions for collective and individual transport coefficient: mobility and diffusivity tensors, and viscosity tensors.
- The longitudinal diffusivity vanishes at the glass transition. From this fact, we infer a decrease in the efficiency of transverse forces upon lowering the temperature, in the vicinity of T_{MCT}
- The odd diffusivity saturates to a constant as the mode-coupling temperature is approached.
- All the entries of the mobility tensor vanish at the glass transition.
- Both the shear and the odd viscosity diverge at the glass transition.
- We put forward a mode-coupling theory for a lifted dynamics inspired by active Brownian particle.
- For this lifted dynamics, we find that the ergodicity breaking scenario is left unaltered by the nonequilibrium drive, as for transverse forces.
- In the ergodic phase, the lifted dynamics is faster than its equilibrium counterpart, similarly for what occurs with transverse forces.

CHAPTER 7

IRREVERSIBLE MONTE CARLO ALGORITHMS IN GLASS FORMERS: EVENT-CHAIN AND COLLECTIVE SWAP

7.1	The model	136
7.2	Monte Carlo schemes	137
7.2.1	Metropolis Monte-Carlo (MMC)	138
7.2.2	Swap Monte Carlo	138
7.2.3	Event chain Monte Carlo (ECMC)	138
7.2.4	Collective Swap (cSwap)	140
7.3	Tests of ergodicity	142
7.3.1	Numerical test	142
7.3.2	Analytical test	143
7.4	Relaxation times	145
7.4.1	Echoes from transverse forces	147
7.4.2	Faster than the fastest	147
7.5	Dense jammed packings	149
7.6	Outlook	149

In the previous chapters, we have studied the overdamped Langevin dynamics with transverse forces in dense liquids. This dynamics was meant to be a minimal, paradigmatic model to study the speedup obtained in glassy systems by translational degrees of freedom driven out of equilibrium, while preserving the Boltzmann distribution in the steady state. In this Chapter, we study the celebrated Event Chain Monte Carlo (ECMC) algorithm, a nonequilibrium Monte Carlo scheme that exploits the idea of lifting to perform driven, collective translations of chains of particles, in a model of polydisperse hard disks. Very much like what was witnessed for transverse forces, the efficiency of ECMC compared to the standard, Metropolis algorithm decreases upon

increasing the glassiness of the system. However, the driven and collective moves characteristic of ECMC need not be confined only to particle translations, as in principle, other degrees of freedom can experience a nonequilibrium drive. For glassy systems, an equilibrium Monte Carlo scheme called Swap is known to achieve astronomical speedups by allowing for the exchanges of particle radii. We propose an algorithm that performs driven, collective swaps in continuously polydisperse systems of hard disks, bringing the event-chain ideas to the space of particle diameters. As the glassiness of the system increases, the efficiency of our algorithm with respect to Swap increases too. By combining our novel algorithm with ECMC for particle translations, we achieve a speedup of ≈ 40 with respect to the state-of-the art Swap. As an application, we show that our algorithm can be used to produce very dense jammed packings of disks.

We depart from the paradigmatic overdamped Langevin dynamics to address the efficiency of irreversible Monte Carlo schemes. As a matter of fact, Monte Carlo algorithms, together with Molecular dynamics simulations, are the way-to-go numerical schemes when confronted with sampling a given target distribution. For example, for the Kob-Andersen model addressed in Chapter 4, equilibrium Monte Carlo schemes are an order of magnitude faster than the corresponding equilibrium overdamped Langevin dynamics [35].

Recently, an efficient Monte Carlo algorithm was developed for size polydisperse fluids, where local Monte Carlo moves are performed in an enlarged configuration space composed of particle positions and diameters [119, 33, 203]. The sequential swap of particle pairs respects detailed balance and ensures that the particle size distribution is conserved [119]. The resulting swap Monte Carlo algorithm (hereafter called ‘Swap’) allows equilibration at very low temperatures, exploiting dynamic pathways unavailable to the local dynamics [203]. Swap paved the way for numerous physical studies [30, 210, 235] and computational developments [31, 218]. Diameter dynamics can be implemented in molecular dynamics, both in thermal equilibrium [34] or in gradient descent [150, 51]. For hard particles, this optimization strategy was exploited to produce jammed packings with large stability and novel physical properties [51, 122, 44].

The Swap algorithm samples the Boltzmann distribution owing to reversible evolution rules obeying detailed balance. We saw however in Chapter 1 that giving up detailed-balance—while preserving the target distribution—can be rewarded with sampling acceleration. Ironically, the seminal 1953 article [188] by Metropolis *et al.* presented an algorithm to sample the Boltzmann distribution for simple fluids whose elementary moves did not, strictly speaking, satisfy detailed balance, since the labels of the moving particles were updated according to a fixed order.

A successful implementation of these idea on irreversibility for particle models is the event-chain Monte Carlo (ECMC) algorithm [23]. Following the *lifting* prescription introduced in Chapter 1, ECMC operates in an enlarged configuration space where irreversible, collective particle translations are performed. For hard disks near their hexatic ordering transition, ECMC offers a two orders of magnitude speedup that led to a better understanding of the phase diagram [22]. This approach was extended in various directions [193, 194, 140, 147, 139, 192, 121, 41], but a quantitative benchmark in dense disordered states is lacking.

Furthermore, in principle, the collective, driven moves that form the backbone of ECMC need not to be confined to the space of particle translations. In polydisperse particle models, another obvious degree of freedom that could be affected by these moves is the diameter of the particles. Here we propose, implement and benchmark irreversible Monte Carlo algorithms where collective and directed particle translations and diameter swaps are performed while maintaining global balance.

We carefully test the respective and combined effects of these moves in a continuously polydisperse models of hard disks displaying glassy dynamics in equilibrium, and that can be compressed towards jamming [44]. We find that the directed translational

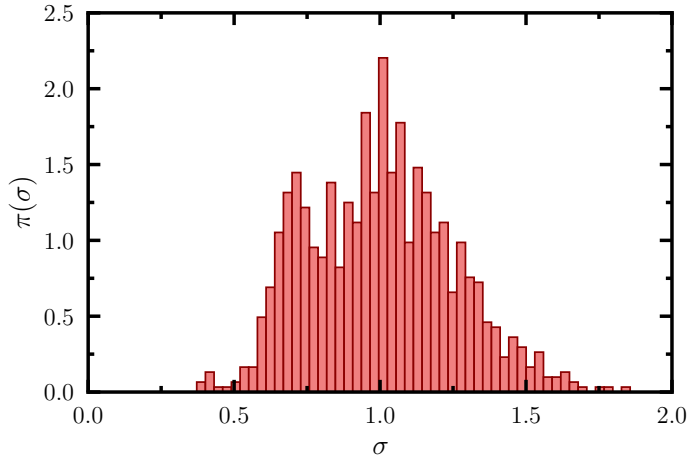


Figure 7.1: Particle size distribution $\pi(\sigma)$ for the system investigated in this work.

moves used in ECMC marginally affect the dynamics, with a speedup that plummets with increasing density, echoing the fate of transverse forces unravelled by our analysis in Chapters 4 - 6. By contrast, irreversible collective swaps (named ‘cSwap’) produce an opposite trend offering a comfortable gain over Swap that improves as density increases. Combining both types of moves in a novel algorithm (named ‘cSwapECMC’) provides an overall computational speedup reaching about 40 over the conventional Swap. In addition, cSwapECMC remains extremely efficient during nonequilibrium compressions, producing jammed packings comparable to gradient descent protocols preserving the particle size distribution.

7.1 The model

We consider a two-dimensional additive mixture of $N = 1024$ hard disks in a periodic square box of linear size L . Lengths are measured in units of the average diameter $\bar{\sigma}$ with a fixed continuous polydispersity $\frac{\sqrt{\sigma^2 - \bar{\sigma}^2}}{\bar{\sigma}}$ of about 25%. The histogram of particles diameters $\pi(\sigma)$ is shown in Fig 7.1. The hard-disk interaction potential $V(r_{ij}, \sigma_i, \sigma_j)$ between two particles, labeled i and j , with diameters σ_i, σ_j is

$$V(r_{ij}, \sigma_i, \sigma_j) \equiv \begin{cases} +\infty & \text{if } r_{ij} \leq \frac{\sigma_i + \sigma_j}{2} \\ 0 & \text{otherwise} \end{cases}, \quad (7.1)$$

and the total interaction energy is $\mathcal{H}(\mathbf{r}^N, \sigma^N) \equiv \sum_{i < j} V(r_{ij}, \sigma_i, \sigma_j)$, where we have used the notation $\mathbf{r}^N \equiv \{\mathbf{r}_1, \dots, \mathbf{r}_N\}$ and $\sigma^N \equiv \{\sigma_1, \dots, \sigma_N\}$ to indicate a given configuration of particle positions and diameters. The probability distribution we are interested in sampling for this system is the Boltzmann distribution $\pi_B(\mathbf{r}^N, \sigma^N) \propto e^{-\beta V(\mathbf{r}^N, \sigma^N)}$. Due to the hard-sphere interaction potential, we have

$$\pi_B(\mathbf{r}^N, \sigma^N) \equiv \begin{cases} 0 & \text{If some pair of particles overlaps} \\ \frac{1}{Z} & \text{Otherwise} \end{cases} \quad (7.2)$$

where $Z \equiv \frac{1}{N!} \sum_{\sigma^N} \int d\mathbf{r}^N e^{-\beta \mathcal{H}(\mathbf{r}^N, \sigma^N)}$ is the partition function of the system, computed over all the possible assignments of particles positions and diameters. Note that, as observed in [213], since a diameter permutation is equivalent to a permutation of the position of the particles, we have that $Z = \int d\mathbf{r}^N e^{-\beta \mathcal{H}(\mathbf{r}^N, \sigma^N)}$ for a fixed permutation of the diameters σ^N .

We control the glassiness of the system by varying the packing fraction is $\phi \equiv N\pi\overline{\sigma^2}/(4L^2)$. We work in a density regime characterized by glassy dynamics, typically much beyond the one explored in [23] for monodisperse systems.

We now proceed to describing the different Monte Carlo dynamics, all tailored to sample π_B , studied in this Chapter.

7.2 Monte Carlo schemes

In this Section, we illustrate the different algorithms investigated in this chapter. First, we recall the condition that each algorithm must obey to admit the Boltzmann distribution in its steady state. We denote by \mathcal{C} denotes a state of the system, and $\pi_t(\mathcal{C})$ the probability of the system to be in configuration \mathcal{C} at time t . This distribution evolves in discrete time according to the master equation

$$\pi_{t+1}(\mathcal{C}) = \sum_{\mathcal{C}'} P(\mathcal{C}' \rightarrow \mathcal{C}) \pi_t(\mathcal{C}') \quad (7.3)$$

with $P(\mathcal{C}' \rightarrow \mathcal{C})$ the transition probability from state \mathcal{C}' to state \mathcal{C} . We look for stationary solution $\pi_{ss}(\mathcal{C})$ of Eq. (7.3). Since by definition, $\sum_{\mathcal{C}} P(\mathcal{C} \rightarrow \mathcal{C}') = 1$ for every \mathcal{C} , we obtain

$$\sum_{\mathcal{C}'} P(\mathcal{C} \rightarrow \mathcal{C}') \pi_{ss}(\mathcal{C}') = \sum_{\mathcal{C}'} P(\mathcal{C}' \rightarrow \mathcal{C}) \pi_{ss}(\mathcal{C}'). \quad (7.4)$$

This stationary condition is known in the mathematics Markov chain literature as global balance [166]. It can be satisfied by imposing the detailed balance condition

$$P(\mathcal{C} \rightarrow \mathcal{C}') \pi_{ss}(\mathcal{C}) = P(\mathcal{C}' \rightarrow \mathcal{C}) \pi_{ss}(\mathcal{C}'), \quad (7.5)$$

which is a statement of reversibility of the underlying Markov Chain, equivalent to what was given in Sec. 1.1.1 for overdamped Langevin dynamics.

To compare the efficiency of various algorithms, we need to carefully define a specific unit of time, t_{move} , adapted for each case. The unit of time t_{move} is constructed upon the elementary transitions involved in each algorithm. Incidentally, over the time t_{move} in each algorithm, one overlap detection involving a calculation of neighbor particles distances is needed. From the point of view of CPU time, this is the most costly operation to be performed for each algorithm. Therefore, the unit t_{move} accurately describes also CPU times, as shown later in this Chapter.

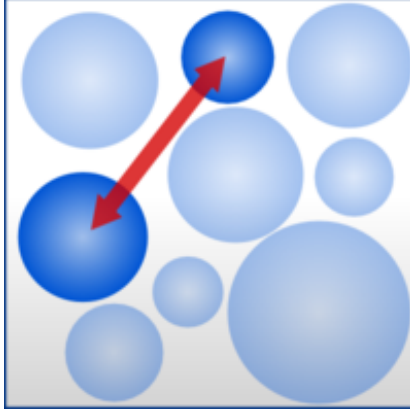


Figure 7.2: Illustration of the Swap Monte Carlo algorithm. During a time t_{move} , a swap of the diameters of the highlighted particles is attempted. Adapted from [203].

7.2.1 Metropolis Monte-Carlo (MMC)

In Metropolis Monte Carlo (MMC) dynamics [166], a random particle is selected uniformly, and a random displacement is uniformly drawn from a square of length δ centered around the origin. We take $\delta = 0.115\bar{\sigma}$ [33]. The displacement is accepted if it creates no overlaps. One such attempt defines t_{move} .

7.2.2 Swap Monte Carlo

In Swap, we randomly alternate translational moves (as in MMC) with particle swaps with probability $p_{\text{swap}} = 0.2$ [203], see Fig. 7.2. During t_{move} , two particles are randomly selected and their radii are exchanged if the swap does not create overlaps. Both the Metropolis and Swap algorithm satisfy the detailed balance condition, which implies that they admit the Boltzmann distribution π_B in their steady state. We now address the irreversible Event Chain algorithm.

7.2.3 Event chain Monte Carlo (ECMC)

We recall the so-called ‘straight’ Event Chain Monte Carlo, as described in [23, 21].

The phase space is lifted by two additional degrees of freedom, an activity label i denoting the driven particle and its direction of self propulsion \mathbf{v} , a two-dimensional vector of unit norm. The state of the system is thus described by a configuration $\mathcal{C} = \{\mathbf{r}^N, \sigma^N, i, \mathbf{v}\}$. During a time interval t_{move} , particle i travels along direction \mathbf{v} until it collides with one of its neighbors, j . The distance $\delta\ell_{ij}$ traveled by i during a move is thus determined by the equation

$$\delta\ell_{ij} = \mathbf{r}_{ji} \cdot \mathbf{v} - \sqrt{\sigma_{ij}^2 - (\mathbf{r}_{ji} \cdot \mathbf{v}_\perp)^2}, \quad (7.6)$$

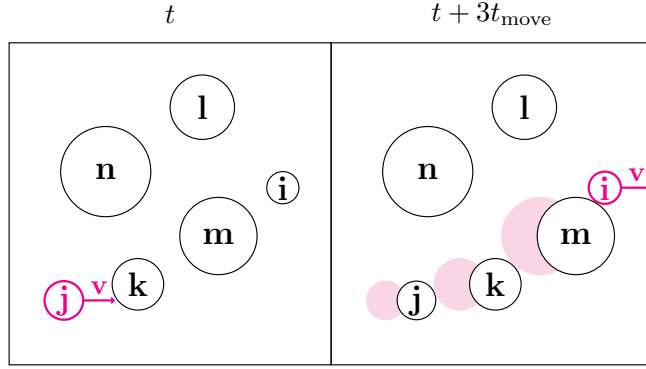


Figure 7.3: Event-chain Monte Carlo algorithm: the lifted set of degrees of freedom, the active label j and the speed direction \mathbf{v} (magenta), produce a directed translational motion of a chain of three particles.

where $\mathbf{r}_{ji} = \mathbf{r}_j - \mathbf{r}_i$ is the vector joining particle i to particle j , $\sigma_{ij} \equiv \frac{\sigma_i + \sigma_j}{2}$ is the effective diameter, and $\mathbf{v}_\perp = (v_y, -v_x)$ is the direction orthogonal to \mathbf{v} . In practice, in the simulations the inter-particle distance \mathbf{r}_{ij} is computed according to the minimum image convention [96] to take periodic boundary conditions into account, and the particle j is identified through an event-driven scheme, by minimizing $\delta\ell_{ik}$ among all possible target particles k , i.e. $j = \arg \min_k \delta\ell_{ik}$.

After an event occurs, a lifting move is performed: the activity label changes from i to j . In the next ECMC move particle j will perform directed motion along the direction \mathbf{v} . The composition of several ECMC moves builds up a chain of particles performing directed motion, see Fig 7.3. When the displacement performed by the active particles add up to a fixed parameter ℓ , which fixes the length of the chain, the activity label and the self propulsion direction are resampled uniformly in their domain of definition, which are respectively the set $\{1, 2, \dots, N\}$ for the activity label and the set $\{\mathbf{e}_x, \mathbf{e}_y\}$ for the self-propulsion, for the case of straight ECMC.

We now give a proof, following the original paper [23], that ECMC admits the Boltzmann distribution in the steady state, once the lifted degrees of freedom are integrated out. We use the following ansatz for the steady state distribution

$$\pi_{ss}(\mathcal{C}) = \frac{1}{2N} \pi_B(\mathbf{r}^N, \sigma^N), \quad (7.7)$$

which means that the lifted degrees of freedom are uniformly distributed in the steady state among the N particle labels and the 2 possible self-propulsion direction, while the positions of the particles and the diameters follow the Boltzmann weight. We need to verify the stationary condition

$$\sum_{\mathcal{C}'} \pi_{ss}(\mathcal{C}') P(\mathcal{C}' \rightarrow \mathcal{C}) = \pi_{ss}(\mathcal{C}) \quad (7.8)$$

with $P(\mathcal{C}' \rightarrow \mathcal{C})$ the probability of transitioning from configuration $\mathcal{C}' = \{\mathbf{r}'^N, \sigma'^N, i', \mathbf{v}'\}$ to configuration $\mathcal{C} = \{\mathbf{r}^N, \sigma^N, i, \mathbf{v}\}$ by displacing a directed chain of particles of length

ℓ . This probability is

$$P(\mathcal{C}' \rightarrow \mathcal{C}) = \frac{1}{2N} \sum_{j=1}^N \delta_{\sigma'^N, \sigma^N} \delta_{\mathbf{r}'^N, \mathbf{r}^{*N}(j, \mathbf{v}')} \quad (7.9)$$

the factor $\frac{1}{2N}$ corresponds to a uniform resampling of the active degrees of freedom, while $\mathbf{r}^{*N}(j, \mathbf{v}'|i')$ is the configuration obtained from \mathbf{r}^N , by displacing a collective chain of length ℓ that starts from the particle with label j along the direction $-\mathbf{v}'$ –note the sign inversion– and terminates at particle i' . This configuration can be uniquely determined upon neglecting the occurrence of simultaneous collisions between three or more disk along a chain. The latter approximation can be rigorously justified by treating the ECMC algorithm as a process continuous in time [198].

Substituting Eq. (7.9) in the stationary condition Eq. (7.8) and using the ansatz for π_{ss} given by Eq. (7.7) we obtain that the condition to be verified is

$$\frac{1}{2N} \sum_{i'=1}^N \sum_{\mathbf{v}'=\mathbf{e}_x, \mathbf{e}_y} \pi_B(\mathbf{r}^{*N}, \sigma^N) = \pi_B(\mathbf{r}^N, \sigma^N), \quad (7.10)$$

which is true, since disks with hard interactions $\pi_B(\mathbf{r}^{*N}, \sigma^N) = \pi_B(\mathbf{r}^N, \sigma^N)$. This concludes our demonstration that ECMC samples the Boltzmann distribution for hard disks.

One can of course design an algorithm where collective translations with ECMC alternate with Swap moves with probability p_s . This produces a new algorithm, here called SwapECMC. We now proceed to bring direct the motion in the space of particle diameters.

7.2.4 Collective Swap (cSwap)

We now show how to perform directed, irreversible, collective moves in diameter space to arrive at cSwap, see Fig. 7.4. We define a one-dimensional array containing the particle labels by order of increasing diameters and the operators $(\mathcal{L}, \mathcal{R})$ acting on the labels: $\mathcal{L}(i)$ returns the label of the particle immediately to the left of i (with a smaller radius); $\mathcal{R}(i)$ returns the label of the particle to the right (with a larger radius). During t_{move} we perform the following operations. A particle i is uniformly selected to become active and the state of the system is described by $\mathcal{C} = \{\mathbf{r}^N, \sigma^N, i\}$. We then determine the largest diameter $\sigma_j \in \sigma^N$ that particle i can adopt without generating an overlap. To preserve the particle size distribution, we now perform a cascade of swaps: $\sigma_i \leftarrow \sigma_j$ (maximal authorized expansion of i), followed by a series of incremental deflations $\sigma_j \leftarrow \sigma_{\mathcal{L}(j)}, \sigma_{\mathcal{L}(j)} \leftarrow \sigma_{\mathcal{L}^2(j)}, \dots, \sigma_{\mathcal{L}^n(j)} \leftarrow \sigma_i$, with n such that $\mathcal{L}^n(j) = \mathcal{R}(i)$, thus completing the cascade. Finally, a lifting event occurs leading to $\mathcal{C}' = \{\mathbf{r}^N, \sigma'^N, \mathcal{L}(i)\}$, where σ'^N is reached after the collective swap. If i is the particle with the smallest diameter, $\mathcal{L}(i)$ is the particle with the largest diameter. To warrant ergodicity, we perform with probability $1/N$ a uniform resampling of the lifting label. Finally, ECMC can be combined with cSwap, leading to a fully irreversible algorithm,

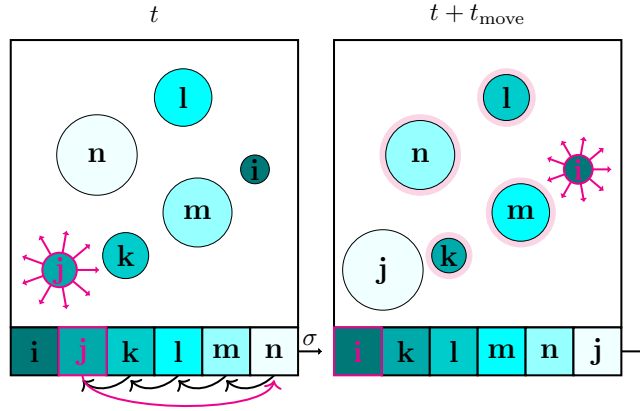


Figure 7.4: Collective Swap algorithm: the active particle (in magenta) inflates while other particles deflate, resulting in a directed motion in diameter space (as seen at the bottom) and a collective swap of five particles.

‘cSwapECMC’. The invention and implementation of irreversible and collective swap moves is our main algorithmic development. While cSwap is broadly applicable for any particle size distribution, its efficiency should be optimal for continuous distributions, or discrete ones with a large number of diameter families. For bidisperse models, cSwap remains rejection-free and irreversible, but loses its collective character.

We must prove that the stationary state of the cSwap dynamics is the Boltzmann distribution, i.e. $\pi_{ss}(\{\mathbf{r}^N, \sigma^N, i\}) = \frac{1}{N}\pi_B(\mathbf{r}^N, \sigma^N)$, where π_B is the Boltzmann distribution for a system of polydisperse hard disks, where now the set of positions \mathbf{r}^N is held fixed, and the factor $\frac{1}{N}$ is the uniform distribution for lifting. Denoting by $p(\mathcal{C} \rightarrow \mathcal{C}')$ the transition probability from $\mathcal{C} = \{\mathbf{r}^N, \sigma^N, i\}$ to $\mathcal{C}' = \{\mathbf{r}^N, \sigma'^N, i'\}$, we must prove that the stationarity condition

$$\sum_{\mathcal{C}'} \pi_{ss}(\mathcal{C}') p(\mathcal{C}' \rightarrow \mathcal{C}) = \pi_{ss}(\mathcal{C}) \quad (7.11)$$

is satisfied by $\pi_{ss} = \pi_B/N$. The left-hand side is decomposed into label resampling and collective swaps:

$$p(\mathcal{C}' \rightarrow \mathcal{C}) = \frac{1}{N^2} \delta_{\sigma'^N, \sigma} + \left(1 - \frac{1}{N}\right) \delta_{\mathcal{C}', \mathcal{C}^*}, \quad (7.12)$$

where \mathcal{C}^* is the configuration leading to \mathcal{C} after a cSwap move (we show below that \mathcal{C}^* exists and is unique). Substituting (7.12) into (7.11), using the definition of π_{ss} and $\sum_{\mathcal{C}} = \sum_j \sum_{\sigma^N}$, we get

$$\frac{1}{N} \pi_B(\mathbf{r}^N, \sigma^N) + \left(1 - \frac{1}{N}\right) \pi_B(\mathbf{r}^N, \sigma^{*N}) = \pi_B(\mathbf{r}^N, \sigma^N).$$

Since for hard disks, π_B is uniform over allowed configurations, stationarity is proven. Finally we construct the configuration $\mathcal{C}^* = \{\mathbf{r}^N, \sigma^{*N}, i^*\}$ that will reach $\mathcal{C} = \{\mathbf{r}^N, \sigma^N, i\}$. We first transform $\sigma_{\mathcal{R}(i)} \leftarrow \sigma_{\mathcal{R}^2(i)}$ if the change does not generate any overlap. We then

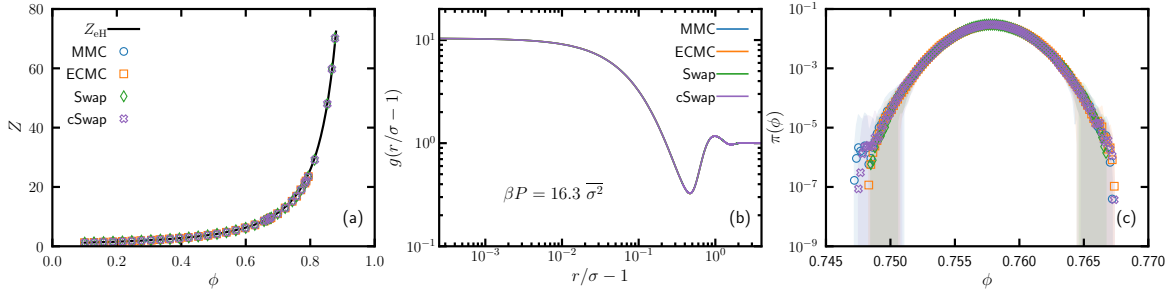


Figure 7.5: Numerical test of ergodicity for the cSwap and ECMC algorithms. (a) Equation of state $Z(\phi)$ for the polydisperse hard disks system. (b) Rescaled radial distribution function $g(r/\sigma - 1)$ as a function of the distance from its first peak $r/\sigma - 1$. (c) Probability distribution function of the packing fractions $\pi(\phi)$ explored by the system during NPT simulations at $\beta P = 16.3 \bar{\sigma}^2$.

repeat this operation for $\mathcal{R}^2(i)$, $\mathcal{R}^3(i)$, etc. After n iterations, either the transformation $\sigma_{\mathcal{R}^n(i)} \leftarrow \sigma_{\mathcal{R}^{n+1}(i)}$ is no longer allowed, or the largest particle is reached. When n is reached, we set $i^* = \mathcal{R}^n(i)$ and transform $\sigma_{\mathcal{R}^n(i)} \leftarrow \sigma_{\mathcal{R}(i)}$. The resulting configuration defines σ^{*N} , as directly verified by performing a cSwap move on \mathcal{C}^* .

7.3 Tests of ergodicity

The above reasoning establishes the stationarity of the Boltzmann distribution. The general proof of ergodicity of the algorithm, as obtained for ECMC [198], is left for future work. Here we provide a set of numerical and analytical tests to support our claim of ergodicity.

7.3.1 Numerical test

We present numerical tests supporting the ergodicity of the cSwap and ECMC algorithms. The first test is the numerical calculation of the equation of state $Z(\phi)$ of the polydisperse system considered in the main text. The equation of state relates the reduced pressure $Z = \frac{\beta P}{\rho}$ to the packing fraction ϕ . Here P is the pressure applied to the system, ρ is the number density and $\beta^{-1} = k_B T$. It can be obtained from simulations in the NPT ensemble, where one has access to the running averages of Z and ϕ at fixed applied pressure P . The results are shown in Fig. 7.5(a), where they are compared with an extension to polydisperse systems of the empirical Henderson formula [129, 234] which reads

$$Z_{\text{eff}} = \frac{1 - \left(1 - \frac{\bar{\sigma}^2}{\sigma^2}\right)\phi + (b - 3)\frac{\bar{\sigma}^2}{\sigma^2}\phi^2}{(1 - \phi)^2}, \quad (7.13)$$

$$b \equiv \frac{16}{3} - \frac{4\sqrt{3}}{\pi}.$$

The agreement with the empirical formula and with the conventional Metropolis and Swap algorithms is excellent, and this serves as a guide to detect deviations from one algorithm to another. We find that all algorithms agree with each other.

We next compare the rescaled radial distribution function $g(r/\sigma)$ in the NPT ensemble in Fig. 7.5(b). Its expression is given by

$$g(x) \equiv \sum_{\substack{i,j \\ i < j}} C_{ij} \int_{x_b}^{x_b + \Delta x} \delta \left(x' - \frac{r_{ij}}{\sigma_{ij}} \right) dx'$$

$$C_{ij} \equiv \frac{1}{2\pi(x_b + \Delta x/2)\Delta x \sigma_{ij}^2 \rho(N-1)} \quad (7.14)$$

where $\sigma_{ij} \equiv \frac{1}{2}(\sigma_i + \sigma_j)$, $\rho = N/L^2$ is the number density of the system, and we collect the rescaled interparticle distances in a histogram with bin width Δx . $x_b = b\Delta_x$ is the coordinate of the b -th bin, with b chosen so that $x_b \leq x < x_b + \Delta x$. Again, the curves obtained with the different algorithms superimpose on each other.

Finally, we report in Fig. 7.5(c) the histogram of the packing fractions explored during an NPT simulation, $\pi(\phi)$, for a fixed pressure P . Again all algorithms explore the same fluctuations, including in the tails of the distribution, showing that the same Boltzmann distribution is indeed properly sampled in all our algorithms.

7.3.2 Analytical test

Here we prove the ergodicity of the cSwap dynamics in the case of a small polydisperse system at low densities. The discrete-time dynamics we consider is made up only by cSwap moves, the positions of the disks \mathbf{r}^N being fixed at all times. The state of the system $\mathcal{C} = \{\sigma^N, i\}$ is specified by assigning a diameter to each of the N particles –the resulting permutation of diameters is denoted by σ^N – and by the lifting degree of freedom i , i.e. the label of the active particle. The system can access a subset of $N! \times N$ configurations. The configurations in the subset satisfy the non-overlapping hard disks condition. The probability $\pi_t(\mathcal{C})$ for the system to be in state \mathcal{C} at time t obeys the discrete time Markov dynamics

$$\pi_{t+1}(\mathcal{C}) = \sum_{\mathcal{C}'} P(\mathcal{C}' \rightarrow \mathcal{C}) \pi_t(\mathcal{C}'), \quad (7.15)$$

with P the transition matrix encoding the probability to jump from one configuration to another during a discrete time-step. The convergence properties of the dynamics are encoded in the spectrum of P . Proving that the cSwap dynamics is ergodic amounts to showing that the spectrum of P has a unique, nondegenerate, eigenvalue $\lambda = 1$ lying on the unit circle, and that all the other eigenvalues have a norm strictly smaller than 1 [202].

We consider the case where $N = 4$ and the particles are far away from each other, so that no overlap between them can be generated upon permutation of the radii. To write down the transition matrix describing the cSwap dynamics, we decompose

the configuration space into a tensor product $S_4 \otimes i$, where S_4 is an element of the permutation group of 4 elements, and i is the lifting degree of freedom labeling the active, expanding particle. The permutations are labeled by natural numbers in the following way:

$$\begin{aligned}
1 &\equiv \{1, 2, 3, 4\} & 2 &\equiv \{2, 3, 4, 1\} & 3 &\equiv \{3, 4, 1, 2\} & 4 &\equiv \{4, 1, 2, 3\} \\
5 &\equiv \{1, 3, 4, 2\} & 6 &\equiv \{3, 4, 2, 1\} & 7 &\equiv \{4, 2, 1, 3\} & 8 &\equiv \{2, 1, 3, 4\} \\
9 &\equiv \{1, 2, 4, 3\} & 10 &\equiv \{2, 4, 3, 1\} & 11 &\equiv \{4, 3, 1, 2\} & 12 &\equiv \{3, 1, 2, 4\} \\
13 &\equiv \{2, 4, 1, 3\} & 14 &\equiv \{4, 1, 3, 2\} & 15 &\equiv \{1, 3, 2, 4\} & 16 &\equiv \{3, 2, 4, 1\} \\
17 &\equiv \{2, 3, 1, 4\} & 18 &\equiv \{3, 1, 4, 2\} & 19 &\equiv \{1, 4, 2, 3\} & 20 &\equiv \{4, 2, 3, 1\} \\
21 &\equiv \{2, 1, 4, 3\} & 22 &\equiv \{1, 4, 3, 2\} & 23 &\equiv \{4, 3, 2, 1\} & 24 &\equiv \{3, 2, 1, 4\}
\end{aligned} \tag{7.16}$$

Here the numbers inside the brackets denote the index of the particles, ordered according to their diameters, from the smallest to the largest. For example, $\{2, 3, 4, 1\}$ is the configurations where particle with label 1 has the largest diameter, particle with label 4 has the second largest diameter, and so on. If the system is in a configuration where particle 3 is the active one, we would have $\mathcal{C} = \{2, 3, 4, 1\} \otimes 3$.

With this notation, the transition matrix can be written as a 24×24 block matrix, each block being made by a 4×4 sub-block. Transitions between blocks represent changes in the diameter assignments for the different particles, while transitions within a block represent change in the active degree of freedom. The transition matrix P describing the cSwap dynamics is

The dot symbol \cdot denote 4×4 matrices whose entries are all zeros. The diagonal block is a sum of two terms, $D_4 \equiv A_4 + B_4$. The block of type A_4 encodes transitions involving only the active degree of freedom,

$$A_4 \equiv \begin{bmatrix} \alpha & \alpha & \alpha & \alpha \\ \alpha & \alpha & \alpha & \alpha \\ \alpha & \alpha & \alpha & \alpha \\ \alpha & \alpha & \alpha & \alpha \end{bmatrix}, \quad (7.18)$$

with $\alpha = 1/4^2 = 1/16$. They are associated to random resampling of the activity label, and they are used here to ensure that P is ergodic. The blocks B_i encode transitions

generated by the cSwap moves, involving an inflation of the active particle and the cascade of swaps. They are given by:

$$B_1 \equiv \begin{bmatrix} \circ & \circ & \circ & 1 - \frac{1}{4} \\ \circ & \circ & \circ & \circ \\ \circ & \circ & \circ & \circ \\ \circ & \circ & \circ & \circ \end{bmatrix} \quad B_2 \equiv \begin{bmatrix} \circ & \circ & \circ & \circ \\ 1 - \frac{1}{4} & \circ & \circ & \circ \\ \circ & \circ & \circ & \circ \\ \circ & \circ & \circ & \circ \end{bmatrix} \quad (7.19)$$

$$B_3 \equiv \begin{bmatrix} \circ & \circ & \circ & \circ \\ \circ & \circ & \circ & \circ \\ \circ & 1 - \frac{1}{4} & \circ & \circ \\ \circ & \circ & \circ & \circ \end{bmatrix} \quad B_4 \equiv \begin{bmatrix} \circ & \circ & \circ & \circ \\ \circ & \circ & \circ & \circ \\ \circ & \circ & \circ & \circ \\ \circ & \circ & 1 - \frac{1}{4} & \circ \end{bmatrix},$$

with the symbol ‘ \circ ’ denoting the entries with value 0.

The matrix P is doubly stochastic, i.e. the sum of all the elements belonging to a fixed row, or fixed column, is one. A stationary solution of the stochastic process associated with P is given by

$$\pi_{ss} \equiv \frac{1}{4 \times 4!} \bigoplus_{i=1}^{24} [1, 1, 1, 1]^T, \quad (7.20)$$

which is the tensor product of the Boltzmann distribution for hard disks times a uniform distribution of the active degree of freedom among the 4 particles. To show ergodicity, we inspect the spectrum of P . Its eigenvalues λ are shown in the complex plane in Fig. 7.6. The only eigenvalue lying on the unit circle is $\lambda = 1$, thus proving the ergodicity of the cSwap Markov chain. We observe that the other eigenvalues tend to accumulate at the vertices of an octagon inside the unit circle. This is a consequence of the introduction of a refreshment probability for the label of the active particle. Without such a refreshment dynamics, the Markov chain would be periodic, and there would be $2N$ eigenvalues lying on the unit circle. The introduction of a refreshment rate pushes the eigenvalues inside the unit circle, making the Markov Chain aperiodic.

7.4 Relaxation times

We run simulations in the NVT ensemble [96] comparing MMC, ECMC, Swap, SwapECMC, cSwap and cSwapECMC for increasing packing fractions. After careful equilibration, we measure a representative time correlation function for $2d$ glass-formers, namely the time autocorrelation of the global hexatic order $C_\psi(t)$ [89]. It is defined as

$$C_\psi \equiv \frac{\langle \psi^*(t)\psi(0) \rangle}{\langle |\psi(0)|^2 \rangle}, \quad (7.21)$$

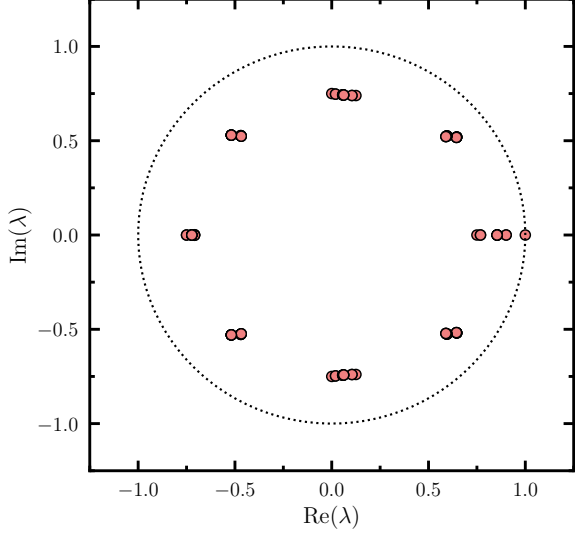


Figure 7.6: Representation in the complex plane of the eigenvalues λ of the transition matrix P given by Eq. (7.17) for the cSwap dynamics in the case of a system of $N = 4$ particles. The dotted line is the unit circle.

where $\psi(t)$ is the global hexatic order parameter. It is a sum of local terms $\psi(t) \equiv \frac{1}{N} \sum_{i=1}^N \phi_{6,i}(t)$ where the local hexatic order parameter for particle i , $\phi_{6,i}(t)$ is

$$\phi_{6,i}(t) \equiv \frac{1}{n_i} \sum_{j=1}^{n_i} e^{6i\theta_{ij}}, \quad (7.22)$$

with the sum running over the n_i neighbors of particle i , defined through a Voronoi tessellation, constructed using the freud library [226], and θ_{ij} is the angle between the vector $\mathbf{r}_{ij} \equiv \mathbf{r}_i - \mathbf{r}_j$ and the vector \mathbf{e}_x .

From the time decay of C_ψ we define the relaxation time τ_α , such that $C_\psi(\tau_\alpha) = e^{-1}$. For each algorithm, we collect the evolution of the correlation time $\tau_\alpha(\phi)$ measured in units of Nt_{move} in Fig. 7.7(a). The most costly part of Monte Carlo moves is the overlap detection involving a sum over neighbors. Since one such sum is needed over the time t_{move} in each algorithm, the comparison in Fig. 7.7(b) accurately describes CPU times. Each algorithm displays hallmarks of glassy dynamics, and we follow for about 5 decades the slowing down. The algorithms are split into two families, depending on the presence of swap moves. In appendix I, we show that these results are robusts upon changing the form of the continuously polydisperse distribution, and upon changing the size of the system.

We now address the speedup provided by nonequilibrium moves in the two families of algorithm.

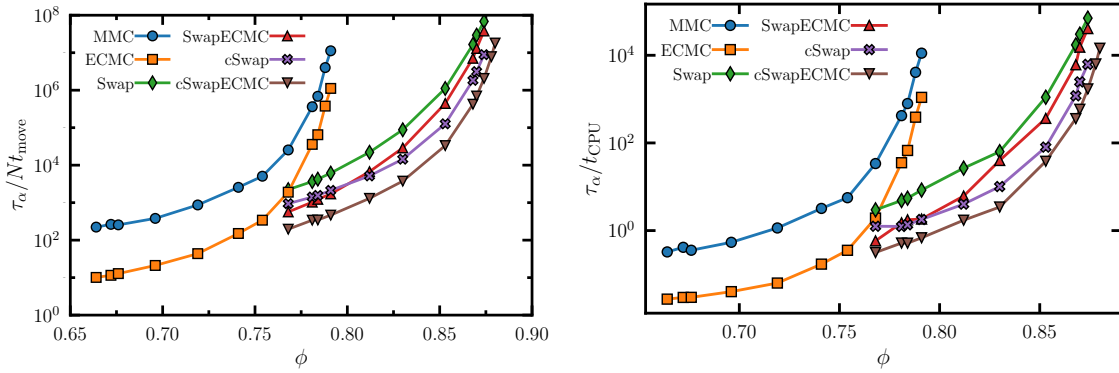


Figure 7.7: (a) Equilibrium relaxation time of six different Monte Carlo algorithms as a function of packing fraction. MMC and the faster ECMC fall out of equilibrium much before the four swap algorithms. The large speedup offered by Swap can be further improved using irreversible MC moves, cSwapECMC providing a further speedup of about 40 near $\phi = 0.88$. (b) Equilibrium relaxation times of the six algorithms investigated in the main text, in units of CPU time. Here $t_{\text{CPU}} = 1$ second.

7.4.1 Echoes from transverse forces

MMC and ECMC only contain translations and equilibration becomes difficult above $\phi \approx 0.79$. Yet, ECMC clearly outperforms MMC throughout the entire density range, but the edge of ECMC over MMC is lost as ϕ increases. This is demonstrated in Fig. 7.8(a), which shows that the ratio of their relaxation times decreases from ≈ 22 in the fluid, down to ≈ 10 near $\phi = 0.79$. This suggests that the irreversibility introduced by the directed chain moves does not help the system to discover new, faster pathways across configuration space. This interpretation is confirmed by the snapshots in Figs. 7.8(b, c) showing particle displacements with respect to the system's center of mass from the same initial condition, using either MMC or ECMC. Despite the very different particle moves in both dynamics, the long time relaxation proceeds along a similar path. This trend in the efficiency and the robustness of the long time relaxation trajectory against the nonequilibrium drive are very much reminiscent of what we saw in the minimal model of transverse forces.

7.4.2 Faster than the fastest

By contrast, the four algorithms employing particle swaps sample the Boltzmann distribution much faster than MMC and ECMC and only become inefficient near $\phi \approx 0.88$, see Fig. 7.7. All algorithms thus display a dramatic speed up compared to MMC and ECMC. Using Swap as a reference, we again observe that the introduction of translational chains in SwapECMC provides a modest acceleration over conventional Swap of about 5 at $\phi = 0.77$, decreasing to about 2 at the largest density (see Fig. 7.9). There-

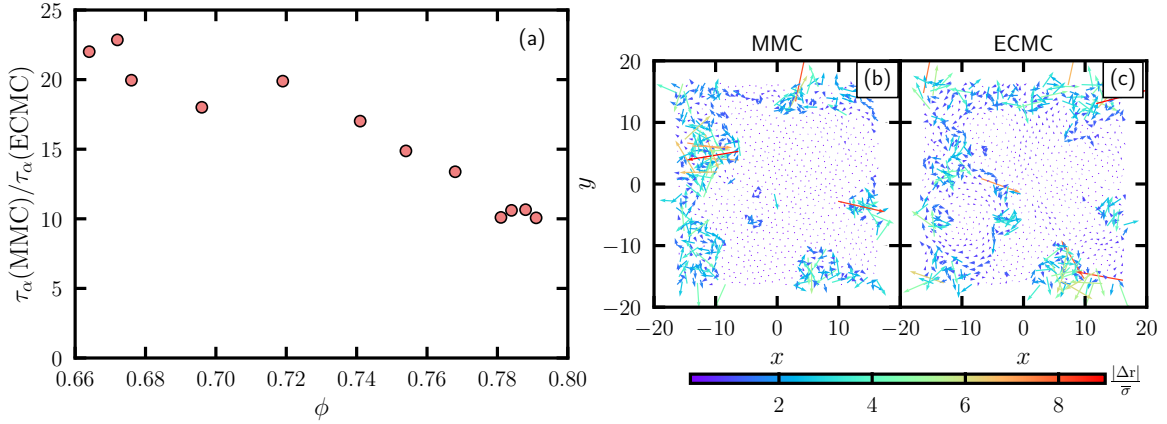


Figure 7.8: (a) The speedup offered by ECMC over MC decreases with density. (b, c) Comparison of the displacement field relative to the center of mass after a time comparable to the relaxation time starting from the same initial condition at $\phi = 0.79$ using MMC ($t = 4.6 \times 10^6 N t_{\text{move}}$) or ECMC ($t = 2.2 \times 10^5 N t_{\text{move}}$). Despite different dynamic rules, both algorithms follow similar dynamic pathways.

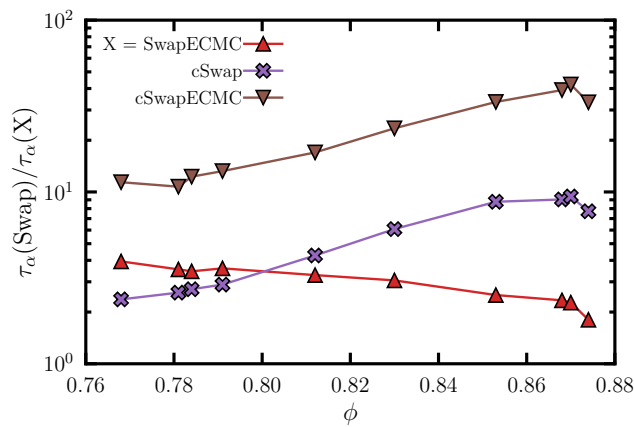


Figure 7.9: Acceleration provided by three novel algorithms (SwapECMC, cSwap, cSwapECMC) with respect to conventional swap Monte Carlo. In cSwapECMC, the combination of collective swaps and chain moves provides the fastest algorithm with a speed up increasing with ϕ and reaching 40.

fore, coupling Swap to ECMC is not very helpful. The situation is more favorable when collective swap moves are introduced, as the speedup offered by the irreversibility in cSwap now grows with density, as demonstrated in Fig. 7.9, to reach a factor about 10 near $\phi = 0.88$ over Swap. These results suggest that it is useful to combine cSwap and ECMC into cSwapECMC, where both translational and diameter moves are now collective and irreversible. Getting the best of both types of moves, cSwapECMC now offers a comfortable speed up over Swap that increases from 10 to about 40 at the largest packing fraction studied, clearly outperforming the swap Monte Carlo algorithm.

7.5 Dense jammed packings

An interesting avenue for our algorithms is the production of jammed disk packings, which are typically produced using specific nonequilibrium compression protocols [178, 206]. Using conventional MMC for compressions, the jamming packing fraction ϕ_J can be reached using *NPT* Monte Carlo [96]. The simplest protocol starts from an equilibrium hard disk configuration at ϕ_{init} , before suddenly turning the pressure to infinity [40]. At long times, the packing fraction saturates to a value ϕ_J , which is an increasing function of ϕ_{init} [62]. This is confirmed in Fig. 7.10, where the range $\phi_J \sim 0.855 - 0.895$ is covered. Very similar results are obtained using ECMC during compressions, see Fig. 7.10. Note that the preparation of equilibrium configurations for $\phi_{\text{init}} > 0.79$ requires particles swaps [211], which are no longer used during compressions. Interestingly, introducing swaps during compressions from the same range of initial conditions leads to jamming densities that are considerably larger, $\phi_J \approx 0.904 - 0.906$ (Fig. 7.10). At the time of writing, such large packing fractions have only been obtained using gradient descent algorithms simultaneously optimizing diameters and positions to more efficiently pack the particles, followed by geometric triangulation methods [44]. That similar performances can be reached using cSwap suggests that these nonequilibrium algorithms in fact explore pathways similar to the ones allowed by swap moves. In addition, the very weak dependence of ϕ_J on ϕ_{init} rationalizes the surprising efficiency of augmented gradient-descent algorithms. A major advantage of cSwap is that the particle size distribution is strictly conserved, rather than annealed, during the compression.

7.6 Outlook

Using swap and event-chain Monte Carlo as stepping stones, we demonstrate that simple Monte Carlo algorithms with increasing efficiency can be devised, that provide a set of improved computational tools to more efficiently equilibrate deep glassy states. We address here some directions of further research.

On the analytical side, it would desirable to understand how cSwap operates, mim-

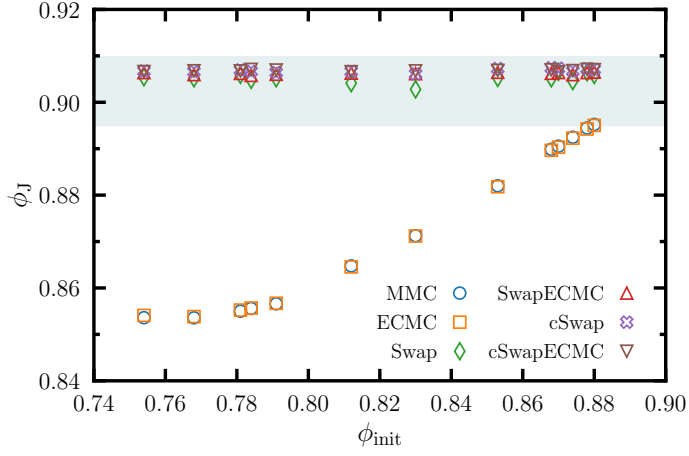


Figure 7.10: Jamming packing fractions ϕ_J obtained after nonequilibrium compressions using different Monte Carlo algorithms, starting from fluid configurations equilibrated at ϕ_{init} . The four swap algorithms reach very large ϕ_J , nearly independently of ϕ_{init} . The light blue band covers the range of densities obtained using augmented gradient-descent techniques [44].

icking, in spirit, the analysis done for transverse forces in this thesis. For instance, we would like to work out a theory of the cSwap dynamics in the high dimensional limit introduced in Chapter 5. When proceeding in this direction, however, there are several issue that demand to be addressed. The first one is to develop a dynamical mean field theory for bidisperse, and polydisperse liquids, even in the absence of Swap dynamics. As a matter of fact, while the analysis of the static for these system was done in [137, 1], the analysis of its dynamics is lacking. This analysis is developed in App. G. The second, perhaps more critical, issue is that is not clear whether the swap dynamics survives in limit of large space dimensions, even though approximate theories suggest so on thermodynamics grounds [138]. This issue is addressed in Appendix H.

For what concerns finite-dimensional, practical implementations, we have just scratched the surface: in order to become new standards, the cSwap algorithm and its derivatives proposed here need to be pushed in several directions. A first encouraging result is the successful scaling of their performances with system size, shown in App. I, in line with results for ECMC and Swap. A less obvious direction is the application to three dimensions, which is the subject of on-going efforts, again with encouraging preliminary results. A third direction concerns the application to glass-former with soft potentials. Swap performances do not decrease with continuous potentials [203], and some extensions of ECMC to continuous potentials were successful [193, 204]. Future work should develop extensions of cSwap for glass-formers with continuous potentials to extend the range of applicability of irreversible Monte Carlo methods in the field of supercooled liquids. All these perspectives directly follow from our work; they should help the development of efficient, versatile and simple to implement sampling methods for disordered systems with a complex free energy landscape.

Contributions of Chapter 7

- We assess the efficiency of the celebrated Event-Chain Monte Carlo (ECMC) algorithm in a polydisperse mixture of hard disks at high density.
- As the density increases we find that ECMC maintains an edge over the equilibrium Metropolis Monte Carlo algorithm, but the efficiency decreases as the dynamics of the system becomes more glassy.
- We design a novel algorithm, collective Swap (cSwap), that performs out of equilibrium, collective, diameter swaps, thus bringing the event-chain ideas in the space of particle diameters.
- We demonstrate that cSwap admits the Boltzmann distribution for hard disks in the steady state, and we provide numerical and analytical evidences that support its ergodicity.
- We compare the performance of cSwap against the state-of-the art, equilibrium, swap algorithm. Remarkably, in the dense regime explored, the efficiency of cSwap over Swap increases as the dynamics of the system slows down, in opposition to what happens for the ECMC algorithm.
- We combine cSwap and ECMC in a novel algorithm, cSwapECMC, which achieves, at the highest density explored, a speedup of ≈ 40 over the the state-of-the art swap algorithm.
- We apply our newly designed algorithm to produce, through fast nonequilibrium compressions, jammed packings at very high densities.

CONCLUSIONS

We conclude this manuscript with an overview of the contributions presented in this thesis, and some further research directions that this work naturally leads to.

In Chapter 1 we introduced the paradigm of equilibrium sampling and the concept of relaxation time by means of an overdamped Langevin dynamics. We described two families of out of equilibrium dynamics that nevertheless sample the Boltzmann distribution. A first one achieves this goal by means of a spatially tuned solenoidal field, while in a second framework, known as lifting, an extended set of degrees of freedom, complemented with nonequilibrium evolution rules, is employed. We identified transverse forces as a candidate to quantitatively assess the performance of irreversible samplers, owing to the their minimal structure, and the fact that the contribution from transverse forces can be clearly written as the perturbation of an otherwise equilibrium process.

In Chapter 2 we built an understanding of transverse forces by studying how they operate for a particle in an external potential. We explored the performance in the convex harmonic well and in the non convex double well potential. In the latter, we found that the time necessary to cross the energy barrier is reduced in the form of prefactor in front of the Arrhenius term, and that the trajectories followed during the barrier crossing process are altered by transverse forces. More generally, we computed a microscopic timescale, the escape rate, which is rescaled by transverse forces, and investigated how the fluctuation-dissipation theorem is modified, and in which situation is preserved.

In Chapter 3 we put transverse forces at work in the p -spin spherical model, a mean field spin glass model. We obtained equations of motion for the correlation and response matrix, and we quantified the acceleration provided by transverse forces. Our approach can be generalized to study nonreciprocal interactions in mean field spin glasses, as well as in fully connected models of neural network. In the latter situation, it is an intriguing question to ask how the behavior of the speedup is affected when switching from a dynamics with thermal noise to one with a stochastic gradient descent supplemented with transverse forces.

In Chapter 4 we studied, by numerical integration of the stochastic dynamics, transverse forces in a dense liquid. Interestingly, the speedup granted by transverse forces is a nonmonotonous function of the temperature, and it decreases as the glassy phase is approached. Concomitantly to this decrease, we observed that the dynamical pathways followed by the particles fold into closed orbits localized within their local cage, a feature quantified by measuring the odd diffusion constant. We also saw that the speedup increases linearly with the strength of transverse forces for large enough values of the nonequilibrium drive. When translating our findings to practical CPU time, we expect

a trade-off between the physical acceleration provided by transverse forces, and the decrease in precision caused by a large drift. A numerical quantification of this trade-off would be helpful in identifying, for a given numerical scheme, the computationally optimal drift strength.

In Chapter 5 and 6, we developed dynamical mean field and mode-coupling theories tailored for transverse forces, rationalizing the results obtained through numerical analysis, and accessing several transport coefficients (mobility, diffusivity, viscosity) together with their odd counterparts. To our knowledge, this is the first time these theories are employed to compute of odd transport coefficients, and the derivation could be extended to active systems, from nonreciprocal interacting assembly of particles to active chiral matter, perhaps employing integration through transient methods [101, 75].

In Chapter 7, we developed a novel algorithm for continuously polydisperse systems of hard disks, the collective Swap. It performs out of equilibrium, collective moves in the space of particle diameters, boosting up the state-of-the-art, Swap algorithm. cSwap is a good candidate to become the novel way-to-go algorithm for Monte Carlo sampling of continuously polydisperse glasses. The natural venues to explore consist in extending it to three dimensions and continuous interactions potentials. On the theoretical side a proof of its ergodicity, as recently done for Event Chain Monte Carlo [198], is desirable.

An interesting question is the determination of the optimal irreversible drift for a given many-body system. This task could be tackled both through analytical and machine learning approaches [151]. Both routes would proceed through the minimization of some cost function, encoding the relaxation time of the dynamics, in the space of possible drifts. The concomitant challenge is then to identify a treatable and meaningful cost function to optimize. It is likely that further insights into the nature of the optimal drift could, and should be gathered from the physics of the system under consideration. Conjectured dynamics designed within this physics-inspired framework might be lifting schemes capable of biasing the motion of dynamical heterogeneities [28], or that mimic externally applied shears. Whether these types of dynamics can be constructed, both in theory and in practice, is an open question.

APPENDIX A

FACILITATED DYNAMICS

This Appendix, which benefits of contributions by Thibaut Arnould de Pirey, addresses an alternative way to speedup the convergence to the target, Boltzmann distribution. It consists in an equilibrium overdamped Langevin dynamics with a space dependent mobility [230, 113, 46, 171]. The possible functional forms that the mobility can take while preserving the Boltzmann distribution are infinite, but we identify a peculiar choice, here referred to as facilitated dynamics, that allows, in principle, to overcome energy barriers. In a parallel development [171], this dynamics has also been recently identified for one-particle systems using a variational principle.

We propose a generalisation the facilitated dynamics to many-body systems, like dense liquids. We show analytically that, in finite-dimensional liquids, this choice surprisingly yields a diffusive behavior at all temperatures and densities. In the region where numerical integration of the facilitated dynamics is feasible, we demonstrate, by means of computer simulations, the presence of an acceleration. We then develop a mode-coupling theory of the facilitated dynamics: using the standard mode-coupling expansion, we show that, perhaps pathologically, no shift in the ergodicity breaking temperature is observed. This suggests that the richness of the facilitated dynamics is encoded in higher order density correlations.

A1 Spatially tuned mobility

To illustrate the philosophy behind the facilitated dynamics let us consider the overdamped Brownian Dynamics of a particle in one dimension, whose position is denoted by x , under the action of an external potential $V(x)$:

$$\dot{x}(t) = -\mu_0 V'(x) + \sqrt{2\mu_0 T} \xi(t) \quad (\text{A.1})$$

where μ_0 is the mobility, T is the temperature and $\xi(t)$ is a white noise with zero average and correlation $\langle \xi(t)\xi(t') \rangle = \delta(t-t')$. As explained in Chapter 1, this is an

equilibrium dynamics with the Boltzmann distribution $\rho_B = \frac{e^{-\beta V(x)}}{\int dy e^{-\beta V(y)}}$ as its stationary distribution. How can we accelerate the relaxation of the system to equilibrium by tuning the mobility of the particle? If the mobility is constant, then we cannot do much, because any value of μ_0 can be absorbed by a time rescaling $t' \equiv \mu_0 t$. The speed up produced by increasing the mobility is equivalent to a change of the units of time.

To obtain an actual speed up one needs to choose a space dependent mobility, which cannot be reabsorbed into a rescaling of time. At the same time we want the new dynamics to sample the Boltzmann distribution $\propto e^{-\beta V(x)}$ in its steady state. We therefore propose the following dynamics:

$$\dot{x}(t) = -\mu(x)V'(x) + T\mu'(x) + \sqrt{2\mu(x)T}\xi(t) \quad (\text{A.2})$$

where Itō discretization is used. Eq. (A.2) describes the motion of a particle with a space dependent mobility under multiplicative noise. We show the Eq. (A.2) is indeed an equilibrium dynamics sampling the Boltzmann distribution in its equilibrium, steady state.

The Fokker-Planck equation associated to Eq. (A.2) is

$$\begin{aligned} \partial_t \rho(x, t) &= \partial_x [\mu(x)V'(x) - T\mu'(x) + T\partial_x \mu(x)] \rho(x, t) \\ &= \partial_x [\mu(x)V'(x) + T\mu(x)\partial_x] \rho(x, t), \end{aligned} \quad (\text{A.3})$$

and one can verify by direct substitution that $\rho_B(x)$ is the steady state of Eq. (A.3).

Next, we verify that Eq. (A.2) is an equilibrium dynamics, in a similar way as was done in Chapter 1 for overdamped Langevin dynamics with constant mobility. The Onsager-Machlup action associated to Eq. (A.2) is [71, 73]

$$\begin{aligned} S(\{x(t)\}) &= \int_0^t d\tau \frac{1}{4T\mu(x(\tau))} [\dot{x}(\tau) + \mu(x(\tau))V'(x(\tau))]^2 \\ &\quad + \int_0^t d\tau \frac{1}{2} [-\mu(x(\tau))V'(x(\tau)) + T\mu'(x(\tau))]' \end{aligned} \quad (\text{A.4})$$

and one can verify, by looking at the ratio between a trajectory $x(\tau)$ and its corresponding time reversal one, $x(t - \tau)$, that detailed balance is obeyed.

A2 Facilitated dynamics

We now need to choose an explicit expression for the mobility $\mu(x)$ to produce a speed up in the equilibration. For the target systems we have in mind the low temperature dynamics is hindered by large energy barriers, that the particle can overcome only through thermally activated jumps. We mentioned in Chapter 1 that the time τ required to jump through a barrier of height ΔV scales in an Arrhenius way as $\tau \propto e^{\beta \Delta V}$. We therefore choose a form of the mobility that can compensate the Arrhenius contribution to the scaling:

$$\mu(x) \equiv \mu_0 e^{\beta V(x)}. \quad (\text{A.5})$$

with μ_0 setting the time scale of the system. Substitution of Eq. (A.5) in Eq. (A.2) yields

$$\dot{x} = \sqrt{2T\mu_0} e^{\frac{\beta}{2}V(x)}\xi(t). \quad (\text{A.6})$$

This is what we call facilitated dynamics. It is a diffusion dynamics with a non-uniform diffusion coefficient: a particle diffuses faster in region of high energy and more slowly in regions of low potential energy.

The time τ needed for barrier crossing with the facilitated dynamics is

$$\tau \propto e^{-\beta V(x_m)} \quad (\text{A.7})$$

with $V(x_m)$ the value of the potential at x_m , where the bottom of the energy well is located. Note that the dependence on the barrier height has disappeared, which suggests that a physical phenomenon usually slowed down by a rugged energy landscape could, with the facilitated dynamics, avoid being sluggish.

We show how to obtain Eq. (A.7), explicitly computing the barrier crossing time τ for a particle in one dimension evolving in a potential landscape $V(x)$ as in Figure 1.1(a). The barrier crossing problem [229] can be tackled by computing the first passage time $\tau(x)$ across x_M , the point of local maximum of the potential $V(x)$, for a particle starting at x . For the facilitated dynamics, $\tau(x)$ satisfies the adjoint equation

$$\mu_0 T e^{\beta V(x)} \partial_x^2 \tau(x) = -1 \quad (\text{A.8})$$

complemented with the boundary conditions $\tau(x_M) = 0$, $\partial_x \tau(x_m) = 0$. The solution to Eq. (A.8) is

$$\tau(x) = \frac{1}{\mu_0 T} \int_x^{x_M} dx' \int_{x_m}^{x'} dy e^{-\beta V(y)}. \quad (\text{A.9})$$

In the low temperature limit, a saddle point approximation yields

$$\tau \equiv \tau(x_m) \approx \frac{1}{\mu_0} \sqrt{\frac{2\pi}{V''(x_m)T}} (x_M - x_m) e^{-\beta V(x_m)}. \quad (\text{A.10})$$

The barrier crossing time depends neither on the barrier height, nor on the potential curvature at the top of the barrier, as is the case for the Kramers' time for usual overdamped Langevin dynamics, displayed in Eq. (1.23).

We demonstrate numerically that the facilitated dynamics samples the Boltzmann distribution in Fig. A.1(a), where we compare the expected Boltzmann distribution ρ_B with the numerical integration of Eq. (A.6), using Euler-Maruyama scheme for the periodic potential

$$V(x) \equiv \frac{1}{2} (1 + \cos 2\pi x) \quad (\text{A.11})$$

in the interval $[0, 1]$ with periodic boundary conditions. The agreement between the predicted distribution and the results from numerical integration confirms that the facilitated dynamics follows the Boltzmann distribution in its equilibrium state. We

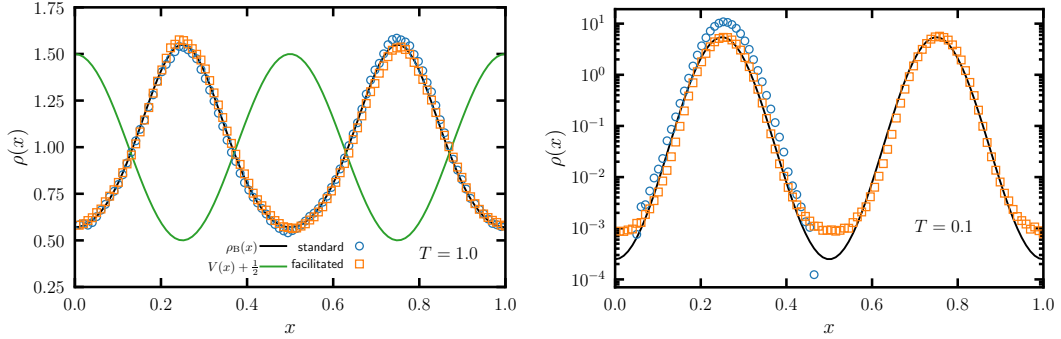


Figure A.1: (a) Comparisons between the histogram of position sampled through numerical integration of the facilitated dynamics for $V(x)$ given by Eq (A.11) against the Boltzmann distribution at $T = 1.0$. (b) Histograms of the position sampled by the facilitated dynamics and the usual overdamped Langevin dynamics for the same potential, at a lower temperature $T = 0.1$. Both dynamics are integrated with the same time step $\Delta t = 1 \times 10^{-5}$ for 2×10^7 steps.

then show in Figure A.1(b) that the facilitated dynamics overcomes energy barriers that otherwise keep the usual overdamped Langevin dynamics confined in the observation time window.

A2.1 Pathological cases

In this section we address the analytical computation of the relaxation time for the facilitated dynamics, following the procedure described in Section 1.2, in the case of two convex potentials, for which a pathological behavior is observed. The first case consists of a triangular potential, where we show that the facilitated dynamics is not confined and the relaxation time is infinite. In the second case, we focus on a convex potential on a finite interval. In this case, the relaxation time of the facilitated dynamics is smaller than its equilibrium counterpart. These behaviors hint at the singular nature of the facilitated dynamics. On the other hand, in the numerical and analytical analysis of model glass formers, periodic boundary conditions are usually applied, leaving room for possible applications that we pursue in the following Sections.

Triangular well

We consider a triangular well potential

$$V(x) = |x|. \quad (\text{A.12})$$

We first review what happens for the usual overdamped Langevin dynamics given by Eq. (A.1). The eigenvalue problem, corresponding to the projection along the real

space of Eq. (1.20), reads

$$\left(-T\partial_x^2 - \delta(x) + \frac{1}{4T}\right)\psi(x) = \frac{\lambda}{\mu_0}\psi(x) \quad (\text{A.13})$$

Which corresponds to the problem of determining the energy spectrum of a quantum particle in an attractive Dirac delta $\delta(x)$ potential. The problem admits a unique bound state as a ground state and has a continuum of delocalized solutions, separated from the ground-state by a gap $\lambda_1 = \frac{1}{4T\mu_0}$. The relaxation time is thus

$$\tau_R = 4T\mu_0 \quad (\text{A.14})$$

For the facilitated dynamics, the eigenvalue problem reads instead

$$\mu_0 T \partial_x^2 R(x) + \lambda e^{-\beta|x|} R(x) = 0 \quad (\text{A.15})$$

with $R(x) \equiv \psi(x)e^{\frac{\beta|x|}{2}}$ the right eigenfunction of the Fokker-Planck operator associated to the facilitated dynamics. The solution to Eq. (A.15) is a linear combination of the Bessel functions of the first and second kind, J_0 and Y_0 [2]

$$\phi(x) = \begin{cases} a_+ J_0(T\sqrt{\lambda\mu_0^{-1}} e^{\frac{\beta x}{2}}) + b_+ Y_0(T\sqrt{\lambda\mu_0^{-1}} e^{\frac{\beta x}{2}}) & \text{if } x > 0 \\ a_- J_0(T\sqrt{\lambda\mu_0^{-1}} e^{-\frac{\beta x}{2}}) + b_- Y_0(T\sqrt{\lambda\mu_0^{-1}} e^{-\frac{\beta x}{2}}) & \text{if } x < 0 \end{cases} \quad (\text{A.16})$$

With the constants a_{\pm}, b_{\pm} determined by the continuity of $\phi(x)$, $\phi'(x)$ in 0 and by the normalization of $\psi(x) \equiv \phi(x)e^{-\frac{\beta|x|}{2}}$. Since such a solution exists for any value $\lambda > 0$, the energy gap between the ground state and the first excited state is 0. This means that

$$\tau_R = +\infty \quad (\text{A.17})$$

And there is no convergence to Boltzmann equilibrium at any finite time. Physically, this means that the facilitated dynamics cannot be confined by the triangular potential, and it escapes toward infinity.

Logarithmic potential

We consider a logarithmic potential [229]

$$V(x) \equiv -2T \log \cos \frac{\pi x}{2a} \quad (\text{A.18})$$

with $-a \leq x \leq a$. For the usual overdamped Langevin dynamics, this problem can be mapped to a quantum problem inside an infinite potential well of width $2a$ [229], and the relaxation time is

$$\tau_R = \frac{4a^2}{3\pi^2 \mu_0 T}. \quad (\text{A.19})$$

For the facilitated dynamics, we want to solve the eigenvalue equation for the right eigenvector $R(x)$,

$$\mu_0 T \partial_x^2 e^{\beta V(x)} R(x) = -\lambda R(x) \quad (\text{A.20})$$

We complement this equation with a reflecting boundary condition

$$J(\pm a, t) = \partial_x r(x)|_{\pm a} = 0 \quad (\text{A.21})$$

which ensures that the particle remains confined between $-a$ and a during the diffusion process.

The problem is easier to solve if we look at the left eigenfunction $L(x)$, defined as

$$L(x) \equiv e^{\beta V(x)} R(x). \quad (\text{A.22})$$

The eigenvalue equation and the boundary conditions read:

$$\begin{cases} \partial_x^2 L(x) + \frac{\lambda}{\mu_0 T} \cos^2 \frac{\pi x}{2a} L(x) &= 0 \\ \partial_x L(x)|_{\pm a} &= 0. \end{cases} \quad (\text{A.23})$$

Introducing a new variable $u = \frac{\pi x}{2a}$ and using the trigonometric identity $\cos^2 u = \frac{1}{2}(1 - \cos 2u)$ we obtain

$$\begin{cases} \partial_u^2 L(u) + (b - 2q \cos 2u)L(u) &= 0 \\ \partial_u L(u)|_{\pm \frac{\pi}{2}} &= 0 \end{cases} \quad (\text{A.24})$$

with $q \equiv \frac{a^2 \lambda}{\pi^2 \mu_0 T}$, $b = 2q$. This is a Mathieu equation [2], its solution are the even and odd Mathieu functions $C(b, q, u), S(b, q, u)$. The spectral gap is determined by imposing the boundary condition in Eq. (A.23) which reads

$$C'(2q, q, \pm \frac{\pi}{2}) = 0 \quad (\text{A.25})$$

for even solutions, and

$$S'(2q, q, \pm \frac{\pi}{2}) = 0 \quad (\text{A.26})$$

for odd solutions. Here the prime denotes a derivative with respect to u . A graph of these curves as a function of q is shown in Fig. A.2. We can see that the curves intersect the x axis for the second time at $q \approx \frac{1}{3}$, implying that the first excited energy level is

$$\lambda \approx \frac{\pi^2 \mu_0 T}{3a^2}, \quad (\text{A.27})$$

and thus implies that the relaxation time is

$$\tau_R \approx \frac{3a^2}{\pi^2 \mu_0 T} \quad (\text{A.28})$$

which is greater than the relaxation time for standard overdamped Langevin dynamics given by Eq. (A.19). In such a convex potential, the facilitated dynamics perform worse than its standard counterpart.

While the two preceding examples serve as caveats concerning the peculiar nature of the facilitated dynamics, the ability of the dynamics to cross the barrier, corroborated by numerical simulations, motivates us to look for an extension of the facilitated dynamics to dense liquids.

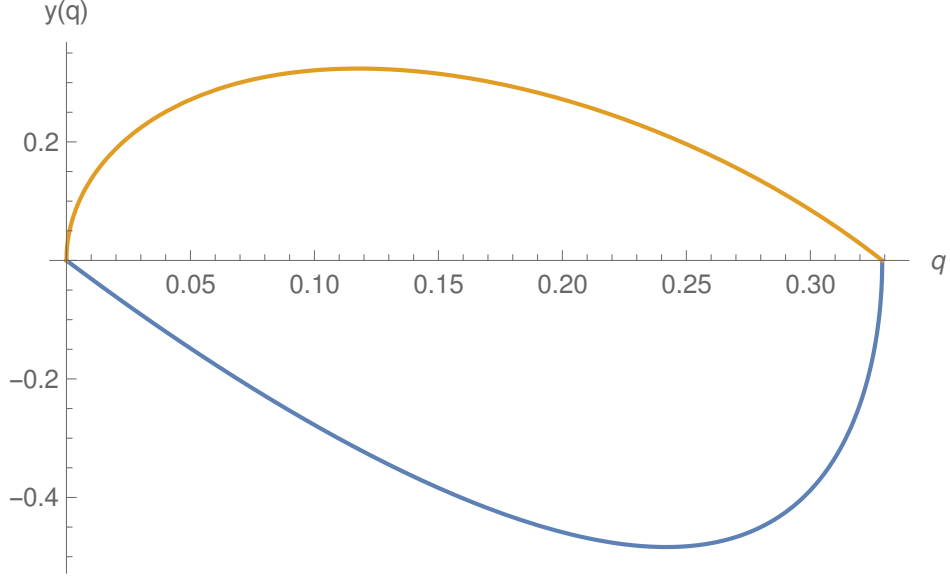


Figure A.2: Derivative of the Mathieu function $C'(2q, q, \pm\frac{\pi}{2})$ (blue), $S'(2q, q, \pm\frac{\pi}{2})$ (orange) as a function of q . The point where the curves pass through zero determines q , and therefore λ .

A3 Facilitated dynamics in dense liquids

We propose an extension of the facilitated dynamics to a d dimensional liquid of N particles interacting through a central potential $\sum_{i < j} V(\mathbf{r}_i - \mathbf{r}_j)$, \mathbf{r}_i being the position of particle i . In our proposal, the mobility now is not only space dependent, but also particle dependent, to be in tune with the particle environment. Eq. (A.2), generalizes to

$$\dot{\mathbf{r}}_i = -\mu_i(\mathbf{r}_i) \sum_{j \neq i} \nabla V(\mathbf{r}_i - \mathbf{r}_j) + T \nabla \mu_i(\mathbf{r}_i) + \sqrt{2T\mu_i(\mathbf{r}_i)} \boldsymbol{\xi}_i(t) \quad (\text{A.29})$$

With $\boldsymbol{\xi}_i(t)$ a white Gaussian noise with zero mean and correlations $\langle \boldsymbol{\xi}_i(t) \otimes \boldsymbol{\xi}_j(t') \rangle = \mathbf{1}_{ij}\delta(t - t')$. Eq. (A.29) is the dynamics for a dense liquid with a space dependent mobility. Following the route provided by the one-dimensional case it can be shown that Eq. (A.29) is time reversible and samples the Boltzmann distribution $\rho_B \propto e^{-\beta \sum_{i < j} V(\mathbf{r}_i - \mathbf{r}_j)}$ in the steady state.

In our choice for a generalization of the facilitated dynamics one considers the potential energy locally felt by each particle through the interaction with the others. The many-body version of the facilitated dynamics is obtained by choosing for the local particle mobility $\mu_i(\mathbf{r}_i)$ the form

$$\mu_i(\mathbf{r}_i) \equiv \mu_0 e^{\beta \sum_{j \neq i} V(\mathbf{r}_i - \mathbf{r}_j)}. \quad (\text{A.30})$$

Note that $\mu_i(\mathbf{r}_i)$ actually depends also on the positions of the particles that interact with \mathbf{r}_i , and we are thus using a lightened notation. With this choice for the mobility,

we obtain the facilitated dynamics for dense liquids:

$$\dot{\mathbf{r}}_i = \sqrt{2\mu_0 T} e^{\beta \sum_{j \neq i} V(\mathbf{r}_i - \mathbf{r}_j)} \boldsymbol{\xi}_i(t) \quad (\text{A.31})$$

Now that we have explicit equations of motions for the facilitated dynamics in the many-body case, it would be interesting to compare its behavior to the one of overdamped Brownian Dynamics in models where a slow down is detected. Due to the exponential form of the mobility, a dynamical mean field theory in the limit $d \rightarrow +\infty$ seems unfeasible. Thus, two natural routes remain: direct numerical integration of Eq. (A.31) and the development of a mode coupling theory, as was done in this thesis for transverse forces. Before doing that, however, we turn to an intriguing result: the diffusion constant in the interacting particle system given by Eq. (A.31) can be determined exactly.

A3.1 Diffusion constant

We consider a system of N interacting particles in d dimensions at fixed volume V and temperature T . The particles motion is described by the facilitated dynamics, Eq. (A.31). We focus on a fixed particle i and we consider its mean squared displacement $\langle [\mathbf{r}_i(t) - \mathbf{r}_i(0)]^2 \rangle$ (we will see that the result does not depend on the choice of the particle):

$$\begin{aligned} \langle [\mathbf{r}_i(t) - \mathbf{r}_i(0)]^2 \rangle &= \int_0^t dt' \int_0^t dt'' \langle \dot{\mathbf{r}}_i(t') \cdot \dot{\mathbf{r}}_i(t'') \rangle \\ &= \left\langle 2\mu_0 T \int_0^t dt' \int_0^t dt'' e^{\frac{\beta}{2} \sum_{j \neq i} V(\mathbf{r}_i(t') - p\mathbf{r}_j(t'))} e^{\frac{\beta}{2} \sum_{j \neq i} V(\mathbf{r}_i(t'') - \mathbf{r}_j(t''))} \right. \\ &\quad \times \boldsymbol{\xi}_i(t') \cdot \boldsymbol{\xi}_i(t'') \Big\rangle \\ &= \left\langle 2\mu_0 T d \int_0^t dt' e^{\beta \sum_{j \neq i} V(\mathbf{r}_i(t') - \mathbf{r}_j(t'))} \right\rangle \end{aligned} \quad (\text{A.32})$$

where $\langle \dots \rangle$ denote an average of the dynamics over the realizations of the noise $\boldsymbol{\xi}_j(t)$ for $j = 1, \dots, N$, and we have made use of the fact that the noise is Gaussian. Note that no force-force correlations implying memory effects appear, in opposition to the usual overdamped Langevin dynamics.

Assuming that the system is ergodic we can replace the time integral of the average over the noise with the equilibrium average in the canonical ensemble

$$\left\langle [\mathbf{r}_i(t) - \mathbf{r}_i(0)]^2 \right\rangle \xrightarrow{t \rightarrow +\infty} \frac{2\mu_0 T d t}{Z(T, V, N) N!} \int d\mathbf{r}_1 \dots d\mathbf{r}_N e^{\beta \sum_{j \neq i} V(\mathbf{r}_i - \mathbf{r}_j)} e^{-\beta \sum_{k < l} V(\mathbf{r}_k - \mathbf{r}_l)} \quad (\text{A.33})$$

where $Z(T, V, N) \equiv \frac{1}{N!} \int d\mathbf{r}_1 \dots d\mathbf{r}_N e^{-\beta \sum_{k < l} V(\mathbf{r}_k - \mathbf{r}_l)}$ is the partition function. We now observe that the factor in the Boltzmann weight involving particle i simplifies with the mobility, so that the integral over $d\mathbf{r}_i$ is unconstrained through all the volume V . This means that:

$$\begin{aligned} \left\langle [\mathbf{r}_i(t) - \mathbf{r}_i(0)]^2 \right\rangle &= \frac{2\mu_0 T dt}{Z(T, V, N) N!} \int d\mathbf{r}_1 \dots d\mathbf{r}_N e^{\beta \sum_{j \neq i} V(\mathbf{r}_i - \mathbf{r}_j)} e^{-\beta \sum_{k < l} V(\mathbf{r}_k - \mathbf{r}_l)} \\ &= \frac{2\mu_0 T dt}{Z(T, V, N) N!} \int d\mathbf{r}_1 \dots d\mathbf{r}_N e^{-\beta \sum_{k < l, k \neq i} V(\mathbf{r}_k - \mathbf{r}_l)} \\ &= \frac{2\mu_0 T dt}{Z(T, V, N) N!} V \int \prod_{j=1, j \neq i}^N d\mathbf{r}_j e^{-\beta \sum_{k < l, k \neq i} V(\mathbf{r}_k - \mathbf{r}_l)} \\ &= 2\mu_0 T dt V \frac{Z(T, V, N-1)(N-1)!}{Z(T, V, N) N!} \end{aligned} \quad (\text{A.34})$$

We now introduce the free energy, $F(T, V, N) \equiv -\frac{1}{\beta} \log Z(T, V, N)$, the density $\rho_0 \equiv \frac{N}{V}$ and the fugacity $z \equiv e^{\beta \mu_{\text{chem}}}$, with the chemical potential $\mu_{\text{chem}} \equiv \frac{\partial F}{\partial N}$ to simplify the previous expression

$$\left\langle [\mathbf{r}_i(t) - \mathbf{r}_i(0)]^2 \right\rangle = \mu_0 T dt \frac{V}{N} e^{-\beta(F(T, V, N-1) - F(T, V, N))} \sim 2\mu_0 T dt \frac{V}{N} e^{\beta \mu_{\text{chem}}} \quad (\text{A.35})$$

so that we can finally write

$$\left\langle [\mathbf{r}_i(t) - \mathbf{r}_i(0)]^2 \right\rangle = \frac{2\mu_0 T dz}{\rho_0} t \equiv 2dDt \quad (\text{A.36})$$

Eq. (A.36) is a remarkable result. Not only we obtained an explicit expression for the diffusion constant, whose analytical computation is often unfeasible for system undergoing standard overdamped Langevin dynamics, but we can also see from its expression that no sign of freezing of the long time diffusion appears at any temperature and dimensions. The dependence from these two parameters appears in fact in D only in a controllable way, through the fugacity and a term linear in T .

The result of this section is an encouraging signal for non trivial behavior of systems undergoing facilitated dynamics, for which we thus proceed with a numerical exploration of a liquid of interacting particles.

A3.2 Numerical exploration

We simulate a system of $N = 128$ particles interacting through the pairwise harmonic potential

$$V(r) = \frac{\epsilon}{2} \left(1 - \frac{r}{\sigma}\right)^2 \theta(r - \sigma) \quad (\text{A.37})$$

where r is the interparticle distance, σ is the particle diameter and ϵ is the strength of interaction of the potential. We measure temperature in units of ϵ/k_B , length in units

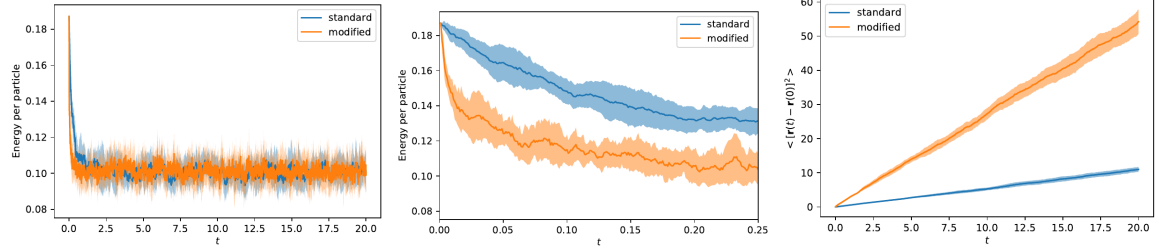


Figure A.3: Comparison between the usual overdamped Langevin dynamics and the facilitated (here denoted ‘modified’) dynamics for harmonic sphere at $T = 0.1$. Left: plots of energy as a function of time. At long times, the average value of the energy and its fluctuations are the same for standard and facilitated dynamics. Center: evolution of the energy at initial times, from which we see that the facilitated dynamics has a faster convergence. Right: mean squared displacement. The mean squared displacement achieved through the facilitated dynamics is an order of magnitude higher than its standard counterpart.

of σ and time in units of $\sigma^2/\mu_0\epsilon$. Periodic boundary conditions are applied, and the size L of the simulation box is determined by the packing fraction $\phi \equiv \pi\sigma^3/6L^3 = 1$. We simulate both standard overdamped Langevin dynamics and the facilitated dynamics, Eq. (A.31) using the Euler-Maruyama scheme. The time step is $\Delta t = 0.0001$.

We simulate the dynamics at the temperature $T = 0.1$, and we compute the potential energy per particle and the average mean squared displacement of the particle in the system as a function of time. We start both the dynamics from the same initial conditions and we simulate 25 independent runs for each temperature, over which we do an average. Results are shown in Fig. A.3. While at the high temperature the two dynamics show a similar convergence rate toward equilibrium, as the temperature is lowered the facilitated dynamics exhibits a faster relaxation, with a higher diffusion constant.

The gain in the relaxation times showed by the Facilitated dynamics translates in a gain in computational time only at high temperature: the exponential term in Eq. (A.31) grows as the temperature is lowered, posing a problem for the numerical convergence of the Facilitated Dynamics. This can be qualitatively seen through a back of the envelope computation: if we assume that the energy per particle has a Gaussian distribution with variance σ_V^2 , the mobility μ has a log-normal distribution, with a variance $e^{\beta^2\sigma_V^2}$, which diverges as $T \rightarrow 0$, assuming $\sigma_V^2 \sim T$.

The back-of-the envelope calculation above suggests that the facilitated dynamics is hardly applicable in practice to low temperature or high density scenarios. On the other hand, the calculation of the diffusion constant makes the facilitated dynamics an appealing theoretical tool to probe the influence of activated events in the theory of the glass transitions, and the interplay between the Boltzmann energy landscape and the dynamics of the system itself. For this reason, we push forward our analytical study

of the facilitated dynamics. In the next Section, we address the mode-coupling theory of the facilitated dynamics.

A4 Mode Coupling Theory

This section is devoted to the development of a mode-coupling theory of the facilitated dynamics. We first take a more general angle, and work with the dynamics with space dependent mobility given by Eq. (A.29).

A4.1 Arbitrary mobility

We perform a computation similar in spirit to the one done in Chapter 6 for the mode coupling theory of transverse forces. The evolution operator associated to Eq. (A.29) is

$$\begin{aligned}\Omega &= \sum_i \nabla_i \cdot (-\mu_i \mathbf{F}_i - T(\nabla_i \mu_i) + T \nabla_i \mu_i) \\ &= \sum_i \nabla_i \cdot (-\mu_i \mathbf{F}_i + T \mu_i \nabla_i)\end{aligned}\tag{A.38}$$

with $\mathbf{F}_i \equiv -\sum_{i < j} \nabla_i V(\mathbf{r}_i - \mathbf{r}_j)$. The operator Ω governs the equation of motion for the probability distribution of the particle positions, $\rho(\mathbf{r}^N)$,

$$\partial_t \rho(\mathbf{r}^N, t) = \Omega \rho(\mathbf{r}^N, t).\tag{A.39}$$

The equilibrium solution is $\rho_B(\mathbf{r}^N) \propto e^{-\beta \sum_{i < j} V(\mathbf{r}_i - \mathbf{r}_j)}$, as $\Omega \rho_B(\mathbf{r}^N) = 0$. We introduce the density mode

$$n(\mathbf{q}) \equiv \sum_i e^{-i\mathbf{q} \cdot \mathbf{r}_i}\tag{A.40}$$

and the dynamical structure factor

$$S(\mathbf{q}, t) \equiv \frac{1}{N} \langle n^*(\mathbf{q}) e^{\Omega t} n(\mathbf{q}) \rangle\tag{A.41}$$

The average $\langle \dots \rangle$ denotes an average over the Boltzmann distribution. The operators act on everything on their right (ρ_B included), unless they are enclosed in parenthesis. We introduce the Laplace transform $f(z) \equiv \int_0^{+\infty} dt e^{-zt} f(t)$ and an operator \mathcal{P} that projects along the space of density modes

$$\mathcal{P} \equiv n(\mathbf{q}) \langle \frac{1}{NS(q)} \langle n^*(\mathbf{q}) \rangle \rangle\tag{A.42}$$

The projection operator \mathcal{P} is accompanied by the operator $\mathcal{Q} \equiv 1 - \mathcal{P}$, which project along the space orthogonal to $n(\mathbf{q})$. Using the projection-operator formalism adopted in Chapter 6 we obtain an equation for the Laplace transform of the dynamical structure factor,

$$zS(q, z) - S(q) = -\omega(q)S(q, z) + \tilde{M}(q, z)S(q, z)\tag{A.43}$$

where we have introduced the decay rate $\omega(q)$ and the memory kernel $\widetilde{M}(q, z)$.

$$\begin{aligned}\omega(q) &= -\frac{1}{NS(q)} \langle n^*(\mathbf{q}) \Omega n(\mathbf{q}) \rangle \\ \widetilde{M}(q, z) &= \frac{1}{NS(q)} \left\langle n^*(\mathbf{q}) \Omega \mathcal{Q} \frac{1}{z - \mathcal{Q} \Omega \mathcal{Q}} \Omega \mathcal{Q}(z) \mathcal{Q} \Omega n(\mathbf{q}) \right\rangle\end{aligned}\quad (\text{A.44})$$

The kernel \widetilde{M} can be expressed in term of its irreducible component. In contrast with the transverse forces case, we do not expect terms orthogonal to \mathbf{q} to be relevant in the dynamics. We therefore follow the prescription of Kawasaki [152], and we introduce an irreducible operator

$$\Omega_{\text{irr}} \equiv \mathcal{Q} \Omega \mathcal{Q} - \mathcal{Q} \Omega n(\mathbf{q}) \rangle \frac{1}{NS(q)\omega(q)} \langle n^*(\mathbf{q}) \Omega \mathcal{Q}. \quad (\text{A.45})$$

Using the resolvent identity

$$\frac{1}{z - \mathcal{Q} \Omega \mathcal{Q}} = \left(1 - \frac{1}{z - \mathcal{Q} \Omega \mathcal{Q}} \mathcal{Q} \Omega n(\mathbf{q}) \rangle \frac{1}{NS(q)\omega(q)} \langle n^*(\mathbf{q}) \Omega \mathcal{Q} \right) \frac{1}{z - \Omega_{\text{irr}}} \quad (\text{A.46})$$

we can write $\widetilde{M}(q, z)$ in term of an irreducible memory kernel $M(q, z)$

$$\widetilde{M}(q, z) = \frac{M(q, z)}{1 + \omega(q)^{-1} M(q, z)} \quad (\text{A.47})$$

with

$$M_{\text{irr}}(q, z) \equiv \frac{1}{NS(q)} \left\langle n^*(\mathbf{q}) \Omega \mathcal{Q} \frac{1}{z - \Omega_{\text{irr}}} \mathcal{Q} \Omega n(\mathbf{q}) \right\rangle. \quad (\text{A.48})$$

The equation for $S(q, z)$, Eq. (A.43) becomes

$$S(q, z) = \frac{S(q)}{z + \frac{\omega(q)}{1 + \omega(q)^{-1} M(q, z)}}, \quad (\text{A.49})$$

or passing to the representation in time,

$$\partial_t S(q, t) = -\omega(q) S(q) - \int_0^t d\tau \omega(q)^{-1} M(q, t - \tau) \partial_\tau S(q, \tau). \quad (\text{A.50})$$

From a formal point of view, this is the standard equation for the evolution of a correlation function obtained through the Mori-Zwanzig projection operator formalism. We now compute the rate $\omega(q)$:

$$\begin{aligned}\omega(q) &= -\frac{1}{NS(q)} \langle n^*(\mathbf{q}) \Omega n(\mathbf{q}) \rangle \\ &= -\frac{1}{NS(q)} \sum_i \langle n^*(\mathbf{q}) \nabla_i \cdot (-\mu_i \mathbf{F}_i + T \mu_i \nabla_i) n(\mathbf{q}) \rangle \\ &= +\frac{i}{NS(q)} \sum_i \mathbf{q} \cdot \langle e^{i\mathbf{q} \cdot \mathbf{r}_i} (-\mu_i \mathbf{F}_i + T \mu_i \nabla_i) n(\mathbf{q}) \rangle \\ &= +\frac{i}{NS(q)} \sum_i \mathbf{q} \cdot \langle e^{i\mathbf{q} \cdot \mathbf{r}_i} (-\mu_i \mathbf{F}_i + T \mu_i \nabla_i) n(\mathbf{q}) \rangle \\ &= \frac{T q^2}{NS(q)} \sum_i \langle \mu_i(\mathbf{r}_i) \rangle \\ &= \frac{T q^2}{S(q)} \langle \mu(0) \rangle\end{aligned}\quad (\text{A.51})$$

where we have introduced the Fourier transform of the mobility field

$$\mu(\mathbf{q}) \equiv \frac{1}{N} \sum_i e^{-i\mathbf{q}\cdot\mathbf{r}_i} \mu_i(\mathbf{r}_i). \quad (\text{A.52})$$

Note that $\mu(0)$ is the Fourier transform of the mobility field evaluated at $\mathbf{q} = 0$. The standard result $\omega(q) = \frac{\mu_0 T q^2}{S(q)}$ is recovered when $\mu_i(\mathbf{r}_i) = \mu_0$, since in that case $\mu(0) = 1$.

We proceed by performing a mode coupling expansion of the memory kernel.

A4.2 Mode coupling expansion

To compute $M(q, t)$ in Eq.(A.48), we must resort to approximation schemes. At the moment, it is unclear how the mode-coupling expansion should be implemented in the presence of a spatially dependent mobility field, that can in principle generate higher-order dynamical correlations among the particles. Here we take the most pedestrian approach, and adopt the usual mode-coupling expansion in terms of products of density modes:

$$\mathcal{Q}\Omega n(\mathbf{q}) \approx \frac{1}{2} \sum_{\mathbf{k}_1, \mathbf{k}_2} \frac{1}{N^2 S(k_1) S(k_2)} \langle n^*(\mathbf{k}_1) n^*(\mathbf{k}_2) \mathcal{Q}\Omega n(\mathbf{q}) \rangle n(\mathbf{k}_1) n(\mathbf{k}_2) \quad (\text{A.53})$$

The average on the right hand side is composed by two term:

$$\langle n^*(\mathbf{k}_1) n^*(\mathbf{k}_2) \mathcal{Q}\Omega n(\mathbf{q}) \rangle = \langle n^*(\mathbf{k}_1) n^*(\mathbf{k}_2) \Omega n(\mathbf{q}) \rangle - \langle n^*(\mathbf{k}_1) n^*(\mathbf{k}_2) \mathcal{P}\Omega n(\mathbf{q}) \rangle. \quad (\text{A.54})$$

Let us compute the first one

$$\begin{aligned} \langle n^*(\mathbf{k}_1) n^*(\mathbf{k}_2) \Omega n(\mathbf{q}) \rangle &= \sum_i \langle n^*(\mathbf{k}_1) n^*(\mathbf{k}_2) \nabla_i \cdot (-\mu_i \mathbf{F}_i + T \mu_i \nabla) n(\mathbf{q}) \rangle \\ &= - \sum_i \langle \nabla_i (n^*(\mathbf{k}_1) n^*(\mathbf{k}_2)) \cdot (-\mu_i \mathbf{F}_i + T \mu_i \nabla) n(\mathbf{q}) \rangle \\ &= T \sum_i i \mathbf{q} \cdot \langle \nabla_i (n^*(\mathbf{k}_1) n^*(\mathbf{k}_2)) \mu_i e^{-i\mathbf{q}\cdot\mathbf{r}_i} \rangle \\ &= -TN \delta_{\mathbf{k}_2 + \mathbf{k}_1, \mathbf{q}} [\mathbf{q} \cdot \mathbf{k}_1 \langle n^*(\mathbf{k}_2) \mu(\mathbf{q} - \mathbf{k}_1) \rangle + \mathbf{q} \cdot \mathbf{k}_2 \langle n^*(\mathbf{k}_1) \mu(\mathbf{q} - \mathbf{k}_2) \rangle] \end{aligned} \quad (\text{A.55})$$

The $\delta_{\mathbf{k}_2 + \mathbf{k}_1, \mathbf{q}}$ comes from the translational invariance of the system. The second term of Eq. (A.54) is, using a convolution approximation,

$$\begin{aligned} \langle n^*(\mathbf{k}_1) n^*(\mathbf{k}_2) \mathcal{P}\Omega n(\mathbf{q}) \rangle &= \langle n(\mathbf{k}_1)^* n(\mathbf{k}_2)^* n(\mathbf{q}) \rangle \omega(q) \\ &\approx N \delta_{\mathbf{k}_1 + \mathbf{k}_2, \mathbf{q}} S(k_1) S(k_2) S(q) \omega(q) \\ &= NT q^2 \delta_{\mathbf{k}_1 + \mathbf{k}_2, \mathbf{q}} S(k_1) S(k_2) \langle \mu(0) \rangle \end{aligned} \quad (\text{A.56})$$

Summing the two contributions, Eq. (A.54) can be rewritten as

$$\begin{aligned} \langle n^*(\mathbf{k}_1) n^*(\mathbf{k}_2) \mathcal{Q}\Omega n(\mathbf{q}) \rangle &= NT \rho_0 S(k_1) S(k_2) \langle \mu(0) \rangle \delta_{\mathbf{k}_1 + \mathbf{k}_2, \mathbf{q}} \\ &\times [\mathbf{q} \cdot \mathbf{k}_1 \tilde{c}_{\mu, \mathbf{q}}(\mathbf{k}_2) + \mathbf{q} \cdot \mathbf{k}_2 \tilde{c}_{\mu, \mathbf{q}}(\mathbf{k}_1)] \end{aligned} \quad (\text{A.57})$$

where we have introduced a 'direct correlation function'-like quantity $\widetilde{c}_{\mu,\mathbf{q}}(\mathbf{k})$ dressed by the dynamics that we denote by

$$\rho_0 \widetilde{c}_{\mu,\mathbf{q}}(\mathbf{k}) \equiv 1 - \frac{\langle n(\mathbf{k})^* \mu(\mathbf{k}) \rangle}{\langle \mu(0) \rangle S(\mathbf{q} - \mathbf{k}) S(k)}. \quad (\text{A.58})$$

For $\mu = \mu_0$, $\widetilde{c}_{\mu,\mathbf{q}}(\mathbf{k})$ reduces to the usual direct correlation function $c|\mathbf{q} - \mathbf{k}|$. The next approximation concerns the evolution of the density correlations

$$\begin{aligned} \langle n(\mathbf{k}_4)^* n(\mathbf{k}_3)^* e^{\Omega_{\text{irr}} t} n(\mathbf{k}_2) n(\mathbf{k}_1) \rangle &\approx \langle n(\mathbf{k}_4)^* n(\mathbf{k}_3)^* e^{\Omega t} n(\mathbf{k}_2) n(\mathbf{k}_1) \rangle \\ &\approx N^2 S(\mathbf{k}_1, t) S(\mathbf{k}_2, t) [\delta_{\mathbf{k}_1, \mathbf{k}_3} \delta_{\mathbf{k}_2, \mathbf{k}_4} + \delta_{\mathbf{k}_1, \mathbf{k}_4} \delta_{\mathbf{k}_2, \mathbf{k}_3}] \end{aligned} \quad (\text{A.59})$$

Putting everything together, we can rewrite the memory kernel as

$$\begin{aligned} M_{\text{irr}}(q, t) &\approx \frac{1}{4N^5 S(q)} \sum_{\mathbf{k}_1, \mathbf{k}_2, \mathbf{k}_3, \mathbf{k}_4} \frac{1}{S(k_1) S(k_2) S(k_3) S(k_4)} \\ &\times \langle n^*(\mathbf{k}_1) n^*(\mathbf{k}_2) \mathcal{Q} \Omega n(\mathbf{q}) \rangle \langle n(\mathbf{q})^* \Omega \mathcal{Q} n(\mathbf{k}_3) n(\mathbf{k}_4) \rangle \\ &\times \langle n(\mathbf{k}_3)^* n(\mathbf{k}_4)^* e^{\Omega_{\text{irr}} t} n(\mathbf{k}_1) n(\mathbf{k}_2) \rangle \\ &= \frac{1}{2N^3} \sum_{\mathbf{k}_1, \mathbf{k}_2} \frac{1}{S(k_1)^2 S(k_2)^2} |\langle n^*(\mathbf{k}_1) n^*(\mathbf{k}_2) \mathcal{Q} \Omega n(\mathbf{q}) \rangle|^2 S(\mathbf{k}_1, t) S(\mathbf{k}_2, t) \\ &= \frac{T^2 \rho_0^2}{2N S(q)} \sum_{\mathbf{k}_1} \langle \mu(0) \rangle^2 [\mathbf{q} \cdot \mathbf{k}_1 \widetilde{c}_{\mu,\mathbf{q}}(\mathbf{q} - \mathbf{k}_1) + \mathbf{q} \cdot (\mathbf{q} - \mathbf{k}_1) \widetilde{c}_{\mu,\mathbf{q}}(\mathbf{k}_1)]^2 \\ &\times S(\mathbf{k}_1, t) S(\mathbf{q} - \mathbf{k}_1, t) \\ &= \frac{T^2 \rho_0 \langle \mu(0) \rangle^2}{2S(q)} \int \frac{d\mathbf{k}}{(2\pi)^3} [\mathbf{q} \cdot \mathbf{k}_1 \widetilde{c}_{\mu,\mathbf{q}}(\mathbf{q} - \mathbf{k}_1) + \mathbf{q} \cdot (\mathbf{q} - \mathbf{k}_1) \widetilde{c}_{\mu,\mathbf{q}}(\mathbf{k}_1)]^2 \\ &\times S(\mathbf{k}_1, t) S(\mathbf{q} - \mathbf{k}_1, t) \end{aligned} \quad (\text{A.60})$$

Or using the definition of the frequency $\omega(q)$

$$\begin{aligned} \omega^{-1}(q) M(q, t) &= \frac{T \rho_0 \langle \mu(0) \rangle}{2q^2} \int \frac{d\mathbf{k}}{(2\pi)^3} [\mathbf{q} \cdot \mathbf{k} \widetilde{c}_{\mu,\mathbf{q}}(\mathbf{q} - \mathbf{k}) + \mathbf{q} \cdot (\mathbf{q} - \mathbf{k}) \widetilde{c}_{\mu,\mathbf{q}}(\mathbf{k})]^2 \\ &\times S(\mathbf{k}, t) S(\mathbf{q} - \mathbf{k}, t) \end{aligned} \quad (\text{A.61})$$

Together with Eq (A.58) is the expression for the irreducible memory kernel in the mode coupling approximations of a dynamics with a spatially dependent mobility. For $\mu_i(\mathbf{r}_i) = \mu_0$, the usual expression is recovered.

We can now specialize to the case of facilitated dynamics

A4.3 Mode coupling theory for facilitated dynamics

We take for $\mu_i(\mathbf{r}_i)$ the expression given by Eq. (A.30), the choice leading to the facilitated dynamics. In this case, a calculation similar to the one done for the diffusion

constant in Section A3.1 shows that

$$\begin{aligned}\langle \mu(0) \rangle &= \mu_0 \frac{\phi}{\rho_0} \\ \omega(q) &= q^2 \mu_0 T \frac{\phi}{\rho_0} \\ \langle n(\mathbf{q}) * \mu(\mathbf{q}) \rangle &= \langle \mu(0) \rangle = \mu_0 \frac{\phi}{\rho_0} \\ \rho_0 \tilde{c}_{\mu, \mathbf{q}}(\mathbf{k}) &= 1 - \frac{1}{S(|\mathbf{q} - \mathbf{k}|)S(k)} = \rho_0 \tilde{c}_{\mu, \mathbf{q}}(\mathbf{q} - \mathbf{k}).\end{aligned}\tag{A.62}$$

The resulting equation of motion for the dynamics structure factor $S(q, t)$ is

$$\partial_t S(q, t) = -q^2 \mu_0 T \frac{\phi}{\rho_0} - \int_0^t d\tau \omega(q)^{-1} M_{\text{fd}}(q, t - \tau) \partial_\tau S(q, \tau),\tag{A.63}$$

where M_{fd} is the mode-coupling memory kernel for the facilitated dynamics,

$$\begin{aligned}\omega(q)^{-1} M_{\text{fd}}(q, t - \tau) &= \mu_0 T \phi q^2 \int \frac{d\mathbf{k}}{(2\pi)^3} (\rho_0 c(\mathbf{k}) c(\mathbf{q} - \mathbf{k}) - c(\mathbf{k}) - c(\mathbf{q} - \mathbf{k}))^2 \\ &\quad \times S(\mathbf{k}, t) S(\mathbf{q} - \mathbf{k}, t)\end{aligned}\tag{A.64}$$

Eq. (A.63) and Eq. (A.64) constitute a first attempt at building a mode-coupling theory for the facilitated dynamics. It is however very likely that the nature of the facilitated dynamics cannot be captured by the most common mode-coupling approximation scheme. This is also suggested when trying to locate the glass transition through a schematic approximation, as done in Chapter 6.3.4.

A4.4 Ergodicity breaking within the schematic approximation

We introduce a nonergodicity parameter $\phi_\infty \equiv \lim_{t \rightarrow +\infty} \frac{S(q, t)}{S(q)}$. It can be determined using the long time limit of Eq (A.63):

$$\frac{\phi_\infty}{1 - \phi_\infty} = \omega(q)^{-2} M_{\text{fd}}(q, t \rightarrow \infty).\tag{A.65}$$

As a first approach, we compute the long time limit of the memory kernel within the schematic approximation, as done in Sec. 6.3.4. We obtain

$$\begin{aligned}\omega(q)^{-1} M_{\text{fd}}^{\text{schematic}} &\approx \mu_0 T S_0^2 \frac{\phi}{\rho_0^2} q_0^2 \phi_\infty^2 \int_{|\mathbf{k}|=q_0, |\mathbf{q}-\mathbf{k}|=q_0} \frac{d\mathbf{k}}{(2\pi)^3} \\ &= \frac{\sqrt{3}}{16\pi^2} \mu_0 T S_0^2 \frac{\phi}{\rho_0^2} q_0^3\end{aligned}\tag{A.66}$$

where as customary in the schematic approximation, q_0 is the wavevector corresponding to the first peak of the structure factor, and S_0 is the amplitude of the peak. Substitution of this expression in Eq. (A.65) yields

$$\frac{\phi_\infty}{1 - \phi_\infty} = \frac{\lambda_{\text{eq}}}{\mu_0 T q_0^2} \phi_\infty^2\tag{A.67}$$

with $\lambda_{\text{eq}} = \frac{\sqrt{3}}{16\pi^2} \frac{\mu_0 T S_0^2}{\rho_0} q_0^3$. This equation is the same as the one found for the usual overdamped Langevin dynamics, as reproduced in Chapter 6.3.4, and thus a glass transition at the same location as for usual overdamped Langevin dynamics is expected to take place. This is in contrast with our finding for the diffusion constant.

Further efforts to understand the facilitated dynamics and its possible applications could proceed along two directions: the first one consists in employing more sophisticated numerical schemes for the integration of the equations of motion, in the spirit of [46, 171]. Although a lower temperature below which numerical integration becomes unfeasible is probably always present, the hope is to push this boundary to temperatures low enough to be able to measure the diffusion coefficient for the facilitated dynamics in a glassy phase and compare it with the prediction obtained here. On the analytical side, there is certainly more to be explored by means of mode-coupling theory. One could for example study what happens when only terms involving pairwise interactions are kept in the expression of $\mu_i(\mathbf{r}_i)$, i.e. by writing

$$\begin{aligned}\mu_i(\mathbf{r}_i) &= e^{\beta \sum_j V(\mathbf{r}_i - \mathbf{r}_j)} = \mu_0 \Pi_j e^{\beta V(\mathbf{r}_i - \mathbf{r}_j)} \\ &\equiv \mu_0 \Pi_j (1 + \tilde{f}(\mathbf{r}_{ij})) \approx 1 + \sum_j \tilde{f}(\mathbf{r}_{ij})\end{aligned}\tag{A.68}$$

with $\tilde{f}(\mathbf{r}_{ij})$ a 'negative temperature Mayer functions'. This procedure would lead to consider only contribution from terms with a pairwise nature, and in this case the standard mode-coupling expansion schemes could prove more fruitful and faithful. Another possibility could be to resort to generalized mode coupling theory, an extension of mode-coupling designed to take into account higher order density correlations [142].

APPENDIX B

BREAKING DETAILED BALANCE ACCELERATES RELAXATION: A PROOF FOR DISCRETE STATES SYSTEMS

In this Section we show that breaking detailed balance in a Markov chain while preserving the stationary distribution reduces the time to reach the stationary state. We follow the proof of Ichiki and Ohzeki [136] for discrete-state Markov processes in continuous time. Let $P_i(t)$ be the probability that the system is in state i at time t . The probability $P_i(t)$ evolves in time according to the master equation

$$\frac{dP_i(t)}{dt} = \sum_{j=1}^N \omega_{ij} P_j(t) - \sum_{j=1}^N \omega_{ji} P_i(t) \quad (\text{B.1})$$

where ω_{ij} is the transition rate from state j to state i . We assume the resulting Markov chain to be irreducible. For the system to admit a given steady state distribution π_i , the transition rates must satisfy

$$\sum_{j=1}^N \omega_{ij} \pi_j = \sum_{j=1}^N \pi_i \omega_{ji} \quad (\text{B.2})$$

This condition of stationarity of π_i , known in the Markov chain literature as global balance, can be satisfied by imposing the sufficient condition

$$\omega_{ij} \pi_j = \omega_{ji} \pi_i \quad (\text{B.3})$$

for all configurations i, j . Eq. (B.3) is the detailed balance condition for discrete Markov chains. It is a sufficient, but not necessary, condition for Eq. (B.2) to be true.

The master equation Eq. (B.1) can be rewritten in a rotated basis:

$$\frac{dR_i(t)}{dt} = \sum_{j=1}^N W_{ij} R_j(t) \quad (\text{B.4})$$

with $R_i(t) \equiv P_i(t)/\sqrt{\pi_i}$, $W_{ij} \stackrel{i \neq j}{\equiv} \pi_i^{-1/2} \omega_{ij} \pi_j^{1/2}$ and $W_{ii} \equiv -\sum_{j \neq i} \omega_{ji}$. The matrix \mathbf{W} is symmetric only when the detailed balance condition Eq. (B.3) holds, but in general, the symmetric part of \mathbf{W} is negative semi-definite, and the Perron-Frobenius theorem ensures that \mathbf{W} has a non-degenerate eigenvector, $\sqrt{\pi_i}$, with eigenvalue $\lambda_0 = 0$, which is also the largest eigenvalue in its spectrum. We see therefore that exponential relaxation to the steady state is ensured, with a relaxation rate given by (minus) the largest non zero eigenvalue of the spectrum.

Eq. (B.4) is the starting point of the proof by Ichiki and Ohzeki concerning the relaxation times of an irreversible Markov chain, which we hereafter reproduce. The outcome of the proof is the possibility to accelerate the relaxation dynamics by breaking detailed balance. We start from Eq. (B.4), and we note that \mathbf{W} can always be decomposed as the sum of a symmetric part $\mathbf{S} \equiv \frac{\mathbf{W} + \mathbf{W}^T}{2}$ and in an antisymmetric part $\mathbf{A} \equiv \frac{\mathbf{W} - \mathbf{W}^T}{2}$:

$$\mathbf{W} = \mathbf{S} + \mathbf{A}. \quad (\text{B.5})$$

The matrix \mathbf{S} is associated to a reversible Markov process with equilibrium distribution π_i , as we now demonstrate. We express the dynamical process $\frac{dR_i(t)}{dt} = \sum_j S_{ij} R_j(t)$ back to its original basis $P_i(t) \equiv \sqrt{\pi_i} R_i(t)$,

$$\frac{d}{dt} P_i(t) = \sum_{j=1}^N \sigma_{ij} P_j(t) - \sum_{j=1}^N \sigma_{ji} P_i(t) \quad (\text{B.6})$$

where the matrix σ_{ij} is related to the stochastic process ω_{ij} for the original, possibly nonreversible process of Eq. (B.1) by:

$$\sigma_{ij} = \frac{1}{2} \left[\omega_{ij} + \frac{\pi_i}{\pi_j} \omega_{ji} \right], \quad (\text{B.7})$$

To show that Eq. (B.6) is a reversible Markov process in continuous time, we need to show that

- (i) $\sigma_{ij} \geq 0$.
- (ii) $\sum_{j \neq i} \sigma_{ji} = -\sigma_{ii} = \sum_{j \neq i} \omega_{ji}$ for any fixed i , i.e. the sum of the escape rates from state i is the same as the one of the original process.
- (iii) Detailed balance with respect to the stationary distribution π_i is obeyed: $\sigma_{ij} \pi_j = \sigma_{ji} \pi_i$

Property (i) is obvious from Eq. (B.6) and the fact that $\omega_{ij} \geq 0$. Property (ii) can be proven using the stationary condition $\sum_j \omega_{ij} \pi_j = \sum_{j \neq i} \omega_{ij} \pi_i$:

$$\sum_{j \neq i} \sigma_{ji} = \frac{1}{2} \sum_{j \neq i} \omega_{ji} + \frac{1}{2} \sum_{j \neq i} \frac{\pi_j}{\pi_i} \omega_{ij} = \frac{1}{2} \sum_{j \neq i} \omega_{ji} + \frac{1}{2\pi_i} \sum_{j \neq i} \omega_{ji} \pi_i = \sum_{j \neq i} \omega_{ji}. \quad (\text{B.8})$$

Property (iii) is verified with an explicit computation

$$\sigma_{ij}\pi_j = \frac{1}{2} \left[\omega_{ij} + \frac{\pi_i}{\pi_j} \omega_{ji} \right] \pi_j = \pi_i \frac{1}{2} \left[\omega_{ji} + \frac{\pi_j}{\pi_i} \omega_{ij} \right] = \pi_i \sigma_{ji}. \quad (\text{B.9})$$

The above reasoning proves that σ_{ij} describes an equilibrium Markov process in continuous time with equilibrium distribution π_i . The matrix \mathbf{A} can thus be seen as a nonequilibrium perturbation of an otherwise equilibrium process.

We are going to prove that, for any fixed \mathbf{S}

$$\operatorname{Re} \lambda_1^W - \lambda_1^S \leq 0 \quad (\text{B.10})$$

where λ_1^W and λ_1^S are the first eigenvalues below zero of the matrices \mathbf{W} and \mathbf{S} , respectively. Relation (B.10) implies that the relaxation times of a dynamics that breaks detailed balance are shorter than their equilibrium counterparts.

To prove the statement, we introduce the characteristic polynomials $p_W(\lambda)$ and $p_S(\lambda)$. For a square N -dimensional matrix \mathbf{M} and a complex number λ the characteristic polynomial $p_M(\lambda)$ is defined as

$$p_M(\lambda) \equiv \det(\lambda \mathbf{1}_N - \mathbf{M}) \quad (\text{B.11})$$

where $\mathbf{1}_N$ is the N -dimensional identity matrix. The spectrum of \mathbf{M} is determined by solving the equation $p_M(\lambda) = 0$. The proof of relation (B.10) is done by establishing two inequalities regarding the characteristic polynomials $p_W(\lambda)$ and $p_S(\lambda)$:

$$p'_W(\lambda) \Big|_{\lambda=0} \geq p'_S(\lambda) \Big|_{\lambda=0} \quad (\text{B.12})$$

$$\left| \frac{p_W(\lambda)}{\lambda} \right| \geq \frac{p_S(\lambda)}{\operatorname{Re} \lambda} \quad \forall \lambda \text{ s.t. } \lambda_1^S < \operatorname{Re} \lambda < \lambda_0^S \quad (\text{B.13})$$

A graphical representation of these two properties is given in Fig. B.1. The two propositions combined together give relation (B.10).

Instrumental to the proof will be the Ostrowsky-Taussky inequality [131], which states that, if \mathbf{M} is a matrix such that $\frac{\mathbf{M} + \mathbf{M}^\dagger}{2}$ is positive definite, then

$$|\det \mathbf{M}| \geq \det \left(\frac{\mathbf{M} + \mathbf{M}^\dagger}{2} \right). \quad (\text{B.14})$$

Proof of Eq. (B.14). Let us define an Hermitian matrix $\mathbf{S}_M \equiv \frac{1}{2}(\mathbf{M} + \mathbf{M}^\dagger)$ and a skew-Hermitian matrix $\mathbf{A}_M \equiv \frac{1}{2}(\mathbf{M} - \mathbf{M}^\dagger)$, so that $\mathbf{M} = \mathbf{S}_M + \mathbf{A}_M$. The Ostrowski-Taussky inequality is equivalent to

$$|\det(\mathbf{1} + \mathbf{S}_M^{-1} \mathbf{A}_M)| \geq 1. \quad (\text{B.15})$$

To proceed further, note that the spectrum of $\mathbf{S}_M^{-1} \mathbf{A}_M$ is complex. Let t_k be an eigenvalue of $\mathbf{S}_M^{-1} \mathbf{A}_M$ with associated eigenvector \mathbf{u}_k , $\mathbf{S}_M^{-1} \mathbf{A}_M \mathbf{u}_k = t_k \mathbf{u}_k$. Multiplying both side of this equation by $\mathbf{S}_M^{1/2}$, and introducing the vector $\mathbf{u}'_k \equiv \mathbf{S}_M^{1/2} \mathbf{u}_k$, we obtain

$$\mathbf{S}_M^{-1/2} \mathbf{A}_M \mathbf{S}_M^{-1/2} \mathbf{u}'_k = t_k \mathbf{u}'_k. \quad (\text{B.16})$$

Note that to write this equation, we used the fact that the matrix \mathbf{S}_M is positive definite. We have thus shown that \mathbf{u}'_k is an eigenvector of the matrix $\mathbf{S}_M^{-1/2} \mathbf{A}_M \mathbf{S}_M^{-1/2}$ with eigenvalue t_k . Since $\mathbf{S}_M^{-1/2} \mathbf{A}_M \mathbf{S}_M^{-1/2}$ is Skew-Hermitian, t_k is imaginary. This means that

$$|\det(\mathbf{1} + \mathbf{S}_M^{-1} \mathbf{A}_M)| = \Pi_k |1 + t_k| \geq 1, \quad (\text{B.17})$$

which proves Eq. (B.15), and thus the Ostrowsky-Taussky inequality in Eq. (B.14).

We now have all the tools needed to derive properties (B.12) and (B.13).

Proof of property (B.12). We apply Ostrowski-Taussky inequality Eq. (B.14) to the matrix $\mathbf{M} \equiv \lambda \mathbf{1}_N - \mathbf{W}$, with λ real and positive:

$$\det(\lambda \mathbf{1}_N) - \mathbf{W} \geq \det(\lambda \mathbf{1}_N - \mathbf{S}) \quad (\text{B.18})$$

Note that $\frac{\mathbf{M} + \mathbf{M}^\dagger}{2} = \lambda \mathbf{1}_N - \mathbf{S}$, which is positive definite for $\lambda \geq 0$. We can therefore write

$$p_W(\lambda) \geq p_S(\lambda), \forall \lambda \geq 0 \quad (\text{B.19})$$

Since we know that $p_W(\lambda) = p_S(\lambda) = 0$ and that the characteristic polynomial is a smooth function of λ , this statement implies property (B.12).

Proof of property (B.13). We start by looking at $p_W(\lambda)$:

$$\begin{aligned} p_W(\lambda) &= \det\left(\lambda \mathbf{1}_N - \mathbf{W} + \frac{(\lambda \mathbf{1}_N - \mathbf{W})^\dagger}{2} - \frac{(\lambda \mathbf{1}_N - \mathbf{W})^\dagger}{2}\right) \\ &= \det(\lambda \mathbf{1}_N - \mathbf{S} + \mathbf{A}) \\ &= \det(\lambda \mathbf{1}_N - \mathbf{\Lambda}_S + \mathbf{A}) \\ &= \lambda \det(\lambda \mathbf{1}_{N-1} - \tilde{\mathbf{\Lambda}}_S + \tilde{\mathbf{A}}) \end{aligned} \quad (\text{B.20})$$

$\mathbf{\Lambda}_S$ is the diagonal matrix associated to \mathbf{S} , and $\tilde{\mathbf{M}}$ denotes the $N - 1$ -dimensional matrix obtained by removing from the N -dimensional matrix \mathbf{M} its first row and its

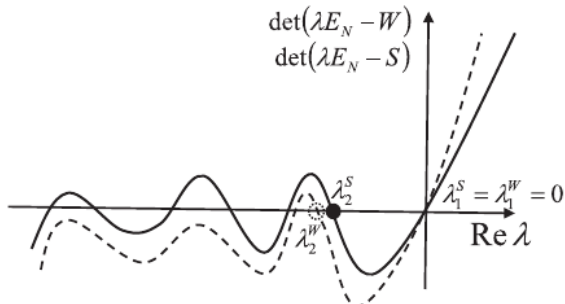


Figure B.1: Graphical interpretation of the proof of Ichiki and Ohzuki, taken from [136]. The plot shows characteristic polynomials of W (dashed line) and S (solid line). Eq. (B.12) enforces the dashed to be above the solid line for $\text{Re } \lambda = 0^+$, while Eq. (B.13) guarantees the solid line to be above the dashed one until the horizontal axis is hit again.

first column. The last passage is justified by the fact that $(\lambda \mathbf{1}_N - \Lambda_S + \mathbf{A})_{11} = \lambda - \lambda_0^S = \lambda$. We now apply the Ostrowski-Taussky inequality Eq. (B.14) to the matrix $\mathbf{M} \equiv \lambda \mathbf{1}_{N-1} - \tilde{\Lambda}_S + \tilde{\mathbf{A}}$:

$$|\det \lambda \mathbf{1}_{N-1} - \tilde{\Lambda}_S + \tilde{\mathbf{A}}| \geq \det (\operatorname{Re} \lambda \mathbf{1}_{N-1} - \tilde{\lambda}) \quad (\text{B.21})$$

Note that $\frac{\mathbf{M} + \mathbf{M}^\dagger}{2} = \operatorname{Re} \lambda \mathbf{1}_{N-1} - \tilde{\lambda}$ is positive definite for $\lambda_1^S < \operatorname{Re} \lambda < \lambda_0^S$, thus defining the interval where the equality holds. Using the relation (B.20) on both sides of the inequality we obtain the result

$$\left| \frac{p_W(\lambda)}{\lambda} \right| \geq \frac{p_S(\lambda)}{\operatorname{Re} \lambda} \quad \forall \lambda \text{ s.t. } \lambda_1^S < \operatorname{Re} \lambda < \lambda_0^S \quad (\text{B.22})$$

which is property (B.13), and the proof is concluded. We have thus showed that breaking detailed balance in discrete Markov processes accelerates relaxation towards the stationary distribution.

APPENDIX C

THE CONDUCTANCE BOUNDS THE MIXING TIME

In this Appendix we consider a Markov Chain in discrete space and time. Following [173], we introduce the mixing time t_{mix} , a complementary quantity to the relaxation time that tracks the convergence of a probability distribution to its target stationary measure, considering a worst-case scenario for the initial condition. The mixing time is bounded from above and below by the conductance Φ^* , which is, in a nutshell, the smallest transition probability for a Markov Chain, when a conditioning on the starting set is taken into account. The bound on the mixing time is

$$\frac{C}{\Phi^*} \leq t_{\text{mix}} \leq \frac{C'}{\Phi^{*2}} \log \frac{1}{\pi_{\min}} \quad (\text{C.1})$$

where $\pi_{\min} \equiv \min_{i \in \Omega} \pi_{\text{ss}}(i)$, with Ω the set of possible configurations of states i and π_{ss} the stationary state of the Markov chain. While the constants C and C' depend on whether the Markov chain is reversible or not, the dependence on the conductance is the same for all Markov chains. Since, as we will show, the conductance is the same for a reversible Markov chain with equilibrium distribution π_{ss} and a lifted Markov chain with the same steady state distribution, it gives information on the maximal efficiency achievable using lifting schemes. If a reversible Markov chain has a mixing time closer to the upper bound $\sim \frac{1}{\Phi^{*2}}$, there is then hope for an effective lifting to achieve a square-root reduction of the mixing time of the system [63].

C1 Definition of the mixing time

We denote by $P(i, j)$ the transition probability from state i to state j of the Markov chain under consideration. The master equation in discrete time for the time dependent probability $\pi_t(i)$ is

$$\pi_{t+1}(i) = \sum_{j \in \Omega} \pi_t(j) P(j, i) \quad (\text{C.2})$$

The steady state distribution π_{ss} satisfies the stationary condition

$$\pi_{ss}(i) = \sum_{j \in \Omega} \pi_{ss}(j) P(j, i) \quad (\text{C.3})$$

Given an initial condition π_0 , the distribution at time t can be constructed by iteratively applying Eq. (C.2):

$$\pi_t(i) = \sum_{j \in \Omega} \pi_0(j) P^t(j, i) \equiv \pi_0 P^t(i) \quad (\text{C.4})$$

with $P^t(j, i)$ the j, i entry of the matrix \mathbf{P}^t .

To define the mixing time, we first introduce the distance from stationarity $d(t)$ as

$$d(t) \equiv \sup_{\mu} \|\mu P^t - \pi_{ss}\|_{\text{TV}} \quad (\text{C.5})$$

where μ is a probability distribution defined on Ω , and $\|\cdot\|_{\text{TV}}$ denotes the total variation distance

$$\|\mu P^t - \pi_{ss}\|_{\text{TV}} \equiv \frac{1}{2} \sum_{j \in \Omega} \left| \sum_i \mu(i) P^t(i, j) - \pi_{ss}(j) \right| \quad (\text{C.6})$$

The distance from stationarity is a measure of how close a Markov chain that has evolved up to time t is to the stationary distribution π_{ss} .

The mixing time is defined by fixing a conventional cutoff of $1/4$ for the distance from stationarity

$$d(t_{\text{mix}}) \equiv \frac{1}{4}. \quad (\text{C.7})$$

After defining the mixing time, we turn to the definition of the conductance.

C2 The conductance

To define the conductance, we first introduce the ergodic flow $\Phi(S)$ from a given set $S \subseteq \Omega$

$$\Phi^* \equiv \frac{\sum_{i \in S} \sum_{j \in S^c} \pi_{ss}(i) P(i, j)}{\pi_{ss}(S)}, \quad (\text{C.8})$$

where S^c is the set complementary to S in Ω . In other words, the ergodic flow $\Phi(S)$ is the conditional probability of observing a transition that exits through the boundaries of S , given that within S the system is in its steady state. The conductance Φ^* is then defined as the smallest possible ergodic flow,

$$\Phi^* \equiv \min_{S | \pi_{ss}(S) \leq 1/2} \Phi(S). \quad (\text{C.9})$$

The condition $\pi(S) \leq 1/2$ is introduced because, using the fact that in the steady state $\sum_{i \in S} \sum_{j \in S^c} \pi_{ss}(i) P(i, j) = \sum_{i \in S^c} \sum_{j \in S} \pi_{ss}(i) P(i, j)$, it can be showed that $\phi(S^c) < \phi(S)$ provided that $\pi(S) > 1/2$.

A simple example of computation of the conductance is given by a random walker on a lattice of size L . At every discrete time, the random walker can move to the left site or to the right site with probability $1/2$. The minimum ergodic flow is achieved choosing for S a block of length $L/2$, which gives a conductance $\Phi^* = \frac{2}{L}$. The bounds for the mixing time in Eq. (C.1) then reads $O(L) \leq t_{\text{mix}} \leq O(L^2 \log L)$.

We proceed by defining lifted Markov chains and their relation with conductance and reduction of the mixing time.

C2.1 Lifted Markov chains, and their conductance

In the Markov chain literature [63], a *lifting* of the configuration space Ω is a larger configuration space $\hat{\Omega}$ and a surjective function $f : \hat{\Omega} \rightarrow \Omega$ that collapses a state $\alpha \in \hat{\Omega}$ onto a state $i \in \Omega$. Note that multiple states of the lifted space can be mapped to the same configuration of the original space. For a fixed configuration $i \in \Omega$, we denote by $f^{-1}(i) \subseteq \hat{\Omega}$ the set of configurations $\alpha \in \hat{\Omega}$ such that $f(\alpha) = i$. The lifted configuration space is accompanied by a lifted steady state distribution $\hat{\pi}_{\text{ss}}$ and a lifted transition probability matrix $\hat{P}(\alpha, \beta)$. In order to define a lifting of the Markov chain $P(i, j)$, they must obey two properties. The first one is that upon integrating out the variables of the extended phase space, the distribution $\hat{\pi}_{\text{ss}}$ must collapse onto π_{ss} , namely

$$\sum_{\alpha \in f^{-1}(i)} \hat{\pi}_{\text{ss}}(\alpha) = \pi_{\text{ss}}(i) \quad (\text{C.10})$$

the second property relates, in a non unique manner, the probability flows of the lifted Markov chain the ones of its collapsed counterpart:

$$\sum_{\alpha \in f^{-1}(i)} \sum_{\beta \in f^{-1}(j)} \hat{\pi}_{\text{ss}}(\alpha) P(\alpha, \beta) = \pi_{\text{ss}}(i) P(i, j). \quad (\text{C.11})$$

In particular, Eq. (C.11) implies that lifted Markov chains do not open new transition channels in the collapsed configurations space, but can accelerate the existing one, hopefully by transforming diffusive transition processes into ballistic ones. In this thesis, we were interested mainly in liftings of the form $\hat{\Omega} = \Omega \times V$ with V a new set of extra degrees of freedom (the self-propulsions in the active particle analogy in Chapter 1, or the activity label and self-propulsion direction for the Event Chain Monte Carlo algorithm in Chapter 7).

The conductance $\hat{\Phi}^*$ of a lifted Markov chain cannot be larger than the one of its original counterpart. This is because using Eq. (C.10) and Eq. (C.11) we have

$$\hat{\Phi}(f^{-1}(S)) \equiv \frac{\sum_{\alpha \in f^{-1}(S)} \sum_{\beta \in f^{-1}(S)^c} \hat{P}(\alpha, \beta) \hat{\pi}_{\text{ss}}(\alpha)}{\pi_{\text{ss}}(f^{-1}(S))} = \Phi(S) \quad (\text{C.12})$$

for every S belonging to the original configuration space Ω . In particular this implies that $\hat{\Phi}^* \leq \Phi^*$. The lower bound presented in Eq. (C.1) for the mixing time remains

valid also for the lifted Markov chain, and there is room for improvement in the case where the t_{mix} is closer to the upper bound in the original chain and closer to the lower bound in the lifted Markov chain.

C3 Proof of the lower bound for t_{mix}

C3.1 Preliminary lemmas

Before proceeding with the proof of the lower bound, we discuss two useful results. The first one is a possible rewriting of the total variation distance between two probability distributions μ and ν on Ω

$$\|\mu - \nu\|_{\text{TV}} = \sum_{\substack{i \in \Omega \\ \mu(i) \geq \nu(i)}} [\mu(i) - \nu(i)], \quad (\text{C.13})$$

which can be shown in the following way

$$\begin{aligned} \|\mu - \nu\|_{\text{TV}} &= \frac{1}{2} \sum_{i \in \Omega} |\mu(i) - \nu(i)| \\ &= \frac{1}{2} \sum_{\substack{i \in \Omega \\ \mu(i) \geq \nu(i)}} [\mu(i) - \nu(i)] + \frac{1}{2} \sum_{\substack{i \in \Omega \\ \mu(i) \leq \nu(i)}} [\nu(i) - \mu(i)] \\ &= \frac{1}{2} \sum_{\substack{i \in \Omega \\ \mu(i) \geq \nu(i)}} [\mu(i) - \nu(i)] + \frac{1}{2} \sum_{\substack{i \in \Omega \\ \mu(i) \leq \nu(i)}} [\nu(i) - \mu(i)] \\ &\quad + \frac{1}{2} \sum_{\substack{i \in \Omega \\ \mu(i) \geq \nu(i)}} [\nu(i) - \mu(i)] - \frac{1}{2} \sum_{\substack{i \in \Omega \\ \mu(i) \geq \nu(i)}} [\nu(i) - \mu(i)] \\ &= \sum_{\substack{i \in \Omega \\ \mu(i) \geq \nu(i)}} [\mu(i) - \nu(i)] + \frac{1}{2} \sum_{i \in \Omega} [\pi(i) - \mu(i)] \\ &= \sum_{\substack{i \in \Omega \\ \mu(i) \geq \nu(i)}} [\mu(i) - \nu(i)], \end{aligned} \quad (\text{C.14})$$

where we made use of the fact that $\sum_{i \in \Omega} \mu(i) = \sum_{i \in \Omega} \nu(i) = 1$.

The second useful lemma is the fact that the total variation distance, defined in Eq. (C.5) is a decreasing function of time, $d(t+1) \leq d(t)$. For two arbitrary distributions on Ω , μ and ν , we have

$$\|\mu P - \nu P\|_{\text{TV}} \leq \|\mu - \nu\|_{\text{TV}} \quad (\text{C.15})$$

since, using the triangle equality, we have

$$\begin{aligned}
 \|\mu P - \nu P\|_{\text{TV}} &= \frac{1}{2} \sum_i |\sum_j \mu(j)P(j,i) - \nu(j)P(j,i)| \\
 &\leq \frac{1}{2} \sum_{i,j \in \Omega} |\mu(j) - \nu(j)|P(j,i) \\
 &= \frac{1}{2} \sum_{i \in \Omega} |\mu(i) - \nu(i)| = \|\mu - \nu\|_{\text{TV}}.
 \end{aligned} \tag{C.16}$$

Through Eq. (C.15), we have

$$\begin{aligned}
 d(t+1) &= \sup_{\mu} \|\mu P^{t+1} - \pi_{\text{ss}}\|_{\text{TV}} \\
 &= \sup_{\mu} \|\mu P^{t+1} - \pi_{\text{ss}} P^{t+1}\|_{\text{TV}} \\
 &\leq \sup_{\mu} \|\mu P^t - \pi_{\text{ss}} P^t\|_{\text{TV}} \\
 &= \sup_{\mu} \|\mu P^t - \pi_{\text{ss}}\|_{\text{TV}} = d(t),
 \end{aligned} \tag{C.17}$$

which concludes our preliminary demonstration. Note that in particular, Eq. (C.15) implies that

$$\|\mu P^{t+1} - \nu P^t\|_{\text{TV}} \leq \|\mu P^t - \nu P^{t-1}\|_{\text{TV}} \leq \dots \leq \|\mu P - \nu\|_{\text{TV}}. \tag{C.18}$$

This inequality will be useful later.

C3.2 Proof of Eq. (C.1)

Following [173], we start by observing that

$$d(t) = \sup_{\mu} \|\mu P^t - \pi_{\text{ss}}\|_{\text{TV}} \geq \|\mu P^t - \pi_{\text{ss}}\|_{\text{TV}} \equiv d_S(t) \tag{C.19}$$

where for a fixed subsets of configuration $S \subseteq \Omega$ we have defined μ_S as $\pi_S / \pi_{\text{ss}}(S)$, with

$$\pi_S(i) \equiv \begin{cases} 0 & \text{if } i \notin S \\ \pi_{\text{ss}}(i) & \text{if } i \in S \end{cases} \tag{C.20}$$

Since $d(t) \geq d_S(t)$ and $d(t+1) \leq d(t)$, $d_S(t+1) \leq d_S(t)$, we have $t_{\text{mix}} \geq t_S$, with $d_S(t_S) \equiv 1/4$. Therefore, we can find a lower bound by estimating t_S and maximizing this time over all the set S such that $\pi(S) \leq 1/2$, to make a connection with the conductance.

Using the triangle inequality for $\|\cdot\|_{\text{TV}}$, we have

$$\|\mu_S P^t - \pi_{\text{ss}}\|_{\text{TV}} + \|\mu_S P^t - \mu_S\|_{\text{TV}} \geq \|\mu_S - \pi\|_{\text{TV}} \tag{C.21}$$

Taking $t = t_S$, the inequality becomes, by definition of t_S

$$\frac{1}{4} + \|\mu_S P^{t_S} - \mu_S\|_{\text{TV}} \geq \|\mu_S - \pi\|_{\text{TV}} \quad (\text{C.22})$$

The term on the right hand side can be estimated as follows

$$\begin{aligned} \|\mu_S - \pi\|_{\text{TV}} &= \frac{1}{2} \sum_{i \in \Omega} |\mu_S - \pi_{\text{ss}}(i)| \\ &= \sum_{\substack{i \in \Omega \\ \mu_S(i) \leq \pi(i)}} [\pi(i) - \mu_S(i)] \\ &= \sum_{i \in S^c} \pi(i) = 1 - \pi(S) \geq \frac{1}{2} \end{aligned} \quad (\text{C.23})$$

The second term on the left hand side of Eq. (C.22) is bounded by the ergodic flow of S ,

$$\|\mu_S P^{t_S} - \mu_S\|_{\text{TV}} \leq t_S \Phi(S). \quad (\text{C.24})$$

Physically, this means that the conductance imposes an upper limit to the rate at which $\mu_S P^t$ drifts away from its initial condition as the Markov chain evolves in time. To see this consider

$$\begin{aligned} \|\mu_S P^{t_S} - \mu_S\|_{\text{TV}} &= \left\| \sum_{r=0}^{t_S-1} \mu_S P^{r+1} - \mu_S P^r \right\|_{\text{TV}} \\ &\leq \sum_{r=0}^{t_S-1} \|\mu_S P^{r+1} - \mu_S P^r\|_{\text{TV}} \\ &\leq t_S \|\mu_S P - \mu_S\|_{\text{TV}} \end{aligned} \quad (\text{C.25})$$

where in the last passage we made use of Eq. (C.18).

$$t_S \|\mu_S P - \mu_S\|_{\text{TV}} = t_S \sum_{\substack{i \in \Omega \\ \mu_S P(i) \geq \mu_S(i)}} \mu_S P(i) - \mu_S(i) \quad (\text{C.26})$$

From the definition of μ_S in Eq. (C.20), we see that the inequality $\mu_S P(i) \geq \mu_S(i)$ is true if and only if $i \notin S$. The equation above reduces to

$$\begin{aligned} t_S \|\mu_S P - \mu_S\|_{\text{TV}} &= t_S \sum_{i \in S^c} \mu_S P(i) - \mu_S(i) \\ &= t_S \sum_{i \in S^c} \sum_{j \in S} \mu_S(j) P(j, i) - \mu_S(i) \\ &= t_S \frac{\sum_{i \in S^c} \sum_{j \in S} \mu_S(j) P(j, i)}{\pi_{\text{ss}}(S)} \\ &= t_S \Phi(S). \end{aligned} \quad (\text{C.27})$$

When passing from the second to the third line, we have used the definition of μ_S , and the fact that $\mu_S(i) = 0$ if $i \in S^c$. We have thus proved Eq. (C.24). The triangle inequality in Eq. (C.22) thus becomes

$$t_S \geq \frac{1}{4\Phi(S)} \quad (\text{C.28})$$

A minimization over S yields the desired result

$$t_{\text{mix}} \geq \sup_{S|\pi_{\text{ss}}(S) \leq 1/2} t_S \geq \sup_{S|\pi_{\text{ss}}(S) \leq 1/2} \frac{1}{4\Phi(S)} = \frac{1}{4\Phi^*}, \quad (\text{C.29})$$

and we have completed the proof. The constant C in Eq. (C.1) is thus $C = 1/4$.

APPENDIX D

p-SPIN WITH ICHIKI-OHZEKI DYNAMICS

D1 Dynamical equations for the *p*-spin evolving under the IO dynamics

We consider two copies of the spherical *p*-spin model evolving according to the Ichiki-Ohzeki (IO) dynamics, for which the equations of motion read

$$\partial_t \sigma_i^{(1)} = -\frac{\partial \mathcal{H}}{\partial \sigma_i^{(1)}} + \gamma \frac{\partial \mathcal{H}}{\partial \sigma_i^{(2)}} - \mu^{(1)}(t) \sigma_i^{(1)} + \gamma \mu^{(2)}(t) \sigma_i^{(2)} + \sqrt{2T} \xi_i^{(1)} \quad (\text{D.1})$$

$$\partial_t \sigma_i^{(2)} = -\frac{\partial \mathcal{H}}{\partial \sigma_i^{(2)}} - \gamma \frac{\partial \mathcal{H}}{\partial \sigma_i^{(1)}} - \mu^{(2)}(t) \sigma_i^{(2)} - \gamma \mu^{(1)}(t) \sigma_i^{(1)} + \sqrt{2T} \xi_i^{(2)} \quad (\text{D.2})$$

where $\mu^{(a)}(t)$ are elastic constants that enforce the spherical constraints $\sum_{i=1}^N \left\langle \left(\sigma_i^{(a)} \right)^2(t) \right\rangle = N$ for $a = 1, 2$, $\xi_i^{(a)}$ are independent Gaussian white noises $\left\langle \xi_i^{(a)}(t) \xi_j^{(b)}(t') \right\rangle = \delta_{ab} \delta_{ij} \delta(t - t')$ and the total Hamiltonian of the system \mathcal{H} reads

$$\mathcal{H} \left[\{\sigma_i\}_{i=1,\dots,N,a=1,2}^{(a)} \right] = - \sum_{i_1 < \dots < i_p} J_{i_1 \dots i_p} \sum_{a=1,2} \sigma_{i_1}^{(a)} \dots \sigma_{i_p}^{(a)} \quad (\text{D.3})$$

Note that the couplings $J_{i_1 \dots i_p}$ have the same realization for both systems, and they are independently distributed according to a Gaussian distribution of mean 0 and variance $\frac{p!}{2N^{p-1}}$.

We suppose that the systems start from an initial equilibrium condition at a temperature $T \equiv \beta^{-1}$, which is kept constant throughout the dynamical evolution. Our goal is to derive effective dynamical equations of motion for the spins in the two system by averaging over the disorder. To achieve this, we use standard path integral techniques as carried out in [67] and further detailed in [14] or [56]. The starting point is the partition function for the dynamics of the composite system in Eq. (D.1) at temperature T . The initial condition for the two subsystems is given by two independent

realization of the Boltzmann distribution at temperature T . We have therefore

$$1 \equiv Z = \int \mathcal{D}\boldsymbol{\sigma}_0 \frac{1}{Z_{\text{eq}}} e^{-\beta \mathcal{H}[\sigma_0^{(1)}, \sigma_0^{(2)}]} \\ \times \int \mathcal{D}\boldsymbol{\sigma} \mathcal{D}\hat{\boldsymbol{\sigma}} \exp \left[-\sum_{i=1}^N \int_0^t d\tau \hat{\sigma}_i^{(1)} \left(\partial_\tau \sigma_i^{(1)} + \frac{\partial \mathcal{H}}{\partial \sigma_i^{(1)}} - \gamma \frac{\partial \mathcal{H}}{\partial \sigma_i^{(2)}} + \mu^{(1)} \sigma_i^{(1)} - \gamma \mu^{(2)} \sigma_i^{(2)} \right) \right. \\ \left. + \hat{\sigma}_i^{(2)} \left(\partial_\tau \sigma_i^{(2)} + \frac{\partial \mathcal{H}}{\partial \sigma_i^{(2)}} + \gamma \frac{\partial \mathcal{H}}{\partial \sigma_i^{(1)}} + \mu^{(2)} \sigma_i^{(2)} + \gamma \mu^{(1)} \sigma_i^{(2)} \right) - T (\hat{\sigma}_i^{(1)})^2 - T (\hat{\sigma}_i^{(2)})^2 \right] \quad (\text{D.4})$$

with Z_{eq} the static partition function of the system, $Z_{\text{eq}} \equiv \int \mathcal{D}\boldsymbol{\sigma}_0 e^{-\beta \mathcal{H}[\boldsymbol{\sigma}_0]}$. We are using a vector notation for the spin variables, $\boldsymbol{\sigma}(t) = (\sigma^{(1)}(t), \sigma^{(2)}(t))^T$, the auxiliary field $\hat{\boldsymbol{\sigma}}(t) = (\hat{\sigma}^{(1)}(t), \hat{\sigma}^{(2)}(t))^T$ and the initial condition $\boldsymbol{\sigma}_0(t) = (\sigma^{(1)}(0), \sigma^{(2)}(0))^T$. As noted in [132], since we are using thermalized initial conditions, we must resort to the replica trick in order to average Z over the disorder:

$$\frac{1}{Z_{\text{eq}}} = \lim_{n \rightarrow 0} Z_{\text{eq}}^{n-1} \quad (\text{D.5})$$

and follow the dynamics of each replica. However, since the initial condition belongs to the replica symmetric phase, the dynamics of the different replicas are decoupled and it suffices to follow the behavior of any single one among them. By using notation of the form $(\sigma^{(a)} \cdot \sigma^{(b)}) (t, t') \equiv \sum_{i=1}^N \sigma_i^{(a)}(t) \sigma_i^{(b)}(t')$, with a and b indices identifying the two systems, we can write in the thermodynamic limit

$$\overline{Z} = \int \mathcal{D}\boldsymbol{\sigma}(0) \mathcal{D}\boldsymbol{\sigma} \mathcal{D}\hat{\boldsymbol{\sigma}} \exp \left\{ -\sum_{i=1}^N \left[\int d\tau \hat{\sigma}_i^{(1)} \left(\partial_\tau \sigma_i^{(1)} + \mu^{(1)} \sigma_i^{(1)} - \gamma \mu^{(2)} \sigma_i^{(2)} \right) - T (\hat{\sigma}_i^{(1)})^2 \right. \right. \\ \left. \left. + \hat{\sigma}_i^{(2)} \left(\partial_\tau \sigma_i^{(2)} + \mu^{(2)} \sigma_i^{(2)} + \gamma \mu^{(1)} \sigma_i^{(1)} \right) - T (\hat{\sigma}_i^{(2)})^2 \right] \right. \\ \left. + \frac{1}{4N^{p-1}} \int dt \int dt' I_1(t, t') + \frac{1}{4TN^{p-1}} \int dt I_2(t) \right\} \quad (\text{D.6})$$

With

$$\begin{aligned}
 I_1(t, t') &\equiv p \left(\hat{\sigma}^{(1)} \cdot \hat{\sigma}^{(1)} \right) \left(\sigma^{(1)} \cdot \sigma^{(1)} \right)^{p-1} + p(p-1) \left(i\hat{\sigma}^{(1)} \cdot \sigma^{(1)} \right) \left(\sigma^{(1)} \cdot \hat{\sigma}^{(1)} \right) \left(\sigma^{(1)} \cdot \sigma^{(1)} \right)^{p-2} \\
 &\quad - \gamma \left[p \left(\hat{\sigma}^{(1)} \cdot \hat{\sigma}^{(1)} \right) \left(\sigma^{(1)} \cdot \sigma^{(2)} \right)^{p-1} + p(p-1) \left(\hat{\sigma}^{(1)} \cdot \sigma^{(2)} \right) \left(\sigma^{(1)} \cdot \hat{\sigma}^{(1)} \right) \left(\sigma^{(1)} \cdot \sigma^{(2)} \right)^{p-2} \right] \\
 &\quad + p \left(\hat{\sigma}^{(1)} \cdot \hat{\sigma}^{(2)} \right) \left(\sigma^{(1)} \cdot \sigma^{(2)} \right)^{p-1} + p(p-1) \left(\hat{\sigma}^{(1)} \cdot \sigma^{(2)} \right) \left(\sigma^{(1)} \cdot \hat{\sigma}^{(2)} \right) \left(\sigma^{(1)} \cdot \sigma^{(2)} \right)^{p-2} \\
 &\quad + \gamma \left[p \left(\hat{\sigma}^{(1)} \cdot \hat{\sigma}^{(2)} \right) \left(\sigma^{(1)} \cdot \sigma^{(1)} \right)^{p-1} + p(p-1) \left(\hat{\sigma}^{(1)} \cdot \sigma^{(1)} \right) \left(\sigma^{(1)} \cdot \hat{\sigma}^{(2)} \right) \left(\sigma^{(1)} \cdot \sigma^{(1)} \right)^{p-2} \right] \\
 &\quad - \gamma \left[p \left(\hat{\sigma}^{(1)} \cdot \hat{\sigma}^{(1)} \right) \left(\sigma^{(2)} \cdot \sigma^{(1)} \right)^{p-1} + p(p-1) \left(\hat{\sigma}^{(1)} \cdot \sigma^{(1)} \right) \left(\sigma^{(2)} \cdot \hat{\sigma}^{(1)} \right) \left(\sigma^{(2)} \cdot \sigma^{(1)} \right)^{p-2} \right] \\
 &\quad + \gamma^2 \left[p \left(\hat{\sigma}^{(1)} \cdot \hat{\sigma}^{(1)} \right) \left(\sigma^{(2)} \cdot \sigma^{(2)} \right)^{p-1} + p(p-1) \left(\hat{\sigma}^{(1)} \cdot \sigma^{(2)} \right) \left(\sigma^{(2)} \cdot \hat{\sigma}^{(1)} \right) \left(\sigma^{(2)} \cdot \sigma^{(2)} \right)^{p-2} \right] \\
 &\quad - \gamma \left[p \left(\hat{\sigma}^{(1)} \cdot \hat{\sigma}^{(2)} \right) \left(\sigma^{(2)} \cdot \sigma^{(2)} \right)^{p-1} + p(p-1) \left(\hat{\sigma}^{(1)} \cdot \sigma^{(2)} \right) \left(\sigma^{(2)} \cdot \hat{\sigma}^{(2)} \right) \left(\sigma^{(2)} \cdot \sigma^{(2)} \right)^{p-2} \right] \\
 &\quad - \gamma^2 \left[p \left(\hat{\sigma}^{(1)} \cdot \hat{\sigma}^{(2)} \right) \left(\sigma^{(2)} \cdot \sigma^{(1)} \right)^{p-1} + p(p-1) \left(\hat{\sigma}^{(1)} \cdot \sigma^{(1)} \right) \left(\sigma^{(2)} \cdot \hat{\sigma}^{(2)} \right) \left(\sigma^{(2)} \cdot \sigma^{(1)} \right)^{p-2} \right] \\
 &\quad + (1 \leftrightarrow 2, \gamma \leftrightarrow -\gamma)
 \end{aligned} \tag{D.7}$$

and

$$\begin{aligned}
 \frac{1}{2} I_2(t, 0) &\equiv p \left(\hat{\sigma}^{(1)} \cdot \sigma_0^{(1)} \right) \left(\sigma^{(1)} \cdot \sigma_0^{(1)} \right)^{p-1} - \gamma p \left(\hat{\sigma}^{(1)} \cdot \sigma_0^{(1)} \right) \left(\sigma^{(2)} \cdot \sigma_0^{(1)} \right)^{p-1} \\
 &\quad + p \left(\hat{\sigma}^{(1)} \cdot \sigma_0^{(2)} \right) \left(\sigma^{(1)} \cdot \sigma_0^{(2)} \right)^{p-1} - \gamma p \left(\hat{\sigma}^{(1)} \cdot \sigma_0^{(2)} \right) \left(\sigma^{(2)} \cdot \sigma_0^{(2)} \right)^{p-1} \\
 &\quad + (1 \leftrightarrow 2, \gamma \leftrightarrow -\gamma)
 \end{aligned} \tag{D.8}$$

We now exploit the thermodynamic limit $N \rightarrow \infty$ through a saddle point evaluation of the path integral. In order to do so, we introduce a set of dynamical overlaps in the partition function:

$$\begin{aligned}
 \bar{Z} &= \int \mathcal{D}\mathbf{Q} \Pi_{a,b=1,2} \delta \left(NQ_1^{(ab)}(t, t') - \hat{\sigma}^{(a)} \cdot \hat{\sigma}^{(b)} \right) \delta \left(NQ_2^{(ab)}(t, t') - \sigma^{(a)} \cdot \sigma^{(b)} \right) \\
 &\quad \times \delta \left(NQ_3^{(ab)}(t, t') - \hat{\sigma}^{(a)} \cdot \sigma^{(b)} \right) \delta \left(NQ_4^{(ab)}(t, t') - \sigma^{(a)} \cdot \hat{\sigma}^{(b)} \right) \\
 &\quad \times \delta \left(NQ_5^{(ab)}(t) - \hat{\sigma}^{(a)} \cdot \sigma_0^{(b)} \right) \times \delta \left(NQ_6^{(ab)}(t) - \sigma^{(a)} \cdot \sigma_0^{(b)} \right) \times (\text{r.h.s. Eq. (D.6)}) \\
 &= \int \mathcal{D}\mathbf{P} \int \mathcal{D}\mathbf{Q} \Pi_{a,b=1,2} \exp \left[iN \int dt dt' \left(P_1^{(ab)}(t, t') Q_1^{(ab)} - P_1^{(ab)}(t, t') \hat{\sigma}^{(a)} \cdot \hat{\sigma}^{(b)} \right) \right] \\
 &\quad \times \exp \left[iN \int dt dt' \left(P_2^{(ab)} Q_2^{(ab)} - P_2^{(ab)} \sigma^{(a)} \cdot \sigma^{(b)} \right) \right] \\
 &\quad \times \exp \left[iN \int dt dt' \left(P_3^{(ab)}(t, t') Q_3^{(ab)} - P_3^{(ab)} \hat{\sigma}^{(a)} \cdot \sigma^{(b)} \right) \right] \\
 &\quad \times \exp \left[iN \int dt dt' \left(P_4^{(ab)}(t, t') Q_4^{(ab)} - P_4^{(ab)} \sigma^{(a)} \cdot \hat{\sigma}^{(b)} \right) \right] \\
 &\quad \times \exp \left[iN \int dt \left(P_5^{(ab)} Q_5^{(ab)} - P_5^{(ab)} \hat{\sigma}^{(a)} \cdot \sigma_0^{(b)} \right) \right] \\
 &\quad \times \exp \left[iN \int dt \left(P_6^{(ab)} Q_6^{(ab)} - P_6^{(ab)} \sigma^{(a)} \cdot \sigma_0^{(b)} \right) \right] \times (\text{r.h.s of Eq. (D.6)})
 \end{aligned} \tag{D.9}$$

The dynamical overlaps have a natural interpretation if one introduces the correlation and the response matrices $\mathbf{C}(t, t')$ and $\mathbf{R}(t, t')$:

$$C_{ab}(t, t') \equiv \frac{1}{N} \sum_i \langle \sigma_i^{(a)}(t) \sigma_i^{(b)}(t') \rangle \quad (\text{D.10})$$

$$R_{ab}(t, t') \equiv \frac{1}{N} \sum_i \langle \sigma_i^{(a)}(t) \hat{\sigma}_i^{(b)}(t') \rangle \quad (\text{D.11})$$

We therefore see that in the thermodynamic limit the following self consistent relations hold:

$$\begin{cases} Q_2^{(ab)}(t, t') &= C_{ab}(t, t') \\ Q_3^{(ab)}(t, t') &= R_{ab}(t', t) \\ Q_4^{(ab)}(t, t') &= R_{ab}(t, t') \\ Q_5^{(ab)}(t) &= C_{ab}(t, 0) \\ Q_6^{(ab)}(t) &= R_{ab}(t, 0) \end{cases} \quad (\text{D.12})$$

Note that $Q_3^{(ab)}(t, t') = Q_4^{(ba)}(t', t)$. Moreover, we claim that, as in the standard case [241], $Q_1^{(ab)} = 0$. The saddle point equations are obtained by differentiating the argument of the exponentials in Eq. (D.6) with respect to the set of dynamical overlaps

$Q_i^{(ab)}$ and they read:

$$\left\{
 \begin{array}{ll}
 iP_1^{(11)} &= \frac{p}{4}Q_2^{(11)p-1} - \gamma\frac{p}{4}\left(Q_2^{(12)p-1} + Q_2^{(21)p-1}\right) + \gamma^2\frac{p}{4}Q_2^{(22)p-1} \\
 iP_2^{(11)} &= 0 \\
 iP_3^{(11)} &= \frac{p}{4}(p-1)Q_4^{(11)}Q_2^{(11)p-2} + \gamma\frac{p}{4}(p-1)Q_4^{(12)}Q_2^{(11)p-2} \\
 &\quad - \gamma\frac{p}{4}(p-1)Q_4^{(21)}Q_2^{(21)p-2} - \gamma^2\frac{p}{4}(p-1)Q_4^{(11)}Q_2^{(21)p-2} \\
 iP_4^{(11)} &= \frac{p}{4}(p-1)Q_3^{(11)}Q_2^{(11)p-2} + \gamma\frac{p}{4}(p-1)Q_3^{(21)}Q_2^{(11)p-2} \\
 &\quad - \gamma\frac{p}{4}(p-1)Q_3^{(12)}Q_2^{(12)p-2} - \gamma^2\frac{p}{4}(p-1)Q_3^{(11)}Q_2^{(12)p-2} \\
 iP_5^{(11)} &= \frac{p}{2T}Q_5^{(11)} - \gamma\frac{p}{2T}Q_5^{(21)} \\
 iP_6^{(11)} &= 0 \\
 \\
 iP_1^{(12)} &= \frac{p}{4}Q_2^{(12)p-1} - \gamma\frac{p}{4}\left(Q_2^{(22)p-1} - Q_2^{(11)p-1}\right) - \gamma^2\frac{p}{4}Q_2^{(22)p-1} \\
 iP_2^{(12)} &= 0 \\
 iP_3^{(12)} &= \frac{p}{4}(p-1)Q_4^{(12)}Q_2^{(12)p-2} - \gamma\frac{p}{4}(p-1)Q_4^{(11)}Q_2^{(12)p-2} - \\
 &\quad \gamma\frac{p}{4}(p-1)Q_4^{(22)}Q_2^{(22)p-2} + \gamma^2\frac{p}{4}(p-1)Q_4^{(21)}Q_2^{(22)p-2} \\
 iP_4^{(12)} &= \frac{p}{4}(p-1)Q_3^{(12)}Q_2^{(12)p-2} + \gamma\frac{p}{4}(p-1)Q_3^{(11)}Q_2^{(11)p-2} \\
 &\quad + \gamma\frac{p}{4}(p-1)Q_3^{(22)}Q_2^{(12)p-2} + \gamma^2\frac{p}{4}(p-1)Q_3^{(21)}Q_2^{(11)p-2} \\
 iP_5^{(12)} &= \frac{p}{2T}Q_5^{(12)} - \gamma\frac{p}{2T}Q_5^{(22)} \\
 iP_6^{(12)} &= 0 \\
 \\
 iP_1^{(21)} &= \frac{p}{4}Q_2^{(21)p-1} - \gamma\frac{p}{4}\left(Q_2^{(11)p-1} - Q_2^{(22)p-1}\right) - \gamma^2\frac{p}{4}Q_2^{(12)p-1} \\
 iP_2^{(21)} &= 0 \\
 iP_3^{(21)} &= \frac{p}{4}(p-1)Q_4^{(21)}Q_2^{(21)p-2} + \gamma\frac{p}{4}(p-1)Q_4^{(11)}Q_2^{(11)p-2} \\
 &\quad + \gamma\frac{p}{4}(p-1)Q_4^{(22)}Q_2^{(21)p-2} + \gamma^2\frac{p}{4}(p-1)Q_4^{(12)}Q_2^{(11)p-2} \\
 iP_4^{(21)} &= \frac{p}{4}(p-1)Q_3^{(21)}Q_2^{(21)p-2} - \gamma\frac{p}{4}(p-1)Q_3^{(11)}Q_2^{(21)p-2} \\
 &\quad - \gamma\frac{p}{4}(p-1)Q_3^{(22)}Q_2^{(12)p-2} + \gamma^2\frac{p}{4}(p-1)Q_3^{(12)}Q_2^{(22)p-2} \\
 iP_5^{(21)} &= \frac{p}{2T}Q_5^{(21)} + \gamma\frac{p}{2T}Q_5^{(11)} \\
 iP_6^{(21)} &= 0 \\
 \\
 iP_1^{(22)} &= \frac{p}{4}Q_2^{(22)p-1} + \gamma\frac{p}{4}\left(Q_2^{(12)p-1} + Q_2^{(21)p-1}\right) + \gamma^2\frac{p}{4}Q_2^{(11)p-1} \\
 iP_2^{(22)} &= 0 \\
 iP_3^{(22)} &= \frac{p}{4}(p-1)Q_4^{(22)}Q_2^{(22)p-2} - \gamma\frac{p}{4}(p-1)Q_4^{(21)}Q_2^{(22)p-2} \\
 &\quad + \gamma\frac{p}{4}(p-1)Q_4^{(12)}Q_2^{(12)p-2} - \gamma^2\frac{p}{4}(p-1)Q_4^{(22)}Q_2^{(12)p-2} \\
 iP_4^{(22)} &= \frac{p}{4}(p-1)Q_3^{(22)}Q_2^{(22)p-2} - \gamma\frac{p}{4}(p-1)Q_3^{(12)}Q_2^{(22)p-2} \\
 &\quad + \gamma\frac{p}{4}(p-1)Q_3^{(21)}Q_2^{(21)p-2} - \gamma^2\frac{p}{4}(p-1)Q_3^{(22)}Q_2^{(21)p-2} \\
 iP_5^{(22)} &= \frac{p}{2T}Q_5^{(22)} + \gamma\frac{p}{2T}Q_5^{(12)} \\
 iP_6^{(22)} &= 0
 \end{array}
 \right. \tag{D.13}$$

Note that $iP_2 = iP_6 = 0$ because $Q_1 = 0$ and because of causality, which implies that $Q_3^{(ab)}(t, t')Q_4^{(ab)}(t, t') = 0$. Substitution of the saddle point expressions of Eq. (D.13) in Eq. (D.9), together with Eq. (D.12) yields the effective dynamical equations for the spins of the system. Using a vector notation, $\boldsymbol{\sigma}(t) = [\sigma^{(1)} \quad \sigma^{(2)}]^T$, we obtain

$$\partial_t \boldsymbol{\sigma}(t) = -(\mathbf{1}_2 + \gamma \mathbf{A}) \cdot \boldsymbol{\mu}(t) \cdot \boldsymbol{\sigma}(t) + \int_0^t d\tau \mathbf{M}_{\mathbf{R}}(t, \tau) \cdot \boldsymbol{\sigma}(\tau) + \frac{1}{T} (\mathbf{1}_2 + \gamma \mathbf{A}) \cdot \mathbf{C}_0(p, t) \cdot \boldsymbol{\sigma}(0) + \boldsymbol{\Xi}(t) \quad (\text{D.14})$$

where $\mu_{ab}(t) \equiv \delta_{ab}\mu^{(a)}(t)$, and the correlations of the noise $\boldsymbol{\Xi}(t)$ are

$$\langle \boldsymbol{\Xi}(t) \boldsymbol{\Xi}(t') \rangle = 2T\delta(t - t')\mathbf{1}_2 + \mathbf{D}(t, t') \quad (\text{D.15})$$

while the expression for the memory kernel $\mathbf{M}_{\mathbf{R}}(t, t')$, the noise correlations $\mathbf{D}(t, t')$ and the coupling with the initial conditions $\mathbf{C}_0(t, 0)$ are the following:

$$\begin{aligned} \mathbf{M}_{\mathbf{R}}(t, \tau) &= \frac{p(p-1)}{2} \\ &\times \begin{bmatrix} C_{11}^{p-2}(R_{11} + \gamma R_{12}) - \gamma C_{21}^{p-2}(R_{21} + \gamma R_{22}) & C_{12}^{p-2}(R_{12} - \gamma R_{11}) - \gamma C_{22}^{p-2}(R_{22} - \gamma R_{21}) \\ C_{21}^{p-2}(R_{21} + \gamma R_{22}) + \gamma C_{11}^{p-2}(R_{11} + \gamma R_{12}) & C_{22}^{p-2}(R_{22} - \gamma R_{21}) + \gamma C_{12}^{p-2}(R_{12} - \gamma R_{11}) \end{bmatrix} \end{aligned} \quad (\text{D.16})$$

$$\mathbf{D}(t, t') \equiv (\mathbf{1}_2 + \gamma \mathbf{A}) \cdot \mathbf{C}_0(p, t) \cdot (\mathbf{1}_2 + \gamma \mathbf{A}^T) \quad (\text{D.17})$$

$$C_0(p, t, 0)_{ij} = \frac{p}{2} C_{ij}^{p-1}(t, 0) \quad (\text{D.18})$$

From Eq. (D.14) by using the definition (D.10) and the equalities

$$R_{ab}(t, t') = \left\langle \frac{\delta \sigma^{(a)}(t)}{\delta \xi^{(b)}(t')} \right\rangle \quad (\text{D.19})$$

$$\langle \xi^{(a)}(t) \sigma^{(b)}(t') \rangle = 2T R_{ba}(t', t) + \int d\tau [\mathbf{D}(t, \tau) \cdot \mathbf{R}^T(t', \tau)]_{ab} \quad (\text{D.20})$$

we obtain

$$\partial_t \mathbf{R}(t, t') = -(\mathbf{1}_2 + \gamma \mathbf{A}) \cdot \boldsymbol{\mu}(t) \cdot \mathbf{R}(t, t') + \int_{t'}^t d\tau \mathbf{M}_{\mathbf{R}}(t, \tau) \cdot \mathbf{R}(\tau, t') + \delta(t - t')\mathbf{1}_2 \quad (\text{D.21})$$

$$\begin{aligned} \partial_t \mathbf{C}(t, t') &= -(\mathbf{1}_2 + \gamma \mathbf{A}) \cdot \boldsymbol{\mu}(t) \cdot \mathbf{C}(t, t') + \int_0^t d\tau \mathbf{M}_{\mathbf{R}}(t, \tau) \cdot \mathbf{C}(\tau, t') + 2T \mathbf{R}^T(t', t) \\ &+ \int_0^{t'} d\tau \mathbf{D}(t, \tau) \cdot \mathbf{R}^T(t', \tau) + \frac{1}{T} (\mathbf{1}_2 + \gamma \mathbf{A}) \cdot \mathbf{C}_0(p, t) \cdot \mathbf{C}(0, t') \end{aligned} \quad (\text{D.22})$$

By imposing the spherical constraint $\sum_{i=1}^N \left\langle \left(\sigma_i^{(a)} \right)^2(t) \right\rangle = N$ for $a = 1, 2$ one can find a self-consistent expression for the restoring forces $\boldsymbol{\mu}(t)$. If we denote the diagonal part of a matrix by $\text{Diag}(\mathbf{A})_{ab} \equiv \delta_{ab} A_{ab}$ the spherical constraint condition reads $\text{Diag}(\mathbf{C}(t, t)) = 1$. By differentiating with respect to t we get

$$\lim_{t' \rightarrow t} \text{Diag}(\partial_t \mathbf{C}(t, t') + \partial_{t'} \mathbf{C}(t, t')) = \lim_{t' \rightarrow t} \text{Diag}(\partial_t \mathbf{C}(t, t') + \partial_{t'} \mathbf{C}^T(t', t)) = 0 \quad (\text{D.23})$$

which leads to

$$\begin{aligned} \boldsymbol{\mu}(t) = & \text{Diag} \left[T\mathbf{1}_2 + \int_0^t d\tau \mathbf{M}(t, \tau) \cdot \mathbf{C}^T(t, \tau) + \int_0^t d\tau \mathbf{D}(t, \tau) \cdot \mathbf{R}^T(t, \tau) \right. \\ & \left. + \frac{1}{T} (\mathbf{1}_2 + \gamma \mathbf{A}) \cdot \mathbf{C}_0(p, t) \cdot \mathbf{C}^T(t, 0) \right] \end{aligned} \quad (\text{D.24})$$

Since the dynamics of the system starts within the steady state, we assume that time translation invariance holds: $\mathbf{C}(t, t') \equiv \mathbf{C}(t - t')$ and $\mathbf{R}(t, t') \equiv \mathbf{R}(t - t')$. The equations of motion for the response and correlation matrices therefore read, when taking $t' = 0$

$$\partial_t \mathbf{R}(t) = -(\mathbf{1}_2 + \gamma \mathbf{A}) \cdot \boldsymbol{\mu}(t) \cdot \mathbf{R}(t) + \int_{t'}^t d\tau \mathbf{M}_{\mathbf{R}}(t - \tau) \cdot \mathbf{R}(\tau) + \delta(t) \mathbf{1}_2 \quad (\text{D.25})$$

$$\begin{aligned} \partial_t \mathbf{C}(t) = & -(\mathbf{1}_2 + \gamma \mathbf{A}) \cdot \boldsymbol{\mu}(t) \cdot \mathbf{C}(t) + \int_0^t d\tau \mathbf{M}_{\mathbf{R}}(t - \tau) \cdot \mathbf{C}(\tau) + \frac{1}{T} (\mathbf{1}_2 + \gamma \mathbf{A}) \cdot \mathbf{C}_0(p, t) \\ & \quad (\text{D.26}) \end{aligned}$$

$$\begin{aligned} \boldsymbol{\mu}(t) = & \text{Diag} \left[T\mathbf{1}_2 + \int_0^t d\tau \mathbf{M}(t - \tau) \cdot \mathbf{C}^T(t - \tau) + \int_0^t d\tau \mathbf{D}(t - \tau) \cdot \mathbf{R}^T(t - \tau) \right. \\ & \left. + \frac{1}{T} (\mathbf{1}_2 + \gamma \mathbf{A}) \cdot \mathbf{C}_0(p, t) \cdot \mathbf{C}^T(t) \right] \\ & \quad (\text{D.27}) \end{aligned}$$

For numerical purposes it is more convenient to work with the integrated response matrix $\mathbf{F}(t, t')$ [155], defined by

$$F_{ab}(t, t') \equiv - \int_{t'}^t d\tau R_{ab}(t, \tau) \quad (\text{D.28})$$

since it has a smoother relaxation than $\mathbf{R}(t, t')$. The equations of motion in the time translation invariant regime are

$$\partial_t \mathbf{F}(t) = -\mathbf{1}_2 - (\mathbf{1}_2 + \gamma \mathbf{A}) \cdot \boldsymbol{\mu}(t) \cdot \mathbf{F}(t) + \int_{t'}^t d\tau \mathbf{M}_{\mathbf{F}}(t - \tau) \cdot \mathbf{F}(\tau) \quad (\text{D.29})$$

$$\begin{aligned} \partial_t \mathbf{C}(t) = & -(\mathbf{1}_2 + \gamma \mathbf{A}) \cdot \boldsymbol{\mu}(t) \cdot \mathbf{C}(t) + \int_0^t d\tau \mathbf{M}_{\mathbf{F}}(t - \tau) \cdot \mathbf{C}(\tau) + \frac{1}{T} (\mathbf{1}_2 + \gamma \mathbf{A}) \cdot \mathbf{C}_0(p, t) \\ & \quad (\text{D.30}) \end{aligned}$$

$$\begin{aligned} \boldsymbol{\mu}(t) = & \text{Diag} \left[T\mathbf{1}_2 + \int_0^t d\tau \mathbf{M}_{\mathbf{F}}(t - \tau) \cdot \mathbf{C}^T(t - \tau) + \int_0^t d\tau \mathbf{D}(t - \tau) \cdot \partial_{\tau} \mathbf{F}^T(t - \tau) \right. \\ & \left. + \frac{1}{T} (\mathbf{1}_2 + \gamma \mathbf{A}) \cdot \mathbf{C}_0(p, t) \cdot \mathbf{C}^T(t) \right] \\ & \quad (\text{D.31}) \end{aligned}$$

and the memory kernel $\mathbf{M}_{\mathbf{F}}(t)$ that reads

$$\begin{aligned} \mathbf{M}_{\mathbf{F}}(t - \tau) \equiv & -\frac{p(p-1)}{2} \times \\ & \begin{bmatrix} C_{11}^{p-2} (\partial_{\tau} F_{11} + \gamma \partial_{\tau} F_{12}) - \gamma C_{21}^{p-2} (\partial_{\tau} F_{21} + \gamma \partial_{\tau} F_{22}) & C_{12}^{p-2} (\partial_{\tau} F_{12} - \gamma \partial_{\tau} F_{11}) - \gamma C_{22}^{p-2} (\partial_{\tau} F_{22} - \gamma \partial_{\tau} F_{21}) \\ C_{21}^{p-2} (\partial_{\tau} F_{21} + \gamma \partial_{\tau} F_{22}) + \gamma C_{11}^{p-2} (\partial_{\tau} F_{11} + \gamma \partial_{\tau} F_{12}) & C_{22}^{p-2} (\partial_{\tau} F_{22} - \gamma \partial_{\tau} F_{21}) + \gamma C_{12}^{p-2} (\partial_{\tau} F_{12} - \gamma \partial_{\tau} F_{11}) \end{bmatrix} \end{aligned} \quad (\text{D.32})$$

the companion initial conditions are $\mathbf{C}(0) \equiv \mathbf{1}_2$, $\mathbf{F}(0) = \mathbf{0}$. Together with Eq. (D.14), these equations correspond to Eqs. (3.5, 3.6, 3.7, 3.8) presented in the main text.

In the following section we provide the reader with some details on the algorithm implemented to integrate the dynamical equations.

D2 Numerical Integration of the dynamical equations

We present here the integration scheme adopted to numerically solve the dynamical equations of motion, Eqs. (D.29, D.30, D.31). The basic idea for the algorithm was first given in [102] in the context of the mode coupling equations. It was then applied to the aging of the p -spin model in [155] and generalised in [27] for the case of non stationary systems. A pedagogical description of the algorithm can be found in [92].

To integrate Eqs. (D.29, D.30, D.31), we take a grid of M points with a discretisation step Δt , so that any function $f(t)$ can be discretised as $f_k \equiv f(t_k)$ with $t_k \equiv k\Delta t$. Suppose that we know the first n value of the correlation and the integrated response along the discretized line and that we want to know their value at the step $n + 1$. By resorting to finite difference approximations, we can obtain a set of non-linear equation for the variable $\mathbf{V}_i \equiv [\mathbf{C}_i \quad \mathbf{F}_i]$ of the form

$$\mathbf{V}_{n+1} = \mathbf{NL}(\mathbf{V}_0, \mathbf{V}_1, \dots, \mathbf{V}_n, \mathbf{V}_{n+1}) \quad (\text{D.33})$$

where \mathbf{NL} is a generic nonlinear operator. This set of equation can be solved iteratively starting from the initial condition $\mathbf{V}_{n+1} = \mathbf{V}_n$. Once convergence is achieved, one can move to the next point along the discretised line. This is the propagation step.

Once all the values of \mathbf{C} and \mathbf{F} have been obtained along the grid, one performs a decimation and a rescaling to compress the information obtained and reach longer times. Half of the points are discarded by performing the substitution $\mathbf{V}_{2i} \rightarrow \mathbf{V}_i$ for $i = 0, \dots, M - 1$ and the time step is rescaled by a factor two, $\Delta t \rightarrow 2\Delta t$. The propagation step is then repeated starting from the point $n + 1 = \frac{M}{2}$. Large times can be quickly achieved by iterating these two steps.

The finite difference approximations that we adopt are the following. For the left hand side of Eqs. (D.29, D.30) the time derivative of a function at step $k + 1$, $\partial_t f_{k+1}$ can be approximated as

$$\partial_t f_{k+1} = \frac{1}{2\Delta t} (3f_{k+1} - 4f_k + f_{k-1}) + O(\Delta t^2) \quad (\text{D.34})$$

while the integrals on the right hand side have the general form

$$I_{n+1} \equiv \int_0^{t_{n+1}} d\tau A(t - \tau) \partial_\tau B(t - \tau) C(\tau) \quad (\text{D.35})$$

$$J_{n+1} \equiv \int_0^{t_{n+1}} d\tau A(t - \tau) \partial_\tau B(t - \tau) C(\tau) \quad (\text{D.36})$$

and they can be approximated as

$$I_{n+1} = \sum_{j=0}^n \frac{1}{4} (A_{n+1-j} + A_{n-j}) (B_{n-j} - B_{n+1-j}) (C_j + C_{j+1}) + O(\Delta t^2) \quad (\text{D.37})$$

$$J_{n+1} = \sum_{j=0}^n \frac{1}{4} (A_{n+1-j} + A_{n-j}) (B_{n-j} - B_{n+1-j}) (C_{n+1-j} + C_{n-j}) + O(\Delta t^2) \quad (\text{D.38})$$

$$(\text{D.39})$$

For the results presented in the main text we have adopted a grid of $M = 1024$ points and an initial timestep of $\Delta t = 10^{-10}$.

D3 aFDT for the IO dynamics of the *p*–spin

We make the following *ansatz* concerning the form of the violation of the FDT for the Twisted Dynamics of the *p*–spin:

$$\frac{1}{T} [\mathbf{C}(t) - \mathbf{C}(0)] = \mathbf{F}(t) \cdot (\mathbf{1}_2 + \gamma \mathbf{A}) \quad (\text{D.40})$$

that is, an analogous form of the FDT relation holds if one looks at the proper combination of response functions. We call this the aFDT relation. In this section we will show that this relation is indeed satisfied by Eqs. (D.29, D.30, D.31). The strategy of the proof is the following: starting from Eqs. (D.30, D.31) and the aFDT we will obtain Eq. (D.29). To do so, we first rewrite Eq. (D.40) in a differential form:

$$\frac{1}{T} \partial_t \mathbf{C}(t) = \partial_t \mathbf{F}(t) \cdot (\mathbf{1}_2 + \gamma \mathbf{A}) \quad (\text{D.41})$$

using Eq. (D.41) we can rewrite the memory kernel \mathbf{M}_F in a simpler form:

$$\mathbf{M}_F(t - \tau) = \frac{1}{T} (\mathbf{1}_2 + \gamma \mathbf{A}) \cdot \partial_\tau \mathbf{C}_0(t - \tau) \quad (\text{D.42})$$

We now proceed to compute the left hand side of Eq. (D.41) using Eq. (D.26):

$$\begin{aligned} \frac{1}{T} \partial_t \mathbf{C}(t) &= -\frac{1}{T} (\mathbf{1}_2 + \gamma \mathbf{A}) \cdot \boldsymbol{\mu}(t) \cdot \mathbf{C}(t) + \frac{1}{T} \int_0^t d\tau \mathbf{M}_F(t - \tau) \cdot \mathbf{C}(\tau) \\ &\quad + \frac{1}{T^2} (\mathbf{1}_2 + \gamma \mathbf{A}) \cdot \mathbf{C}_0(t) \\ &= -(\mathbf{1}_2 + \gamma \mathbf{A}) \cdot \left(\frac{1}{T} \mathbf{1}_2 + \mathbf{F}(t) \cdot (\mathbf{1}_2 + \gamma \mathbf{A}) \right) + \frac{1}{T} \int_0^t d\tau \mathbf{M}_F(t - \tau) \cdot \mathbf{C}(\tau) \\ &\quad + \frac{1}{T^2} (\mathbf{1}_2 + \gamma \mathbf{A}) \cdot \mathbf{C}_0(t) \end{aligned} \quad (\text{D.43})$$

$$\begin{aligned} \boldsymbol{\mu}(t) &= \text{Diag} \left[T \mathbf{1}_2 + \int_0^t d\tau \mathbf{M}_F(t - \tau) \cdot \mathbf{C}^T(t - \tau) + \int_0^t d\tau \mathbf{D}(t - \tau) \cdot \partial_\tau \mathbf{F}^T(t - \tau) \right. \\ &\quad \left. + \frac{1}{T} (\mathbf{1}_2 + \gamma \mathbf{A}) \cdot \mathbf{C}_0(p - 1, t) \cdot \mathbf{C}^T(t) \right] \end{aligned} \quad (\text{D.44})$$

to evaluate the time integral, we can use Eq. (D.42), integration by parts, the aFDT relation and the boundary condition $\mathbf{C}(0) = \mathbf{1}_2$, $\mathbf{F}(0) = \mathbf{0}$ to obtain

$$\frac{1}{T} \int_0^t d\tau \mathbf{M}_{\mathbf{F}}(t - \tau) \cdot \mathbf{C}(\tau) = \frac{1}{T^2} \left(\frac{p}{2} \mathbf{1}_2 - \mathbf{C}_0(t) \right) + \int_0^t d\tau \mathbf{M}_{\mathbf{F}}(t - \tau) \cdot \mathbf{F}(\tau) \cdot (\mathbf{1}_2 + \gamma \mathbf{A}) \quad (\text{D.45})$$

$$\int_0^t d\tau \mathbf{D}(t - \tau) \cdot \partial_{\tau} \mathbf{F}^{\mathbf{T}}(t - \tau) = \frac{1}{2T} (\mathbf{1}_2 + \gamma \mathbf{A}) \cdot \int_0^t d\tau \mathbf{C}_0 \cdot \partial_{\tau} \mathbf{C}^{\mathbf{T}}(\tau) \quad (\text{D.46})$$

$$\int_0^t d\tau \mathbf{M}_{\mathbf{F}}(t - \tau) \cdot \mathbf{C}^{\mathbf{T}}(t - \tau) = \frac{1}{T} \left[\frac{p}{2} \mathbf{1}_2 - \mathbf{C}_0(t) \cdot \mathbf{C}^{\mathbf{T}}(t) - \frac{1}{T} \int_0^t d\tau \mathbf{C}_0(t - \tau) \cdot \partial_{\tau} \mathbf{C}^{\mathbf{T}}(\tau) \right] \quad (\text{D.47})$$

So that $\boldsymbol{\mu}$ reads after simplifying and taking the diagonal part:

$$\boldsymbol{\mu}(t) = \left(T + \frac{p}{2T} \right) \mathbf{1}_2 \equiv \boldsymbol{\mu}_{\infty} \quad (\text{D.48})$$

putting everything back in Eq. (D.43) and simplifying we get that

$$\frac{1}{T} \partial_t \mathbf{C}(t) = \partial_t \mathbf{F}(t) \cdot (\mathbf{1}_2 + \gamma \mathbf{A}) \quad (\text{D.49})$$

with $\partial_t \mathbf{F}(t)$ given by Eq. (D.29), and the proof is completed.

APPENDIX E

CHIRAL ACTIVE BATHS AND SYMMETRIC TRACERS

Over the course of my thesis, due to the expertise developed in the area of nonreciprocal forces and projection operator methods, I have been involved in a research project in chiral active matter. This Appendix presents the topic in a form close to the eventual submission. This work was done in collaboration with Cory Hargus, Julien Tailleur, and Frédéric van Wijland.

Chiral active matter [175] refers to systems of particles that harness energy from the environment and convert it in a form of biased self-propulsion, that breaks the inversion symmetry of the system. It has received much interest in recent years, as a framework to describe a variety of systems in biology and synthetic soft matter, from sperm cells [228] to asymmetrically shaped self-phoretic colloids [260].

Here we ask ourselves how a bath of chiral active matter affects the dynamics of an embedded passive tracer. This applies to its transport properties and possible ratchet effects. In the microscopic world, where fluctuations play an important role, the minimal theoretical ingredients necessary to build a ratchet are well-known: irreversible dynamics coupled to a spatially asymmetric shape or potential can generate directed motion, from which work can be extracted [88, 183]. In the last two decades, microscopic ratchets have been devised using nonequilibrium baths [52, 53, 114] and probes of various shapes. Even more recently, active baths have been used to construct microscopic engines [167, 259]. One spectacular realization is that of a gear with asymmetric (chiral) teeth, which rotates when placed in a bacterial bath [80, 9].

Conversely, even a symmetric object may become a rotational ratchet when placed in a chiral active bath, composed of self-driven particles with a propensity to turn in a particular direction [174]. In this case, the bath itself contains both ingredients, breaking time-reversal and mirror symmetries. Indeed, the breaking of time-reversal and mirror symmetries in the microscopic dynamics permits exotic transport properties

otherwise prohibited by Onsager's reciprocal relations, such as odd transport phenomena [13, 123, 126, 223], which have been previously seen in this thesis as a byproduct of transverse forces. In the presence of multiple tracers interacting with such a kind of bath, exotic forms of clustering formation and rotation [120] have been observed.

E1 Model

We consider an extended rigid tracer of arbitrary shape and typical size ℓ evolving under Hamiltonian dynamics and interacting with a chiral active bath in two dimensions. The tracer has mass m and moment of inertia I . Its state is characterized by its position \mathbf{R} , momentum \mathbf{P} , orientation Θ and angular momentum L . The equations of motion of the tracer read

$$\begin{aligned}\dot{\mathbf{R}} &= \frac{1}{m} \mathbf{P}, & \dot{\Theta} &= \frac{1}{I} L, \\ \dot{\mathbf{P}} &= \mathbf{F}_{\text{bath}} & \dot{L} &= \Gamma_{\text{bath}}\end{aligned}\tag{E.1}$$

where \mathbf{F}_{bath} and Γ_{bath} are the total force and torque on the object due to pairwise interactions between elementary constituents of the tracer with the bath particles. The bath is composed chiral active Brownian particles (cABPs) [179], whose equations of motion are

$$\begin{aligned}\zeta \dot{\mathbf{r}}_i &= \mathbf{F}_{\text{tracer},i} + f_0 \mathbf{u}_i + \sqrt{2\zeta D_t} \boldsymbol{\eta}_i, \\ \dot{\theta}_i &= \omega_0 + \sqrt{2D_r} \xi_i\end{aligned}\tag{E.2}$$

where $\mathbf{F}_{\text{int},i}$ accounts for pairwise interactions between bath particles, the force on bath particle i due to the tracer is $\mathbf{F}_{\text{tracer},i}$, and where f_0 is the active propulsion force oriented along the director \mathbf{u}_i . Pairwise interactions are assumed to be reciprocal, *i.e.* satisfying $\sum_i \mathbf{F}_{\text{tracer},i} = -\mathbf{F}_{\text{bath}}$. The active bath described by Eq. (E.2) displays two microscopic active timescales: the persistence length $\ell_p := \frac{f_0}{D_r \zeta}$ and the gyroradius $\ell_g := \frac{f_0}{\omega_0 \zeta}$.

E2 Main results

We first present qualitative results coming from Molecular Dynamics simulations of Eq. (E.1) and Eq. (E.2) obtained by C. Hargus. Fig. E.1 illustrates three differently shaped objects which, when placed in a bath of chiral active Brownian particles, exhibit qualitative differences in their motion. Namely, an isotropic disk inherits from the bath particles an emergent chiral random motion (Fig. E.1(a)), imbuing the object with odd diffusivity [126], as previously noted in [174]. This is quantified by plotting the antisymmetric component of the velocity autocorrelations as a function of time (Fig. E.1(d)). When isotropy is broken, but invariance by central symmetry is preserved, for example in an elongated rod-like object, the object will generically experience a torque from the chiral active particles causing it to rotate systematically in one direction (Fig. E.1(b))

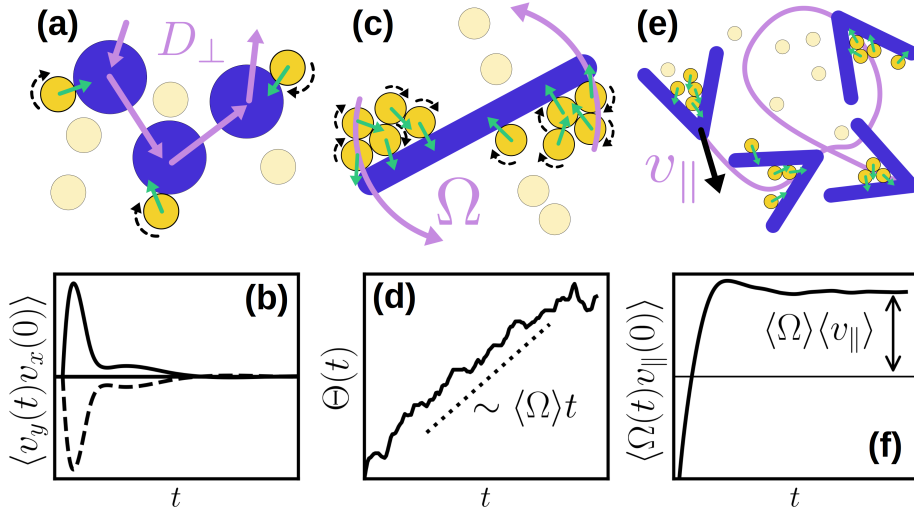


Figure E.1: Odd dynamics and ratchet currents of differently-shaped passive objects in a bath of cABPs. **(a)** A passive disc (blue) inherits chiral random motion of the opposite sign of the bath particles (yellow) through collisions. **(b)** This results in odd diffusion, manifesting in antisymmetric velocity correlations (solid line) which are odd under time-reversal (dashed line). **(c)** An immobilized rod breaks the isotropy of the bath, resulting in asymmetric accumulation of cABPs driving a net torque $\langle \Gamma \rangle_b$. **(d)** For a mobile rod, this torque is balanced in steady state by the angular friction, resulting in a constant angular velocity. Translational and rotational dynamics are decoupled due to central symmetry. **(e)** A passive wedge further breaks this central symmetry, behaving as both a rotational and translational ratchet. **(f)** Translation-rotation coupling and ratchet currents are visible in the time correlation of Ω and v_{\parallel} . The bottom row shows simulation results for $\ell_p = 10$ and $\ell_g = 10$. . This figure was realised by Cory Hargus.

as its nonzero angular velocity shows (Fig. E.1(e)). When the rod is deformed into a wedge, thus suppressing any rotational invariance and breaking one of its symmetry axes, the object effectively becomes an actively-driven chiral particle itself (Fig. E.1(e)), and the combination of actively-driven translations and rotations leads to ballistic-like motion on the timescale of active particle reorientation, and enhanced odd diffusion on long timescales (Fig. E.1(f)). We complement these numerical results with an analytical approach in which we coarsen out the bath degrees of freedom. This simplification comes at the cost of an adiabatic approximation.

In the spirit of Van Kampen [250], we shall assume that the bath degrees of freedom evolve over much shorter time scales than those of the tracer. In this adiabatic approximation, the structure of the bath is completely determined by the instantaneous configuration of the tracer. The implementation of the adiabatic approximation is described in deeper detail in the next sections, the outcome of which is the following Langevin equation for the tracer

$$\begin{bmatrix} \dot{\mathbf{P}} \\ \dot{L} \end{bmatrix} = \begin{bmatrix} \langle \mathbf{F} \rangle_b \\ \langle \Gamma \rangle_b \end{bmatrix} - \underbrace{\begin{bmatrix} \zeta_{PP} & \zeta_{PL} \\ \zeta_{LP} & \zeta_{LL} \end{bmatrix}}_{\zeta} \begin{bmatrix} m^{-1} \mathbf{P} \\ I^{-1} L \end{bmatrix} + \underbrace{\begin{bmatrix} \xi_P(t) \\ \xi_L(t) \end{bmatrix}}_{\xi}. \quad (\text{E.3})$$

Upon adiabatic elimination of the active bath degrees of freedom, three effects are produced on the tracer: a constant drift, an instantaneous friction ζ and a Markovian noise ξ . The translational and rotational degrees of freedom of the tracer, which are now coupled one with each other, are thus directly affected.

These equations feature a collection of nine friction coefficients ζ and of three white Gaussian noises ξ whose correlations are characterized by nine diffusion constants λ ,

$$\langle \xi(t) \otimes \xi(t') \rangle = 2\lambda \delta(t - t') \quad (\text{E.4})$$

Depending on the shape of the tracer, the friction and noise may depend on the instantaneous tracer orientation Θ except, due to the bath isotropy implied by Eq. (E.2), ζ_{LL} and λ_{LL} , while translation invariance prohibits dependence on \mathbf{R} and \mathbf{P} .

The outcome of our theoretical procedure is to provide expressions for ζ and λ in terms of steady-state averages over the bath degrees of freedom at fixed tracer coordinates, as written out in Eqs. (E.5) and (E.6). The friction matrix ζ reads

$$\zeta = \int_0^{+\infty} d\tau \begin{bmatrix} \langle \delta\mathbf{F}(\tau) \otimes \nabla_{\mathbf{R}} \log \rho_b(0) \rangle_b & \langle \delta\mathbf{F}(\tau) \partial_\theta \log \rho_b(0) \rangle_b \\ \langle \delta\Gamma(\tau) \nabla_{\mathbf{R}}^T \log \rho_b(0) \rangle_b & \langle \delta\Gamma(\tau) \partial_\theta \log \rho_b(0) \rangle_b \end{bmatrix} \quad (\text{E.5})$$

with $\delta\mathbf{F} = \mathbf{F} - \langle \mathbf{F} \rangle_b$, $\delta\Gamma = \Gamma - \langle \Gamma \rangle_b$ the fluctuation of the active bath forces acting on the tracer. The matrix λ encodes the noise correlations, and it is given by

$$\lambda = \int_0^{+\infty} d\tau \begin{bmatrix} \langle \delta\mathbf{F}(\tau) \otimes \delta\mathbf{F}(0) \rangle_b & \langle \delta\mathbf{F}(\tau) \delta\Gamma(0) \rangle_b \\ \langle \delta\Gamma(\tau) \delta\mathbf{F}^T(0) \rangle_b & \langle \delta\Gamma(\tau) \delta\Gamma(0) \rangle_b \end{bmatrix}. \quad (\text{E.6})$$

Equation (E.3) is the most general description of the tracer dynamics within the adiabatic approximation. As highlighted in Figure E.1, in addition to being subjected to a translational drift, the tracer generically feels a constant torque as well. Due to the chirality of the bath itself, the object need not be chiral to experience a net torque. We now specialize Eq. (E.3) to the various shapes of Fig. E.1.

E2.1 Swirling disk

We start with a circular tracer, which has only translational degrees of freedom. Due to rotational symmetry, we have $\langle \mathbf{F} \rangle_b = \mathbf{0}$, and Eq.(E.3) reduces to

$$\dot{\mathbf{P}} = -\frac{1}{m} \zeta_{PP} \cdot \mathbf{P} + \boldsymbol{\xi}_P(t). \quad (\text{E.7})$$

When $\omega_0 = 0$ the bath is made by achiral ABPs, which, together with the isotropy of the system imposes $\zeta = \zeta_{\parallel} \mathbb{1}$, $\lambda = \lambda_{\parallel} \mathbb{1}$ and we recover the result of [240]. However, when $\omega_0 \neq 0$, the friction and noise matrices are no longer constrained to be diagonal. The isotropy of the system therefore imposes $\zeta_{PP} = \zeta_{\parallel} \mathbb{1} + \zeta_{\perp} \mathbf{A}$, $\lambda = \lambda_{\parallel} \mathbb{1} + \lambda_{\perp} \mathbf{A}$, with $\mathbf{A} = \begin{bmatrix} 0 & -1 \\ 1 & 0 \end{bmatrix}$. The physical consequence of such a structure of the friction and noise matrices is the emergence of odd diffusion for the passive disk. Such an effect is quantified by a finite odd diffusivity [126] $D_{\perp} = \frac{1}{2m^2} \int_0^{+\infty} d\tau \langle \mathbf{P}(\tau) \cdot \mathbf{A} \mathbf{P}(0) \rangle = \int_0^{+\infty} \langle v_y(t) v_x(0) \rangle$, as shown in Fig. E.1(d). The dynamical evolution of Eq. (E.7) is irreversible because upon time-reversal ω_0 remains unchanged (unlike the magnetic field in the Lorentz force for a charged particle [205]) but observables that are even in ω_0 will be consistent with Boltzmann statistics. We can therefore introduce an effective temperature $T_{\text{eff}} = \lambda_{\parallel}/\zeta_{\parallel}$, such that $\langle \mathbf{P}^2 \rangle = 2mT_{\text{eff}}$. This leads to the following expression for the odd diffusion constant

$$D_{\perp} = T_{\text{eff}} \frac{\zeta_{\perp}}{\zeta_{\parallel}^2 + \zeta_{\perp}^2}. \quad (\text{E.8})$$

Interestingly, one can show that in this adiabatic context, the odd mobility of the tracer, defined as $\mu_{\perp} = \lim_{t \rightarrow \infty} \frac{\delta \dot{R}_y}{\delta f_x}$ when a constant force $\mathbf{f} = f \mathbf{e}_x$ is applied on the tracer obeys the effective Einstein relation $\mu_{\perp} = T_{\text{eff}}^{-1} D_{\perp}$.

E2.2 Spinning rod

To pinpoint the effects of the chiral bath upon the orientational degree of freedom, we consider the case of an anisotropic, achiral tracer, such as a rod. Due to the anisotropy of the tracer and the chirality of the bath, we expect the average torque $\langle \Gamma \rangle_b$ to be nonzero. This is because two particles hitting either side of the rod at the same location will experience asymmetric fates as the particles will slide along

the obstacle according to their chirality. This creates a heterogeneous density profile and a net torque. This was indeed observed in [55] for a chiral active particle in an anisotropic confining potential. Due to the twofold rotational symmetry of the rod, Eqs. (E.5) and (E.6) show that the off-diagonal elements of λ and ζ coupling rotation and translational degrees of freedom must vanish. Thus the translation motion of the rod is odd-diffusive, just as in the previous case of the disk, while rotation is now present and described by

$$\dot{L} = \langle \Gamma \rangle_b - \frac{\zeta_{LL}}{I} L + \xi_L(t). \quad (\text{E.9})$$

In the steady state, we thus expect the tracer to spin with a constant average angular velocity Ω given by

$$\Omega = \frac{\langle \Gamma \rangle_b}{\zeta_{LL}}, \quad (\text{E.10})$$

as shown in Fig. E.1(e) or in [174]. The range of validity of the adiabatic limit, and of the accompanying effective Green-Kubo relations, is much more subtle than for the disk. In the presence of a constant drift, another time scale Ω^{-1} controls the motion of the tracer. For the adiabatic regime to hold, we must *a posteriori* verify that this emergent time scale is larger than D_r^{-1} and ω_0^{-1} . This is a consequence of the transport coefficients coupling rotation and translation vanishing due to central symmetry of the rod: $\langle \Gamma(t) F_i(0) \rangle_{\omega_0} = \langle \Gamma(0) F_i(t) \rangle_{-\omega_0} = 0$. This decoupling is warranted for the rod — which can be rotated into itself by a rotation of π — as for any object exhibiting central symmetry.

E2.3 Steering wedge

Finally we consider the case of a wedge, which exhibits no central symmetry. All the entries in λ and ζ have to be considered, because rotational and translational dynamics are now coupled. However, due to the mirror symmetry of the wedge, ζ exhibits only five independent elements. The wedge behaves as both a rotational and translational ratchet. The translational drift is a function of the wedge orientation only, $\langle \mathbf{F} \rangle_b = \langle \mathbf{F} \rangle_b(\Theta)$. The tracer itself can be pictured as an effective chiral active Brownian particle, where its self-propulsion velocity is determined by its instantaneous spinning orientation. While, in the adiabatic approximation, generalized frictions and diffusivities sometimes appear to be connected by an effective temperature, in general their relationship may be more complex, and this calls for further numerical simulations.

In the next Section, we derive, within the adiabatic approximation, Eq. (E.3).

E3 Effective Langevin equation for the tracer

E3.1 Setting up the stage

In this Section, we derive the effective underdamped Langevin equation of motion for the tracer in the adiabatic limit, Eq. (E.3) of the main text. We consider a rigid tracer of arbitrary shape, with mass m and momentum of inertia I , interacting with a bath of chiral active particles. Our starting point are the equation of motion of the tracer and the active bath, which are Eqs. (E.1) and (E.2) of the main text.

The probability density for the full system $\rho(\mathbf{R}, \mathbf{P}, \Theta, L, \mathbf{r}^N, \mathbf{u}^N)$ evolves according to the Fokker-Planck equation

$$\partial_t \rho = (\mathcal{L}_T + \mathcal{L}_{\text{bath}}) \rho \quad (\text{E.11})$$

where \mathcal{L}_T and \mathcal{L}_B are respectively the evolution operator acting on the tracer and the bath degrees of freedom:

$$\begin{aligned} \mathcal{L}_T &= -\frac{\mathbf{P}}{m} \cdot \nabla_{\mathbf{R}} - \mathbf{F} \cdot \nabla_{\mathbf{P}} - \frac{L}{I} \partial_{\Theta} - \Gamma_{\text{bath}} \partial_L \\ \mathcal{L}_B &= \sum_i \frac{1}{\zeta} \nabla_{\mathbf{r}_i} \cdot [-\mathbf{F}_{\text{tracer},i} - f_0 \mathbf{u}_i + D_t \nabla_{\mathbf{r}_i}] + \partial_{\theta_i} [-\omega_0 + D_r \partial_{\theta_i}]. \end{aligned} \quad (\text{E.12})$$

To implement the adiabatic approximation, we introduce a dimensionless parameter

$$h \equiv \sqrt{\frac{\epsilon}{m\sigma^2}} \tau_{\text{R,bath}}, \quad (\text{E.13})$$

where σ and ϵ are the strength and length scale of the interaction potential between the bath particles and the tracer, and

$$\tau_{\text{R,bath}} \equiv \frac{\ell^2}{D_{\parallel,\text{bath}}} \quad (\text{E.14})$$

is the typical relaxation time of the bath, with $D_{\parallel,\text{bath}}$ the longitudinal diffusion constant of the cABPs given that the tracer is fixed at a given position and orientation. The adiabatic limit is obtained when the mass of the tracer is large enough, so that $h \ll 1$. We then introduce a rescaled time $t^*h \equiv t$, a rescaled mass $m^*h^{-2} \equiv m$, a rescaled momentum $\mathbf{P}^*h^{-1} \equiv \mathbf{P}$, a rescaled angular momentum $L^*h^{-1} \equiv L$, and a rescaled moment of inertia $I^* = h^{-2}I$. Using these rescaled variables, Eq. (E.11) becomes

$$\partial_{t^*} \rho = \left(\mathcal{L}_T^* + \frac{1}{h} \mathcal{L}_{\text{bath}} \right) \rho \quad (\text{E.15})$$

with $\mathcal{L}_T^* = -\frac{\mathbf{P}^*}{m^*} \cdot \nabla_{\mathbf{R}}^* - \mathbf{F} \cdot \nabla_{\mathbf{P}^*} - \frac{L^*}{I^*} \partial_{\Theta} - \Gamma_{\text{bath}} \partial_{L^*}$. To lighten up the notation, we drop the $*$ symbol in what follows.

E3.2 Projection operator formalism

In this Section we implement the projection operator formalism, to integrate out the degrees of freedom of the active chiral bath. The idea is to introduce an operator \mathcal{P} that project in the space orthogonal to the evolution of the chiral bath, i.e. such that

$$\mathcal{P}\mathcal{L}_{\text{bath}} = \mathcal{L}_{\text{bath}}\mathcal{P} = 0. \quad (\text{E.16})$$

We also require the idempotent property $\mathcal{P}\mathcal{P} = \mathcal{P}$, which defines a projection operator. Our choice for \mathcal{P} is

$$\mathcal{P} \dots = \rho_{\text{bath}}(\{\mathbf{r}^N, \theta^N\} | \mathbf{R}, \mathbf{P}, \Theta, L) \int d\mathbf{r}'^N d\theta'^N \dots \quad (\text{E.17})$$

where $\rho_{\text{bath}}(\{\mathbf{r}^N, \theta^N\} | \mathbf{R}, \mathbf{P}, \Theta, L)$ is the steady state distribution of the active chiral bath, when the degrees of freedom of the tracer are held fixed. It satisfies the partial differential equation

$$\mathcal{L}_{\text{bath}}\rho_{\text{bath}} = 0. \quad (\text{E.18})$$

The idea behind this choice of \mathcal{P} is that at a given time in the evolution of the tracer, the bath relaxes instantaneously to its steady state distribution, and the tracer degrees of freedom are effectively frozen. The space over which \mathcal{P} projects is thus tailored to capture this kind of dynamics with widely separated timescales.

The action of \mathcal{P} on ρ induces the definition of a tracer density distribution, $\rho_{\text{T}}(\mathbf{R}, \mathbf{P}, \Theta, L, t)$:

$$\begin{aligned} \mathcal{P}\rho(\mathbf{R}, \mathbf{P}, L, \Theta, \mathbf{r}^N, \theta^N, t) &= \rho_{\text{bath}}(\{\mathbf{r}^N, \theta^N\} | \mathbf{R}, \mathbf{P}, \Theta, L) \int d\mathbf{r}'^N d\theta'^N \rho(\mathbf{R}, \mathbf{P}, \mathbf{r}^N, \theta^N, t) \\ &\equiv \rho_{\text{bath}}(\{\mathbf{r}^N, \theta^N\} | \mathbf{R}, \mathbf{P}, \Theta, L) \rho_{\text{T}}(\mathbf{R}, \mathbf{P}, \Theta, L, t). \end{aligned} \quad (\text{E.19})$$

Our goal is to obtain an equation of motion for the tracer density distribution, ρ_{T} . We introduce a projection operator $\mathcal{Q} \equiv 1 - \mathcal{P}$ orthogonal to \mathcal{P} and, Using Eq. (E.11) and Eq. (E.16) we get

$$\begin{aligned} \partial_t \mathcal{P}\rho &= \mathcal{P}\mathcal{L}_{\text{T}}\mathcal{P}\rho + \mathcal{P}\mathcal{L}_{\text{T}}\mathcal{Q}\rho \\ \partial_t \mathcal{Q}\rho &= \mathcal{Q}\mathcal{L}_{\text{T}}\mathcal{P}\rho + \mathcal{Q}\mathcal{L}_{\text{T}}\mathcal{Q}\rho + \frac{1}{h} \mathcal{Q}\mathcal{L}_{\text{bath}}\mathcal{Q}\rho. \end{aligned} \quad (\text{E.20})$$

We have thus formally decoupled the evolution of ρ into two parts, one belonging to the space projected over by \mathcal{P} , and the other belonging to the orthogonal space. To proceed further, we will exploit the separation between the timescale for the evolution of the tracer and the one for the evolution of the bath, implemented via the small parameter h .

E3.3 Adiabatic approximation

We solve the equation for $\mathcal{Q}\rho$ in Eq. (E.20) by expanding in powers of h :

$$\mathcal{Q}\rho = q_0 + hq_1 + O(h^2). \quad (\text{E.21})$$

The equation for q_0 reads, from Eq. (E.20),

$$\mathcal{Q}\mathcal{L}_{\text{bath}}q_0 = \mathcal{L}_{\text{bath}}q_0 = 0 \quad (\text{E.22})$$

This equation is solved for $q_0 = \rho_{\text{bath}}$ or $q_0 = 0$. The former can be excluded because by definition $\mathcal{P}q_0 = 0$, while $\mathcal{P}\rho_{\text{bath}} = \rho_{\text{bath}}$. We thus conclude that $q_0 = 0$.

To first order in h , Eq. (E.20) becomes

$$\mathcal{Q}\mathcal{L}_{\text{bath}}q_1 + \mathcal{Q}\mathcal{L}_{\text{T}}\mathcal{P}\rho = 0, \quad (\text{E.23})$$

which admits the formal solution

$$q_1 = \mathcal{Q} \left(\int_0^{+\infty} ds e^{\mathcal{L}_{\text{bath}}s} \right) \mathcal{Q}\mathcal{L}_{\text{T}}\mathcal{P}\rho, \quad (\text{E.24})$$

as can indeed be verified:

$$\begin{aligned} \mathcal{Q}\mathcal{L}_{\text{bath}}q_1 &= \mathcal{Q}\mathcal{L}_{\text{bath}}\mathcal{Q} \left(\int_0^{+\infty} ds e^{\mathcal{L}_{\text{bath}}s} \right) \mathcal{Q}\mathcal{L}_{\text{T}}\mathcal{P}\rho \\ &= \mathcal{Q}\mathcal{L}_{\text{bath}} \left(\int_0^{+\infty} ds e^{\mathcal{L}_{\text{bath}}s} \right) \mathcal{Q}\mathcal{L}_{\text{T}}\mathcal{P}\rho \\ &= \mathcal{Q} \left(\int_0^{+\infty} ds \frac{d}{ds} e^{\mathcal{L}_{\text{bath}}s} \right) \mathcal{Q}\mathcal{L}_{\text{T}}\mathcal{P}\rho \\ &= -\mathcal{Q}\mathcal{L}_{\text{T}}\mathcal{P}\rho. \end{aligned} \quad (\text{E.25})$$

We thus have, for $\mathcal{Q}\rho$,

$$\mathcal{Q}\rho = h\mathcal{Q} \left(\int_0^{+\infty} ds e^{\mathcal{L}_{\text{bath}}s} \right) \mathcal{Q}\mathcal{L}_{\text{T}}\mathcal{P}\rho + O(h^2). \quad (\text{E.26})$$

Substituting the above expression in the first line of Eq. (E.20) and neglecting higher orders in h we obtain

$$\partial_t \mathcal{P}\rho = \rho_{\text{bath}} \partial_t \rho_{\text{T}} \approx \mathcal{P}\mathcal{L}_{\text{T}}\mathcal{P}\rho + \mathcal{P}\mathcal{L}_{\text{T}}\mathcal{Q} \left(\int_0^{+\infty} ds e^{\frac{1}{h}\mathcal{L}_{\text{bath}}s} \right) \mathcal{Q}\mathcal{L}_{\text{T}}\mathcal{P}\rho. \quad (\text{E.27})$$

This is the formal evolution equation for ρ_{T} in the adiabatic limit. We now proceed to the computation of its different terms.

E3.4 Explicit computation

The first term in Eq. (E.27) reads:

$$\begin{aligned}
 \mathcal{P}\mathcal{L}_T\mathcal{P}\rho &= -\mathcal{P} \left(\mathbf{F} \cdot \nabla_{\mathbf{P}} + \frac{1}{m} \mathbf{P} \cdot \nabla_{\mathbf{R}} + \frac{1}{I} L \partial_{\Theta} + \Gamma \partial_L \right) \rho_T \rho_{\text{bath}} \\
 &= -\mathcal{P} \rho_{\text{bath}} \left[\mathbf{F} \cdot \nabla_{\mathbf{P}} + \frac{1}{m} \mathbf{P} \cdot ((\nabla_{\mathbf{R}} \log \rho_{\text{bath}}) + \nabla_{\mathbf{R}}) \right. \\
 &\quad \left. + \Gamma \partial_L + \frac{1}{I} L [(\partial_{\Theta} \log \rho_{\text{bath}}) + \partial_{\Theta}] \right] \rho_T \\
 &= -\rho_{\text{bath}} \left[\langle \mathbf{F} \rangle_B \cdot \nabla_{\mathbf{P}} + \frac{1}{m} \mathbf{P} \cdot \nabla_{\mathbf{R}} + \langle \Gamma \rangle_B \partial_L + \frac{1}{I} L \partial_{\Theta} \right] \rho_T
 \end{aligned} \tag{E.28}$$

where

$$\langle \dots \rangle_b \equiv \int d\mathbf{r}^N d\theta^N \dots \rho_{\text{bath}}(\{\mathbf{r}^N, \theta^N\} | \mathbf{R}, \mathbf{P}, \Theta, L) \tag{E.29}$$

is an average over the steady state distribution of the active bath when the tracer degrees of freedom are held fixed. To keep the notation light, we omitted the arguments of the function, but it should be remembered that ρ_T and $\langle \dots \rangle_b$ depends only on the tracer degrees of freedom. When passing from the second to the third line of Eq. (E.28), we used the fact that

$$\langle [\nabla_{\mathbf{R}} \log \rho_{\text{bath}}] \rangle_b = \nabla_{\mathbf{R}} \langle 1 \rangle_b = 0 \tag{E.30}$$

and that the same is true for $\langle \partial_{\Theta} \log \rho_{\text{bath}} \rangle_b$. Due to the anisotropy of the tracer and the chirality of the bath, we admit that a net nonzero average force and torque can be exerted on the tracer, $\langle \mathbf{F}_{\text{bath}} \rangle_b \neq 0$, $\langle \Gamma_{\text{bath}} \rangle_b \neq 0$.

We compute separately different components of the second term in the r.h.s. of Eq. (E.27). The first one is

$$\begin{aligned}
 \mathcal{Q}\mathcal{L}_T\mathcal{P}\rho &= -\rho_{\text{bath}} \left[(\mathbf{F}_{\text{bath}} - \langle \mathbf{F}_{\text{bath}} \rangle_b) \cdot \nabla_{\mathbf{P}} + \frac{1}{m} \mathbf{P} \cdot (\nabla_{\mathbf{R}} \log \rho_{\text{bath}}) \right. \\
 &\quad \left. + (\Gamma_{\text{bath}} - \langle \Gamma_{\text{bath}} \rangle_b) \partial_L + \frac{1}{I} L (\partial_{\Theta} \log \rho_{\text{bath}}) \right] \rho_T \\
 &\equiv -\rho_{\text{bath}} \left[\delta \mathbf{F}_{\text{bath}} \cdot \nabla_{\mathbf{P}} + \frac{1}{m} \mathbf{P} \cdot (\nabla_{\mathbf{R}} \log \rho_{\text{bath}}) \right. \\
 &\quad \left. + \delta \Gamma_{\text{bath}} \partial_L + \frac{1}{I} (\partial_{\Theta} \log \rho_{\text{bath}}) \right] \rho_T
 \end{aligned} \tag{E.31}$$

where we defined the fluctuations of the force and the torque exerted from the bath to the tracer, $\delta \mathbf{F}_{\text{bath}} \equiv \mathbf{F}_{\text{bath}} - \langle \mathbf{F}_{\text{bath}} \rangle_b$, $\delta \Gamma_{\text{bath}} \equiv \Gamma_{\text{bath}} - \langle \Gamma_{\text{bath}} \rangle_b$.

Using Eq. (E.31) we can compute

$$\begin{aligned}
 & \mathcal{P} \mathcal{L}_T \mathcal{Q} \left(\int_0^{+\infty} ds e^{\frac{1}{\hbar} \mathcal{L}_{\text{bath}} s} \right) \mathcal{Q} \mathcal{L}_T \mathcal{P} \rho = \mathcal{P} \mathcal{L}_T \left(\int_0^{+\infty} ds e^{\frac{1}{\hbar} \mathcal{L}_{\text{bath}} s} \right) \mathcal{Q} \mathcal{L}_T \mathcal{P} \rho \\
 &= \rho_{\text{bath}} \int d\mathbf{r}^N d\theta^N \mathcal{L}_T \left(\int_0^{+\infty} ds e^{\frac{1}{\hbar} \mathcal{L}_{\text{bath}} s} \right) \mathcal{Q} \mathcal{L}_T \mathcal{P} \rho \\
 &= \rho_{\text{bath}} \int d\mathbf{r}^N d\theta^N \left[\mathbf{F} \cdot \nabla_{\mathbf{P}} + \frac{1}{m} \mathbf{P} \cdot \nabla_{\mathbf{R}} + \frac{1}{I} L \partial_{\Theta} + \Gamma \partial_L \right] \left(\int_0^{+\infty} ds e^{\frac{1}{\hbar} \mathcal{L}_{\text{bath}} s} \right) \rho_{\text{bath}} \\
 &\quad \times \left[\delta \mathbf{F}_{\text{bath}} \cdot \nabla_{\mathbf{P}} + \frac{1}{m} \mathbf{P} \cdot (\nabla_{\mathbf{R}} \log \rho_{\text{bath}}) + \delta \Gamma_{\text{bath}} \partial_L + \frac{1}{I} (\partial_{\Theta} \log \rho_{\text{bath}}) \right] \rho_T \\
 &= \rho_{\text{bath}} \int d\mathbf{r}^N d\theta^N \left[\mathbf{F} \cdot \nabla_{\mathbf{P}} + \frac{1}{m} \mathbf{P} \cdot \nabla_{\mathbf{R}} + \frac{1}{I} L \partial_{\Theta} + \Gamma \partial_L \right] \rho_{\text{bath}} \left(\int_0^{+\infty} ds e^{\frac{1}{\hbar} \mathcal{L}_{\text{bath}} s} \right) \\
 &\quad \times \left[\delta \mathbf{F}_{\text{bath}} \cdot \nabla_{\mathbf{P}} + \frac{1}{m} \mathbf{P} \cdot (\nabla_{\mathbf{R}} \log \rho_{\text{bath}}) + \delta \Gamma_{\text{bath}} \partial_L + \frac{1}{I} (\partial_{\Theta} \log \rho_{\text{bath}}) \right] \rho_T \\
 &= \rho_{\text{bath}} \left\langle \left[\mathbf{F} \cdot \nabla_{\mathbf{P}} + \frac{1}{m} \mathbf{P} \cdot \nabla_{\mathbf{R}} + \Gamma \partial_L + \frac{1}{I} L \partial_{\Theta} \right] \left(\int_0^{+\infty} ds e^{\frac{1}{\hbar} \mathcal{L}_{\text{bath}} s} \right) \right. \\
 &\quad \left. \times \left[\delta \mathbf{F}_{\text{bath}} \cdot \nabla_{\mathbf{P}} + \frac{1}{m} \mathbf{P} \cdot (\nabla_{\mathbf{R}} \log \rho_{\text{bath}}) + \delta \Gamma_{\text{bath}} \partial_L + \frac{1}{I} (\partial_{\Theta} \log \rho_{\text{bath}}) \right] \right\rangle_b \rho_T
 \end{aligned} \tag{E.32}$$

Let us look at some terms to have an idea of how the calculation proceeds. We get diffusion terms of the form

$$\begin{aligned}
 \int_0^{+\infty} ds \left\langle (\mathbf{F} \cdot \nabla_{\mathbf{P}}) e^{\frac{1}{\hbar} \mathcal{L}_{\text{bath}} s} (\delta \mathbf{F}_{\text{bath}} \cdot \nabla_{\mathbf{P}}) \right\rangle_b &= \nabla_{\mathbf{P}} \cdot \int_0^{+\infty} ds \left\langle \left(e^{\frac{1}{\hbar} \mathcal{L}_{\text{bath}}^\dagger s} \mathbf{F} \right) \otimes \delta \mathbf{F}_b \right\rangle_b \cdot \nabla_{\mathbf{P}} \\
 &= \nabla_{\mathbf{P}} \cdot \int_0^{+\infty} ds \langle \delta \mathbf{F}_b(s) \otimes \delta \mathbf{F}_b(0) \rangle_b \cdot \nabla_{\mathbf{P}} \\
 &\equiv \nabla_{\mathbf{P}} \cdot \boldsymbol{\lambda}_{PP}(\Theta) \cdot \nabla_{\mathbf{P}}
 \end{aligned} \tag{E.33}$$

with $\mathcal{L}_{\text{bath}}^\dagger$ the operator adjoint to $\mathcal{L}_{\text{bath}}$, and friction terms of the form

$$\begin{aligned}
 \int_0^{+\infty} ds \left\langle (\mathbf{F} \cdot \nabla_{\mathbf{P}}) e^{\frac{1}{\hbar} \mathcal{L}_{\text{bath}} s} \mathbf{P} \cdot [\nabla_{\mathbf{R}} \log \rho_{\text{bath}}] \right\rangle_b &= \nabla_{\mathbf{P}} \cdot \int_0^{+\infty} ds \langle \delta \mathbf{F}_b(s) \otimes [\nabla_{\mathbf{R}} \log \rho_{\text{bath}}] \rangle_b \cdot \frac{1}{m} \mathbf{P} \\
 &\equiv \frac{1}{m} \nabla_{\mathbf{P}} \cdot \boldsymbol{\zeta}_{PP}(\Theta) \cdot \mathbf{P}
 \end{aligned} \tag{E.34}$$

where the force-force correlation matrix $\boldsymbol{\lambda}_{PP}(\Theta)$ and the momentum friction matrix $\boldsymbol{\zeta}_{PP}(\Theta)$ are the ones appearing in Eq. (3) of the main text. Note that friction and diffusion terms coupling the orientational and translational degrees of freedom are also admitted. Terms involving $\nabla_{\mathbf{R}}$, ∂_{Θ} on the left side of the average in Eq. (E.32) vanish. For example

$$\frac{L}{I} \int_0^{+\infty} ds \left\langle \partial_{\Theta} e^{\frac{1}{\hbar} \mathcal{L}_{\text{bath}} s} \frac{1}{m} \mathbf{P} \cdot [\nabla_{\mathbf{R}} \log \rho_{\text{bath}}] \right\rangle_b = \frac{L}{Im} \mathbf{P} \cdot \partial_{\Theta} \langle [\nabla_{\mathbf{R}} \log \rho_{\text{bath}}] \rangle_b = 0. \tag{E.35}$$

Plugging Eq. (E.31) - (E.32) into Eq. (E.27) we finally obtain

$$\begin{aligned} \partial_t \rho_T(\mathbf{R}, \mathbf{P}, \Theta, L) = & \left\{ - \begin{bmatrix} m^{-1} \mathbf{P} \\ I^{-1} L \end{bmatrix} \cdot \begin{bmatrix} \nabla_{\mathbf{R}} \\ \partial_{\Theta} \end{bmatrix} - \begin{bmatrix} \langle \mathbf{F}_{\text{bath}} \rangle_b \\ \langle \Gamma_{\text{bath}} \rangle_b \end{bmatrix} \cdot \begin{bmatrix} \nabla_{\mathbf{P}} \\ \partial_L \end{bmatrix} \right. \\ & \left. + \begin{bmatrix} \nabla_{\mathbf{P}} \\ \partial_L \end{bmatrix} \zeta(\Theta) \begin{bmatrix} m^{-1} \mathbf{P} \\ I^{-1} L \end{bmatrix} + \begin{bmatrix} \nabla_{\mathbf{P}} \\ \partial_L \end{bmatrix} \boldsymbol{\lambda}(\Theta) \begin{bmatrix} \nabla_{\mathbf{P}} \\ \partial_L \end{bmatrix} \right\} \rho_T(\mathbf{R}, \mathbf{P}, \Theta, L) \end{aligned} \quad (\text{E.36})$$

Where the friction and noise matrices $\zeta(\Theta)$, $\boldsymbol{\lambda}(\Theta)$ are given by Eq. (E.5) and Eq. (E.6). Eq. (E.36) describes the effective evolution of the probability distribution of the tracer once the bath degrees of freedom have been integrated out within an adiabatic approximation. The stochastic process associated to this equation is given by Eq. (E.3). This concludes our derivation for the dynamics of a passive tracer in an active chiral bath.

Extensions of the results presented here shall focus on numerical and analytical investigations of what happens beyond the adiabatic regime, when the timescale of motion of the tracer is comparable to the one of the bath [111]. Out of the adiabatic regime, the bath time correlation function could develop power law decays and lead to superdiffusion, as observed in [118]. How this form of superdiffusion couples to odd transport is an open question. Further development could also proceed toward understanding how chiral active bath mediate the interactions between multiple tracers, as done in [117] for the achiral case. In the latter case, we expect nonreciprocal interactions, akin to transverse forces, to arise from the chiral active bath. From there, there would be hope to understand in a bottom-top approach the cluster dynamics observed in assemblies of passive colloids immersed in chiral baths [179].

APPENDIX F

THE IRREDUCIBLE MEMORY KERNEL

In this appendix we justify the choice for the irreducible memory kernel made in Eq. (6.58). We first review how the irreducible memory kernel is introduced in the equilibrium case, when $\gamma = 0$. Following Kawasaki [152], the starting point is the observation that the evolution operator $\Omega \equiv D_0 \sum_i \nabla_i [\beta \mathbf{F}_i + \nabla_i]$ can be mapped to a Hermitian operator $H \equiv e^{\frac{\beta\mathcal{H}}{2}} \Omega e^{-\frac{\beta\mathcal{H}}{2}}$. It can be written in a manifestly Hermitian form as

$$H = - \sum_i \mathbf{U}_i^\dagger \cdot \mathbf{U}_i, \quad (\text{F.1})$$

with $\mathbf{U}_i \equiv \sqrt{D_0} \left[-\nabla_i + \frac{\beta}{2} \mathbf{F}_i \right]$. Going back to the non-Hermitian representation we see that

$$\Omega = - \sum_i e^{-\frac{\beta\mathcal{H}}{2}} \mathbf{U}_i^\dagger e^{\frac{\beta\mathcal{H}}{2}} \cdot e^{-\frac{\beta\mathcal{H}}{2}} \mathbf{U}_i e^{\frac{\beta\mathcal{H}}{2}} \equiv - \sum_i \mathbf{O}_i^\times \cdot \mathbf{O}_i, \quad (\text{F.2})$$

with

$$\begin{aligned} \mathbf{O}_i^\times &= \sqrt{D_0} \nabla_i, \\ \mathbf{O}_i &= \sqrt{D_0} \left[-\nabla_i + \beta \mathbf{F}_i \right]. \end{aligned} \quad (\text{F.3})$$

At this point, one can insert any generic projection operator \mathcal{P}_i and its orthogonal counterpart $\mathcal{Q}_i \equiv \mathcal{I} - \mathcal{P}_i$. For consistency with the notation of the main text, we also enclose Ω between the orthogonal projector $\mathcal{Q} = \mathcal{I} - \mathcal{P}$, defined from Eq. (6.48):

$$\begin{aligned} \mathcal{Q}\Omega\mathcal{Q} &= -\mathcal{Q} \left(\sum_i \mathbf{O}_i^\times \mathcal{P}_i \cdot \mathbf{O}_i - \sum_i \mathbf{O}_i^\times \mathcal{Q}_i \cdot \mathbf{O}_i \right) \mathcal{Q} \\ &\equiv -\delta\Omega + \Omega^{\text{irr}}. \end{aligned} \quad (\text{F.4})$$

What remains to do is to properly choose the projection operator \mathcal{P} , in such a way that a renormalization of the memory kernel occurs: $\tilde{M}(q, z) = \frac{M(q, z)}{1 + cM(q, z)}$, with c some q -dependent constant. Following Cichocki and Hess [64] we take

$$\mathcal{P}_i \equiv \dots e^{-i\mathbf{q} \cdot \mathbf{r}_i} \rangle \langle e^{i\mathbf{q} \cdot \mathbf{r}_i} \dots, \quad (\text{F.5})$$

leading to the following expression for $\delta\Omega$

$$\delta\Omega = \frac{D_0\beta^2}{N} \dots \mathcal{Q}\mathbf{f}(\mathbf{q})\rangle \cdot \langle \mathbf{f}^*(\mathbf{q})\mathcal{Q} \dots \quad (\text{F.6})$$

Note that this is different from the choice of Kawasaki, which is instead

$$\mathcal{P}_j^{\text{Kawasaki}} = \dots \mathbf{O}_j e^{-i\mathbf{q}\cdot\mathbf{r}_j} \rangle \frac{1}{D_0 q^2} \langle e^{i\mathbf{q}\cdot\mathbf{r}_j} \mathbf{O}_j^\times \dots \quad (\text{F.7})$$

which leads to, using the fact that particles are equivalent,

$$\begin{aligned} \delta\Omega^{\text{Kawasaki}} &= \dots \Omega n(\mathbf{q})\rangle \frac{1}{\langle n^*(\mathbf{q})\Omega n(\mathbf{q})\rangle} \langle n^*(\mathbf{q})\Omega \dots \\ &= \frac{D_0\beta^2}{N} \dots \mathcal{Q} f_{\parallel}(\mathbf{q})\rangle \langle f_{\parallel}^*(\mathbf{q})\mathcal{Q} \dots \end{aligned} \quad (\text{F.8})$$

We see that in equilibrium, the operator $\delta\Omega^{\text{Kawasaki}}$ contains only contributions from the longitudinal currents.

We now turn to the general situation with $\gamma \neq 0$. In this case one can see that an analogous decomposition for Ω_γ can be made, with an extra term to take into account the presence of transverse forces:

$$\Omega_{-\gamma} = -\mathbf{O}^\times \cdot (\mathbf{1} - \gamma\mathbf{A}) \cdot \mathbf{O}. \quad (\text{F.9})$$

Using the projection operator P_i defined in Eq. (F.5) we obtain

$$\begin{aligned} \Omega_{-\gamma}^{\text{irr}} &= \mathcal{Q}\mathbf{O}^\times\mathcal{Q}_i \cdot (\mathbf{1} - \gamma\mathbf{A}) \cdot \mathbf{O} \\ &= D_0\mathcal{Q} \sum_j \nabla_j \mathcal{Q}_j \cdot (\mathbf{1} - \gamma\mathbf{A}) [-\beta\mathbf{F}_j + \nabla_j] \mathcal{Q}, \end{aligned} \quad (\text{F.10})$$

which is Eq. (6.58) shown in the main text.

APPENDIX G

GLASSY BIDISPERSE FLUIDS IN LARGE DIMENSIONS

This Appendix addresses the development of a dynamical mean field theory for bidisperse fluids in the large dimensional limit. The motivation behind this work is twofold. First we desire to set a stepping stone toward the development of a dynamical mean field theory for the Swap algorithm, discussed in Chapter 7, which by construction, requires at least two different species of particles. The dynamics of bidisperse mixture in large dimensions without particle diameters swaps thus constitutes the benchmark against which the swap dynamics needs to be compared. At the moment, bidisperse mixtures in the large dimensional limit have been studied from a thermodynamics viewpoint through an ansatz in the static calculation [137, 1], and the situation is analogous for the Swap dynamics [138]. Second, the study of the dynamics of polydisperse mixture is interesting per se, as it would bring an interesting, mean field companion to recent finite-dimensional studies on polydisperse systems that resort to the mode-coupling approximation schemes [170].

We consider a binary mixture of N_A large particles of type A and N_B small particles of type B evolving under an equilibrium overdamped Langevin dynamics in d dimensions,

$$\zeta \dot{\mathbf{R}}_i^\mu(t) = \mathbf{F}_i^\mu + \sqrt{2\zeta T} \boldsymbol{\xi}_i^\mu(t), \quad (\text{G.1})$$

where i is the particle label and μ denotes its species, $\mu = A, B$. The noise $\boldsymbol{\xi}_i^\mu(t)$ is Gaussian with correlations $\langle \boldsymbol{\xi}_i^\mu(t) \otimes \boldsymbol{\xi}_j^\nu(t') \rangle = \mathbf{1}\delta(t-t')\delta_{\mu\nu}\delta_{ij}$. The particles interact through a pairwise potential, $\mathbf{F}_i^\mu = -\sum_{\nu=A,B} \sum_j \mathbf{F}_{ij}^{\mu\nu}(t)$, with $\mathbf{F}_{ij}^{\mu\nu} \equiv -\nabla_i v_{\mu\nu}(|\mathbf{R}_i^\mu(t) - \mathbf{R}_j^\nu(t)|)$, where $v_{\mu\nu}(r) = v(\frac{r}{\ell_{\mu\nu}})$, and $\ell_{\mu\nu} \equiv \frac{\ell_\mu + \ell_\nu}{2}$, is the effective interaction diameter of the two species.

Each species has a packing fraction $\varphi_\mu \equiv \rho_\mu V d \ell_\mu^d / 2^d$, with $\rho_\mu \equiv \frac{N_\mu}{V}$ the number density of the species. To control the concentration fraction of small particles we introduce the parameter $x \equiv \frac{\varphi_B}{\varphi_A + \varphi_B}$. Following [137], in order to have a well defined packing

fraction ratio for the two species, we choose the following scaling for the diameter ratio of particles of species A and B :

$$\frac{\ell_A}{\ell_B} \equiv 1 + \frac{\delta}{d} \quad (\text{G.2})$$

with δ a parameter controlling the size ratio, which remains of order $O(1)$ in d .

We now address the dynamics of this bidisperse mixture.

G1 One-particle process

The starting point is the one-particle process for particles of species $\mu = A, B$. As for the monodisperse case [177] we write $\mathbf{R}_i^\mu(t) = \mathbf{R}_i^\mu(0) + \mathbf{u}_i^\mu(t)$. The one-particle process can then be derived following the same procedure described in Chapter 5, disregarding the presence of transverse forces, which thus reduces to the equilibrium derivation for monodisperse system. The main difference is that the memory kernel involved in the generalized Langevin equation now contains contributions from force-force correlations between particles of the same species and particles of different species. Within a given species, all particles are equivalent, and we can thus drop the index i . The one-particle process for the displacement \mathbf{u}_μ of particle of species μ –note that we moved the species index downward– is therefore

$$\begin{aligned} \zeta \dot{\mathbf{u}}_\mu(t) &= -\beta \int_0^t d\tau M_\mu(t-\tau) \dot{\mathbf{u}}_\mu(\tau) + \boldsymbol{\Xi}_\mu(t) \\ \langle \boldsymbol{\Xi}_\mu(t) \otimes \boldsymbol{\Xi}_\nu(t') \rangle &= \mathbf{1}_{\mu\nu} [2T\zeta\delta(t-t') + M_\mu(t-t')] . \end{aligned} \quad (\text{G.3})$$

The colored Gaussian noise $\boldsymbol{\Xi}_\mu(t)$ has zero mean. Note that the noise affecting particles of one species is independent from the noise affecting a particle of another species, as the force affecting two different particles are statistically independent. The memory kernel $M_\mu(t)$ contains the force-force correlation among a particle of species μ and all the other species

$$M_\mu(t) = \frac{1}{dN_\mu} \left[\sum_{i,j} \left\langle \mathbf{F}_{ij}^{\mu\mu}(t) \cdot \mathbf{F}_{ij}^{\mu\mu}(0) \right\rangle + \sum_{ij} \left\langle \mathbf{F}_{ij}^{\mu\bar{\mu}}(t) \cdot \mathbf{F}_{i,j}^{\mu\bar{\mu}}(0) \right\rangle \right] \quad (\text{G.4})$$

with $\bar{\mu}$ denoting the species complementary to species μ , e.g. $\bar{A} = B$. In the spirit of the dynamical mean field theory, the memory kernel M_μ are self-consistently determined from the knowledge of three independent two-body processes, involving the distance $\mathbf{r}_{\mu\nu}(t) \equiv \mathbf{R}_\mu(0) - \mathbf{R}_\nu(0) + \mathbf{u}_\mu(t) - \mathbf{u}_\nu(t)$ between two interacting particles belonging respectively to species μ and ν . The two-body process is considered in the next Section. Here we address the form taken by M_μ in the large dimensional limit. To this purpose, we introduce the rescaled particle overlap $h_{\mu\nu}(t)$

$$h_{\mu\nu}(t) \equiv d \left(\frac{|\mathbf{r}_{\mu\nu}(t)|}{\ell_{\mu\nu}} - 1 \right) . \quad (\text{G.5})$$

and a rescaled interaction potential $\bar{v}(h)$

$$\bar{v}(h) \equiv v(r). \quad (\text{G.6})$$

In the large dimensional limit, the two memory kernels $M_A(t)$ and $M_B(t)$ become

$$\begin{aligned} \mathcal{M}_A(t) &\equiv \frac{\ell_A^2}{2d^2} M_A(t) = \frac{\hat{\varphi}}{2} \left[(1-x) \int_{-\infty}^{+\infty} dh_0 e^{h_0 - \beta \bar{v}(h_0)} \bar{v}'(h_0) \langle \bar{v}'(h(t)) \rangle_{h_0}^{AA} \right. \\ &\quad \left. + x e^{\frac{\delta}{2}} \int_{-\infty}^{+\infty} dh_0 e^{h_0 - \beta \bar{v}(h_0)} \bar{v}'(h_0) \langle \bar{v}'(h(t)) \rangle_{h_0}^{AB} \right] \\ \mathcal{M}_B(t) &\equiv \frac{\ell_B^2}{2d^2} M_B(t) = \frac{\hat{\varphi}}{2} \left[x \int_{-\infty}^{+\infty} dh_0 e^{h_0 - \beta \bar{v}(h_0)} \bar{v}'(h_0) \langle \bar{v}'(h(t)) \rangle_{h_0}^{BB} \right. \\ &\quad \left. + (1-x) e^{-\frac{\delta}{2}} \int_{-\infty}^{+\infty} dh_0 e^{h_0 - \beta \bar{v}(h_0)} \bar{v}'(h_0) \langle \bar{v}'(h(t)) \rangle_{h_0}^{AB} \right]. \end{aligned} \quad (\text{G.7})$$

where $\hat{\varphi}_\mu \equiv 2^d d\varphi_\mu$ is a rescaled packing fraction, and $\langle \dots \rangle_{h_0}^{\mu\nu}$ denotes an average over the dynamics of the displacement between two interacting particle belonging respectively to the species μ and ν , given that the initial interparticle distance is h_0 .

To give an idea of the computation, we illustrate how one can pass from Eq. (G.4) to Eq. (G.7), focusing on the correlator for the forces that particles B exert on a particle of species A . Owing to the large dimensional limit, the initial interparticle separation is entirely encoded in the radial distribution function $g_{\mu\nu}(r) = e^{-\beta v_{\mu\nu}(r)}$ or in its expression in terms of $h_{\mu\nu} \bar{g}(h_{\mu\nu}) \equiv g_{\mu\nu}(r)$. We thus have, using the limit $d \rightarrow +\infty$,

$$\begin{aligned} \frac{1}{dN_A} \sum_{i \in A, j \in B} \langle \mathbf{F}_{i,j}(t) \cdot \mathbf{F}_{i,j}(0) \rangle &= \frac{\rho_A \rho_B}{dN_A} \int d\mathbf{x} d\mathbf{y} g_{AB}(\mathbf{x} - \mathbf{y}) \langle v'_{AB}(\mathbf{x}(t) - \mathbf{y}(t)) \rangle_{\mathbf{x}-\mathbf{y}}^{AB} v'_{AB}(\mathbf{x} - \mathbf{y}) \\ &= \frac{\rho_B}{d} \int d\mathbf{r}_0 g_{AB}(\mathbf{r}_0) v'_{AB}(\mathbf{r}_0) \langle v'_{AB}(\mathbf{r}(t)) \rangle_{\mathbf{r}_0}^{AB} \\ &= \frac{\rho_B S_d}{d} \int_0^{+\infty} dr_0 r_0^{d-1} g_{AB}(\mathbf{r}_0) v'_{AB}(\mathbf{r}_0) \langle v'_{AB}(\mathbf{r}(t)) \rangle_{\mathbf{r}_0}^{AB} \\ &= \rho_B S_d \left(\frac{\ell_A + \ell_B}{2} \right)^d \int_{-\infty}^{+\infty} dh_0 e^{h_0} \bar{g}(h_0) \bar{v}'(h_0) \langle \bar{v}'(h(t)) \rangle_{h_0}^{AB} \\ &= \rho_B S_d \ell_B^d \left(1 + \frac{\delta}{2d} \right)^d \int_{-\infty}^{+\infty} dh_0 e^{h_0} \bar{g}(h_0) \bar{v}'(h_0) \langle \bar{v}'(h(t)) \rangle_{h_0}^{AB} \\ &= \frac{d^2}{\ell_A^2} \hat{\varphi}_B e^{\frac{\delta}{2}} \int_{-\infty}^{+\infty} dh_0 e^{h_0} \bar{g}(h_0) \bar{v}'(h_0) \langle \bar{v}'(h(t)) \rangle_{h_0}^{AB} \\ &= \frac{d^2}{\ell_A^2} \hat{\varphi} x e^{\frac{\delta}{2}} \int_{-\infty}^{+\infty} dh_0 e^{h_0 - \beta \bar{v}(h_0)} \bar{v}'(h_0) \langle \bar{v}'(h(t)) \rangle_{h_0}^{AB}, \end{aligned} \quad (\text{G.8})$$

with $S_d \equiv dV_d$ the surface of a unit sphere in d dimensions. The final line of Eq. (G.8) is precisely the term appearing the second line of Eq. (G.7). The other terms can be computed in a similar manner.

We now turn to the determination of the two-body processes necessary to close the dynamical mean field equations.

G2 Two-body process

The two-body processes involving the same species can be determined by directly taking the time derivative of $\mathbf{r}_{\mu\mu}$ while sorting out from the memory kernel the two-body force between the two particles:

$$\begin{aligned}\zeta \dot{\mathbf{r}}_{\mu\mu} &= -\nabla v_{\mu\mu}(\mathbf{r}_{\mu\mu}) - \frac{\beta}{2} \int_0^t d\tau M_\mu(t-\tau) \dot{\mathbf{r}}_{\mu\mu}(\tau) + \Xi_{\mu\mu}(t) \\ \langle \Xi_{\mu\mu}(t) \otimes \Xi_{\nu\nu}(t') \rangle &= \delta_{\mu\nu} \mathbf{1} \left[T\zeta \delta(t-t') + \frac{1}{2} M_\mu(t-t') \right]\end{aligned}\quad (\text{G.9})$$

The determination of the equation of motion for the distance \mathbf{r}_{AB} between particles of different species proceeds in a slightly different manner. We first consider the equations of motion for the single particle displacement \mathbf{u}_A , \mathbf{u}_B separately, while keeping outside of the memory kernel the interaction between the two specific particles A and B :

$$\begin{aligned}\zeta \dot{\mathbf{u}}_A &= -\nabla v(\mathbf{r}_{AB}) - \beta \int_0^t d\tau M_A(t-\tau) \dot{\mathbf{u}}_A + \Xi_A(t) \\ \zeta \dot{\mathbf{u}}_B &= \nabla v(\mathbf{r}_{AB}) - \beta \int_0^t d\tau M_B(t-\tau) \dot{\mathbf{u}}_B + \Xi_B(t)\end{aligned}\quad (\text{G.10})$$

We introduce the Laplace transform $\tilde{\mathbf{u}}(s) \equiv \int_0^{+\infty} e^{-st} \mathbf{u}(s) dt$ and write

$$\begin{aligned}\widetilde{K}_A(s) [s\tilde{\mathbf{u}}_A - \mathbf{u}_A(0)] &= -\nabla \tilde{v}(s) + \tilde{\Xi}_A(s) \\ \widetilde{K}_B(s) [s\tilde{\mathbf{u}}_B - \mathbf{u}_B(0)] &= \nabla \tilde{v}(s) + \tilde{\Xi}_B(s)\end{aligned}\quad (\text{G.11})$$

with

$$\begin{aligned}\widetilde{K}_\mu(s) &= 2T\zeta + \widetilde{M}_\mu(s) \\ \langle \tilde{\Xi}_\mu(s) \otimes \tilde{\Xi}_\nu(s') \rangle &= \mathbf{1} \delta_{\mu\nu} \frac{\widetilde{K}_\mu(s) + \widetilde{K}_\mu(s')}{s + s'}\end{aligned}\quad (\text{G.12})$$

We can multiply the first and the second line of Eq. (G.11) by $\widetilde{K}_B(s)$ and $\widetilde{K}_A(s)$ respectively, subtracting the second from the first, and dividing both terms by $\widetilde{K}_A(s) + \widetilde{K}_B(s)$. We finally obtain

$$\widetilde{K}_{AB}(s) [s\tilde{\mathbf{r}}_{AB}(s) - \mathbf{r}_{AB}(0)] = -\nabla \tilde{v}(s) + \tilde{\Xi}_{AB}(s) \quad (\text{G.13})$$

with $\tilde{\Xi}_{AB}(s)$ a Gaussian colored noise with zero mean, and

$$\begin{aligned}\widetilde{K}_{AB}(s) &\equiv \frac{\widetilde{K}_A(s)\widetilde{K}_B(s)}{\widetilde{K}_A(s) + \widetilde{K}_B(s)} \\ \langle \tilde{\Xi}_{AB}(s) \otimes \tilde{\Xi}_{AB}(s') \rangle &= \mathbf{1} \frac{\widetilde{K}_{AB}(s) + \widetilde{K}_{AB}(s')}{s + s'}\end{aligned}\quad (\text{G.14})$$

the two-body process between species A and B is therefore an equilibrium process with a memory kernel given by the geometric mean of the kernels governing the single-particle dynamics of each species. We have thus self-consistently closed the dynamical mean field equation. In the next Section, we study the long time limit of the memory kernels.

G3 Long time plateau of the memory kernel

The memory kernel $\widetilde{K}(s)$, can be separated into two contribution:

$$\lim_{s \rightarrow 0} \widetilde{K}_{AB,f}(s) \equiv \lim_{s \rightarrow 0} \widetilde{K}_{AB,f}(s) + \frac{M_{AB,\infty}}{s}. \quad (\text{G.15})$$

$\widetilde{K}_{AB,f}(s \rightarrow 0) < +\infty$ is a regular term in the zero frequency limit, while the second term diverges when $M_{AB,\infty}$ is different from 0. An analogous decomposition can be done for the memory kernels M_A and M_B :

$$\widetilde{M}_A(s \rightarrow 0) \equiv M_{\mu,f}(s \rightarrow 0) + \frac{M_{\mu,\infty}}{s}. \quad (\text{G.16})$$

The plateau value $M_{AB,\infty}$ is related to $M_{\mu,\infty}$. This can be explicitly seen by computing its singular part

$$\begin{aligned} \widetilde{K}_{AB}(s) &= \frac{\left(T\zeta + M_{A,f}(s) + \frac{M_{A,\infty}}{s}\right)\left(T\zeta + M_{B,f}(s) + \frac{M_{B,\infty}}{s}\right)}{2T\zeta + M_{A,f}(s) + M_{B,f}(s) + \frac{M_{A,\infty} + M_{B,\infty}}{s}} \\ &= \widetilde{K}_{AB,f}(s) + \frac{M_{A,\infty}M_{B,\infty}}{s(M_{A,\infty} + M_{B,\infty})} \end{aligned} \quad (\text{G.17})$$

from which we read

$$M_{AB,\infty} = \frac{M_{A,\infty}M_{B,\infty}}{M_{A,\infty} + M_{B,\infty}}. \quad (\text{G.18})$$

The plateau value of the memory kernel for the inter-species process is related, through a geometric mean by the ones of the processes between particles of the same species.

We thus see that there can be three distinct dynamical regimes:

- $M_{A,\infty} = 0$ and $M_{B,\infty} = 0$, which implies $M_{AB,\infty} = 0$, corresponding to the ergodic phase.
- $M_{\mu,\infty} \neq 0$ and $M_{\bar{\mu},\infty} = 0$, which implies $M_{AB,\infty} = 0$. This correspond to a single glass phase found in [137], where only the particles of one species are arrested.
- $M_{A,\infty} \neq 0$ and $M_{B,\infty} \neq 0$, which implies $M_{AB,\infty} \neq 0$. In this double-glass phase [137], particles of both species are arrested.

The temperature below which $M_{\mu,\infty} \neq 0$ is determined using the same approach described in Chapter 5.5.1. The self-consistent equations read

$$\begin{aligned}\mathcal{M}_{A,\infty} &= \frac{\hat{\varphi}}{2} \left[(1-x) \int_{-\infty}^{+\infty} dh_0 e^{h_0 - \beta \bar{v}(h_0)} \bar{v}'(h_0) \langle \bar{v}'(h) \rangle_{h_0}^{AA} \right. \\ &\quad \left. + x e^{\frac{\delta}{2}} \int_{-\infty}^{+\infty} dh_0 e^{h_0 - \beta \bar{v}(h_0)} \bar{v}'(h_0) \langle \bar{v}'(h) \rangle_{h_0}^{AB} \right] \\ \mathcal{M}_{B,\infty} &= \frac{\hat{\varphi}}{2} \left[x \int_{-\infty}^{+\infty} dh_0 e^{h_0 - \beta \bar{v}(h_0)} \bar{v}'(h_0) \langle \bar{v}'(h) \rangle_{h_0}^{BB} \right. \\ &\quad \left. + (1-x) e^{-\frac{\delta}{2}} \int_{-\infty}^{+\infty} dh_0 e^{h_0 - \beta \bar{v}(h_0)} \bar{v}'(h_0) \langle \bar{v}'(h) \rangle_{h_0}^{AB} \right]. \\ \langle \bar{v}'(h) \rangle_{h_0}^{\mu\mu} &= \frac{1}{(\pi \mathcal{M}_{\mu,\infty})^{1/2}} \int d\Xi_{\mu,\infty} e^{-\frac{\Xi_{\mu,\infty}^2}{\mathcal{M}_{\mu,\infty}}} \int dh p_B(h, |\mathcal{M}_{\mu,\infty}, \Xi_{\mu,\infty}, h_0) \bar{v}'(h) \\ \langle \bar{v}'(h) \rangle_{h_0}^{AB} &= \frac{1}{(\pi \mathcal{M}_{AB,\infty})^{1/2}} \int d\Xi_{AB,\infty} e^{-\frac{\Xi_{AB,\infty}^2}{\mathcal{M}_{AB,\infty}}} \int dh p_B(h, |\mathcal{M}_{AB,\infty}, \Xi_{AB,\infty}, h_0) \bar{v}'(h)\end{aligned}\tag{G.19}$$

with $p_B(h, |\mathcal{M}_\infty, \Xi_\infty, h_0)$ the steady state distribution for the two-body gap h , given a fixed plateau value of the memory kernel \mathcal{M}_∞ , long time noise realisation Ξ_∞ and initial condition h_0 :

$$\begin{aligned}p_B(h, |\mathcal{M}_\infty, \Xi_\infty, h_0) &\equiv \frac{e^{-\beta w(h|\mathcal{M}_\infty, \Xi_\infty, h_0)}}{\int dh' e^{-\beta w(h'|\mathcal{M}_\infty, \Xi_\infty, h_0)}} \\ w(h|\mathcal{M}_\infty, \Xi_\infty, h_0) &\equiv \frac{1}{4} \mathcal{M}_\infty (h - h_0)^2 - \Xi_\infty h.\end{aligned}\tag{G.20}$$

Eq. (G.19) allows, in principle to determine the location of the dynamical glass transition in bidisperse fluids in large dimensions. In the next section, we make a connection with the static result presented in [137] by means of a Gaussian ansatz.

G4 Connection with Ikeda *et al.* [137]

The equations for the memory kernels $M_{A,\infty}, M_{B,\infty}$ can be turned into equations for the plateau value of the mean squared displacement of particles of species μ , $\Delta_\mu \equiv \lim_{t \rightarrow \infty} \frac{d}{\ell_\mu^2} \langle \mathbf{u}_\mu^2(t) \rangle$, performing a calculation analogous to the one of Section 5.7:

$$\begin{aligned}\Delta_\mu &= \frac{1}{\beta^2 \mathcal{M}_{\mu,\infty}} \\ \Delta_{AB} &\equiv \frac{\Delta_A + \Delta_B}{2}\end{aligned}\tag{G.21}$$

In the ergodic phase particles diffuse at long times and $\Delta_\mu + \infty$. When dynamical arrest occurs for particles of species μ , then we have Δ_μ has a finite value, which has the physical meaning of the size of the cage in which particles are trapped.

The equations for the plateaus then read, once they are expressed in terms of Δ_μ

$$\begin{aligned} \frac{1}{\Delta_A} &= \hat{\varphi} \left[(1-x) \int_{-\infty}^{+\infty} dh e^{-h} \log q_{\Delta_A}(h) \frac{\partial}{\partial \Delta_A} q_{\Delta_A}(h) \right. \\ &\quad \left. + x e^{\frac{\delta}{2}} \int_{-\infty}^{+\infty} dh e^{-h} \log q_{\Delta_{AB}}(h) \frac{\partial}{\partial \Delta_{AB}} q_{\Delta_{AB}}(h) \right] \\ \frac{1}{\Delta_B} &= \hat{\varphi} \left[x \int_{-\infty}^{+\infty} dh e^{-h} \log q_{\Delta_B}(h) \frac{\partial}{\partial \Delta_B} q_{\Delta_B}(h) \right. \\ &\quad \left. + (1-x) e^{-\frac{\delta}{2}} \int_{-\infty}^{+\infty} dh e^{-h} \log q_{\Delta_{AB}}(h) \frac{\partial}{\partial \Delta_{AB}} q_{\Delta_{AB}}(h) \right] \end{aligned} \quad (\text{G.22})$$

with

$$q_\Delta(h) \equiv \int \frac{dz}{\sqrt{2\pi\Delta}} e^{-\beta\bar{v}(h+\Delta/2+z)} e^{-\frac{z^2}{2\Delta}}. \quad (\text{G.23})$$

In the case of a hard sphere potential, when $\bar{v}(h) = +\infty$ if $h \leq 0$ and 0 otherwise, $q_\Delta(h)$ reduces to

$$q_\Delta(h) = \frac{1}{2} \left[1 + \operatorname{erf} \left(\frac{h + \Delta/2}{\sqrt{2\Delta}} \right) \right] \quad (\text{G.24})$$

and we the equations of Ikeda *et al.* [137]. The iterative solution of Eq. (G.22) shows that, for opportunely chosen values of the size ratio difference δ and the relative concentration x one can obtain, by varying $\hat{\varphi}$ a transition from a liquid phase to a single glass phase, where only particle of type A are arrested, to a double glass phase where both particle of type A and B are frozen. In Fig. G.1, we show the resulting dynamical phase diagram reproducing the results in [137].

G5 Generalization to multi-component mixtures

We present an immediate generalization of Eq. (G.22) for the case of polydisperse mixture with a discrete number m of families $\mu = A, B, C, \dots$. Each family has a typical interaction diameter ℓ_μ , which scales in the large dimensional limit as

$$\frac{\ell_\mu}{\ell_{\min}} = 1 + \frac{\delta_\mu}{d} \quad (\text{G.25})$$

with $\ell_{\min} \equiv \min_\mu \ell_\mu$ the minimal diameter among the different species, which implies that $\delta_\mu \geq 0$. We introduce then m volume fractions $x_\mu \equiv \frac{\varphi_\mu}{\sum_\nu \varphi_\nu}$, which satisfy the condition $\sum_\nu x_\nu = 1$. Eq. (G.22) then generalizes to

$$\frac{1}{\Delta_\mu} = \hat{\varphi} \sum_\nu x_\nu e^{\frac{\delta_\mu - \delta_\nu}{2}} \int_{-\infty}^{+\infty} dh e^{-h} \log q_{\Delta_\mu}(h) \frac{\partial}{\partial \Delta_{\mu\nu}} q_{\Delta_{\mu\nu}}(h). \quad (\text{G.26})$$

with $\Delta_{\mu\nu} \equiv \frac{\Delta_\mu + \Delta_\nu}{2}$. Based on the double glass transition observed in the bidisperse case, it is then reasonable to expect multiple glass transitions o arise in the presence of

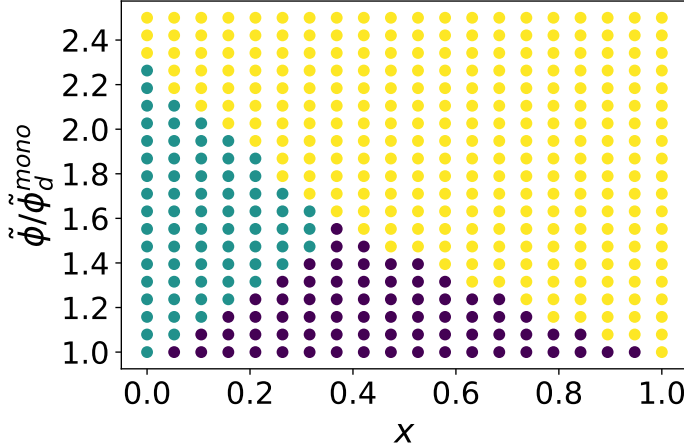


Figure G.1: Dynamical phase diagram of the bidisperse fluid for $\delta = 3.0$. $\hat{\varphi}_d^{\text{mono}} \approx 4.8067$ is the critical packing fraction for the glass transition of monodisperse hard spheres. Violet points: fully ergodic phase ($\Delta_\mu = +\infty$ for $\mu = A, B$); Green points: single glass phase ($\Delta_A < +\infty$, $\Delta_B = \infty$) with particles of type A dynamical arrested; yellow points: double glass phase ($\Delta_A < +\infty$, $\Delta_B = \infty$) with both particles of type A and B dynamically frozen. This is image reproduces results reported in [137]

many families of particles, if their distribution is carefully chosen. We solved Eq. (G.26) in the case of $m = 3$, choosing the following hierarchical distribution for the volume fractions

$$\begin{aligned}\hat{\varphi}_A &= \frac{\hat{\varphi}}{1 + x + x^2} \\ \hat{\varphi}_B &= x\hat{\varphi}_A \\ \hat{\varphi}_C &= x\hat{\varphi}_B\end{aligned}\tag{G.27}$$

with particles of type C the one with the smallest diameter. The results are shown in Fig G.2. By varying $\hat{\varphi}$ and the control parameter x , multiple glass transitions are observed, as we pass from an ergodic liquid to a single, double and triple glass where particle undergo dynamical arrest consecutively upon varying the total density, starting from the largest ones.

In this Appendix, we have presented some ongoing work on the dynamics of bidisperse, and polydisperse liquids in the large dimensional limit. Natural directions of development of this work are a more complete investigation of which discrete distributions of the polydispersity give rise to multiple glass transitions and which distributions do not. Further insights into the dynamics of the particles in the ergodic case could be obtained by means of numerical integration [185], and shed light on the nature, in mean field, of the different relaxation channels exploited by particles of different sizes. For continuously polydisperse mixture it has been shown in a recent work [1], by means of static calculations, that both in the case of exponential and nearly monodisperse distributions there exists a regime where only particles above a threshold size vitrify, with

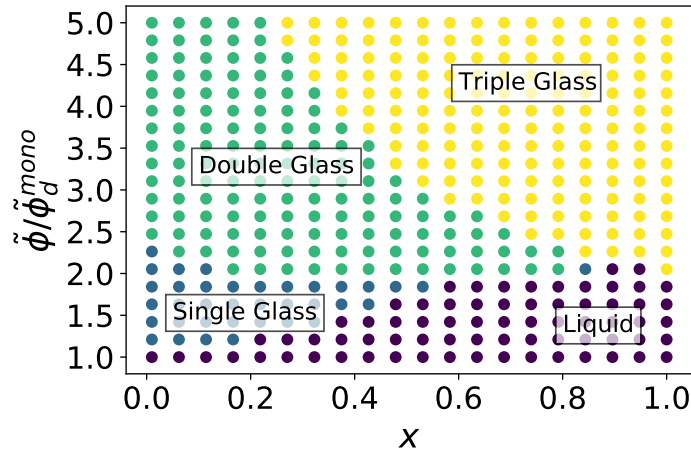


Figure G.2: Dynamical phase diagram of a ternary mixture in infinite dimensions for $\delta_A = 6.0$, $\delta_B = 3.0$ and $\delta_C = 0$.

a critical behavior of the cage size for particle with a size close to the threshold. How does the dynamics of the particles look like in this regime is an intriguing question, that could be addressed through the approach illustrated here.

APPENDIX H

DOES SWAP IN LARGE DIMENSIONS WORK?

This Appendix contains some theoretical considerations on the behavior of the Swap algorithm in the high dimensional limit. The Swap algorithm, and its collective version presented in Chapter 7, achieve in continuously polydisperse supercooled liquids a speedup of many orders of magnitude with respect to the ordinary Metropolis dynamics. Beyond its practical applications, the acceleration provided by Swap has sprouted many theoretical reflections [258, 29] concerning the interplay between static and dynamic properties of supercooled liquids. Our understanding of how the swap algorithm bypass the sluggishness of supercooled liquids is incomplete. A static ansatz in the high dimensional limit, based on the replica method [138], a mode-coupling approach [245, 246] and extrapolation to the large dimensional limit of numerical simulations [31] suggest that the Swap algorithm shifts the dynamical ergodicity breaking temperature. During my thesis, I attempted to build a dynamical mean field theory of the Swap dynamics for liquids in large dimensions. However, while doing so, it became apparent that the Swap dynamics in the large dimensional limit either reduces to normal dynamics, or samples a different glassy state from the one obtained without particle swaps.

H1 Swap dynamics with continuous diameter distribution

We consider a continuously polydisperse liquid of interacting particles in d dimensions, and compare two types of equilibrium dynamics. The first one is the usual overdamped Langevin dynamics

$$\begin{aligned}\zeta \dot{\mathbf{r}}_i &= -\frac{\partial H_\sigma(\mathbf{r}^N)}{\partial \mathbf{r}_i} + \sqrt{2\zeta T} \boldsymbol{\xi}_i(t) \\ &= -\sum_{j \neq i} \partial_{\mathbf{r}_i} v(|\mathbf{r}_i - \mathbf{r}_j|, \sigma_i, \sigma_j) + \sqrt{2\zeta T} \boldsymbol{\xi}_i(t)\end{aligned}\tag{H.1}$$

where $\xi_i(t)$ is a Gaussian white noise with correlations $\langle \xi_i(t) \otimes \xi_j(t') \rangle = \delta_{ij} \mathbf{1}\delta(t - t')$, ζ the friction coefficient, σ_i is the diameter of particle i , and $v(r, \sigma, \sigma')$ is an isotropic pairwise interaction potential that depends on the diameters σ, σ' of the interacting particles, as well as on their distance r . The Hamiltonian $H_\sigma(\mathbf{r}^N) = \sum_{i < j} v(r_{ij}, \sigma_i, \sigma_j)$ is the energy of the system given a configurations of diameters σ^N , which are quenched variables in the usual dynamics.

The second dynamics is a continuous version of the Swap dynamics, whose formulation in the underdamped case was proposed in [34]. Now the diameters are annealed variables, allowed to evolve under the action of an external potential $\sum_i w(\sigma_i)$. The Hamiltonian of the system $H(\mathbf{r}^N, \sigma^N)$ is

$$H(\mathbf{r}^N, \sigma^N) \equiv \sum_{i < j} v(r_{ij}, \sigma_i, \sigma_j) + \sum_i w(\sigma_i) = H_\sigma(\mathbf{r}^N) + \sum_i w(\sigma_i) \quad (\text{H.2})$$

and the corresponding Swap overdamped Langevin dynamics is

$$\begin{aligned} \zeta \dot{\mathbf{r}}_i &= - \sum_{j \neq i} \partial_{\mathbf{r}_i} v(|\mathbf{r}_i - \mathbf{r}_j|, \sigma_i, \sigma_j) + \sqrt{2\zeta T} \xi_i(t) \\ \zeta_{\text{sw}} \dot{\sigma}_i &= - \sum_{j \neq i} \partial_{\sigma_i} v(|\mathbf{r}_i - \mathbf{r}_j|, \sigma_i, \sigma_j) - \partial_{\sigma_i} w(\sigma_i) + \sqrt{2T\zeta_{\text{sw}}} \chi(t) \end{aligned} \quad (\text{H.3})$$

with the Gaussian white noise $\chi(t)$ has zero mean and correlations $\langle \chi_i(t) \chi_j(t') \rangle = \delta_{ij} \delta(t - t')$. The ratio ζ/ζ_{sw} sets the relative timescale of motion of the diameters with respect to the translational degrees of freedom.

H1.1 Determination of w : annealed and quenched averages

The external potential $w(\sigma)$ is determined by matching the value of equilibrium observables in the two systems, as we now show. Let $O(\mathbf{r}^N, \sigma^N)$ be a generic observable that depends both on the position and diameters of the liquid. Using the dynamics with quenched diameters given by Eq. (H.1), the equilibrium value of $O(\mathbf{r}^N, \sigma^N)$ is given by the quenched average $\langle \dots \rangle_\sigma$, where the realization of the diameter is fixed.

$$\langle O(\mathbf{r}^N, \sigma^N) \rangle_\sigma = \frac{1}{Z_\sigma} \int d\mathbf{r}^N e^{-\beta H_\sigma(\mathbf{r}^N)} O(\mathbf{r}^N, \sigma^N), \quad (\text{H.4})$$

where the partition function Z_σ is

$$Z_\sigma \equiv \int d\mathbf{r}^N e^{-\beta H_\sigma(\mathbf{r}^N)}. \quad (\text{H.5})$$

On the other hand, the annealed average $\langle \dots \rangle$, obtained by letting the particles' positions and diameters evolve through Eq. (H.3) is

$$\langle O(\mathbf{r}^N, \sigma^N) \rangle \equiv \frac{1}{Z} \int d\mathbf{r}^N d\sigma^N e^{-\beta H(\mathbf{r}^N, \sigma^N)} O(\mathbf{r}^N, \sigma^N) \quad (\text{H.6})$$

with the new annealed partition function Z ,

$$Z \equiv \int d\mathbf{r}^N d\sigma^N e^{-\beta H(\mathbf{r}^N, \sigma^N)}. \quad (\text{H.7})$$

We now impose the quenched average, after averaging over all the realizations of the diameter distribution $\pi(\sigma^N)$, to match the annealed average:

$$\begin{aligned} \langle O(\mathbf{r}^N, \sigma^N) \rangle &= \int d\sigma^N \pi(\sigma^N) \langle O(\mathbf{r}^N, \sigma^N) \rangle_\sigma \\ &= \int d\sigma^N \pi(\sigma^N) \frac{1}{Z_\sigma} \int d\mathbf{r}^N e^{-\beta H_\sigma(\mathbf{r}^N)} O(\mathbf{r}^N, \sigma^N) \end{aligned} \quad (\text{H.8})$$

Using the definition of quenched and annealed average, Eq. (H.8) leads to the condition

$$\pi(\sigma^N) = \frac{Z_\sigma}{Z} e^{-\beta \sum_i w(\sigma_i)} \quad (\text{H.9})$$

Eq. (H.9) establishes a relation between the potential w and the diameter distribution π . The partition function Z_σ involves many-body interactions between the diameters, while the exponential on the right hand side of Eq. (H.9) factorizes into a product of single body terms. This means, interestingly, that for Eq. (H.9) to be valid the distribution $\pi(\sigma^N)$ must involve high order correlations among the diameter of the particles. Conversely if this were not the case, we would need to replace the one-body potential $\sum_i w(\sigma_i)$ with a many-body one, which would lead to interactions among the particle diameters.

H1.2 Infinite-dimensional limit

We now explore how to take the infinite dimensional limit of Eq. (H.3). Following the criterion suggested by Ikeda *et al.* [137, 1], and adopted in App. G for bidisperse mixtures, we introduce rescaled particle diameters $s_i \equiv d \left(\frac{\sigma_i}{\sigma_0} - 1 \right)$, with σ_0 a reference diameter, and a rescaled interparticle distance $h_{ij} \equiv d \left(\frac{r_{ij}}{\sigma_0} - 1 \right)$. We also introduce rescaled potentials $\bar{v}(h, s, s') \equiv v(r, \sigma, \sigma')$ and $\bar{w}(s) \equiv w(\sigma)$. The first line of Eq. (H.3) becomes

$$\zeta \dot{\mathbf{r}}_i = -d \sum_{j \neq i} \hat{\mathbf{r}}_{ij} \partial_{h_{ij}} \bar{v}(h_{ij}, s_i, s_j) + \sqrt{2T\zeta} \xi_i(t) \quad (\text{H.10})$$

with $\hat{\mathbf{r}}_{ij} \equiv \frac{|\mathbf{r}_i - \mathbf{r}_j|}{r_{ij}}$. Here the different terms have the same scaling in d , as already observed in Chapter 5: looking at component $\alpha = 1, \dots, d$ of Eq. (H.10), we have

$$\zeta \underbrace{\dot{r}_{i,\alpha}}_{O(d^{-1})} = -d \sum_{\substack{j \neq i \\ O(d^{1/2})}} \underbrace{\hat{r}_{ij,\alpha}}_{\text{contribution from fluctuating terms}} \bar{v}'(h_{ij}, s_i, s_j) + \sqrt{2T\zeta} \xi_{\alpha,i}(t). \quad (\text{H.11})$$

The dynamical evolution unfolds over a time of order $O(1)$ in d if we work with the rescaled friction coefficient $\hat{\zeta} \equiv d^{-2}\zeta$.

For the dynamics of the diameters, we have

$$\zeta_{\text{sw}} d^{-1} \sigma_0 \dot{\sigma}_i = -\frac{d}{\sigma_0} \underbrace{\sum_{j \neq i} \partial_{s_i} \bar{v}(h_{ij}, s_i, s_j)}_{O(d^{1/2})} - \frac{d}{\sigma_0} \bar{w}'(s_i) + \sqrt{2T\zeta_{\text{sw}}} \chi_i(t), \quad (\text{H.12})$$

or, after book-keeping the orders of d

$$\zeta_{\text{sw}} O(d^{-1}) = O(d^{3/2}) + O(d) + O(\sqrt{\zeta_{\text{sw}}}). \quad (\text{H.13})$$

We have then two possibilities in choosing the scaling of ζ_{sw} , both leading to pathological dynamics. The first one is $\zeta_{\text{sw}} = d^2 \hat{\zeta}_{\text{sw}}$, which represents an attempt at constraining the dynamics of the diameters to unfold on the same timescale of the translational degrees of freedom. However, in this case the first term on the right hand side of Eq. (H.12) dominates, and we expect the diameter to instantaneously freeze around the minimum of the potential $\sum_{i < j} \bar{v}(h, s, s')$. The second choice is $\zeta_{\text{sw}} = d^{5/2} \hat{\zeta}_{\text{sw}}$, which makes the ratio $\frac{\hat{\zeta}}{\zeta_{\text{sw}}} \sim O(d^{-1/2})$, implying that the diameters are frozen in the times over which the dynamics of the translational degrees of freedom unfolds, and the annealed dynamics Eq. (H.3) never takes place.

In the next section, we show that a similar freezing scenario is to be expected for the case of a bidisperse mixture where the swap dynamics is implemented through jump processes, without introducing correlation between the diameters, neither at the level of the diameter distribution nor of the potential w .

H2 Swap rates in large dimensions

In this Section, we consider a binary mixture in large dimension. We consider N particles in a volume V . Each particle i has a label μ_i identifying its species, $\mu_i = \mu_A, \mu_B$, and its corresponding diameter σ_{μ_i} . The position of the particles \mathbf{R}_i evolve according to the usual overdamped Langevin dynamics

$$\dot{\zeta} \mathbf{R}_i = - \sum_{j \neq i} v(R_{ij}, \sigma_i, \sigma_j) + \sqrt{2T\zeta} \xi_i(t) \quad (\text{H.14})$$

with $v(R_{ij}, \sigma_i, \sigma_j)$ an interaction potential as described below Eq. (H.1). On top of the evolution of translational degrees of freedom, a particle i is allowed to change from species $\mu_i = A$ (B) to species $\bar{\mu}_i = B$ (A) with rate ω_i . These rates are tuned so that the equilibrium distribution of the dynamics is the Boltzmann distribution

$$\rho_B \propto \exp \left[-\beta \sum_{i < j} v(R_{ij}, \sigma_{\mu_i}, \sigma_{\mu_j}) + \Delta\mu_{\text{chem}} (N_A - N_B) \right] \quad (\text{H.15})$$

The chemical potential difference $\Delta\mu_{\text{chem}}$ is determined by fixing the average particle number concentration $\langle \frac{N_A}{N} \rangle \equiv n_A = 1 - n_B$, and it mimics the effects of a diameter

reservoir in contact with the system. An example of rates that satisfy the detailed balance condition and that lead to the Boltzmann distribution given by Eq. (H.15) are

$$\omega_i \equiv \frac{1}{\tau_{sw}} e^{-\frac{\beta}{2} \left[\sum_{j \neq i} v(R_{ij}, \sigma_{\bar{\mu}_i}, \sigma_{\mu_j}) - v(R_{ij}, \sigma_{\mu_i}, \sigma_{\mu_j}) \right] + \Delta \mu_{chem} (\delta_{\mu_i, B} - \delta_{\mu_i, A})}. \quad (\text{H.16})$$

The argument of the exponential is half of the energy difference between the state where particle i has changed species and the state where particle i has kept its initial species. The time τ_{sw} fixes the typical time scale over which the particle change species

In the large dimensional limit, the rates ω_i behave pathologically, as they either grow or decay exponentially in \sqrt{d} . To see this, we adopt rescaled variables for the diameters $s_{\mu_i} \equiv d \left(\frac{\sigma_{\mu_i}}{\sigma_0} - 1 \right)$, and for the overlap $R_{ij} \equiv d \left(\frac{R_{ij}}{\sigma_0} - 1 \right)$, with σ_0 a reference length scale of the system. Using the rescaled potential defined above Eq. (H.10) the difference in the potential energy of interaction becomes

$$\begin{aligned} \sum_{j \neq i} \left[v(R_{ij}, \sigma_{\bar{\mu}_i}, \sigma_{\mu_j}) - v(R_{ij}, \sigma_{\mu_i}, \sigma_{\mu_j}) \right] &= \sum_{j \neq i} \left[v(R_{ij}, \sigma_{\mu_i} \left(1 + \frac{s_{\bar{\mu}_i} - s_{\mu_i}}{d} \right), \sigma_{\mu_j}) - v(R_{ij}, \sigma_{\mu_i}, \sigma_{\mu_j}) \right] \\ &\approx \sum_{j \neq i} \frac{s_{\bar{\mu}_i} - s_{\mu_i}}{d} \sigma_{\mu_i} \frac{\partial v(R_{ij}, \sigma_{\mu_i}, \sigma_{\mu_j})}{\partial \sigma_{\mu_i}} \\ &= (s_{\bar{\mu}_i} - s_{\mu_i}) \sum_{j \neq i} \sigma_0^{-1} \frac{\partial \bar{v}(h_{ij}, s_{\mu_i}, s_{\mu_j})}{\partial s_{\mu_i}} + O(d^{-1/2}) \\ &\sim (s_{\bar{\mu}_i} - s_{\mu_i}) \times O(d^{1/2}). \end{aligned} \quad (\text{H.17})$$

In the first line, we have used the fact that $\frac{\sigma_{\bar{\mu}_i}}{\sigma_{\mu_i}} = 1 + \frac{s_{\bar{\mu}_i} - s_{\mu_i}}{d} + O(d^{-2})$. The calculation in Eq. (H.17) shows that the rates at which particles turn from one species to another depend exponentially on \sqrt{d} , in stark contrast with the dynamics of the position of the particles, which unfolds over a time $O(1)$ in the space dimension. Moreover, if we assume that the interaction potential is a monotonously increasing function of s , $\partial_s \bar{v}(h, s, s') > 0$, then the sign in the last line of Eq. (H.17) is equal to the sign of $s_{\bar{\mu}_i} - s_{\mu_i}$. This implies that the rates at which small particles turn to large ones are of order $O(e^{-\sqrt{d}})$, which suggests that the swap dynamics is completely frozen in the large dimensional limit. An example of a potential for which $\partial_s \bar{v}(h, s, s') > 0$ is a power law potential of the form

$$v(r, \sigma, \sigma') \equiv \varepsilon \left(\frac{\frac{1}{2}(\sigma + \sigma')}{r} \right)^{ad} \quad (\text{H.18})$$

with $a > 0$, and of order $O(1)$ in the space dimension d . Using rescaled diameter and distances, this potential becomes

$$\begin{aligned} v(r, \sigma, \sigma') &\approx \varepsilon \left(1 + \frac{s + s'}{2d} \right)^{ad} \times \left(1 + \frac{h}{2d} \right)^{-ad} \\ &= \varepsilon e^{-ah + \frac{a}{2}(s+s')} \equiv \bar{v}(h, s, s'), \end{aligned} \quad (\text{H.19})$$

for which $\partial_s \bar{v}(h, s, s') > 0$.

In this Appendix, we presented some arguments that suggest that the Swap dynamics becomes either trivial or singular in the large dimensional limit. The fact that a similar feature might be observed also for the facilitated dynamics explored in Appendix A is intriguing, as both swap and –at least, in theory– the facilitated dynamics are extremely effective in finite dimensional systems. Our considerations are somewhat supported by the observation that Swap Monte Carlo loses its effectiveness as the space dimension is increased in numerical simulations [31]. We speculate that the shift in the mean field glass transition temperature found using approximated static calculations [138] implicitly relies on the assumption that the swap dynamics is capable, even in the infinite dimensional limit, to explore metastable states of a different nature than its counterpart without swaps. This assumption is put to the test by the preliminary observation presented here.

APPENDIX I

ADDITIONAL RESULT FOR CSWAP

I1 A model with a different polydispersity

To show that the efficiency of the cSwap algorithm does not depend on the specific polydispersity of the model studied in the main text, we study the relaxation dynamics of a second model. It consists of $N = 1024$ hard disks with a diameter distribution following a power law, $\pi(\sigma) \propto \sigma^{-3}$, with $\sigma_{\min} \leq \sigma \leq \sigma_{\max}$, as studied earlier [32]. We recall that the units of length are chosen so that $\bar{\sigma} = 1$. We have chosen the support of the diameter distribution such that the polydispersity is $\Delta = 23\%$. We ran *NVT* simulations using the six different algorithms studied in the main text at a large packing fraction, $\phi = 0.86$, where we measured the time decay of C_ψ . The results are shown in Fig. I.1. The hierarchy of speedups obtained by the different algorithm, and their relative values, is comparable to the results reported in the main text for a similar value of ϕ .

I2 Changing the length of the chain in ECMC

When using the ECMC algorithm, it is also possible to measure times using the number of directed chains of particles that have moved [23]. When comparing ECMC with other types of algorithms, however, this choice is a poor indicator of its efficiency, as it hides the number of particles—and hence of event determinations—that are involved in each chain. This is demonstrated in Fig. I.2(a), where the time relaxation of C_ψ is shown as a function the number of chain displaced during an ECMC in the *NVT* ensemble, for different values of the chain length ℓ . When times are measured according to the number of chains displaced, longer chains have a stronger impact on the system relaxation. However, if one measures times in units of Nt_{move} , thus counting individual particle displacements, we see that all the relaxation curves now collapse. This collapse implies that the efficiency of ECMC (in CPU time) is nearly independent of ℓ .

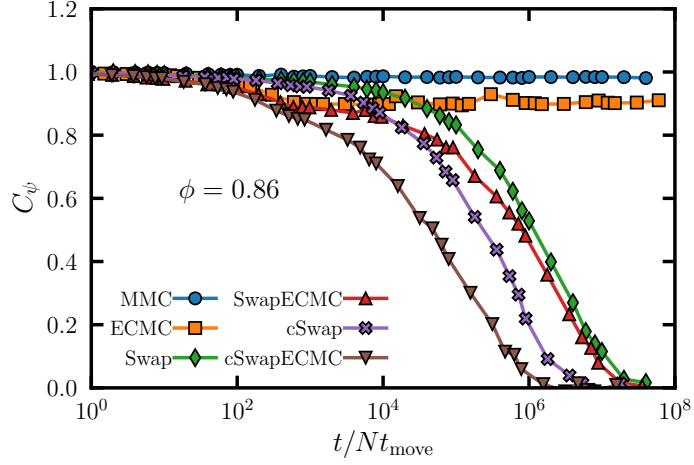


Figure I.1: Time dependence of the hexatic correlation function for a system of $N = 1024$ particles with a power law distribution of the diameters. Time is measured in units of Nt_{move} , and the efficiency of the algorithms that involve swap moves is comparable to the results shown in Fig. 2 of the main text near $\phi \approx 0.85$.

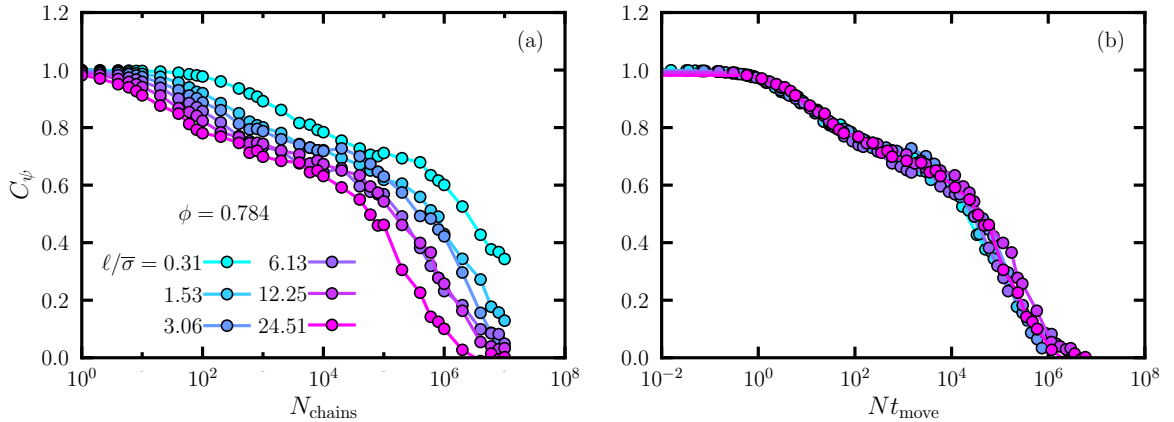


Figure I.2: Equilibrium correlation function for the ECMC dynamics, using different values of the chain length ℓ . Time is measured in units of (a) the number of chains displaced, and (b) Nt_{move} .

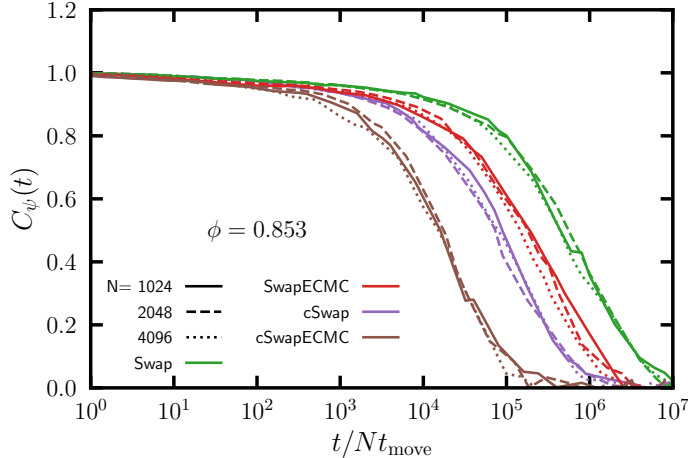


Figure I.3: Time dependence of the hexatic correlation function for systems of different sizes using the Swap, SwapECMC, cSwap and cSwapECMC algorithms in the NVT ensemble.

I3 Efficiency of the algorithms as a function of system size

In this section we address the question of how the gain provided by SwapECMC, cSwap and cSwapECMC behaves with the size of the system. We study the relaxation dynamics for polydisperse systems of $N = 1024$, 2048 , and 4096 hard disks, with the polydispersity defined as in Sec. I1. To avoid uncontrolled fluctuations in the distribution of the diameters and make a clear comparison between different system sizes, we generate the diameters $\{\sigma_i\}_{i=1,\dots,N}$ in each system of N particles in the following way: we first take N numbers $a_i = i/N$ with a uniform spacing in the interval $[0, 1]$. From each number a_i , the diameter σ_i is generated using the following relation

$$\sigma_i = \frac{\sigma_{\max}}{\sqrt{1 - a_i + a_i \left(\frac{\sigma_{\max}}{\sigma_{\min}}\right)^2}}, \quad (\text{I.1})$$

which maps a random number generated from the uniform distribution in the interval $[0, 1]$ to a random number generated from a power law distribution $\propto \sigma^{-3}$ between σ_{\min} and σ_{\max} .

We run NVT simulations using the Swap, SwapECMC, cSwap, cSwapECMC algorithms for the three system sizes at a high packing fraction $\phi = 0.853$, and we track the decay of the correlation function $C_\psi(t)$. The resulting curves, displayed in Fig I.3, demonstrate that the gain provided by the different algorithms is constant with respect to the size of the system. This is in line with previous results regarding swap efficiency in glass-formers.

CHAPTER I

BIBLIOGRAPHY

- [1] H. Kim and A. Ikeda, In preparation.
- [2] Milton Abramowitz and Irene A Stegun. *Handbook of mathematical functions with formulas, graphs, and mathematical tables*. Vol. 55. US Government printing office, 1948.
- [3] Elisabeth Agoritsas, Thibaud Maimbourg, and Francesco Zamponi. *Out-of-equilibrium dynamical equations of infinite-dimensional particle systems I. The isotropic case*. 2019.
- [4] Elisabeth Agoritsas, Thibaud Maimbourg, and Francesco Zamponi. “Out-of-equilibrium dynamical equations of infinite-dimensional particle systems. II. The anisotropic case under shear strain”. In: *Journal of Physics A: Mathematical and Theoretical* 52.33 (2019), p. 334001.
- [5] Berni Julian Alder and Thomas Everett Wainwright. “Phase transition for a hard sphere system”. In: *The Journal of chemical physics* 27.5 (1957), pp. 1208–1209.
- [6] Michael P Allen and Dominic J Tildesley. *Computer simulation of liquids*. Oxford university press, 2017.
- [7] Alexander Amini, Ava Soleimany, Sertac Karaman, and Daniela Rus. “Spatial uncertainty sampling for end-to-end control”. In: *arXiv preprint arXiv:1805.04829* (2018).
- [8] Christophe Andrieu, Nando De Freitas, Arnaud Doucet, and Michael I Jordan. “An introduction to MCMC for machine learning”. In: *Machine learning* 50 (2003), pp. 5–43.
- [9] L Angelani, A Costanzo, and R Di Leonardo. “Active ratchets”. In: *Europhysics Letters* 96.6 (2011), p. 68002.
- [10] Charles Austen Angell. “Structural instability and relaxation in liquid and glassy phases near the fragile liquid limit”. In: *Journal of non-crystalline solids* 102.1-3 (1988), pp. 205–221.
- [11] Simon Apers, Alain Sarlette, and Francesco Ticozzi. “Fast Mixing with Quantum Walks vs. Classical Processes”. In: *Quantum Information Processing (QIP) 2017*. 2017.
- [12] JE Avron. “Odd viscosity”. In: *Journal of statistical physics* 92 (1998), pp. 543–557.
- [13] Debarghya Banerjee, Anton Souslov, Alexander G Abanov, and Vincenzo Vitelli. “Odd viscosity in chiral active fluids”. In: *Nature communications* 8.1 (2017), p. 1573.

- [14] Alain Barrat. “The p-spin spherical spin glass model”. In: *arXiv preprint cond-mat/9701031* (1997).
- [15] Alain Barrat, Raffaella Burioni, and Marc Mézard. “Dynamics within metastable states in a mean-field spin glass”. In: *Journal of Physics A: Mathematical and General* 29.5 (1996), p. L81.
- [16] Jean-Louis Barrat and Ludovic Berthier. “Computer simulations of the glass transition and glassy materials”. In: *arXiv preprint arXiv:2206.01013* (2022).
- [17] Jean-Louis Barrat and Ludovic Berthier. “Computer simulations of the glass transition and glassy materials”. In: *Comptes Rendus. Physique* 24.S1 (2023), pp. 1–16. URL: <https://doi.org/10.5802/crphys.129>.
- [18] Gérard Ben Arous, Yan V Fyodorov, and Boris A Khoruzhenko. “Counting equilibria of large complex systems by instability index”. In: *Proceedings of the National Academy of Sciences* 118.34 (2021), e2023719118.
- [19] Ulf Bengtzelius, W Gotze, and A Sjolander. “Dynamics of supercooled liquids and the glass transition”. In: *Journal of Physics C: solid state Physics* 17.33 (1984), p. 5915.
- [20] Anthony Benois, Marie Jardat, Vincent Dahirel, Vincent Démery, Jaime Agudo-Canalejo, Ramin Golestanian, and Pierre Illien. “Enhanced diffusion of tracer particles in nonreciprocal mixtures”. In: *Physical Review E* 108.5 (2023), p. 054606.
- [21] Etienne Bernard. “Algorithms and applications of the Monte Carlo method: Two-dimensional melting and perfect sampling”. PhD thesis. Université Pierre et Marie Curie-Paris VI, 2011.
- [22] Etienne P. Bernard and Werner Krauth. “Two-Step Melting in Two Dimensions: First-Order Liquid-Hexatic Transition”. In: *Phys. Rev. Lett.* 107 (15 2011), p. 155704. DOI: [10.1103/PhysRevLett.107.155704](https://doi.org/10.1103/PhysRevLett.107.155704). URL: <https://link.aps.org/doi/10.1103/PhysRevLett.107.155704>.
- [23] Etienne P. Bernard, Werner Krauth, and David B. Wilson. “Event-chain Monte Carlo algorithms for hard-sphere systems”. In: *Phys. Rev. E* 80 (5 2009), p. 056704. DOI: [10.1103/PhysRevE.80.056704](https://doi.org/10.1103/PhysRevE.80.056704). URL: <https://link.aps.org/doi/10.1103/PhysRevE.80.056704>.
- [24] Ludovic Berthier and Jean-Louis Barrat. “Nonequilibrium dynamics and fluctuation-dissipation relation in a sheared fluid”. In: *The Journal of Chemical Physics* 116.14 (2002), pp. 6228–6242.
- [25] Ludovic Berthier, Jean-Louis Barrat, and Jorge Kurchan. “A two-time-scale, two-temperature scenario for nonlinear rheology”. In: *Physical Review E* 61.5 (2000), p. 5464.
- [26] Ludovic Berthier and Giulio Biroli. “Theoretical perspective on the glass transition and amorphous materials”. In: *Reviews of modern physics* 83.2 (2011), p. 587.

- [27] Ludovic Berthier, Giulio Biroli, J-P Bouchaud, Walter Kob, Kunimasa Miyazaki, and David R Reichman. “Spontaneous and induced dynamic correlations in glass formers. II. Model calculations and comparison to numerical simulations”. In: *The Journal of chemical physics* 126.18 (2007).
- [28] Ludovic Berthier, Giulio Biroli, Jean-Philippe Bouchaud, Luca Cipelletti, and Wim van Saarloos. *Dynamical heterogeneities in glasses, colloids, and granular media*. Vol. 150. OUP Oxford, 2011.
- [29] Ludovic Berthier, Giulio Biroli, Jean-Philippe Bouchaud, and Gilles Tarjus. “Can the glass transition be explained without a growing static length scale?” In: *The Journal of chemical physics* 150.9 (2019).
- [30] Ludovic Berthier, Patrick Charbonneau, Yuliang Jin, Giorgio Parisi, Beatriz Seoane, and Francesco Zamponi. “Growing timescales and lengthscales characterizing vibrations of amorphous solids”. In: *Proceedings of the National Academy of Sciences* 113.30 (2016), pp. 8397–8401. URL: <https://doi.org/10.1073/pnas.1607730113>.
- [31] Ludovic Berthier, Patrick Charbonneau, and Joyjit Kundu. “Bypassing sluggishness: SWAP algorithm and glassiness in high dimensions”. In: *Phys. Rev. E* 99 (3 2019), p. 031301. DOI: [10.1103/PhysRevE.99.031301](https://doi.org/10.1103/PhysRevE.99.031301). URL: <https://link.aps.org/doi/10.1103/PhysRevE.99.031301>.
- [32] Ludovic Berthier, Patrick Charbonneau, Andrea Ninarello, Misaki Ozawa, and Sho Yaida. “Zero-temperature glass transition in two dimensions”. In: *Nature communications* 10.1 (2019), p. 1508.
- [33] Ludovic Berthier, Daniele Coslovich, Andrea Ninarello, and Misaki Ozawa. “Equilibrium Sampling of Hard Spheres up to the Jamming Density and Beyond”. In: *Phys. Rev. Lett.* 116 (23 2016), p. 238002. DOI: [10.1103/PhysRevLett.116.238002](https://doi.org/10.1103/PhysRevLett.116.238002). URL: <https://link.aps.org/doi/10.1103/PhysRevLett.116.238002>.
- [34] Ludovic Berthier, Elijah Flenner, Christopher J Fullerton, Camille Scalliet, and Murari Singh. “Efficient swap algorithms for molecular dynamics simulations of equilibrium supercooled liquids”. In: *Journal of Statistical Mechanics: Theory and Experiment* 2019.6 (2019), p. 064004. URL: <https://doi.org/10.1088/1742-5468/ab1910>.
- [35] Ludovic Berthier and Walter Kob. “The Monte Carlo dynamics of a binary Lennard-Jones glass-forming mixture”. In: *Journal of Physics: Condensed Matter* 19.20 (2007), p. 205130. URL: <https://doi.org/10.1088/0953-8984/19/20/205130>.
- [36] Ludovic Berthier and Jorge Kurchan. “Non-equilibrium glass transitions in driven and active matter”. In: *Nature Physics* 9.5 (2013), pp. 310–314.

- [37] Ludovic Berthier and David R Reichman. “Modern computational studies of the glass transition”. In: *Nature Reviews Physics* 5 (2023), pp. 1–15. URL: <https://doi.org/10.1038/s42254-022-00548-x>.
- [38] Ludovic Berthier and Gilles Tarjus. “Critical test of the mode-coupling theory of the glass transition”. In: *Physical Review E* 82.3 (2010), p. 031502.
- [39] Ludovic Berthier and Gilles Tarjus. “Testing “microscopic” theories of glass-forming liquids”. In: *The European Physical Journal E* 34 (2011), pp. 1–10.
- [40] Ludovic Berthier and Thomas A. Witten. “Glass transition of dense fluids of hard and compressible spheres”. In: *Phys. Rev. E* 80 (2 2009), p. 021502. DOI: [10.1103/PhysRevE.80.021502](https://doi.org/10.1103/PhysRevE.80.021502). URL: <https://link.aps.org/doi/10.1103/PhysRevE.80.021502>.
- [41] Joris Bierkens, Sebastiano Grazzi, Gareth Roberts, and Moritz Schauer. “Methods and applications of PDMP samplers with boundary conditions”. In: *arXiv preprint arXiv:2303.08023* (2023).
- [42] Giulio Biroli and Juan P Garrahan. “Perspective: The glass transition”. In: *The Journal of chemical physics* 138.12 (2013).
- [43] Mary L Boas. *Mathematical methods in the physical sciences*. John Wiley & Sons, 2006.
- [44] Viola Bolton-Lum, R. Cameron Dennis, Peter Morse, and Eric Corwin. “The Ideal Glass and the Ideal Disk Packing in Two Dimensions”. In: *arXiv preprint arXiv:2404.07492* (2024).
- [45] L éon Bottou. “Online learning and stochastic approximations”. In: *Online learning in neural networks* 17.9 (1998), p. 142.
- [46] Nawaf Bou-Rabee, Aleksandar Donev, and Eric Vanden-Eijnden. “Metropolis integration schemes for self-adjoint diffusions”. In: *Multiscale modeling & simulation* 12.2 (2014), pp. 781–831.
- [47] Jean-Philippe Bouchaud. “Why is the Dynamics of Glasses Super-Arrhenius?” In: *arXiv preprint arXiv:2402.01883* (2024).
- [48] Freddy Bouchet and Julien Reygner. “Generalisation of the Eyring–Kramers transition rate formula to irreversible diffusion processes”. In: *Annales Henri Poincaré*. Vol. 17. 12. Springer. 2016, pp. 3499–3532.
- [49] George EP Box and Mervin E Muller. “A note on the generation of random normal deviates”. In: *The annals of mathematical statistics* 29.2 (1958), pp. 610–611.
- [50] AJ Bray and AJ McKane. “Instanton calculation of the escape rate for activation over a potential barrier driven by colored noise”. In: *Physical review letters* 62.5 (1989), p. 493.

- [51] Carolina Brito, Edan Lerner, and Matthieu Wyart. “Theory for Swap Acceleration near the Glass and Jamming Transitions for Continuously Polydisperse Particles”. In: *Phys. Rev. X* 8 (3 2018), p. 031050. DOI: [10.1103/PhysRevX.8.031050](https://doi.org/10.1103/PhysRevX.8.031050). URL: <https://link.aps.org/doi/10.1103/PhysRevX.8.031050>.
- [52] Christian Van den Broeck, Ryoichi Kawai, and Pascal Meurs. “Microscopic analysis of a thermal Brownian motor”. In: *Physical review letters* 93.9 (2004), p. 090601.
- [53] Martijn van den Broek, Ralf Eichhorn, and Christian Van den Broeck. “Intrinsic ratchets”. In: *Europhysics Letters* 86.3 (2009), p. 30002.
- [54] Nicolas Brosse, Alain Durmus, and Eric Moulines. “The promises and pitfalls of stochastic gradient Langevin dynamics”. In: *Advances in Neural Information Processing Systems* 31 (2018).
- [55] Lorenzo Caprini, Hartmut Löwen, and Umberto Marini Bettolo Marconi. “Chiral active matter in external potentials”. In: *arXiv preprint arXiv:2306.11133* (2023).
- [56] Tommaso Castellani and Andrea Cavagna. “Spin-glass theory for pedestrians”. In: *Journal of Statistical Mechanics: Theory and Experiment* 2005.05 (2005), P05012.
- [57] Andrea Cavagna. “Supercooled liquids for pedestrians”. In: *Physics Reports* 476.4-6 (2009), pp. 51–124.
- [58] Devlina Chakravarty, Joseph W Schafer, Ethan A Chen, Joseph Thole, and Lauren Porter. “AlphaFold2 has more to learn about protein energy landscapes”. In: *bioRxiv* (2023), pp. 2023–12.
- [59] David Chandler. “Introduction to modern statistical”. In: *Mechanics. Oxford University Press, Oxford, UK* 5 (1987), p. 449.
- [60] David Chandler and Juan P Garrahan. “Dynamics on the way to forming glass: Bubbles in space-time”. In: *Annual review of physical chemistry* 61 (2010), pp. 191–217.
- [61] Patrick Charbonneau, Jorge Kurchan, Giorgio Parisi, Pierfrancesco Urbani, and Francesco Zamponi. “Glass and jamming transitions: From exact results to finite-dimensional descriptions”. In: *Annual Review of Condensed Matter Physics* 8 (2017), pp. 265–288.
- [62] Pinaki Chaudhuri, Ludovic Berthier, and Srikanth Sastry. “Jamming Transitions in Amorphous Packings of Frictionless Spheres Occur over a Continuous Range of Volume Fractions”. In: *Phys. Rev. Lett.* 104 (16 2010), p. 165701. DOI: [10.1103/PhysRevLett.104.165701](https://doi.org/10.1103/PhysRevLett.104.165701). URL: <https://link.aps.org/doi/10.1103/PhysRevLett.104.165701>.
- [63] Fang Chen, László Lovász, and Igor Pak. “Lifting Markov chains to speed up mixing”. In: *Proc. 31st Ann. ACM Symp. Theory of Comp.* 1999, pp. 275–281.

- [64] Bogdan Cichocki and Walter Hess. “On the memory function for the dynamic structure factor of interacting brownian particles”. In: *Physica A: Statistical Mechanics and its Applications* 141.2-3 (1987), pp. 475–488.
- [65] Andrea Crisanti, Heinz Horner, and H J Sommers. “The spherical p-spin interaction spin-glass model: the dynamics”. In: *Zeitschrift für Physik B Condensed Matter* 92 (1993), pp. 257–271.
- [66] Andrea Crisanti and H-J Sommers. “The spherical p-spin interaction spin glass model: the statics”. In: *Zeitschrift für Physik B Condensed Matter* 87.3 (1992), pp. 341–354.
- [67] Leticia F Cugliandolo and Jorge Kurchan. “Analytical solution of the off-equilibrium dynamics of a long-range spin-glass model”. In: *Physical Review Letters* 71.1 (1993), p. 173.
- [68] Leticia F Cugliandolo, Jorge Kurchan, Pierre Le Doussal, and Luca Peliti. “Glassy behaviour in disordered systems with nonrelaxational dynamics”. In: *Physical review letters* 78.2 (1997), p. 350.
- [69] Leticia F Cugliandolo, Jorge Kurchan, and Luca Peliti. “Energy flow, partial equilibration, and effective temperatures in systems with slow dynamics”. In: *Physical Review E* 55.4 (1997), p. 3898.
- [70] Leticia F Cugliandolo and Pierre Le Doussal. “Large time nonequilibrium dynamics of a particle in a random potential”. In: *Physical Review E* 53.2 (1996), p. 1525.
- [71] Leticia F Cugliandolo and Vivien Lecomte. “Rules of calculus in the path integral representation of white noise Langevin equations: the Onsager–Machlup approach”. In: *Journal of Physics A: Mathematical and Theoretical* 50.34 (2017), p. 345001.
- [72] Mark HA Davis. “Piecewise-deterministic Markov processes: A general class of non-diffusion stochastic models”. In: *Journal of the Royal Statistical Society: Series B (Methodological)* 46.3 (1984), pp. 353–376.
- [73] Thibaut Arnoulx De Pirey, Leticia F Cugliandolo, Vivien Lecomte, and Frédéric Van Wijland. “Path integrals and stochastic calculus”. In: *Advances in Physics* 71.1-2 (2022), pp. 1–85.
- [74] David S Dean. “Langevin equation for the density of a system of interacting Langevin processes”. In: *Journal of Physics A: Mathematical and General* 29.24 (1996), p. L613.
- [75] Vincent E Debets and Liesbeth Janssen. “Active glassy dynamics is unaffected by the microscopic details of self-propulsion”. In: *The Journal of Chemical Physics* 157.22 (2022).
- [76] Vincent E Debets and Liesbeth Janssen. “Mode-coupling theory for mixtures of athermal self-propelled particles”. In: *arXiv preprint arXiv:2304.08936* (2023).

- [77] Vincent E Debets, Hartmut Löwen, and Liesbeth MC Janssen. “Glassy dynamics in chiral fluids”. In: *Physical Review Letters* 130.5 (2023), p. 058201.
- [78] Vincent Démery, Olivier Bénichou, and Hugo Jacquin. “Generalized Langevin equations for a driven tracer in dense soft colloids: construction and applications”. In: *New Journal of Physics* 16.5 (2014), p. 053032.
- [79] Vincent Démery and David S Dean. “Perturbative path-integral study of active-and passive-tracer diffusion in fluctuating fields”. In: *Physical Review E* 84.1 (2011), p. 011148.
- [80] Roberto Di Leonardo et al. “Bacterial ratchet motors”. In: *Proceedings of the National Academy of Sciences* 107.21 (2010), pp. 9541–9545.
- [81] Persi Diaconis, Susan Holmes, and Radford M Neal. “Analysis of a nonreversible Markov chain sampler”. In: *Annals of Applied Probability* (2000), pp. 726–752.
- [82] Ken A Dill and Justin L MacCallum. “The protein-folding problem, 50 years on”. In: *science* 338.6110 (2012), pp. 1042–1046.
- [83] Christophe Dress and Werner Krauth. “Cluster algorithm for hard spheres and related systems”. In: *Journal of Physics A: Mathematical and General* 28.23 (1995), p. L597.
- [84] Simon Duane, Anthony D Kennedy, Brian J Pendleton, and Duncan Roweth. “Hybrid monte carlo”. In: *Physics letters B* 195.2 (1987), pp. 216–222.
- [85] Jeffrey M Epstein and Kranthi K Mandadapu. “Time-reversal symmetry breaking in two-dimensional nonequilibrium viscous fluids”. In: *Physical review E* 101.5 (2020), p. 052614.
- [86] MH Ernst and J Robert Dorfman. “Nonanalytic dispersion relations for classical fluids: II. The general fluid”. In: *Journal of Statistical Physics* 12.4 (1975), pp. 311–359.
- [87] Henry Eyring. “The activated complex in chemical reactions”. In: *The Journal of Chemical Physics* 3.2 (1935), pp. 107–115.
- [88] Richard P Feynman, Robert B Leighton, and Matthew Sands. *The Feynman Lectures on Physics Ch. 46 Vol. 1*. 1966.
- [89] Elijah Flenner and Grzegorz Szamel. “Fundamental differences between glassy dynamics in two and three dimensions”. In: *Nature communications* 6.1 (2015), p. 7392.
- [90] Elijah Flenner and Grzegorz Szamel. “Relaxation in a glassy binary mixture: Comparison of the mode-coupling theory to a Brownian dynamics simulation”. In: *Physical Review E* 72.3 (2005), p. 031508.
- [91] Giampaolo Folena, Silvio Franz, and Federico Ricci-Tersenghi. “Rethinking mean-field glassy dynamics and its relation with the energy landscape: The surprising case of the spherical mixed p-spin model”. In: *Physical Review X* 10.3 (2020), p. 031045.

- [92] Giampaolo Folena et al. “The mixed p-spin model: selecting, following and losing states”. In: (2020).
- [93] Silvio Franz and Giorgio Parisi. “Effective potential in glassy systems: theory and simulations”. In: *Physica A: Statistical Mechanics and its Applications* 261.3-4 (1998), pp. 317–339.
- [94] Silvio Franz and Giorgio Parisi. “Phase diagram of coupled glassy systems: A mean-field study”. In: *Physical review letters* 79.13 (1997), p. 2486.
- [95] Silvio Franz, Giorgio Parisi, Maxime Sevelev, Pierfrancesco Urbani, and Francesco Zamponi. “Universality of the SAT-UNSAT (jamming) threshold in non-convex continuous constraint satisfaction problems”. In: *SciPost Physics* 2.3 (2017), p. 019.
- [96] Daan Frenkel and Berend Smit. *Understanding molecular simulation: from algorithms to applications*. Vol. 1. Elsevier, 2001.
- [97] Daan Frenkel and Berend Smit. *Understanding molecular simulation: from algorithms to applications*. Elsevier, 2023.
- [98] HL Frisch, N Rivier, and D Wyler. “Classical hard-sphere fluid in infinitely many dimensions”. In: *Physical review letters* 54.19 (1985), p. 2061.
- [99] Michel Fruchart, Colin Scheibner, and Vincenzo Vitelli. “Odd viscosity and odd elasticity”. In: *Annual Review of Condensed Matter Physics* 14 (2023), pp. 471–510.
- [100] Matthias Fuchs and Michael E Cates. “A mode coupling theory for Brownian particles in homogeneous steady shear flow”. In: *Journal of Rheology* 53.4 (2009), pp. 957–1000.
- [101] Matthias Fuchs and Michael E Cates. “Integration through transients for Brownian particles under steady shear”. In: *Journal of Physics: Condensed Matter* 17.20 (2005), S1681.
- [102] Matthias Fuchs, W Gotze, Ivo Hofacker, and Arnulf Latz. “Comments on the alpha-peak shapes for relaxation in supercooled liquids”. In: *Journal of physics: Condensed matter* 3.26 (1991), p. 5047.
- [103] Christopher J Fullerton and Robert L Jack. “Dynamical phase transitions in supercooled liquids: Interpreting measurements of dynamical activity”. In: *The Journal of Chemical Physics* 138.22 (2013), p. 224506.
- [104] Futoshi Futami, Tomoharu Iwata, Naonori Ueda, and Issei Sato. “Accelerated diffusion-based sampling by the non-reversible dynamics with skew-symmetric matrices”. In: *Entropy* 23.8 (2021), p. 993.
- [105] Yan V Fyodorov and Boris A Khoruzhenko. “Nonlinear analogue of the May-Wigner instability transition”. In: *Proceedings of the National Academy of Sciences* 113.25 (2016), pp. 6827–6832.

- [106] Xuefeng Gao, Mert Gurbuzbalaban, and Lingjiong Zhu. “Breaking reversibility accelerates langevin dynamics for non-convex optimization”. In: *Advances in Neural Information Processing Systems* 33 (2020), pp. 17850–17862.
- [107] Federico Ghimenti, Ludovic Berthier, Grzegorz Szamel, and Frédéric van Wijland. “Irreversible Boltzmann samplers in dense liquids: weak-coupling approximation and mode-coupling theory”. In: *arXiv preprint arXiv:2404.14863* (2024).
- [108] Federico Ghimenti, Ludovic Berthier, Grzegorz Szamel, and Frédéric van Wijland. “Sampling Efficiency of Transverse Forces in Dense Liquids”. In: *Phys. Rev. Lett.* 131 (25 2023), p. 257101. doi: [10.1103/PhysRevLett.131.257101](https://doi.org/10.1103/PhysRevLett.131.257101). URL: <https://link.aps.org/doi/10.1103/PhysRevLett.131.257101>.
- [109] Federico Ghimenti, Ludovic Berthier, Grzegorz Szamel, and Frédéric van Wijland. “Transverse forces and glassy liquids in infinite dimensions”. In: *arXiv preprint arXiv:2402.10856* (2024).
- [110] Federico Ghimenti, Ludovic Berthier, and Frédéric van Wijland. “Irreversible Monte Carlo algorithms for hard disk glasses: from event-chain to collective swaps”. In: *arXiv preprint arXiv:2402.06585* (2024).
- [111] Federico Ghimenti, Cory Hargus, Julien Tailleur, and Frédéric van Wiljand. “In preparation”.
- [112] Federico Ghimenti and Frédéric van Wijland. “Accelerating, to some extent, the p -spin dynamics”. In: *Phys. Rev. E* 105 (5 2022), p. 054137. doi: [10.1103/PhysRevE.105.054137](https://doi.org/10.1103/PhysRevE.105.054137). URL: <https://link.aps.org/doi/10.1103/PhysRevE.105.054137>.
- [113] Mark Girolami and Ben Calderhead. “Riemann manifold langevin and hamiltonian monte carlo methods”. In: *Journal of the Royal Statistical Society Series B: Statistical Methodology* 73.2 (2011), pp. 123–214.
- [114] Andrea Gnoli, Alberto Petri, Fergal Dalton, Giorgio Pontuale, Giacomo Gradenigo, Alessandro Sarracino, and Andrea Puglisi. “Brownian ratchet in a thermal bath driven by coulomb friction”. In: *Physical review letters* 110.12 (2013), p. 120601.
- [115] Wolfgang Götze. *Complex dynamics of glass-forming liquids*. Vol. 143. Oxford University Press on Demand, 2009.
- [116] Wolfgang Götze. “Recent tests of the mode-coupling theory for glassy dynamics”. In: *Journal of Physics: condensed matter* 11.10A (1999), A1.
- [117] Omer Granek, Yariv Kafri, Mehran Kardar, Sunghan Ro, Alexandre Solon, and Julien Tailleur. “Inclusions, Boundaries and Disorder in Scalar Active Matter”. In: *arXiv preprint arXiv:2310.00079* (2023).
- [118] Omer Granek, Yariv Kafri, and Julien Tailleur. “Anomalous transport of tracers in active baths”. In: *Physical Review Letters* 129.3 (2022), p. 038001.

- [119] Tomás S. Grigera and Giorgio Parisi. “Fast Monte Carlo algorithm for super-cooled soft spheres”. In: *Phys. Rev. E* 63 (4 2001), p. 045102. DOI: [10.1103/PhysRevE.63.045102](https://doi.org/10.1103/PhysRevE.63.045102). URL: <https://link.aps.org/doi/10.1103/PhysRevE.63.045102>.
- [120] Daniel Grober, Ivan Palaia, Mehmet Can Uçar, Edouard Hannezo, Andela Šarić, and Jérémie Palacci. “Unconventional colloidal aggregation in chiral bacterial baths”. In: *Nature Physics* 19.11 (2023), pp. 1680–1688.
- [121] Tristan Guyon, Arnaud Guillin, and Manon Michel. “Necessary and sufficient symmetries in Event-Chain Monte Carlo with generalized flows and Application to hard dimers”. In: *arXiv preprint arXiv:2307.02341* (2023).
- [122] Varda F Hagh, Sidney R Nagel, Andrea J Liu, M Lisa Manning, and Eric I Corwin. “Transient learning degrees of freedom for introducing function in materials”. In: *Proceedings of the National Academy of Sciences* 119.19 (2022), e2117622119.
- [123] Ming Han, Michel Fruchart, Colin Scheibner, Suriyanarayanan Vaikuntanathan, Juan J De Pablo, and Vincenzo Vitelli. “Fluctuating hydrodynamics of chiral active fluids”. In: *Nature Physics* 17.11 (2021), pp. 1260–1269.
- [124] Jean-Pierre Hansen and Ian Ranald McDonald. *Theory of simple liquids: with applications to soft matter*. Academic press, 2013.
- [125] Cory Hargus, Jeffrey M Epstein, and Kranthi K Mandadapu. “Odd diffusivity of chiral random motion”. In: *Physical review letters* 127.17 (2021), p. 178001.
- [126] Cory Hargus, Jeffrey M. Epstein, and Kranthi K. Mandadapu. “Odd Diffusivity of Chiral Random Motion”. In: *Physical Review Letters* 127 (17 2021), p. 178001. ISSN: 10797114. DOI: [10.1103/PhysRevLett.127.178001](https://doi.org/10.1103/PhysRevLett.127.178001). URL: <https://journals.aps.org/prl/abstract/10.1103/PhysRevLett.127.178001>.
- [127] Cory Hargus, Katherine Klymko, Jeffrey M Epstein, and Kranthi K Mandadapu. “Time reversal symmetry breaking and odd viscosity in active fluids: Green–Kubo and NEMD results”. In: *The journal of chemical physics* 152.20 (2020).
- [128] Hisao Hayakawa and Michio Otsuki. “Mode-coupling theory of sheared dense granular liquids”. In: *Progress of Theoretical Physics* 119.3 (2008), pp. 381–402.
- [129] Douglas Henderson. “A simple equation of state for hard discs”. In: *Molecular Physics* 30.3 (1975), pp. 971–972.
- [130] W Hess. “Fokker-Planck dynamics of interacting Brownian particles”. In: *Journal of Physics A: Mathematical and General* 14.5 (1981), p. L145.
- [131] Roger A Horn and Charles R Johnson. *Matrix analysis*. Cambridge university press, 2012.
- [132] A Houghton, S Jain, and AP Young. “Role of initial conditions in the mean-field theory of spin-glass dynamics”. In: *Physical Review B* 28.5 (1983), p. 2630.

- [133] Koji Hukushima and Koji Nemoto. “Exchange Monte Carlo method and application to spin glass simulations”. In: *Journal of the Physical Society of Japan* 65.6 (1996), pp. 1604–1608.
- [134] Chii-Ruey Hwang, Shu-Yin Hwang-Ma, and Shuenn-Jyi Sheu. “Accelerating diffusions”. In: *The Annals of Applied Probability* 15.2 (2005), pp. 1433–1444.
- [135] Chii-Ruey Hwang, Shu-Yin Hwang-Ma, and Shuenn-Jyi Sheu. “Accelerating gaussian diffusions”. In: *The Annals of Applied Probability* (1993), pp. 897–913.
- [136] Akihisa Ichiki and Masayuki Ohzeki. “Violation of detailed balance accelerates relaxation”. In: *Physical Review E* 88.2 (2013), p. 020101.
- [137] Harukuni Ikeda, Kunimasa Miyazaki, Hajime Yoshino, and Atushi Ikeda. “Multiple glass transitions and higher-order replica symmetry breaking of binary mixtures”. In: *Physical Review E* 103.2 (2021), p. 022613.
- [138] Harukuni Ikeda, Francesco Zamponi, and Atsushi Ikeda. “Mean field theory of the swap Monte Carlo algorithm”. In: *The Journal of chemical physics* 147.23 (2017).
- [139] Masaharu Isobe, Aaron S. Keys, David Chandler, and Juan P. Garrahan. “Applicability of Dynamic Facilitation Theory to Binary Hard Disk Systems”. In: *Phys. Rev. Lett.* 117 (14 2016), p. 145701. doi: [10.1103/PhysRevLett.117.145701](https://doi.org/10.1103/PhysRevLett.117.145701). URL: <https://link.aps.org/doi/10.1103/PhysRevLett.117.145701>.
- [140] Masaharu Isobe and Werner Krauth. “Hard-sphere melting and crystallization with event-chain Monte Carlo”. In: *The Journal of Chemical Physics* 143.8 (Aug. 2015), p. 084509. ISSN: 0021-9606. doi: [10.1063/1.4929529](https://doi.org/10.1063/1.4929529). URL: <https://doi.org/10.1063/1.4929529>.
- [141] Denis J Evans and Gary P Morriss. *Statistical mechanics of nonequilibrium liquids*. ANU Press, 2007.
- [142] Liesbeth MC Janssen. “Mode-coupling theory of the glass transition: A primer”. In: *Frontiers in Physics* 6 (2018), p. 97.
- [143] Marie Jardat, Vincent Dahirel, and Pierre Illien. “Diffusion of a tracer in a dense mixture of soft particles connected to different thermostats”. In: *Physical Review E* 106.6 (2022), p. 064608.
- [144] Andreas Jaster. “An improved Metropolis algorithm for hard core systems”. In: *Physica A: Statistical Mechanics and its Applications* 264.1-2 (1999), pp. 134–141.
- [145] Erik Kalz, Hidde Derk Vuijk, Iman Abdoli, Jens-Uwe Sommer, Hartmut Löwen, and Abhinav Sharma. “Collisions enhance self-diffusion in odd-diffusive systems”. In: *Physical Review Letters* 129.9 (2022), p. 090601.
- [146] Erik Kalz, Hidde Derk Vuijk, Jens-Uwe Sommer, Ralf Metzler, and Abhinav Sharma. “Oscillatory force autocorrelations in equilibrium odd-diffusive systems”. In: *arXiv preprint arXiv:2302.01263* (2023).

- [147] Sebastian C Kapfer and Werner Krauth. “Cell-veto Monte Carlo algorithm for long-range systems”. In: *Physical Review E* 94.3 (2016), p. 031302.
- [148] Sebastian C. Kapfer and Werner Krauth. “Irreversible Local Markov Chains with Rapid Convergence towards Equilibrium”. In: *Phys. Rev. Lett.* 119 (24 2017), p. 240603. DOI: [10.1103/PhysRevLett.119.240603](https://doi.org/10.1103/PhysRevLett.119.240603). URL: <https://link.aps.org/doi/10.1103/PhysRevLett.119.240603>.
- [149] Sebastian C Kapfer and Werner Krauth. “Sampling from a polytope and hard-disk Monte Carlo”. In: *Journal of Physics: Conference Series*. Vol. 454. 1. IOP Publishing. 2013, p. 012031.
- [150] Geert Kapteijns, Wencheng Ji, Carolina Brito, Matthieu Wyart, and Edan Lerner. “Fast generation of ultrastable computer glasses by minimization of an augmented potential energy”. In: *Phys. Rev. E* 99 (1 2019), p. 012106. DOI: [10.1103/PhysRevE.99.012106](https://doi.org/10.1103/PhysRevE.99.012106). URL: <https://link.aps.org/doi/10.1103/PhysRevE.99.012106>.
- [151] George Em Karniadakis, Ioannis G Kevrekidis, Lu Lu, Paris Perdikaris, Sifan Wang, and Liu Yang. “Physics-informed machine learning”. In: *Nature Reviews Physics* 3.6 (2021), pp. 422–440.
- [152] Kyozi Kawasaki. “Irreducible memory function for dissipative stochastic systems with detailed balance”. In: *Physica A: Statistical Mechanics and its Applications* 215.1-2 (1995), pp. 61–74.
- [153] Kyozi Kawasaki and Jim Gunton. “Renormalization-group and mode-coupling theories of critical dynamics”. In: *Physical Review B* 13.11 (1976), p. 4658.
- [154] Jaron Kent-Dobias. “Arrangement of nearby minima and saddles in the mixed spherical energy landscapes”. In: *SciPost Physics* 16.1 (2024), p. 001.
- [155] Bongsoo Kim and Arnulf Latz. “The dynamics of the spherical p-spin model: From microscopic to asymptotic”. In: *Europhysics Letters* 53.5 (2001), p. 660.
- [156] Harald Kinzelbach and Heinz Horner. “Dynamics of manifolds in random media II: long range correlations in the disordered medium”. In: *Journal de Physique I* 3.9 (1993), pp. 1901–1919.
- [157] Harald Kinzelbach and Heinz Horner. “Dynamics of manifolds in random media: the selfconsistent Hartree approximation”. In: *Journal de Physique I* 3.6 (1993), pp. 1329–1357.
- [158] R. Klein. “Dynamics of Colloidal Suspensions”. In: *Structure and Dynamics of Polymer and Colloidal Systems*. Ed. by Redouane Borsali and Robert Pecora. Dordrecht: Springer Netherlands, 2002, pp. 83–115. ISBN: 978-94-010-0442-8. DOI: [10.1007/978-94-010-0442-8_4](https://doi.org/10.1007/978-94-010-0442-8_4). URL: https://doi.org/10.1007/978-94-010-0442-8_4.

- [159] Walter Kob and Hans C Andersen. “Scaling behavior in the β -relaxation regime of a supercooled Lennard-Jones mixture”. In: *Physical review letters* 73.10 (1994), p. 1376.
- [160] Walter Kob and Hans C Andersen. “Scaling behavior in the dynamics of a supercooled lennard-jones mixture”. In: *Il Nuovo Cimento D* 16 (1994), pp. 1291–1295.
- [161] Walter Kob and Hans C Andersen. “Testing mode-coupling theory for a supercooled binary Lennard-Jones mixture I: The van Hove correlation function”. In: *Physical Review E* 51.5 (1995), p. 4626.
- [162] Walter Kob and Hans C Andersen. “Testing mode-coupling theory for a supercooled binary Lennard-Jones mixture. II. Intermediate scattering function and dynamic susceptibility”. In: *Physical Review E* 52.4 (1995), p. 4134.
- [163] Walter Kob and Jean-Louis Barrat. “Aging effects in a Lennard-Jones glass”. In: *Physical review letters* 78.24 (1997), p. 4581.
- [164] Hendrik Anthony Kramers. “Brownian motion in a field of force and the diffusion model of chemical reactions”. In: *Physica* 7.4 (1940), pp. 284–304.
- [165] W Till Kranz, Matthias Sperl, and Annette Zippelius. “Glass transition for driven granular fluids”. In: *Physical review letters* 104.22 (2010), p. 225701.
- [166] Werner Krauth. *Statistical mechanics: algorithms and computations*. Vol. 13. OUP Oxford, 2006.
- [167] Sudeesh Krishnamurthy, Subho Ghosh, Dipankar Chatterji, Rajesh Ganapathy, and AK Sood. “A micrometre-sized heat engine operating between bacterial reservoirs”. In: *Nature Physics* 12.12 (2016), pp. 1134–1138.
- [168] Florent Krzakala, Andrea Montanari, Federico Ricci-Tersenghi, Guilhem Semerjian, and Lenka Zdeborová. “Gibbs states and the set of solutions of random constraint satisfaction problems”. In: *Proceedings of the National Academy of Sciences* 104.25 (2007), pp. 10318–10323.
- [169] Jorge Kurchan, Giorgio Parisi, and Francesco Zamponi. “Exact theory of dense amorphous hard spheres in high dimension I. The free energy”. In: *Journal of Statistical Mechanics: Theory and Experiment* 2012.10 (2012), P10012.
- [170] Corentin CL Laudicina, Ilian Pihlajamaa, and Liesbeth MC Janssen. “Competing relaxation channels in continuously polydisperse fluids: A mode-coupling study”. In: *Physical Review Research* 5.3 (2023), p. 033121.
- [171] Tony Lelièvre, Grigoris A Pavliotis, Geneviève Robin, Régis Santet, and Gabriel Stoltz. “Optimizing the diffusion of overdamped Langevin dynamics”. In: *arXiv preprint arXiv:2404.12087* (2024).
- [172] E Leutheusser. “Dynamical model of the liquid-glass transition”. In: *Physical Review A* 29.5 (1984), p. 2765.

- [173] David A Levin and Yuval Peres. *Markov chains and mixing times*. Vol. 107. American Mathematical Soc., 2017.
- [174] Jing-Ran Li, Wei-jing Zhu, Jia-Jian Li, Jian-Chun Wu, and Bao-Quan Ai. “Chirality-induced directional rotation of a symmetric gear in a bath of chiral active particles”. In: *New Journal of Physics* 25.4 (2023), p. 043031.
- [175] Benno Liebchen and Demian Levis. “Chiral active matter”. In: *Europhysics Letters* 139.6 (2022), p. 67001.
- [176] Alexander Liliashvili, Jonathan Ónody, and Thomas Voigtmann. “Mode-coupling theory for active Brownian particles”. In: *Physical Review E* 96.6 (2017), p. 062608.
- [177] Chen Liu, Giulio Biroli, David R Reichman, and Grzegorz Szamel. “Dynamics of liquids in the large-dimensional limit”. In: *Physical Review E* 104.5 (2021), p. 054606.
- [178] Boris D Lubachevsky and Frank H Stillinger. “Geometric properties of random disk packings”. In: *Journal of statistical Physics* 60 (1990), pp. 561–583.
- [179] Zhan Ma and Ran Ni. “Dynamical clustering interrupts motility-induced phase separation in chiral active Brownian particles”. In: *The Journal of Chemical Physics* 156.2 (2022).
- [180] Stefan Machlup and Lars Onsager. “Fluctuations and irreversible process. II. Systems with kinetic energy”. In: *Physical Review* 91.6 (1953), p. 1512.
- [181] Christian Maes. “Frenesy: Time-symmetric dynamical activity in nonequilibria”. In: *Physics Reports* 850 (2020), pp. 1–33.
- [182] A. C. Maggs and Werner Krauth. “Large-scale dynamics of event-chain Monte Carlo”. In: *Phys. Rev. E* 105 (1 2022), p. 015309. DOI: [10.1103/PhysRevE.105.015309](https://doi.org/10.1103/PhysRevE.105.015309). URL: <https://link.aps.org/doi/10.1103/PhysRevE.105.015309>.
- [183] Marcelo O Magnasco. “Forced thermal ratchets”. In: *Physical Review Letters* 71.10 (1993), p. 1477.
- [184] Thibaud Maimbourg, Jorge Kurchan, and Francesco Zamponi. “Solution of the dynamics of liquids in the large-dimensional limit”. In: *Physical review letters* 116.1 (2016), p. 015902.
- [185] Alessandro Manacorda, Grégory Schehr, and Francesco Zamponi. “Numerical solution of the dynamical mean field theory of infinite-dimensional equilibrium liquids”. In: *The Journal of chemical physics* 152.16 (2020), p. 164506.
- [186] Rituparno Mandal and Peter Sollich. “Multiple types of aging in active glasses”. In: *Physical Review Letters* 125.21 (2020), p. 218001.
- [187] Riccardo Mannella. “Numerical integration of stochastic differential equations”. In: *Proc. Euroconf. on Supercomputation in Nonlinear and Disordered Systems* (1997), pp. 100–30.

- [188] Nicholas Metropolis, Arianna W. Rosenbluth, Marshall N. Rosenbluth, Augusta H. Teller, and Edward Teller. “Equation of State Calculations by Fast Computing Machines”. In: *The Journal of Chemical Physics* 21.6 (June 1953), pp. 1087–1092. ISSN: 0021-9606. DOI: [10.1063/1.1699114](https://doi.org/10.1063/1.1699114). URL: <https://doi.org/10.1063/1.1699114>.
- [189] Nicholas Metropolis and Stanislaw Ulam. “The monte carlo method”. In: *Journal of the American statistical association* 44.247 (1949), pp. 335–341.
- [190] Marc Mézard and Giorgio Parisi. “Thermodynamics of glasses: A first principles computation”. In: *Journal of Physics: Condensed Matter* 11.10A (1999), A157.
- [191] Marc Mézard, Giorgio Parisi, and Miguel Angel Virasoro. *Spin glass theory and beyond: An Introduction to the Replica Method and Its Applications*. Vol. 9. World Scientific Publishing Company, 1987.
- [192] Manon Michel, Alain Durmus, and Stéphane Sénécal. “Forward event-chain Monte Carlo: Fast sampling by randomness control in irreversible Markov chains”. In: *Journal of Computational and Graphical Statistics* 29.4 (2020), pp. 689–702.
- [193] Manon Michel, Sebastian C. Kapfer, and Werner Krauth. “Generalized event-chain Monte Carlo: Constructing rejection-free global-balance algorithms from infinitesimal steps”. In: *The Journal of Chemical Physics* 140.5 (Feb. 2014), p. 054116. ISSN: 0021-9606. DOI: [10.1063/1.4863991](https://doi.org/10.1063/1.4863991). URL: <https://doi.org/10.1063/1.4863991>.
- [194] Manon Michel, Johannes Mayer, and Werner Krauth. “Event-chain Monte Carlo for classical continuous spin models”. In: *Europhysics Letters* 112.2 (2015), p. 20003.
- [195] Francesca Mignacco, Pierfrancesco Urbani, and Lenka Zdeborová. “Stochasticity helps to navigate rough landscapes: comparing gradient-descent-based algorithms in the phase retrieval problem”. In: *Machine Learning: Science and Technology* 2.3 (2021), p. 035029.
- [196] Ayori Mitsutake, Yuji Sugita, and Yuko Okamoto. “Generalized-ensemble algorithms for molecular simulations of biopolymers”. In: *Peptide Science: Original Research on Biomolecules* 60.2 (2001), pp. 96–123.
- [197] Rémi Monasson. “Structural glass transition and the entropy of the metastable states”. In: *Physical review letters* 75.15 (1995), p. 2847.
- [198] Athina Monemvassitis, Arnaud Guillin, and Manon Michel. “PDMP characterisation of event-chain Monte Carlo algorithms for particle systems”. In: *Journal of Statistical Physics* 190.3 (2023), p. 66.
- [199] Cécile Monthus. “Large deviations for the skew-detailed-balance lifted-Markov processes to sample the equilibrium distribution of the Curie–Weiss model”. In: *Journal of Statistical Mechanics: Theory and Experiment* 2021.10 (2021), p. 103202.

- [200] Wenlong Mou, Yi-An Ma, Martin J Wainwright, Peter L Bartlett, and Michael I Jordan. “High-order Langevin diffusion yields an accelerated MCMC algorithm”. In: *Journal of Machine Learning Research* 22.42 (2021), pp. 1–41.
- [201] G Nägele and J Bergenholz. “Linear viscoelasticity of colloidal mixtures”. In: *The Journal of chemical physics* 108.23 (1998), pp. 9893–9904.
- [202] Mark EJ Newman and Gerard T Barkema. *Monte Carlo methods in statistical physics*. Clarendon Press, 1999.
- [203] Andrea Ninarello, Ludovic Berthier, and Daniele Coslovich. “Models and Algorithms for the Next Generation of Glass Transition Studies”. In: *Phys. Rev. X* 7 (2 2017), p. 021039. DOI: [10.1103/PhysRevX.7.021039](https://doi.org/10.1103/PhysRevX.7.021039). URL: <https://link.aps.org/doi/10.1103/PhysRevX.7.021039>.
- [204] Yoshihiko Nishikawa, Werner Krauth, and AC Maggs. “Liquid-hexatic transition for soft disks”. In: *Physical Review E* 108.2 (2023), p. 024103.
- [205] Jérémie O’Byrne, Yariv Kafri, Julien Tailleur, and Frédéric van Wijland. “Time-(Ir)Reversibility in Active Matter: From Micro to Macro”. In: (2021). eprint: [2104.03030](https://arxiv.org/abs/2104.03030).
- [206] Corey S. O’Hern, Stephen A. Langer, Andrea J. Liu, and Sidney R. Nagel. “Random Packings of Frictionless Particles”. In: *Phys. Rev. Lett.* 88 (7 2002), p. 075507. DOI: [10.1103/PhysRevLett.88.075507](https://doi.org/10.1103/PhysRevLett.88.075507). URL: <https://link.aps.org/doi/10.1103/PhysRevLett.88.075507>.
- [207] Masayuki Ohzeki. “Stochastic gradient method with accelerated stochastic dynamics”. In: *Journal of Physics: Conference Series* 699 (2016), p. 012019. DOI: [10.1088/1742-6596/699/1/012019](https://doi.org/10.1088/1742-6596/699/1/012019). URL: <https://doi.org/10.1088/1742-6596/699/1/012019>.
- [208] Masayuki Ohzeki and Akihisa Ichiki. “Langevin dynamics neglecting detailed balance condition”. In: *Physical Review E* 92.1 (2015), p. 012105.
- [209] Lars Onsager and Stefan Machlup. “Fluctuations and irreversible processes”. In: *Physical Review* 91.6 (1953), p. 1505.
- [210] Misaki Ozawa, Ludovic Berthier, Giulio Biroli, Alberto Rosso, and Gilles Tarjus. “Random critical point separates brittle and ductile yielding transitions in amorphous materials”. In: *Proceedings of the National Academy of Sciences* 115.26 (2018), pp. 6656–6661. URL: <https://doi.org/10.1073/pnas.1806156115>.
- [211] Misaki Ozawa, Ludovic Berthier, and Daniele Coslovich. “Exploring the jamming transition over a wide range of critical densities”. In: *SciPost Physics* 3.4 (2017), p. 027. URL: <https://doi.org/10.21468/SciPostPhys.3.4.027>.
- [212] Misaki Ozawa, Yasutaka Iwashita, Walter Kob, and Francesco Zamponi. “Creating bulk ultrastable glasses by random particle bonding”. In: *Nature Communications* 14.1 (2023), p. 113.

- [213] Misaki Ozawa, Giorgio Parisi, and Ludovic Berthier. “Configurational entropy of polydisperse supercooled liquids”. In: *The Journal of Chemical Physics* 149.15 (2018).
- [214] Jérémie O’Byrne, Yariv Kafri, Julien Tailleur, and Frédéric van Wijland. “Time irreversibility in active matter, from micro to macro”. In: *Nature Reviews Physics* 4.3 (2022), pp. 167–183.
- [215] Alessandro Pacco, Giulio Biroli, and Valentina Ros. “Curvature-driven pathways interpolating between stationary points: the case of the pure spherical 3-spin model”. In: *Journal of Physics A: Mathematical and Theoretical* 57.7 (2024), 07LT01.
- [216] Giorgio Parisi, Pierfrancesco Urbani, and Francesco Zamponi. *Theory of simple glasses*. Cambridge University Press, 2020.
- [217] Giorgio Parisi and Francesco Zamponi. “Mean-field theory of hard sphere glasses and jamming”. In: *Reviews of Modern Physics* 82.1 (2010), p. 789.
- [218] Anshul D. S. Parmar, Misaki Ozawa, and Ludovic Berthier. “Ultrastable Metallic Glasses In Silico”. In: *Phys. Rev. Lett.* 125 (8 2020), p. 085505. DOI: [10.1103/PhysRevLett.125.085505](https://doi.org/10.1103/PhysRevLett.125.085505). URL: <https://link.aps.org/doi/10.1103/PhysRevLett.125.085505>.
- [219] Anshul DS Parmar, Benjamin Guiselin, and Ludovic Berthier. “Stable glassy configurations of the Kob–Andersen model using swap Monte Carlo”. In: *The Journal of Chemical Physics* 153.13 (2020).
- [220] Khoa N Pham et al. “Multiple glassy states in a simple model system”. In: *Science* 296.5565 (2002), pp. 104–106.
- [221] J Pihlajamaa, Corentin CL Laudicina, Thomas Voigtmann, and Liesbeth MC Janssen. “ModeCouplingTheory.jl: A solver for mode-coupling-theory-like integro-differential equations”. In: *Journal of Open Source Software* 8 (2023).
- [222] Estelle Pitard, Vivien Lecomte, and Frédéric Van Wijland. “Dynamic transition in an atomic glass former: A molecular-dynamics evidence”. In: *Europhysics Letters* 96.5 (2011), p. 56002.
- [223] Anthony R. Poggioli and David T. Limmer. “Odd mobility of a passive tracer in a chiral active fluid”. In: (2022), pp. 1–5. URL: <https://arxiv.org/abs/2211.07003v1>.
- [224] Anthony R Poggioli and David T Limmer. “Odd mobility of a passive tracer in a chiral active fluid”. In: *Physical Review Letters* 130.15 (2023), p. 158201.
- [225] Noëlle Pottier. “Relaxation time distributions for an anomalously diffusing particle”. In: *Physica A: Statistical Mechanics and its Applications* 390.16 (2011), pp. 2863–2879. ISSN: 0378-4371. DOI: <https://doi.org/10.1016/j.physa.2011.03.029>. URL: <https://www.sciencedirect.com/science/article/pii/S0378437111002421>.

- [226] Vyas Ramasubramani, Bradley D. Dice, Eric S. Harper, Matthew P. Spellings, Joshua A. Anderson, and Sharon C. Glotzer. “freud: A software suite for high throughput analysis of particle simulation data”. In: *Computer Physics Communications* 254 (2020), p. 107275. ISSN: 0010-4655. DOI: <https://doi.org/10.1016/j.cpc.2020.107275>. URL: <https://www.sciencedirect.com/science/article/pii/S0010465520300916>.
- [227] David R Reichman and Patrick Charbonneau. “Mode-coupling theory”. In: *Journal of Statistical Mechanics: Theory and Experiment* 2005.05 (2005), P05013.
- [228] Ingmar H Riedel, Karsten Kruse, and Jonathon Howard. “A self-organized vortex array of hydrodynamically entrained sperm cells”. In: *Science* 309.5732 (2005), pp. 300–303.
- [229] Hannes Risken and Hannes Risken. *Fokker-planck equation*. Springer, 1996.
- [230] GO Roberts and O Stramer. “Tempered Langevin diffusions and algorithms”. In: *University of Iowa, Department of Statistics and Actuarial Sciences Technical Report* 314 (2002).
- [231] Marshall N Rosenbluth and Arianna W Rosenbluth. “Monte Carlo calculation of the average extension of molecular chains”. In: *The Journal of Chemical Physics* 23.2 (1955), pp. 356–359.
- [232] C Patrick Royall, Francesco Turci, Soichi Tatsumi, John Russo, and Joshua Robinson. “The race to the bottom: approaching the ideal glass?” In: *Journal of Physics: Condensed Matter* 30.36 (2018), p. 363001.
- [233] Yuji Sakai and Koji Hukushima. “Dynamics of one-dimensional Ising model without detailed balance condition”. In: *Journal of the Physical Society of Japan* 82.6 (2013), p. 064003.
- [234] Andrés Santos, Santos Bravo Yuste, and Mariano López De Haro. “Equation of state of a multicomponent d-dimensional hard-sphere fluid”. In: *Molecular Physics* 96.1 (1999), pp. 1–5.
- [235] Camille Scalliet, Benjamin Guiselin, and Ludovic Berthier. “Thirty Milliseconds in the Life of a Supercooled Liquid”. In: *Phys. Rev. X* 12 (4 2022), p. 041028. DOI: [10.1103/PhysRevX.12.041028](https://doi.org/10.1103/PhysRevX.12.041028). URL: <https://link.aps.org/doi/10.1103/PhysRevX.12.041028>.
- [236] Kenneth S Schweizer. “Microscopic theory of the dynamics of polymeric liquids: General formulation of a mode-mode-coupling approach”. In: *The Journal of chemical physics* 91.9 (1989), pp. 5802–5821.
- [237] Udo Seifert. “Entropy production along a stochastic trajectory and an integral fluctuation theorem”. In: *Physical review letters* 95.4 (2005), p. 040602.
- [238] Jagdeep Shah. *Hot carriers in semiconductor nanostructures: Physics and applications*. Elsevier, 2012.

- [239] Alexandre Solon and Jordan M Horowitz. “On the Einstein relation between mobility and diffusion coefficient in an active bath”. In: *Journal of Physics A: Mathematical and Theoretical* 55.18 (2022), p. 184002.
- [240] Alexandre Solon and Jordan M. Horowitz. “On the Einstein relation between mobility and diffusion coefficient in an active bath”. In: *Journal of Physics A: Mathematical and Theoretical* 55 (18 May 2022). ISSN: 17518121. doi: [10.1088/1751-8121/ac5d82](https://doi.org/10.1088/1751-8121/ac5d82).
- [241] Haim Sompolinsky and Annette Zippelius. “Relaxational dynamics of the Edwards-Anderson model and the mean-field theory of spin-glasses”. In: *Physical Review B* 25.11 (1982), p. 6860.
- [242] Robert H Swendsen and Jian-Sheng Wang. “Nonuniversal critical dynamics in Monte Carlo simulations”. In: *Physical review letters* 58.2 (1987), p. 86.
- [243] Grzegorz Szamel. “Mode-coupling theory for the steady-state dynamics of active Brownian particles”. In: *The Journal of chemical physics* 150.12 (2019), p. 124901.
- [244] Grzegorz Szamel. “Theory for the dynamics of dense systems of athermal self-propelled particles”. In: *Physical Review E* 93.1 (2016), p. 012603.
- [245] Grzegorz Szamel. “Theory for the dynamics of glassy mixtures with particle size swaps”. In: *Physical Review E* 98.5 (2018), p. 050601.
- [246] Grzegorz Szamel. “Theory for the single-particle dynamics in glassy mixtures with particle size swaps”. In: *Journal of Statistical Mechanics: Theory and Experiment* 2019.10 (2019), p. 104016.
- [247] Grzegorz Szamel and Hartmut Löwen. “Mode-coupling theory of the glass transition in colloidal systems”. In: *Physical Review A* 44.12 (1991), p. 8215.
- [248] Konstantin S Turitsyn, Michael Chertkov, and Marija Vucelja. “Irreversible Monte Carlo algorithms for efficient sampling”. In: *Physica D: Nonlinear Phenomena* 240.4-5 (2011), pp. 410–414.
- [249] Pierre Turq, Frédéric Lantelme, and Harold L Friedman. “Brownian dynamics: Its application to ionic solutions”. In: *The Journal of Chemical Physics* 66.7 (1977), pp. 3039–3044.
- [250] NG Van Kampen and I Oppenheim. “Brownian motion as a problem of eliminating fast variables”. In: *Physica A: Statistical Mechanics and its Applications* 138.1-2 (1986), pp. 231–248.
- [251] Salvador Elías Venegas-Andraca. “Quantum walks: a comprehensive review”. In: *Quantum Information Processing* 11.5 (2012), pp. 1015–1106.
- [252] Loup Verlet. “Computer” experiments” on classical fluids. II. Equilibrium correlation functions”. In: *Physical Review* 165.1 (1968), p. 201.

- [253] Florian Vogel and Matthias Fuchs. “Stress correlation function and linear response of Brownian particles”. In: *The European Physical Journal E* 43.11 (2020), pp. 1–10.
- [254] Michael te Vrugt and Raphael Wittkowski. “Projection operators in statistical mechanics: a pedagogical approach”. In: *European Journal of Physics* 41.4 (2020), p. 045101.
- [255] Marija Vucelja. “Lifting—a nonreversible Markov chain Monte Carlo algorithm”. In: *American Journal of Physics* 84.12 (2016), pp. 958–968.
- [256] Steven Weinberg. *Lectures on quantum mechanics*. Cambridge University Press, 2015.
- [257] Ulli Wolff. “Collective Monte Carlo updating for spin systems”. In: *Physical Review Letters* 62.4 (1989), p. 361.
- [258] Matthieu Wyart and Michael E Cates. “Does a growing static length scale control the glass transition?” In: *Physical review letters* 119.19 (2017), p. 195501.
- [259] Ruben Zakine, Alexandre Solon, Todd Gingrich, and Frédéric Van Wijland. “Stochastic Stirling engine operating in contact with active baths”. In: *Entropy* 19.5 (2017), p. 193.
- [260] Bo Zhang, Andrey Sokolov, and Alexey Snezhko. “Reconfigurable emergent patterns in active chiral fluids”. In: *Nature communications* 11.1 (2020), p. 4401.
- [261] Robert Zwanzig. “Ensemble method in the theory of irreversibility”. In: *The Journal of Chemical Physics* 33.5 (1960), pp. 1338–1341.
- [262] Robert Zwanzig. *Nonequilibrium statistical mechanics*. Oxford university press, 2001.